© 2020 Wiley-VCH GmbH

ADVANCED FUNCTIONAL MATERIALS

Supporting Information

for *Adv. Funct. Mater.*, DOI: 10.1002/adfm.202004838

Maximizing Chiral Perturbation on Thermally Activated Delayed Fluorescence Emitters and Elaboration of the First Top-Emission Circularly Polarized OLED

*Lucas Frédéric, Alaric Desmarchelier, Romain Plais, Leonid Lavnevich, Gilles Muller, Cassie Villafuerte, Gilles Clavier, Etienne Quesnel, Benoit Racine, Sylvia Meunier-Della-Gatta, Jean-Pierre Dognon, Pierre Thuéry, Jeanne Crassous, Ludovic Favereau, and Grégory Pieters**

Supporting information

General information

Every air or moisture sensitive experiments were carried out under a nitrogen or argon atmosphere in flame dry glassware. Anhydrous solvents were obtained by distillation by the following procedure:

-Tetrahydrofurane: distillated under a nitrogen atmosphere over sodium and benzophenone

-Methylene chloride: distillated under a nitrogen atmosphere over calcium hydride.

Other solvents were used without any other purification.

All commercial reagents, purchased from Aldrich, Alpha Aesar, TCI and Merck were used without further purification.

Progress of reactions was monitored by thin layer chromatography on precoated Merck silica gel plates (60F-254). Visualization was accomplished by UV light (254, 312 and 365 nm).

Flash chromatography was performed with Merck silica gel (40-60 μm) or with a CombiFlash (COMBIFLASH RF, Teledyne Isco) using the appropriate normal phase silica gel columns, eluting with cyclohexane (Cy), ethyl acetate (EA), methylene chloride (CH_2Cl_2) and toluene (tol) mixtures.

^{1}H NMR (400 MHz), ^{13}C NMR (100 MHz), ^{19}F NMR (376 MHz) were recorded on a Bruker Avance 400 MHz spectrometer. Chemical Shifts are reported in parts per million (ppm) downfield from residual solvent peaks and coupling constants are reported as Hertz (Hz). Splitting patterns are designated as singlet (s), doublet (d), triplet (t). Splitting patterns that could not be interpreted or easily visualized are designated as multiplet (m).

UV−visible spectra were recorded on a Cary 50 or a Cary 400 (Agilent) double-beam spectrometer using a 10 mm path quartz cell.
Circular dichroism (CD) spectra were recorded on a Jasco (model J-815) spectropolarimeter equipped with a Peltier thermostated cell holder and Xe laser. Data were recorded at 20°C using a 1mm*1cm cell. The obtained signals were processed by substracting solvent and cell contribution.

Emission spectra were measured on a Fluoromax-3 (Horiba) spectrofluorimeter or Fluoromax-4 (Horiba) or Fluorolog (Horiba). A right-angle configuration was used. Optical density of the samples was checked to be less than 0.1 to avoid reabsorption artifacts. The relative fluorescence quantum yields for solutions were determined using Coumarin 102 (Φ_F = 0.764 in ethanol) or Coumarin 153 (Φ_F = 0.53 in ethanol) as references with the following formula:

$$\Phi_F(x) = \Phi_F(0)\frac{1-10^{-A_0}}{1-10^{-A_x}}\frac{S_x}{S_0}\left(\frac{n_x}{n_o}\right)^2$$

Where $\Phi_F(0)$ is the quantum yield of the reference, A_0 and A_x respectively absorbance of the reference and the studied compound at the excitation wavelength; S_x and S_0 respectively area under the emission peak of the reference and the studied compound; n_x and n_x respectively refractive index of the solvent of the reference and the studied compound. Absolute quantum yields of solid samples were determined with integrating sphere.

The fluorescence decay curves in the ns regime were obtained by the time-correlated single-photon counting (TCSPC) method with a femtosecond laser excitation composed of a Titanium Sapphire laser (Tsunami, Spectra-Physics) pumped by a doubled Nd:YVO4 laser (Millennia Xs, Spectra-Physics). Light pulses at 990 nm from the oscillator were selected by an acousto-optic crystal at a repetition rate of 4 MHz, and then tripled at 330nm by non-linear crystals.

Fluorescence photons were detected at 90° through a monochromator and a polarizer at magic angle by means of a Hamamatsu MCP R3809U photomultiplier, connected to a SPC-630 TCSPC module from Becker & Hickl. The instrumental response function was recorded before each decay measurement with a fwhm (full width at half-maximum) of ~25 ps. The fluorescence data were analyzed using the Globals software package developed at the Laboratory for Fluorescence Dynamics at the University of Illinois at Urbana-Champaign, which includes reconvolution analysis and global non-linear least-squares minimization method. The µs fluorescence decay curves were obtained using an Edinburgh instrument LP920 laser flash photolysis spectrometer combined with an Nd:YAG laser (Continuum) tripled at 355 nm via non-linear crystals. This third harmonic is optimized to pump an OPO that can generate 425 nm signal. The Fluorescence photons were detected at 90° through a long pass filter and a monochromator by means of a Hamamatsu R928 photomultiplier. The Levenberg-Marquardt algorithm was used for non-linear least square fit (tail fit) as implemented in the L900 software (Edinburgh instrument). In order to estimate the quality of the fit, the weighted residuals were calculated.

CPL measurement were recorded with three different apparatus.

The circularly polarized luminescence (CPL) and total luminescence spectra were recorded on an instrument described previously,[S3] operating in a differential photoncounting mode. The light source for excitation was a continuous wave 1000 W xenon arc lamp from a Spex Fluorolog-2 spectrofluorimeter, equipped with excitation and emission monochromators with dispersion of 4 nm/mm (SPEX, 1681B). To prevent artifacts associated with the presence of linear polarization in the emission,[S2] a high quality linear polarizer was placed in the sample compartment, and aligned so that the excitation beam was linearly polarized in the direction of emission detection (z-axis). The key feature of this geometry is that it ensures that the molecules that have been excited and that are subsequently emitting are isotropically distributed in the plane (x,y) perpendicular to the direction of emission detection. The optical system detection consisted of a focusing lens, long pass filter, and 0.22 m monochromator. The emitted light was detected by a cooled EMI-9558B photomultiplier tube operating in photocounting mode. All measurements were performed with quartz cuvettes with a pathlength of 1.0 cm.

The circularly polarized luminescence (CPL) measurements were performed using a commercialized instrument JASCO CPL-300 at room temperature in 10*10mm cell. Beforehand, concentration of solutions was adjust to reach an optical density around 0.2 on a UV-CARY 50. Excitation wavelength and instrument parameters were adapted for every sample. Data pitch was set at 1 nm and spectra displayed are mean values of a minimum of 10 accumulations.

Circularly polarized luminescence (CPL) measurements of thin layer of pure compound and circularly polarized electroluminescence of OLEDs were performed using a home-built (with the help of the JASCO company) CPL spectrofluoropolarimeter. The thin layer samples were excited using a 90° geometry with a Xenon ozone-free lamp 150 W LS. The parameters were: emission bandwidth ~ 1.0 nm, integration time = 4 sec, scan-speed = 50 nm/min, accumulations = 10.

Every CPL measurement in solution were double checked on both apparatus.

Electrochemical measurements were performed with a potentiostat-galvanostat AutoLab PGSTAT 302N controlled by resident General Purpose Electrochemical System (GPES 4.9) software using a conventional single-compartment three-electrode cell. The working and auxiliary electrodes were platinum electrodes and the reference electrode was the saturated potassium chloride calomel electrode (SCE). The supporting electrolyte was 0.2 M Bu_4NPF_6 in CH_2Cl_2 and solutions were purged with argon before the measurements. The scan rate was 200 mV/s. All potentials are given relative to SCE.

Thin films were prepared with the following procedure: 50 µL of TADF compound solution (1 mg/mL in methylene chloride) is poured into a solution of PMMA (50 mg of PMMA into 0.5 mL of

methylene chloride). The solution is then dropped onto a quartz slide. The solvent is let evaporated one night under a saturated atmosphere of methylene chloride.

Every AIE experiment were performed as follow: stock-solutions of each compounds in distillated THF were prepared at $C=10^{-3}$ M. Diluted solution were then prepared at $C=10^{-5}$ M with a mixture THF/water, the fraction of water in volume is annoted f_w. Every emission spectra were recorded with 1cm*1cm cuvette in the same conditions (excitation wavelength, slits size, range of emission) depending on the compound.

Computational methods

Preliminary remarks

TD-DFT with non-hybrid exchange-correlation functionals generally underestimate excitation energys, particularly for charge-transfer states. Charge-transfer excitation energys are generally improved with hybrid functionals and also with range-separated functionals that separate the exchange term of the DFT functional into long- and short-range contributions.[S3] To model the TADF process properly, the geometry of the systems needs to be relaxed for all relevant electronic states. Even TD-DFT is a very tractable method for large molecules, their computational cost with range separated functionals still prevents excited states geometry optimization of our largest systems. Accordingly, we have chosen to optimize the geometries of S0, S1 and T1 states and to evaluate the ΔE_{ST} term with a hybrid functional and to calculate the optical properties with a range-separated functionals.

Geometry optimization

The geometries of the most stable conformers were optimized using density functional theory (DFT) with the ORCA 4 program[S4] along with the resolution of identity approximation.[S5] It speeds up calculation of the Coulomb term for large systems. The PBE0 functional was considered corrected by the empirical dispersion term (D3) proposed by Grimme et al.[S6] with a finite damping as introduced by Becke and Johnson (BJ-damping) to account for the London dispersion energy.[S7] The addition of the BJ-damping provides better results for non-bonded distances and more clear effects of intramolecular dispersion. The split valence plus polarization triple- (def2-TZVP) basis set was used.[S8] Same methods and approximations were applied to optimize the geometries of the excited states S1 and T1 starting from S0 geometry.

Post-process, analysis and visualization of results from ORCA

All calculations (including spectra and excited states properties) were analyzed by using Multiwfn (development version 3.7) software[S9] and visualized by using the VMD 1.9.4 software.[S10]

Visual study of non-covalent interaction

C. Lefevre et al.[S11] proposed a very useful way of studying inter-fragment and intra-fragment interactions, named Independent Gradient Model (IGM). The IGM method was used, as implemented in Multiwfn, to characterize the interaction region and interaction type in the molecules studied in this work.

Excited states

The theoretical electronic absorption spectra and CD spectra were calculated on the optimized ground-state geometry using time-dependent DFT (TD-DFT) with the CAM-B3LYP range-separated functional and def2-TZVP basis set (ORCA 4). It is now well established that range-separated functionals like CAM-B3LYP are mandatory to predict the photophysical properties of molecules.[S3] To get spectra from calculations that can be compared with the experiments we applied a Gaussian broadening function over the single oscillator or rotational strength calculated

values, we included an energy correction and only subsequently we converted the spectra to nm. In a final step, we performed a scaling of the calculated intensities for a better similarity with experimental spectra.

Synthetic procedures

General procedure A, synthesis of **6a-c** :

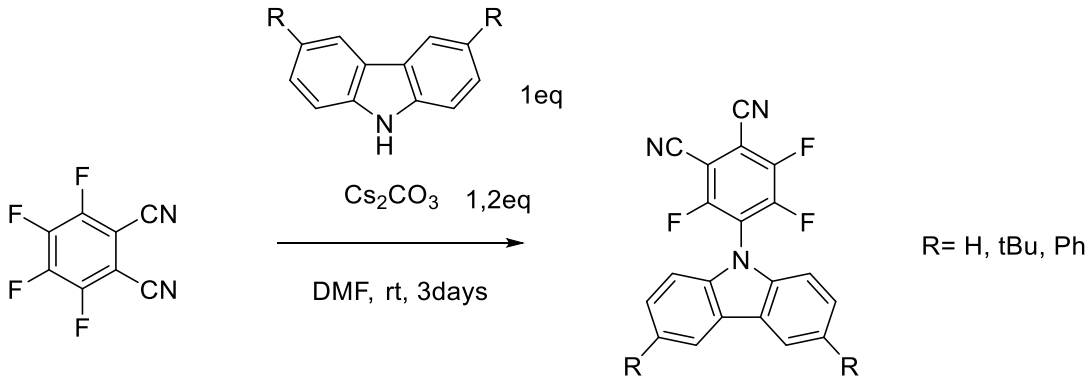

6a-c

Synthesis :

In a dry flask with a stirrer, carbazole derivative (1 eq), tetrafluorophthalonitrile (1 eq) and cesium carbonate (1.2 eq) are loaded. After cooling to 0°C with an ice bath, acetonitrile (C=0.2 mol/L) is added to the flask. The mixture is reacted for 3 days. After no more evolution of the reaction, followed by thin layer chromatography, the reaction mixture is diluted with methylene chloride (scale 1 mmol / 5 mL) and quenched with water (scale 1 mmol / 5 mL). Aqueous layer is extracted three times (scale 1 mmol / 20 mL), organic layers are collected and washed with brine (scale 1 mmol / 10 mL), then dry over $MgSO_4$ and dry under reduced pressure. The solid obtained is then partially purified by flash chromatography to give a mixture of the expected product and tetrafluorophthalonitrile.

General procedure B, synthesis of C' products:

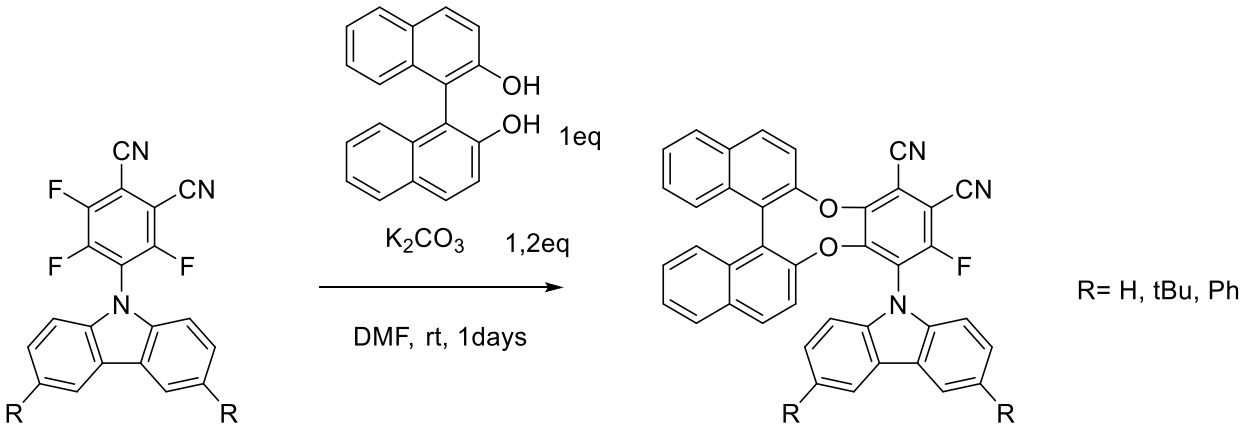

6a-c

C'1,2,3 *(S)/(R)*

Synthesis :

In a dry flask with a stirrer, **6a-c** (1eq), *(S)/(R)*-1,1'-bi(2-naphthol) (1 eq) and potassium carbonate (2 eq) are added under nitrogen. Then DMF (C=0.2 mol/L) is added and the reaction is let under stirring for 24h. After completion of the reaction followed by thin layer chromatography, the reaction mixture is diluted with methylene chloride (scale 1 mmol / 5mL) and quenched with water (scale 1 mmol / 5 mL). Aqueous layers are extracted with methylene chloride three times (scale 1 mmol / 20 mL), organic layers are gathered and washed with brine (scale 1 mmol / 10mL), dry over $MgSO_4$ and solvent was removed under vacuum. The solid obtained was purified by flash chromatography to give the expected product.

General procedure C, synthesis of C products:

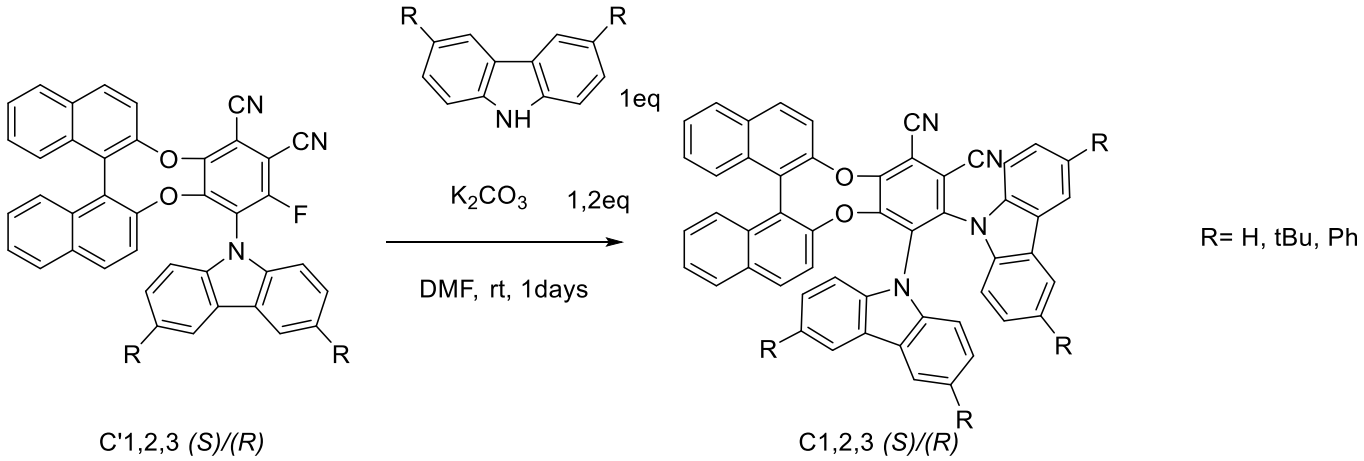

C'1,2,3 *(S)/(R)*

C1,2,3 *(S)/(R)*

Synthesis :

In a dry flask with a stirrer, compound **C'1, 2, 3** (1 eq), corresponding carbazole **5a-c** (1 eq) and potassium carbonate (1.2 eq) are added under nitrogen. Then DMF (C=0.2 mol/L) is added and the reaction is let under stirring for 24h. After completion of the reaction followed by thin layer chromatography, the reaction mixture is diluted with methylene chloride (scale 1 mmol / 5mL) and quenched with water (scale 1 mmol / 5mL). Aqueous layers are extracted with methylene chloride three times (scale 1 mmol / 20 mL), organic layers are gathered and washed with brine (scale 1 mmol / 10 mL), dry over $MgSO_4$ and solvent was removed under vacuum. The solid obtained was purified by flash chromatography to give the expected product.

Compound **B1** *(S)/(R)* :

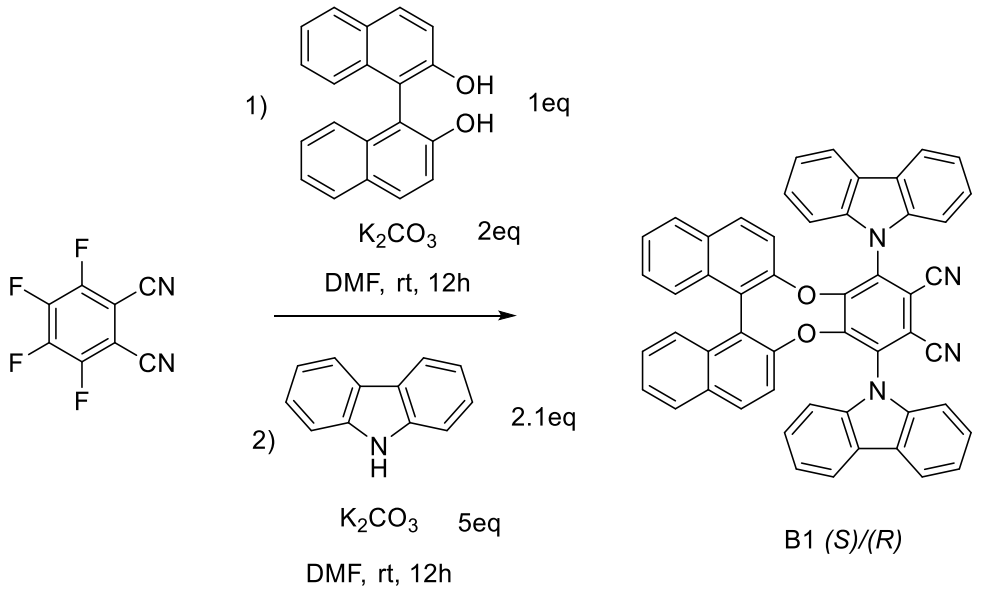

Synthesis :

To a 50 mL flask with a magnetic stirrer under nitrogen, *(S)/(R)*-(-)-1,1'-bi(2-naphthol) (716 mg, 2.5 mmol, 1 eq), tetrafluorophthalonitrile (500 mg, 2.5 mmol, 1 eq) and anhydrous potassium carbonate (691 mg, 5 mmol, 2 eq) were added. Then under nitrogen and stirring, dry DMF (12.5 mL, 0.2 mol/L) was added to dissolve organic compounds. The reaction mixture become pale yellow and is let for 12h. After completion of the reaction monitored by thin layer chromatography, the reaction mixture was diluted with methylene chloride (40 mL) and quenched with water (20 mL) at 0°C. The aqueous layer was extracted 3 times with methylene chloride (3*50 mL), after organic layer were combined and washed with brine (50mL), then dried over $MgSO_4$, solvent was removed under vacuum to give a yellowish/transparent solid. This solid was dissolved in a small amount of methylene chloride (15 mL), then pass through a small pad of silica (eluted with methylene chloride, 150 mL). The resulting product was dried under vacuum to give a yellowish/transparent solid.

Then the solid was introduced into a 50 mL flask with a magnetic stirrer under nitrogen with carbazole (836 mg, 5 mmol, 2 eq) and anhydrous potassium carbonate (1.728 g, 12.5 mmol, 5 eq). Then dry DMF (12.5 mL, 0.2 mol/L) was added under argon and stirring. The reaction is let for 24h. After completion of the reaction monitored by thin layer chromatography, the reaction mixture is quenched with water (20 mL), and diluted with methylene chloride (40 mL). The aqueous layer is extracted 3 times with dichloromethane (3*50 mL). Organic layers are combined and washed with brine (50m L), then dried over magnesium sulfate. The solvent was then removed under vacuum and the solid was purified by flash chromatography (EA/Cy, 0:100 to 5:95) to give **B1** *(S)/(R)* as a yellow solid (1.606 g, 87% yield).

^{1}H NMR (400 MHz, $CDCl_3$) δ 8.22 (d, J = 7.7 Hz, 2H), 8.09 (d, J = 7.4 Hz, 1H), 7.81 (d, J = 8.2 Hz, 2H), 7.75 (d, J = 8.9 Hz, 2H), 7.68 (t, J = 7.6 Hz, 2H), 7.47 (dd, J = 18.5, 7.8 Hz, 4H), 7.40 (ddd, J = 7.9, 4.8, 2.9 Hz, 2H), 7.24 – 7.13 (m, 9H), 6.82 (d, J = 7.9 Hz, 2H), 6.57 (d, J = 8.9 Hz, 2H).

^{13}C NMR (101 MHz, $CDCl_3$) δ 153.1, 149.0, 140.7, 140.6, 135.5, 132.1, 131.66, 131.63, 128.41, 127.3, 127.0, 126.8, 126.7, 126.4, 124.7, 124.6, 124.2, 121.9, 121.4, 121.3, 120.8, 119.9, 114.4, 112.2, 110.0, 109.5.

HRMS (ESI): m/z calculated for C52H28N4O2 [M]+: 740.2212, found [M+H]+: 741.228211.

Compound **B1r** *(S)/(R)* :

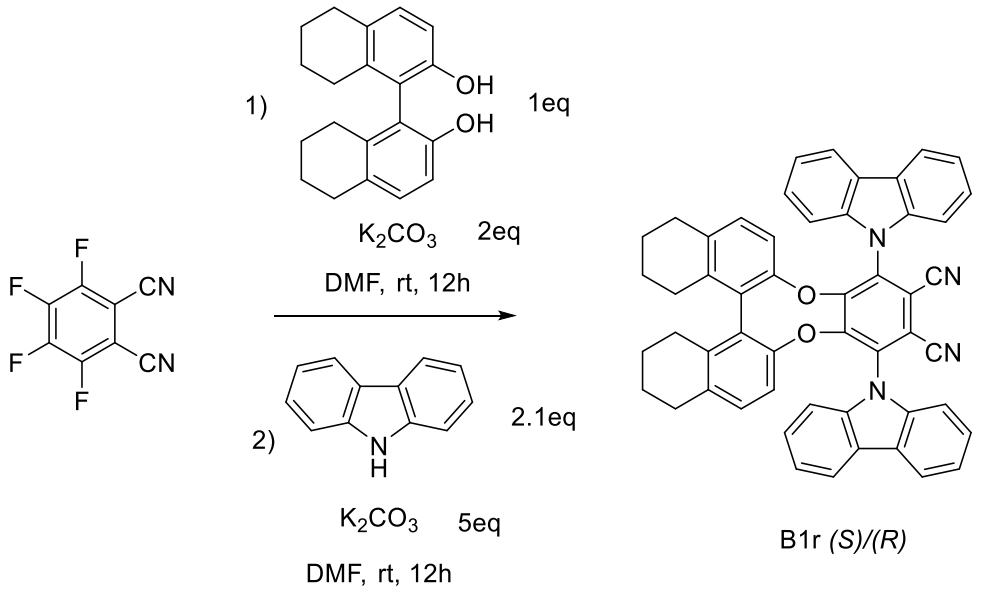

Synthesis :

Synthesis of compound **B1r** *(S)/(R)* follow the same procedure used for compound **B1** *(S)/(R)* with *(S)/(R)*- 5,5′,6,6′,7,7′,8,8′-Octahydro-1,1′-bi-2-naphthol (65 mg, 0.22 mmol, 1 eq), tetrafluorophthalonitrile (44 mg, 0.22 mmol, 1 eq) and anhydrous potassium carbonate (61mg, 0.44mmol, 2eq) in dry DMF (1.1 mL, 0.2 mol/L). For the second step, carbazole (74 mg, 0.44 mmol, 2 eq) and potassium carbonate (152 mg, 1.1 mmol, 5 eq) with the intermediate product were solubilized in DMF (1.1 mL). The product was purified by flash chromatography (EA/Cy, 0:100 to 5:95) to give **B1r** *(S)/(R)* as a yellow solid (124 mg, 75% yield).

^{1}H NMR (400 MHz, $CDCl_3$) δ 8.20 (d, *J* = 7.7 Hz, 2H), 8.12 (dd, *J* = 6.0, 2.8 Hz, 2H), 7.62 (t, *J* = 7.4 Hz, 2H), 7.44 (t, *J* = 7.5 Hz, 2H), 7.38 (d, *J* = 8.1 Hz, 2H), 7.28 (dd, *J* = 5.9, 3.1 Hz, 4H), 6.88 (d, *J* = 8.3 Hz, 2H), 6.84 – 6.77 (m, 2H), 6.17 (d, *J* = 8.3 Hz, 2H), 2.71 (t, *J* = 6.3 Hz, 4H), 2.47 – 2.34 (m, 2H), 2.10 (dt, *J* = 16.3, 5.2 Hz, 2H), 1.78 – 1.57 (m, 6H), 1.55 – 1.36 (m, 3H).

^{13}C NMR (101 MHz, $CDCl_3$) δ 153.8, 149.3, 140.7, 140.3, 137.4, 136.4, 135.0, 130.4, 128.7, 126.7, 126.3, 124.4, 124.2, 121.7, 121.2, 121.1, 120.6, 117.7, 113.3, 112.4, 110.2, 109.5, 29.18, 27.35, 22.51, 22.34.

Compound **B2** *(S)/(R)* :

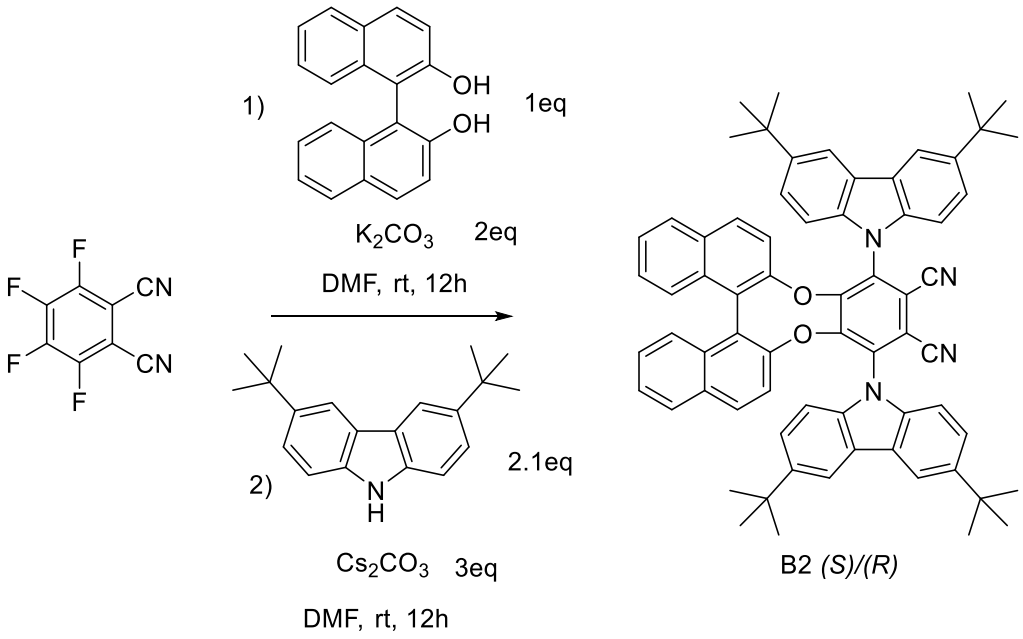

Synthesis :

To a 10 mL flask with a magnetic stirrer, *(S)/(R)*-1,1'-bi(2-naphthol) (64 mg, 0.224 mmol, 1 eq), tetrafluorophthalonitrile (45 mg, 0.224 mmol, 1 eq) and anhydrous potassium carbonate (62 mg, 0.448 mmol, 2 eq) were added. Then under nitrogen and stirring, dry DMF (1.1 mL, 0.2 mol/L) was added to dissolve organic compounds. The reaction mixture become pale yellow and is let for 12h. After completion of the reaction monitored by thin layer chromatography, the reaction mixture was diluted with methylene chloride (10 mL) and quenched with water (5 mL) at 0°C. The aqueous layer was extracted 3 times with methylene chloride (3*10 mL), after organic layer were combined and washed with brine, then dried over $MgSO_4$, solvent was removed under vacuum to give a yellowish/transparent solid. This solid was dissolved in a small amount of methylene chloride (10 mL), then pass through a small pad of silica (eluted with methylene chloride, 100 mL). The resulting product was dried under vacuum to give a yellowish/transparent solid.

Then the solid was introduced into a 10 mL flask with a magnetic stirrer under nitrogen with 3,6-ditertbutylcarbazole (125 mg, 0.447 mmol, 2 eq) and anhydrous cesium carbonate (219 mg, 0.672 mmol, 3 eq) were added. Then dry DMF (2.99 mL, 0.075 mol/L) was added under argon and stirring. The reaction is let for 24h. After completion of the reaction monitored by thin layer chromatography, the reaction mixture is quenched with water (2 mL), and diluted with methylene chloride (10 mL). The aqueous layer is extracted 3 times with dichloromethane (3*20 mL). Organic layers are combined and washed with brine (10 mL), then dried over magnesium sulfate. The solvent was then removed under vacuum and the solid was purified by flash chromatography (EA/Cy, 0:100 to 5:95). The resulting solid was then purified by HPLC giving **B2** (41.8 mg,20% yield) as yellow solid.

HPLC conditions:

Column Xbridge C18 (150x19mm), 5µm. Eluent A: H_2O + 1/1000 formic acid. Eluent B: acetonitrile + 1/1000 formic acid., flowrate: 17mL/min.

Gradient :

t=0min %A 70 %B 30

t=15min %A 0 %B 100

t=30 min %A 0 %B 100

^{1}H NMR (400 MHz, $CDCl_3$) δ 8.23 (d, J = 1.6 Hz, 2H), 8.11 (d, J = 1.6 Hz, 2H), 7.87 (d, J = 8.3 Hz, 2H), 7.80 (d, J = 8.9 Hz, 2H), 7.70 (dd, J = 8.6, 1.9 Hz, 2H), 7.46 (ddd, J = 8.1, 5.5, 2.5 Hz, 2H), 7.33 (d, J = 8.6 Hz, 2H), 7.27 (dd, J = 3.6, 0.7 Hz, 2H), 7.26 – 7.25 (m, 1H), 7.23 (d, J = 1.9 Hz, 1H), 7.21 (d, J = 1.9 Hz, 1H), 6.71 (d, J = 8.6 Hz, 2H), 6.66 (d, J = 8.9 Hz, 2H), 1.57 (s, 18H), 1.37 (s, 18H).

^{13}C NMR (101 MHz, $CDCl_3$) δ 152.9, 149.2, 144.6, 144.1, 139.2, 139.1, 135.7, 132.0, 131.7, 131.4, 128.3, 127.1, 126.8, 126.2, 124.7, 124.6, 124.3, 124.2, 124.1, 120.2, 117.3, 116.7, 114.2, 112.2, 109.4, 108.9, 345.0, 34.7, 32.1, 31.9.

HRMS (ESI): m/z calculated for C68H60N4O2 [M]+: 964.4716, found [M+H]+: 965.4793.

Compound **B3** *(S)/(R)* :

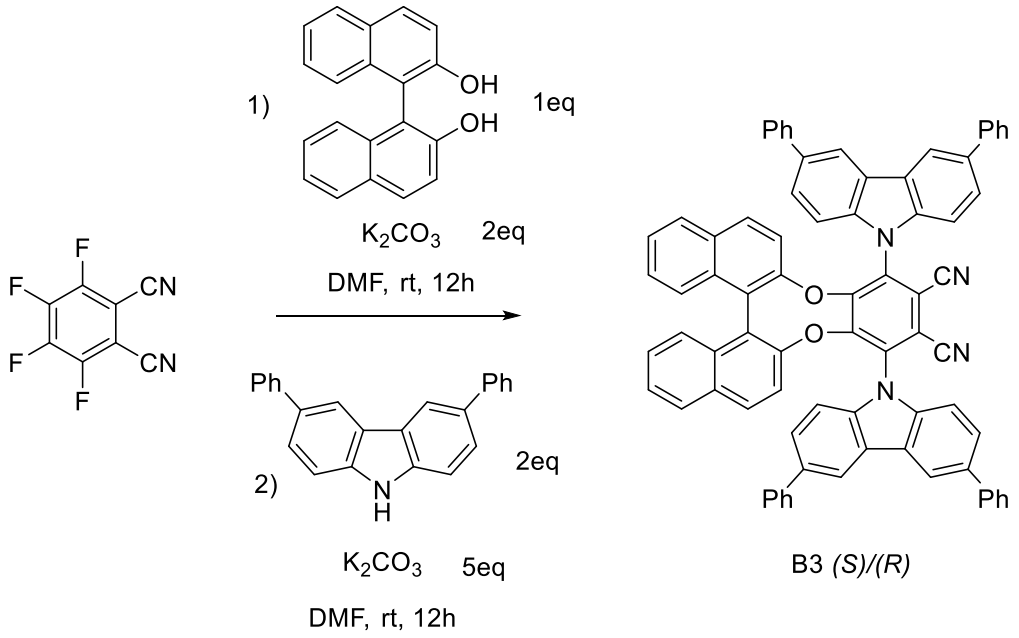

Synthesis :

To a 5 mL flask with a magnetic stirrer, *(S)/(R)*-1,1'-bi(2-naphthol) (72 mg, 0.25 mmol, 1 eq), tetrafluorophthalonitrile (50 mg, 0.25 mmol, 1 eq) and anhydrous potassium carbonate (70 mg, 0.51 mmol, 2 eq) were added. Then under nitrogen and stirring, dry DMF (1.3 mL, 0.2 mol/L) was added to dissolve organic compounds. The reaction mixture become pale yellow and is let for 12h. After completion of the reaction monitored by thin layer chromatography, the reaction mixture was diluted with methylene chloride (10 mL) and quenched with water (5 mL) at 0°C. The aqueous layer was extracted 3 times with methylene chloride (3*10 mL), after organic layers were combined and washed with brine (10mL), then dried over $MgSO_4$, solvent was removed under vacuum to give a yellowish/transparent solid. This solid was dissolved in a small amount of methylene chloride (10 mL), then passed through a small pad of silica (eluted with methylene chloride, 100 mL). The resulting product was dried under vacuum to give a yellowish/transparent solid.

Then the solid was introduced into a 10 mL flask with a magnetic stirrer under nitrogen with 3,6-diphenylcarbazole (160 mg, 0.5 mmol, 2 eq) and anhydrous potassium carbonate (173.1 mg, 1.25 mmol, 5 eq) were added Then dry DMF (3.33 mL, 0.075 mol/L) was added under argon and stirring. The reaction is let for 24h. After completion of the reaction monitored by thin layer chromatography, the reaction mixture is quenched with water (5 mL), and diluted with methylene chloride (10 mL). The aqueous layer is extracted 3 times with dichloromethane (3*20 mL). Organic layers are combined and washed with brine (20 mL), then dried over magnesium sulfate. The solvent was then removed under vacuum and the solid was purified by flash chromatography (EA/Cy, 0:100 to 4:96). The resulting orange solid is then purified by HPLC to give **B3** (135.7 mg, 52% yield) as a yellow powder.

HPLC conditions :

Column Interchim Utpisphere HDO C18 (150x21mm), 5µm. Eluent A: H_2O + 1/1000 formic acid. Eluent B: acetonitrile + 1/1000 formic acid., flowrate: 21mL/min.

Gradient :

t=0min %A 20 %B80

t=24min %A 0 %B 100

t=30 min %A 0 %B 100

^{1}H NMR (400 MHz, $CDCl_3$) δ 8.50 (d, J = 1.5 Hz, 3H), 8.37 (d, J = 1.5 Hz, 3H), 7.96 (dd, J = 8.4, 1.7 Hz, 3H), 7.84 (dt, J = 10.7, 8.3 Hz, 12H), 7.62 – 7.52 (m, 15H), 7.44 (ddt, J = 11.5, 9.7, 5.3 Hz, 15H), 7.28 (ddd, J = 10.5, 7.7, 5.3 Hz, 10H), 6.89 (d, J = 8.5 Hz, 3H), 6.68 (d, J = 8.9 Hz, 3H).

^{13}C NMR (101 MHz, $CDCl_3$) δ 153.0, 149.1, 141.53, 141.48, 140.6, 140.4, 135.6, 135.4, 135.3, 132.2, 131.8, 131.7, 129.1, 128.9, 128.5, 127.6, 127.5, 127.4, 127.2, 127.0, 126.9, 126.6, 126.5, 125.3, 124.9, 124.8, 119.94, 119.89, 119.40, 114.3, 112.3, 110.5, 109.9.

HRMS (ESI): m/z calculated for C76H44N4O2 [M]+: 1044.3464, found [M+H]+: 1045.3538.

3,6-dibromocarbazole

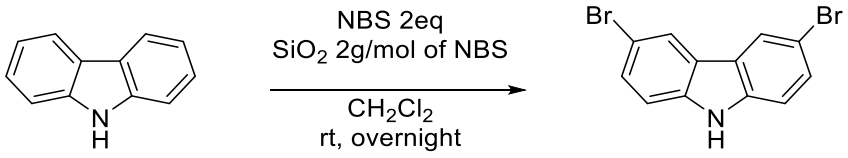

Synthesis :

In a flame dried 1L flask with a stirrer under argon covered with aluminium foil, carbazole (1.67 g, 10 mmol, 1 eq) is solubilized in dry methylene chloride (250 mL). Then beforehand flame dried silica (40 g, 2g/mmol of NBS) is added to the solution. N-bromosuccinimide solution (3.56 g, 20 mmol, 2 eq in 250 mL of methylene chloride), is added dropwise over 1h30. The reaction is let stirred at room temperature overnight. Then the reaction mixture is filtrated over sintered funnel and washed with methylene chloride (100 mL). Organic layers are washed with water and dried over $MgSO_4$. The resulting solid is then purified by flash chromatography (EA/Cy, 0:100 to 1:9) to give the expected product as a beige powder (2.9 g, 89% yield).

^{1}H NMR (400 MHz, Acetone) δ 10.58 (d, J = 49.1 Hz, 1H), 8.35 (s, 2H), 7.60 – 7.42 (m, 4H).

^{13}C NMR (101 MHz, Acetone) δ 140.05, 129.84, 124.82, 124.09, 113.87, 112.47.

Compound **3,6-dibromocarbazole :**

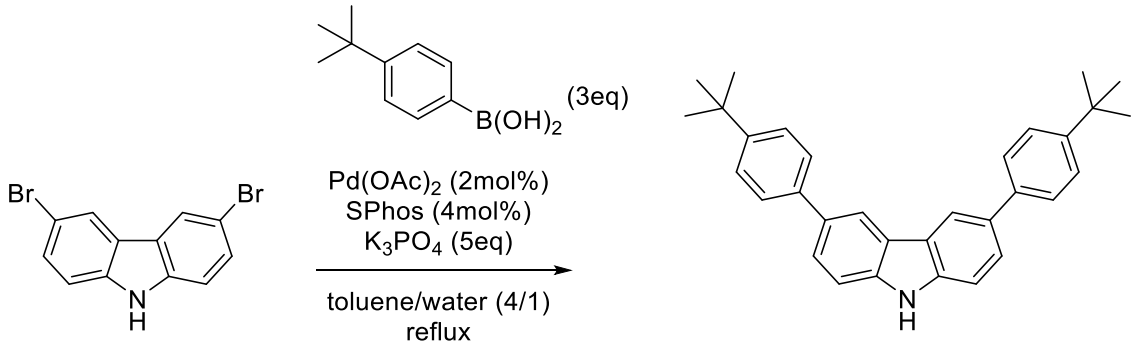

Synthesis :

In a flame dried Schlenck under nitrogen, 3,6-dibromocarbazole (500 mg, 1.538 mmol, 1 eq), 4-tert-butylphenylboronic acid (821 mg, 4.61 mmol, 3 eq), palladium acetate (7 mg, 0.0031 mmol, 2 mol%), SPhos (25.3 mg, 0.062 mmol, 4 mol%) and tripotassium triphosphate (1.63 g, 7.67 mmol, 5 eq) are loaded. Then toluene (6 mL) and water (1 mL) are added. The reaction mixture is heated to reflux (around 110°C) overnight. The content of the Schlenck is then dilute with methylene chloride (20 mL) and water (15 mL). Organic layers are extracted 7 times with methylene chloride (7*20 mL) and thus washed with brine (20 mL) and dried over $MgSO_4$. The resulting solid is then purified by flash chromatography (EA/Cy, 3:97 to 15:85) to give product **5d** as a white powder (240 mg, 36% yield).

^{1}H NMR (400 MHz, $CDCl_3$) δ 8.32 (s, 2H), 8.09 (s, 1H), 7.67 (t, J = 7.4 Hz, 6H), 7.51 (d, J = 8.3 Hz, 6H), 1.39 (s, 18H).

Due to the lack of solubility of this product in common deuterated organic solvents ($CDCl_3$, acetone-d_6, DMSO-d_6, DMF-d_7), no suitable 13C spectrum can be exhibited

Compound **B4** *(S)/(R)* :

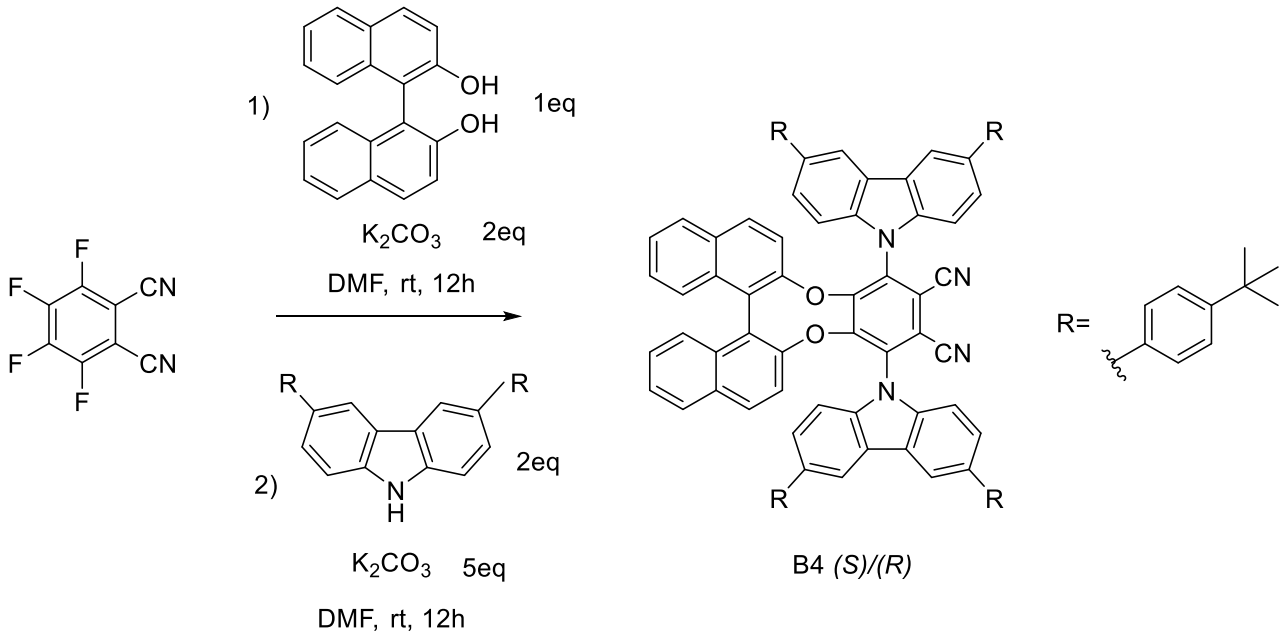

Synthesis :

To a 5mL flask with a magnetic stirrer, *(S)/(R)*-1,1'-bi(2-naphthol) (57 mg, 0.2 mmol, 1 eq), tetrafluorophthalonitrile (40 mg, 0.2 mmol, 1 eq) and anhydrous potassium carbonate (55 mg, 0.4 mmol, 2 eq) were added. Then under nitrogen and stirring, dry DMF (1 mL, 0.2 mol/L) was added to dissolve organic compounds. The reaction mixture become pale yellow and is let for 12h. After completion of the reaction monitored by thin layer chromatography, the reaction mixture was diluted with methylene chloride (10 mL) and quenched with water (5 mL) at 0°C. The aqueous layer was extracted 3 times with methylene chloride, after organic layers were combined and washed with brine, then dried over $MgSO_4$, solvent was removed under vacuum to give a yellowish/transparent solid. This solid was dissolved in a small amount of methylene chloride (10 mL), then pass through a small pad of silica (eluted with methylene chloride, 100 mL). The resulting product was dried under vacuum to give a yellowish/transparent solid.

Then the solid was introduced into a 10 mL flask with a magnetic stirrer under nitrogen with 3,6-para-tertbutyldiphenylcarbazole (172 mg, 1 mmol, 2 eq) and anhydrous potassium carbonate (138 mg, 1 mmol, 5 eq) were added. Then dry DMF (1 mL, 0.2 mol/L) was added under argon and stirring The reaction is let for 24h. After completion of the reaction monitored by thin layer chromatography, the reaction mixture is quenched with water (2 mL), and diluted with methylene chloride (5 mL). The aqueous layer is extracted 3 times with dichloromethane (3*20 mL). Organic layers are combined and washed with brine (20 mL), then dried over magnesium sulfate. The solvent was then removed under vacuum and the solid was purified by flash chromatography (EA/Cy, 0:100 to 3:97) to give product B4 as a yellow solid (62 mg, 24% yield).

^{1}H NMR (400 MHz, Acetone) δ 8.79 (d, J = 1.1 Hz, 2H), 8.62 (d, J = 1.3 Hz, 2H), 8.04 (ddd, J = 26.1, 13.1, 5.2 Hz, 8H), 7.88 (d, J = 8.3 Hz, 4H), 7.62 (dd, J = 10.2, 8.4 Hz, 8H), 7.54 – 7.43 (m, 8H), 7.26 (dd, J = 11.7, 7.3 Hz, 4H), 7.16 (d, J = 8.5 Hz, 2H), 6.79 (d, J = 9.0 Hz, 2H), 1.43 (s, 18H), 1.34 (d, J = 8.9 Hz, 18H).

^{13}C NMR (101 MHz, Acetone) δ 153.9, 150.7, 150.5, 150.0 , 142.0, 139.4, 139.3, 136.6, 135.8, 135.6, 133.1, 132.5, 132.5, 129.5, 128.3, 127.8, 127.7, 127.1, 126.9, 126.7, 126.5, 125.9, 125.6, 125.4, 121.1, 120.2, 119.3, 116.7, 113.8, 111.8, 111.6, 35.1, 35.0, 31.74 , 31.65.

HRMS (ESI): m/z calculated for C92H76N4O2 [M]+: 1268.5968, found [M+H]+: 1269.6041.

Screening table for optimization of **6a:**

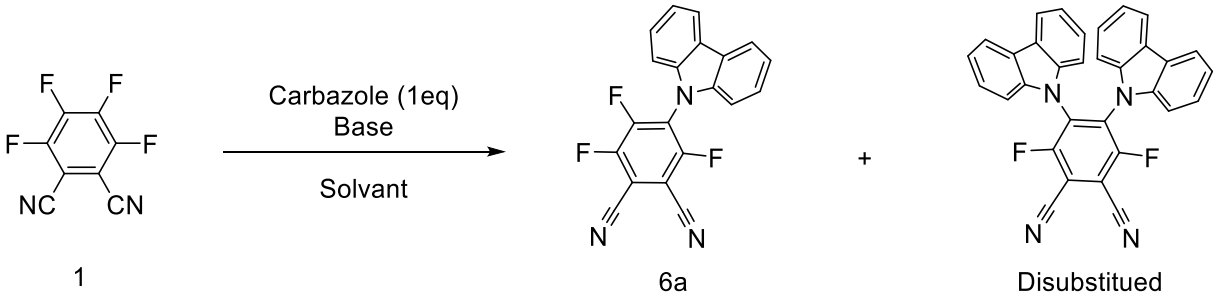

Entry	Base	Solvent	% 6a: disubstitued : residual carbazole
1	K_2CO_3 (1,2 eq)	DMF	32 : 4 : 64
2	K_2CO_3 (1,2 eq)	DMSO	24 : 6 : 70
3	K_2CO_3 (1,2 eq)	ACN	23 : 1 : 76
4	K_2CO_3 (1.2 eq)	THF	0 : 0 : 100
5	K_2CO_3 (4 eq)	DMF	26 : 32 : 42
6	K_2CO_3 (4 eq)	ACN	35 : 1 : 64
7	**Cs_2CO_3 (1,2 eq)**	**ACN**	**69 : 3 : 28**

Table S1: Optimization for compound **6a**

Compound **6a** (R=H)

Synthesis :

6a is obtained following the general procedure A product with carbazole (669 mg, 4 mmol, 1 eq), tetrafluorophthalonitrile (800 mg, 4 mmol, 1 eq) and cesium carbonate (1.56 g, 4.8 mmol, 1.2 eq) in 20 mL of acetonitrile. The crude product is purified by flash chromatography (CH_2Cl_2/Cy, 4/6) to give a yellow solid.

Compound **6b** (R=*t*Bu)

Synthesis :

6b is obtained following the general procedure A with 3,6-ditertbutylcarbazole (279 mg, 1 mmol, 1 eq), tetrafluorophthalonitrile (200 mg, 1 mmol, 1 eq) and cesium carbonate (391 mg, 1.2 mmol, 1.2 eq) in 5 mL of acetonitrile. The crude product is purified by flash chromatography (CH_2Cl_2/Cy, 4/6) to give a yellow solid.

Compound **6c** (R=Ph)

Synthesis :

6c is obtained following the general procedure A with 3,6-diphenylcarbazole (319 g, 1 mmol, 1 eq), tetrafluorophthalonitrile (200 mg, 1 mmol, 1 eq) and cesium carbonate (391 mg, 1.2 mmol, 1.2 eq) in 5 mL of acetonitrile. The crude product is purified by flash chromatography (EA/Cy, 5/95) to give a yellow solid.

Compound **C'1**

Synthesis :

C'1 *(S)/(R)* was obtained following the general procedure B with **6a** (100 mg, considered as 1 eq), *(S)/(R)*-1,1'-bi(2-naphthol) (106 mg, 0.37 mmol, 1 eq) and potassium carbonate (102 mg, 0.74 mmol, 2 eq) in 2 mL of DMF. Flash chromatography was performed (AE/Cy, 1/9) to give compound **C'1** as a yellow solid (122 mg, 23% yield over two steps).

^{1}H NMR (400 MHz, $CDCl_3$) δ 8.18 (dd, J = 16.8, 8.3 Hz, 2H), 8.06 (dd, J = 19.2, 7.9 Hz, 2H), 7.84 (d, J = 8.2 Hz, 1H), 7.73 (d, J = 8.9 Hz, 1H), 7.69 (d, J = 8.8 Hz, 1H), 7.64 – 7.52 (m, 2H), 7.52 – 7.31 (m, 6H), 7.24 – 7.12 (m, 3H), 6.69 (d, J = 8.1 Hz, 1H), 6.51 (d, J = 8.9 Hz, 1H).

^{13}C NMR (101 MHz, $CDCl_3$) δ 158.9, 156.2, 152.7, 152.7, 150.2, 150.2, 149.3, 148.9, 140.3 , 140.2, 132.5, 132.18, 131.96, 131.91, 131.84, 131.7, 128.7, 128.6, 127.5, 126.98, 126.96, 126.74, 126.73, 126.6, 121.8, 121.3, 121.1, 120.6, 120.2, 120.1, 111.8, 111.8, 110.2, 110.1, 109.4, 100.8, 100.6.

^{19}F NMR (376 MHz, $CDCl_3$) δ -109.49 .

HRMS (ESI): m/z calculated for C40H20FN3O2 [M]+: 593.1540, found [M+H]+: 594.1607.

Compound **C'2**

Synthesis :

C'2 *(S)/(R)* was obtained following the general procedure B with **6b** (100 mg, considered as 1 eq), *(S)/(R)*-1,1'-bi(2-naphthol) (63 mg, 0.22 mmol, 1 eq) and potassium carbonate (60 mg, 0.44 mmol, 2 eq) in 1.1 mL of DMF. Flash chromatography was performed (AE/Cy, 1/9) to give compound **C'2** as a yellow solid (49mg, 45% yield over two steps).

^{1}H NMR (400 MHz, $CDCl_3$) δ 8.16 (t, J = 5.6 Hz, 2H), 8.06 (dd, J = 8.3, 4.9 Hz, 2H), 7.85 (d, J = 8.2 Hz, 1H), 7.75 (d, J = 8.8 Hz, 1H), 7.69 (d, J = 8.8 Hz, 1H), 7.64 – 7.54 (m, 2H), 7.46 (d, J = 22.6 Hz, 2H), 7.41 – 7.35 (m, 3H), 7.19 (dd, J = 8.7, 1.9 Hz, 1H), 7.10 (dd, J = 8.5, 2.6 Hz, 1H), 6.60 (dd, J = 10.6, 8.8 Hz, 2H), 1.53 (s, 10H), 1.34 (s, 9H).

^{13}C NMR (101 MHz, $CDCl_3$) δ 156.2, 152.5, 150.2, 149.4, 149.1, 144.8, 144.4, 138.7, 138.7, 132.5, 132.2, 132.0, 131.9, 131.8, 131.6, 128.7, 128.5, 127.6, 127.4, 127.0, 126.8, 126.6, 126.5, 125.9, 125.8, 125.0, 124.9, 124.6, 124.5, 124.4, 124.3, 120.4, 117.1, 116.6, 111.9, 110.2, 109.6, 109.0, 100.7, 100.5, 35.1, 34.8, 32.1, 32.0.

^{19}F NMR (376 MHz, $CDCl_3$) δ -109.00.

HRMS (ESI): m/z calculated for C48H36FN3O2 [M]+: 705.2792, found [M+H]+: 706.2859.

Compound **C'3**

Synthesis :

C'3 *(S)/(R)* was obtained following the general procedure B with **6c** (100 mg, considered as 1 eq), *(S)/(R)*-1,1'-bi(2-naphthol) (57 mg, 0.2 mmol, 1 eq) and potassium carbonate (55 mg, 0.4 mmol, 2 eq) in 1 mL of DMF. Flash chromatography was performed (AE/Cy, 1/9) to give compound **C'3** as a yellow solid (85 mg, 55% yield over two steps).

^{1}H NMR (400 MHz, $CDCl_3$) δ 8.44 (d, J = 1.5 Hz, 1H), 8.32 (d, J = 1.4 Hz, 1H), 8.17 (d, J = 8.9 Hz, 1H), 8.05 (d, J = 8.3 Hz, 1H), 7.85 (dd, J = 8.4, 1.8 Hz, 2H), 7.82 – 7.75 (m, 3H), 7.70 (d, J = 8.8 Hz, 1H), 7.58 – 7.35 (m, 14H), 7.32 – 7.28 (m, 2H), 6.75 (d, J = 8.5 Hz, 1H), 6.59 (d, J = 8.9 Hz, 1H).

^{13}C NMR (101 MHz, CDCl3) δ 158.8, 156.1, 152.6, 152.6, 150.3, 150.3, 149.4, 148.9, 141.43, 141.38, 140.2, 140.0, 135.6, 135.2, 132.5, 132.2, 132.00, 131.99, 131.88, 131.8, 129.1, 128.9, 128.7, 128.60, 127.7, 127.59, 127.55, 127.4, 127.3, 127.0, 127.0, 126.8, 126.67, 126.65, 126.61, 126.5, 125.23, 125.19, 125.05, 125.00, 124.89, 124.87, 120.3, 120.1, 119.7, 119.2, 111.84, 111.81, 110.6, 110.2, 109.9, 109.59, 109.55, 100.9, 100.7.

^{19}F NMR (376 MHz, $CDCl_3$) δ -109.52.

HRMS (ESI): m/z calculated for C52H28FN3O2 [M]+: 745.2166, found [M+H]+: 746.2233.

Compound **C1**

Synthesis :

C1 *(S)/(R)* was obtained following the general procedure C with compound **C'1** (50 mg, 0.08 mmol, 1 eq), carbazole (14 mg, 0.08 mmol, 1 eq) and potassium carbonate (14 mg, 0.1 mmol, 1.2 eq) in 1 mL of DMF. Flash chromatography was performed (CH_2Cl_2/Cy, 4:6) to give compound **C1** as a yellow solid (56 mg, 99% yield).

^{1}H NMR (400 MHz, $CDCl_3$) δ 8.24 (d, J = 8.9 Hz, 1H), 8.09 (d, J = 8.3 Hz, 1H), 7.83 (dd, J = 8.3, 3.7 Hz, 2H), 7.78 (d, J = 7.7 Hz, 1H), 7.68 (dd, J = 11.5, 8.3 Hz, 2H), 7.62 – 7.44 (m, 7H), 7.39 (dd, J = 13.3, 6.2 Hz, 3H), 7.30 (d, J = 7.7 Hz, 1H), 7.13 (dt, J = 14.7, 7.7 Hz, 2H), 6.87 (t, J = 8.2 Hz, 2H), 6.83 – 6.74 (m, 1H), 6.64 – 6.48 (m, 2H), 6.42 (dd, J = 8.4, 5.4 Hz, 3H).

^{13}C NMR (101 MHz, $CDCl_3$) δ 152.7, 152.1, 149.4, 149.2, 139.8, 139.2, 138.19, 138.17, 136.7, 135.2, 132.6, 132.1, 132.0, 131.9, 131.6, 128.7, 128.6, 127.6, 127.5, 127.1, 126.8, 126.6, 126.5, 126.34, 126.30, 125.03, 124.99, 124.7, 124.5, 124.2, 124.0, 123.9, 121.7, 121.07, 121.06, 120.1, 120.7, 120.6, 120.23, 120.17, 119.9, 119.7, 113.2, 112.8, 112.32 110.8, 110.5, 110.1, 109.84, 109.77.

HRMS (ESI): m/z calculated for C52H28N4O2 [M]+: 740.2212, found [M+H]+: 741.2278.

Compound **C2**

Synthesis :

C2 *(S)/(R)* was obtained following the general procedure C with compound **C'2** (30 mg, 0.043 mmol, 1 eq), 3,6-ditertbutylcarbazole (12 mg, 0.043 mmol, 1 eq) and potassium carbonate (7 mg, 0.05 mmol, 1.2 eq) in 1mL of DMF. Flash chromatography was performed (CH_2Cl_2/Cy, 3:7) to give compound **C2** a yellow solid (33 mg, 79% yield).

^{1}H NMR (400 MHz, $CDCl_3$) δ 8.25 (d, J = 8.8 Hz, 1H), 8.11 (d, J = 8.3 Hz, 1H), 7.85 (dd, J = 11.1, 8.5 Hz, 2H), 7.74 – 7.30 (m, 13H), 7.21 (dd, J = 8.6, 1.9 Hz, 1H), 6.69 (d, J = 8.8 Hz, 2H), 6.25 (dd, J = 8.5,

1.9 Hz, 1H), 6.11 (dd, J = 8.6, 1.9 Hz, 1H), 6.03 (d, J = 8.5 Hz, 1H), 5.86 (d, J = 8.6 Hz, 1H), 1.48 (d, J = 3.3 Hz, 9H), 1.34 (d, J = 3.3 Hz, 9H), 1.26 – 1.20 (m, 10H), 1.19 (d, J = 3.4 Hz, 9H).

^{13}C NMR (101 MHz, $CDCl_3$) δ 152.3, 151.5, 149.62, 149.61, 144.6, 144.1, 143.7, 143.6, 138.1, 137.5, 136.3, 136.2, 136.2, 135.2, 132.6, 132.14, 132.09, 131.9, 131.8, 131.6, 128.7, 128.6, 127.5, 127.4, 127.2, 126.8, 126.5, 126.4, 125.15, 125.12, 125.08, 125.05, 124.2, 124.1, 123.9, 122.1, 121.9, 120.8, 120.5, 116.5, 116.0, 115.3, 115.0, 113.4, 112.8, 112.6, 110.2, 109.5, 109.5, 109.3, 109.3, 34.9, 34.8, 34.4, 34.4, 32.2, 32.0, 31.8, 31.8.

HRMS (ESI): m/z calculated for C68H60N4O2 [M]+: 964.4716, found [M+H]+: 965.4783.

Compound **C3**

Synthesis :

C3 *(S)/(R)* was obtained following the general procedure C with compound **C'3** (50 mg, 0.07 mmol, 1 eq), 3,6-diphenylcarbazole (22 mg, 0.07 mmol, 1 eq) and potassium carbonate (11 mg, 0.08 mmol, 1.2 eq) in 1 mL of DMF. Flash chromatography was performed (Toluene/Cy, 8:2) to give **C3** as a yellow solid (58 mg, 79% yield).

1H NMR (400 MHz, $CDCl_3$) δ 8.28 (d, J = 8.9 Hz, 1H), 8.12 (d, J = 8.4 Hz, 1H), 7.92 – 7.81 (m, 5H), 7.72 (dd, J = 18.3, 5.1 Hz, 3H), 7.67 – 7.27 (m, 25H), 7.25 – 7.22 (m, 3H), 6.98 (d, J = 8.5 Hz, 1H), 6.77 – 6.65 (m, 2H), 6.55 (dd, J = 8.6, 2.0 Hz, 2H), 6.45 (d, J = 8.5 Hz, 1H).

13C NMR (101 MHz, $CDCl_3$) δ 153.0, 152.4, 149.5, 149.3, 141.5, 141.4, 141.3, 141.3, 140.2, 139.8, 138.4, 138.3, 137.4, 135.7, 135.5, 134.97, 134.95, 134.8, 132.6, 132.2, 132.1, 131.94, 131.91, 131.8, 129.0, 128.9, 128.83, 128.76, 128.72, 128.6, 127.7, 127.55, 127.52, 127.3, 127.29, 127.28, 127.1, 127.0, 126.93, 126.89, 126.82, 126.77, 126.67, 126.55, 125.9, 125.5, 125.08, 125.04, 124.97, 124.8, 124.1, 124.0, 120.7, 120.2, 119.3, 118.9, 118.2, 117.9, 113.5, 112.9, 112.4, 111.3, 111.2, 110.8, 110.71, 110.67.

HRMS (ESI): m/z calculated for C76H44N4O2 [M]+: 1044.3464, found [M+H]+: 1045.3527.

Photophysical properties

The absorptive dissymmetry factor ($g_{abs}(\lambda)$) is defined as the ratio of molar circular dichroism ($\Delta\varepsilon(\lambda)$) to molar extinction coefficient ($\varepsilon(\lambda)$): [S12]

$$g_{abs}(\lambda) = \frac{\Delta\varepsilon(\lambda)}{\varepsilon(\lambda)}$$

The degree of dissmetry of CPL ($g_{lum}(\lambda)$) is quantified by the relative intensity difference of left and right circularly polarized emission: [S12]

$$g_{lum}(\lambda) = 2 \times \frac{\Delta I(\lambda)}{I(\lambda)}$$

UV-Vis spectra: :

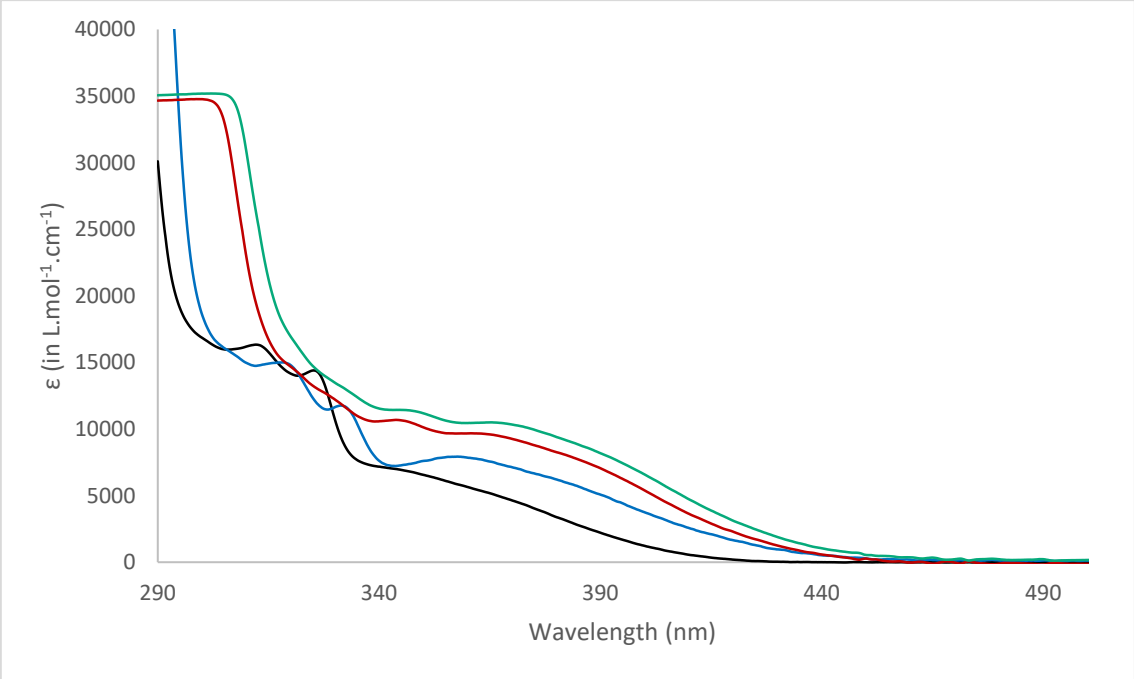

Figure S1: UV-vis spectra of **B1** (black), **B2** (blue), **B3** (red) and **B4** (green) in toluene solution at 298 K.

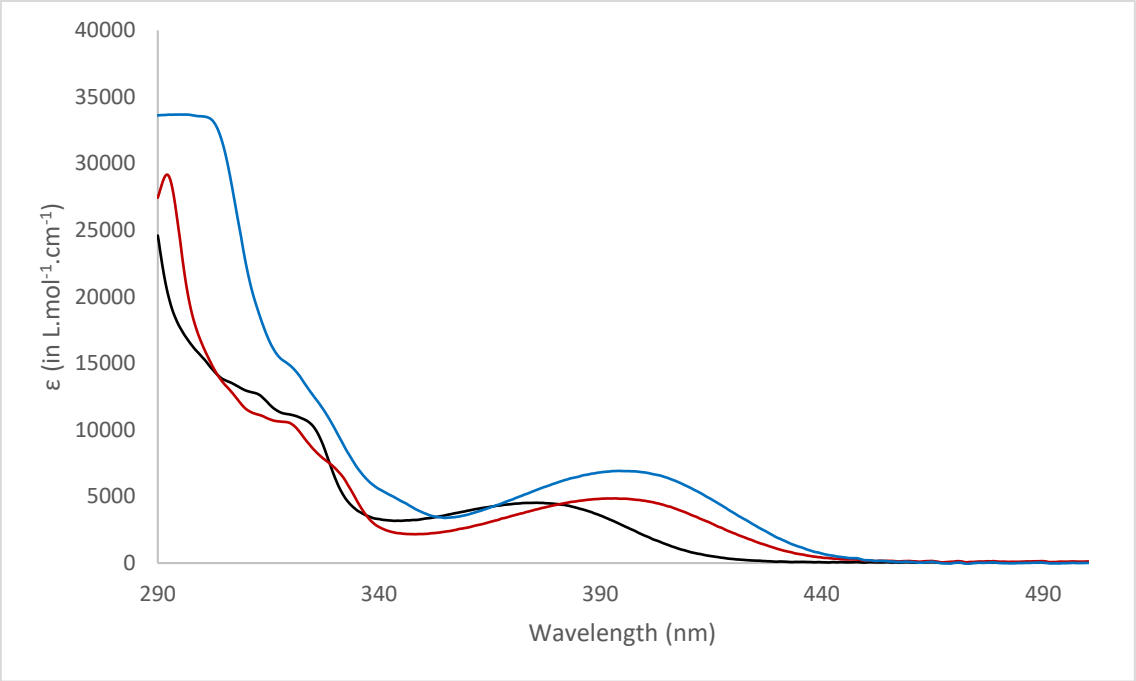

Figure S2: UV-vis spectra of **C'1** (black), **C'2** (red) and **C'3** (blue) in toluene solution at 298 K.

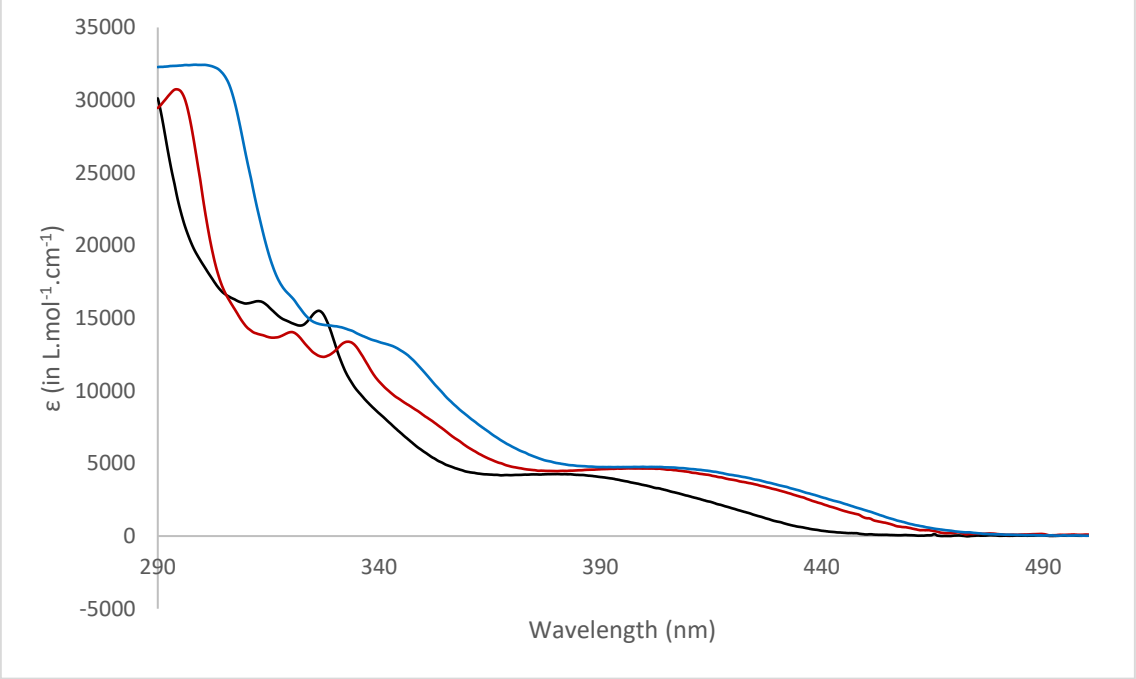

Figure S3: UV-vis spectra of **C1** (black), **C2** (red) and **C3** (blue) in toluene solution at 298 K.

Fluorescence

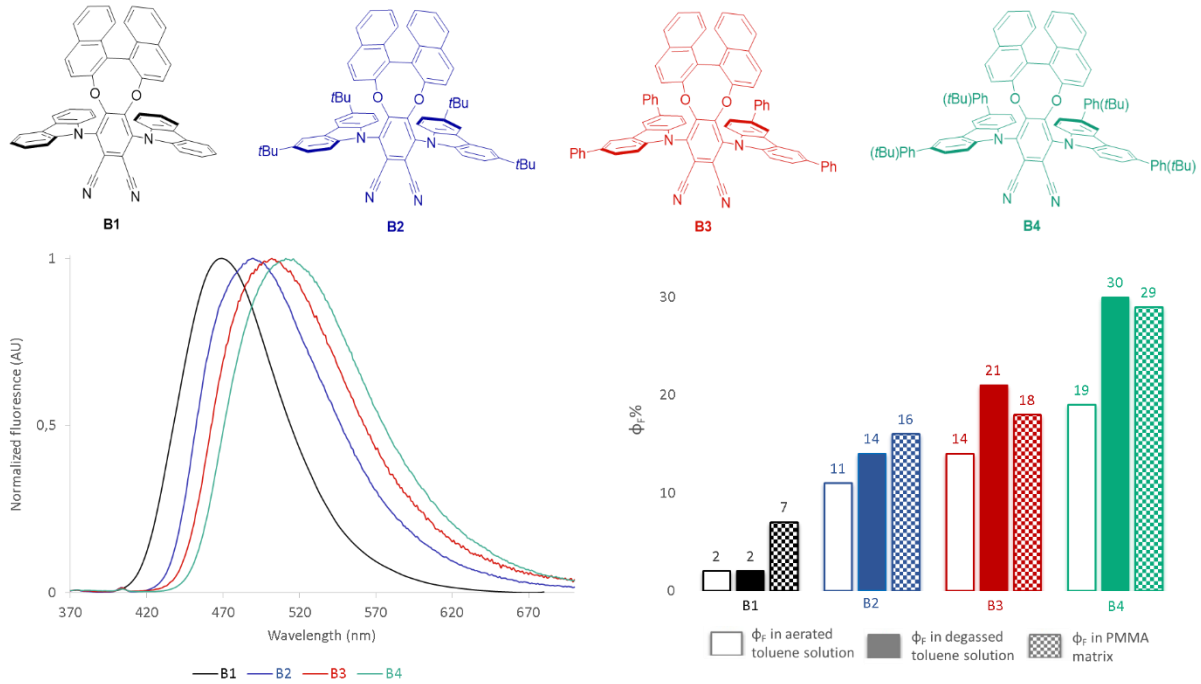

Figure S4: Molecular structure, normalized fluorescence spectra (10 µmol in toluene solution at 298 K) and quantum yield for **B1** (black), **B2** (blue), **B3** (red) and **B4** (green).

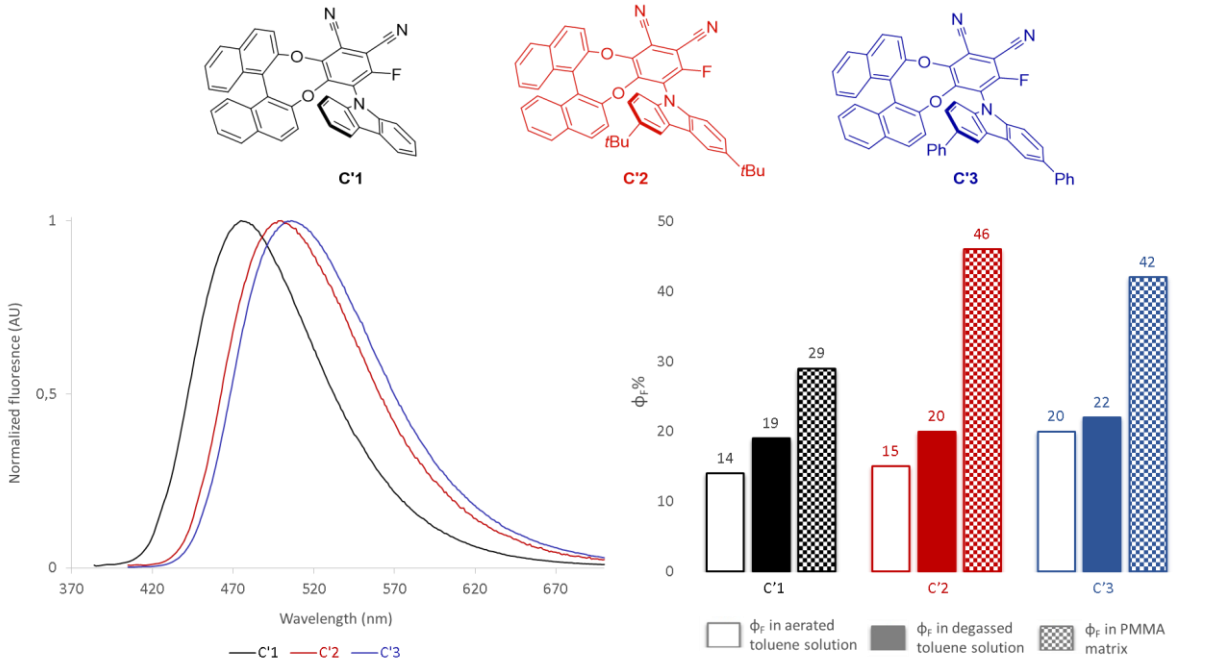

Figure S5: Molecular structure, normalized fluorescence spectra (10 µmol in toluene solution at 298 K) and quantum yield for **C'1** (black), **C'2** (red) and **C'3** (blue).

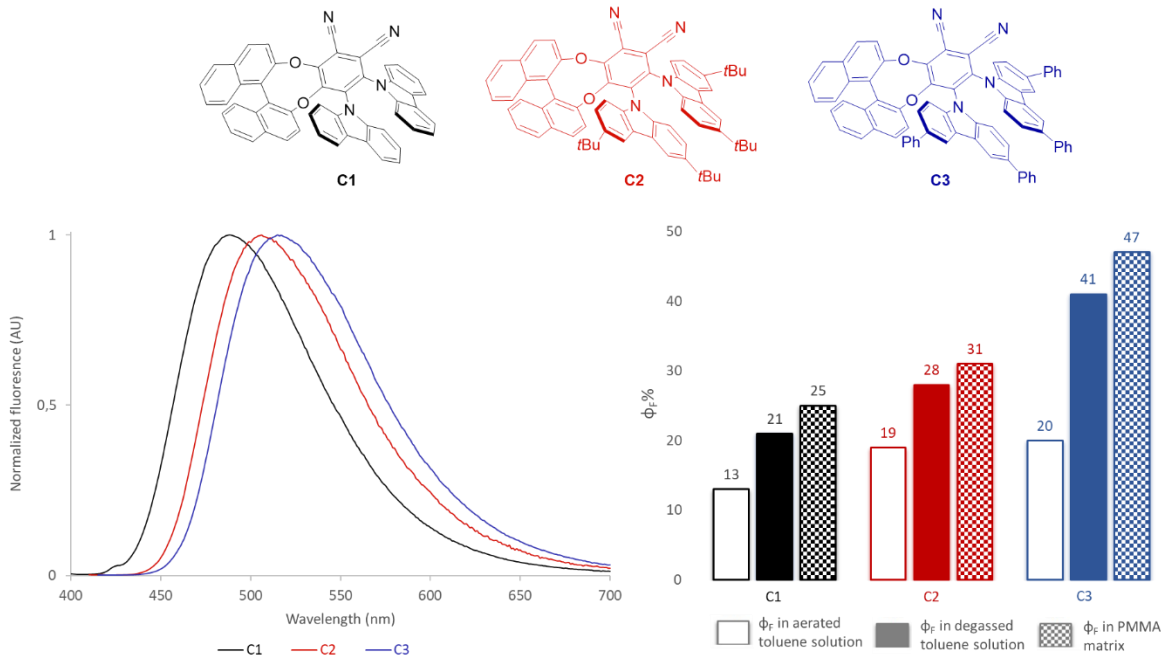

Figure S6: Molecular structure, normalized fluorescence spectra (10 µmol in toluene solution at 298 K) and quantum yield for **C1** (black), **C2** (red) and **C3** (blue).

Every following fluorescence spectra were measured in degazed toluene solution, concentration of each compound is 10^{-5} mol/L, in 1cm*1cm cell or in thin PMMA film.

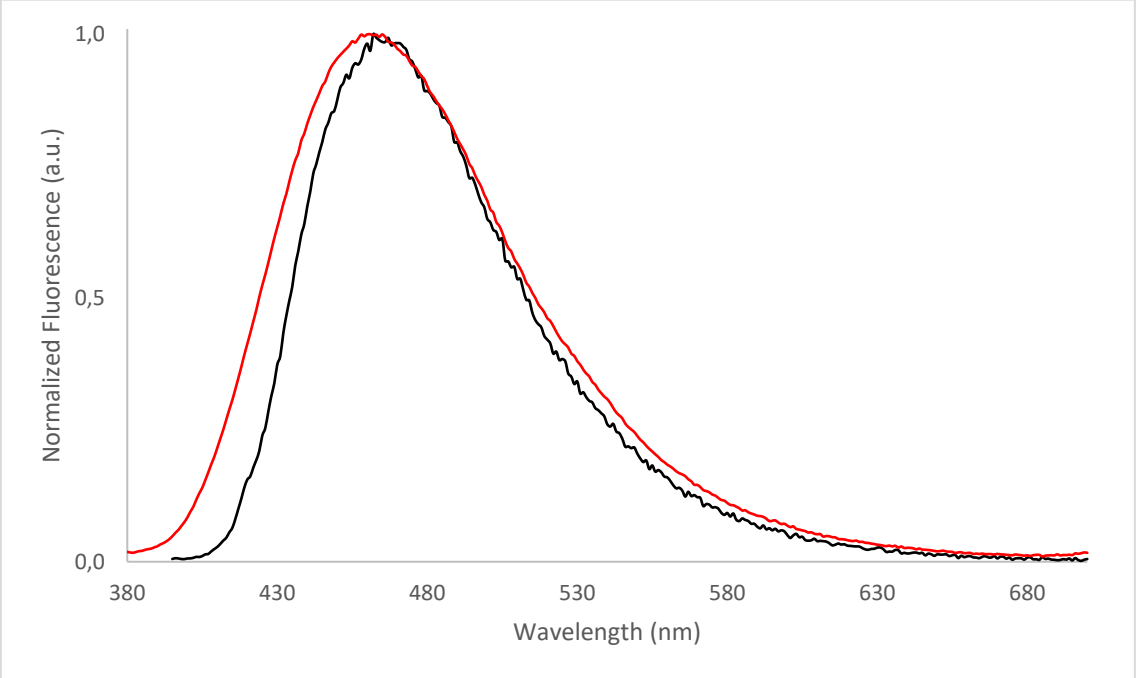

Figure S7: Normalized emission spectra of **B1** in toluene solution excited at 365 nm (black) and in PMMA film excited at 370 nm (red) at 298 K.

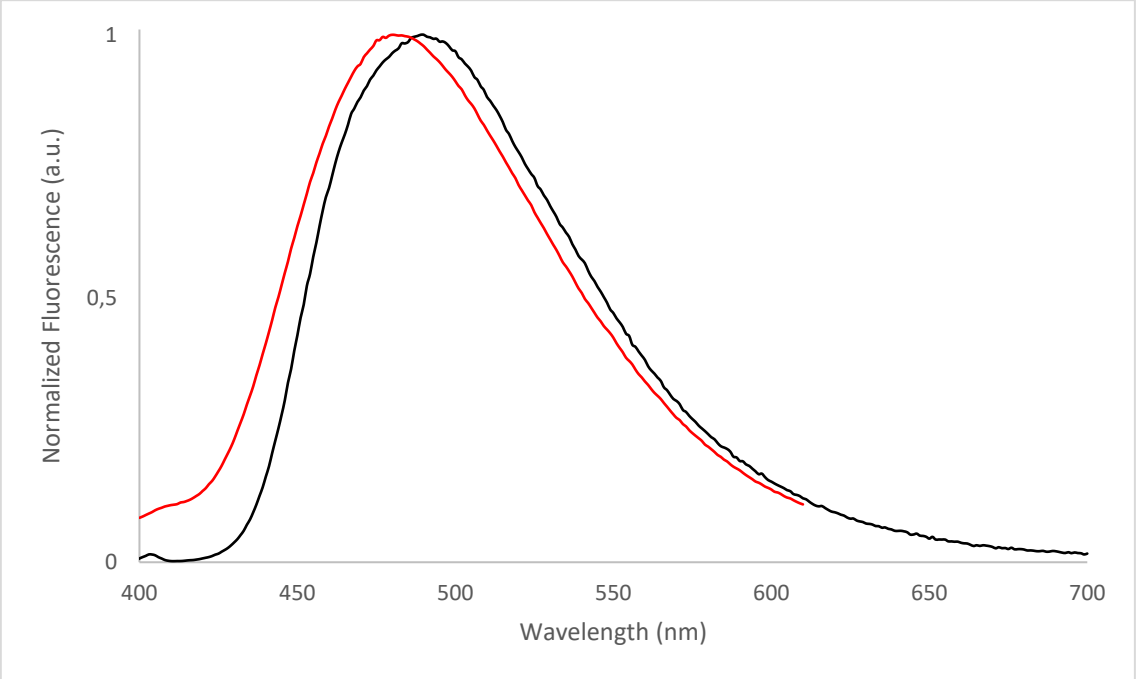

Figure S8: Normalized emission spectra of **B2** in toluene solution excited at 370 nm (black) and in PMMA film excited at 390 nm (red) at 298 K.

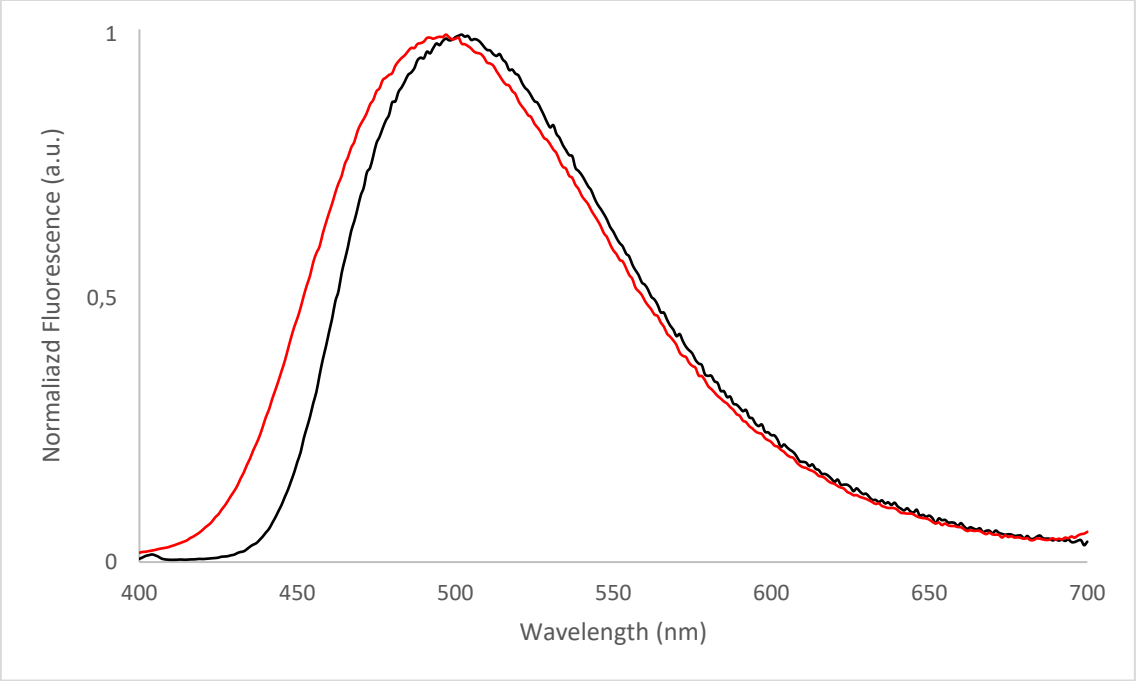

Figure S9: Normalized emission spectra of **B3** in toluene solution excited at 360 nm (black) and in PMMA film excited at 370 nm (red) at 298 K.

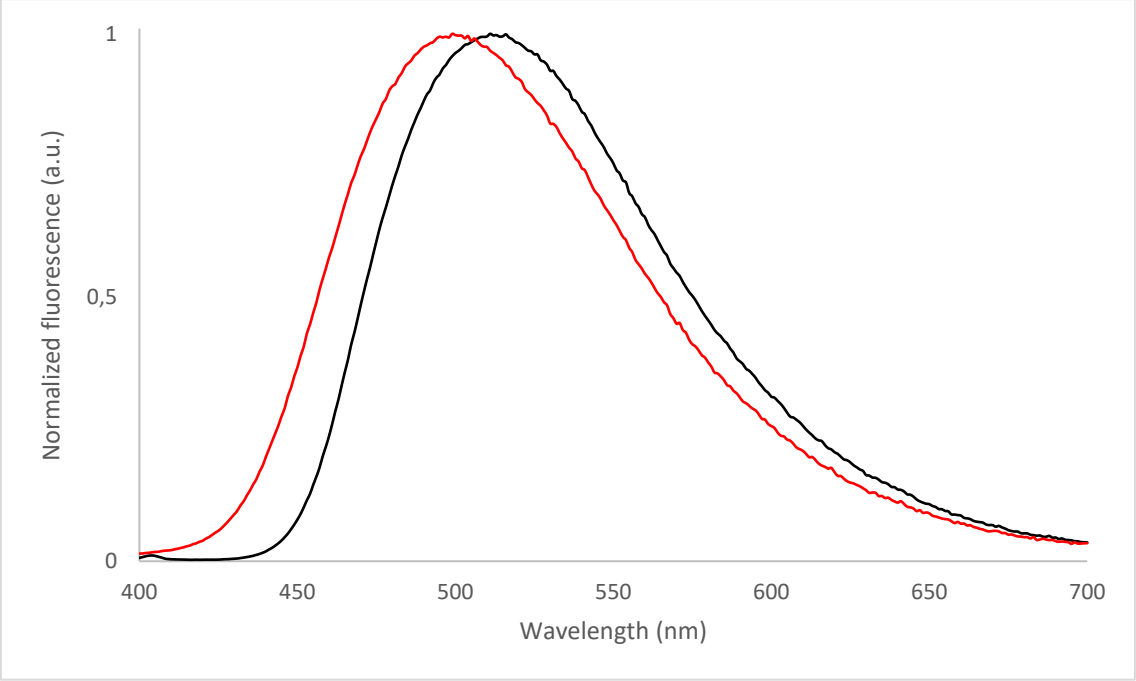

Figure S10: Normalized emission spectra of **B4** in toluene solution excited at 360 nm (black) and in PMMA film excited at 370 nm (red) at 298 K.

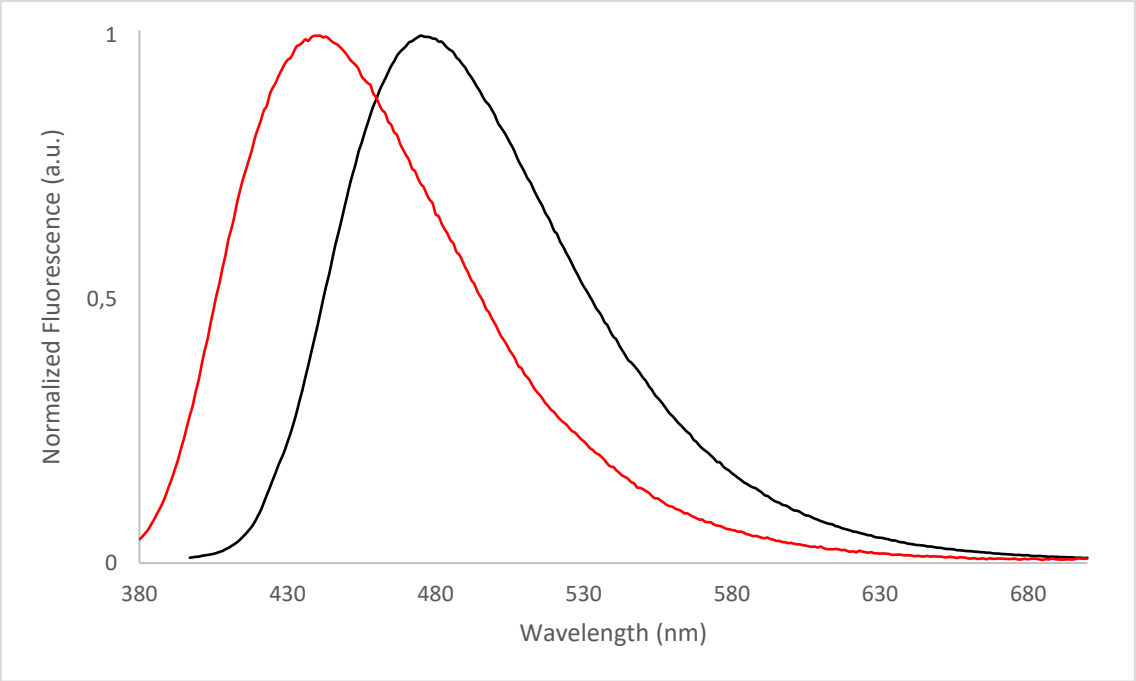

Figure S11: Normalized emission spectra of **C'1** in toluene solution excited at 370 nm (black) and in PMMA film excited at 370 nm (red) at 298 K.

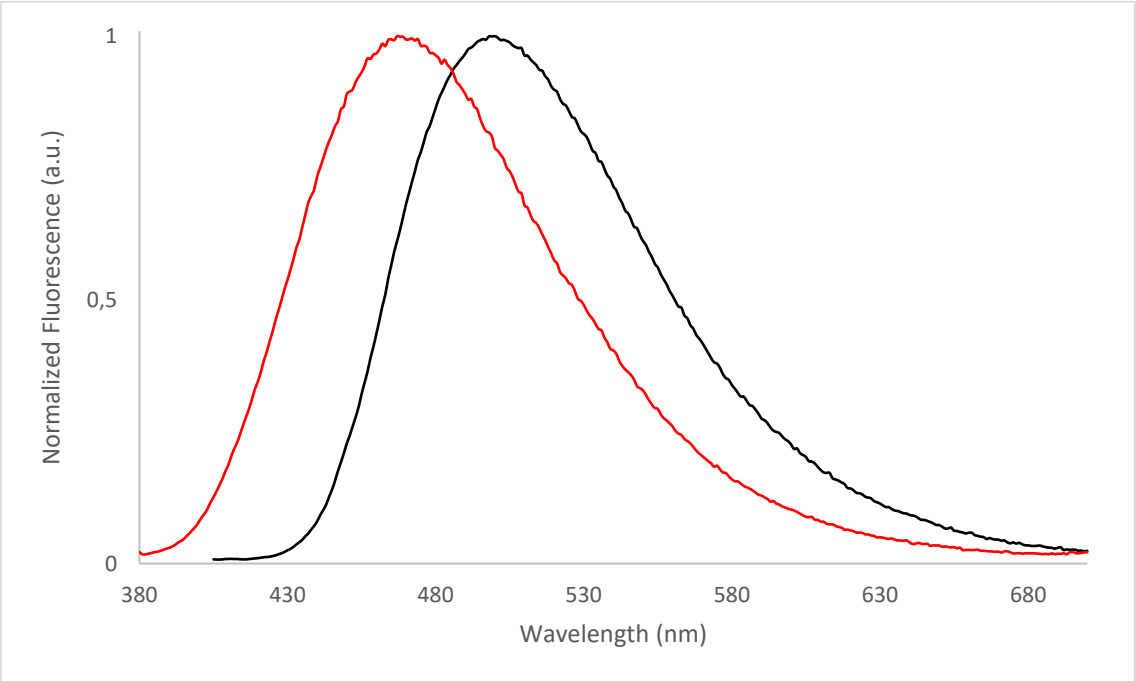

Figure S12: Normalized emission spectra of **C'2** in toluene solution excited at 395 nm (black) and in PMMA film excited at 370 nm (red) at 298 K.

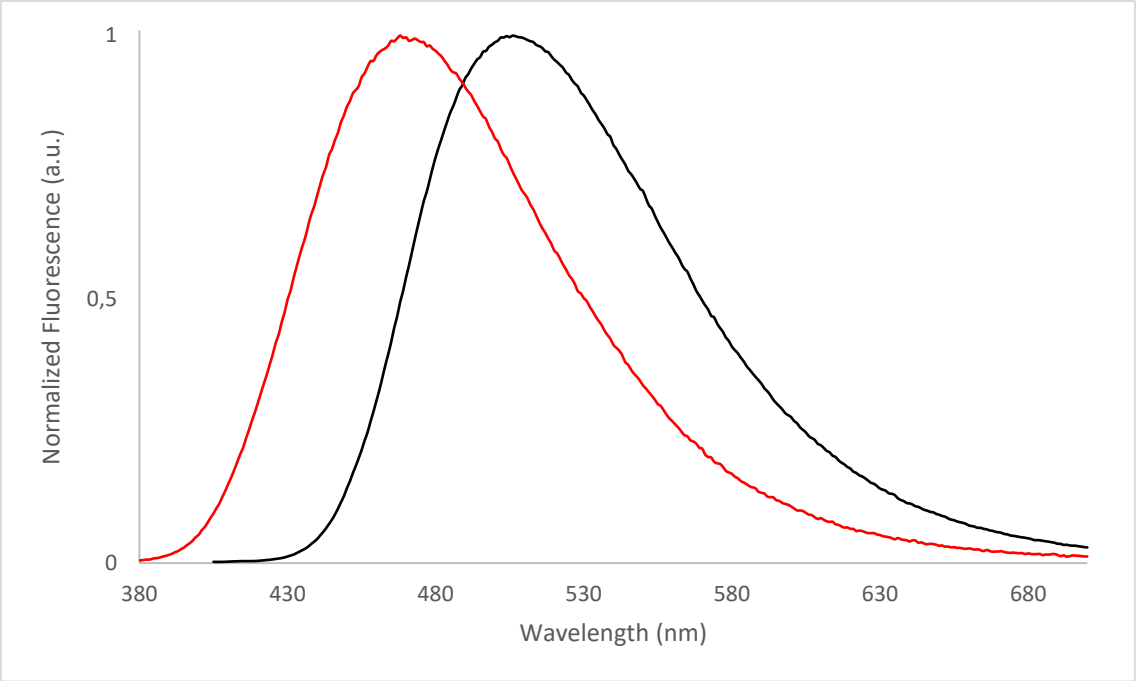

Figure S13: Normalized emission spectra of **C'3** in toluene solution excited at 395 nm (black) and in PMMA film excited at 370 nm (red) at 298 K.

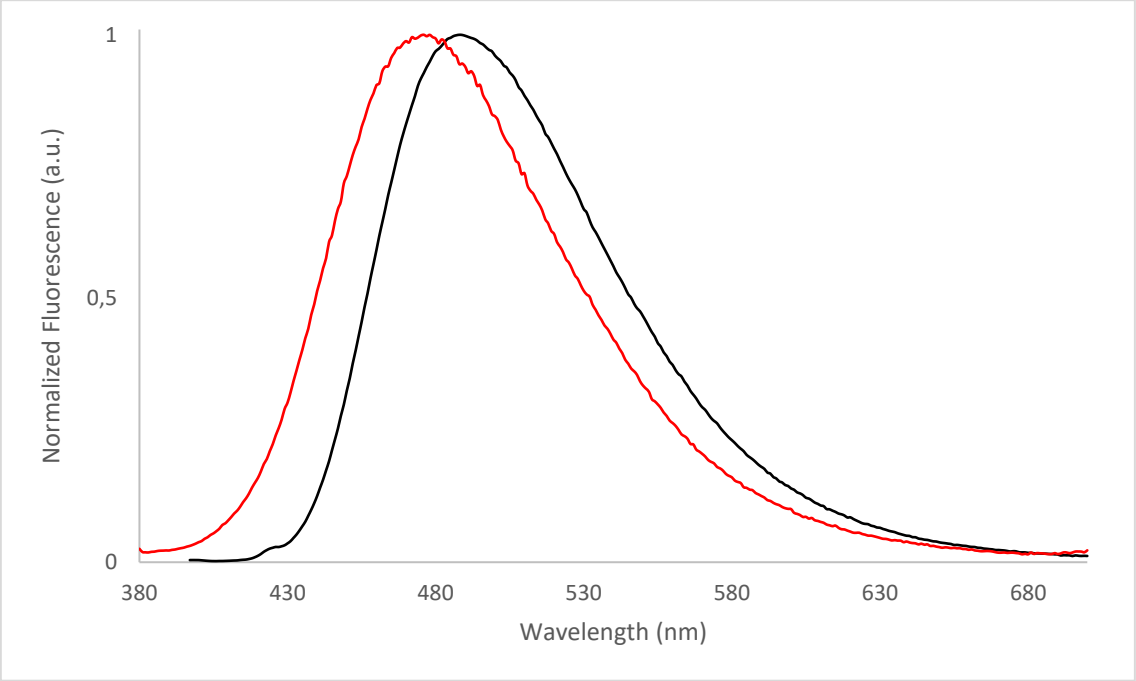

Figure S14: Normalized emission spectra of **C1** in toluene solution excited at 370 nm (black) and in PMMA film excited at 370 nm (red) at 298 K.

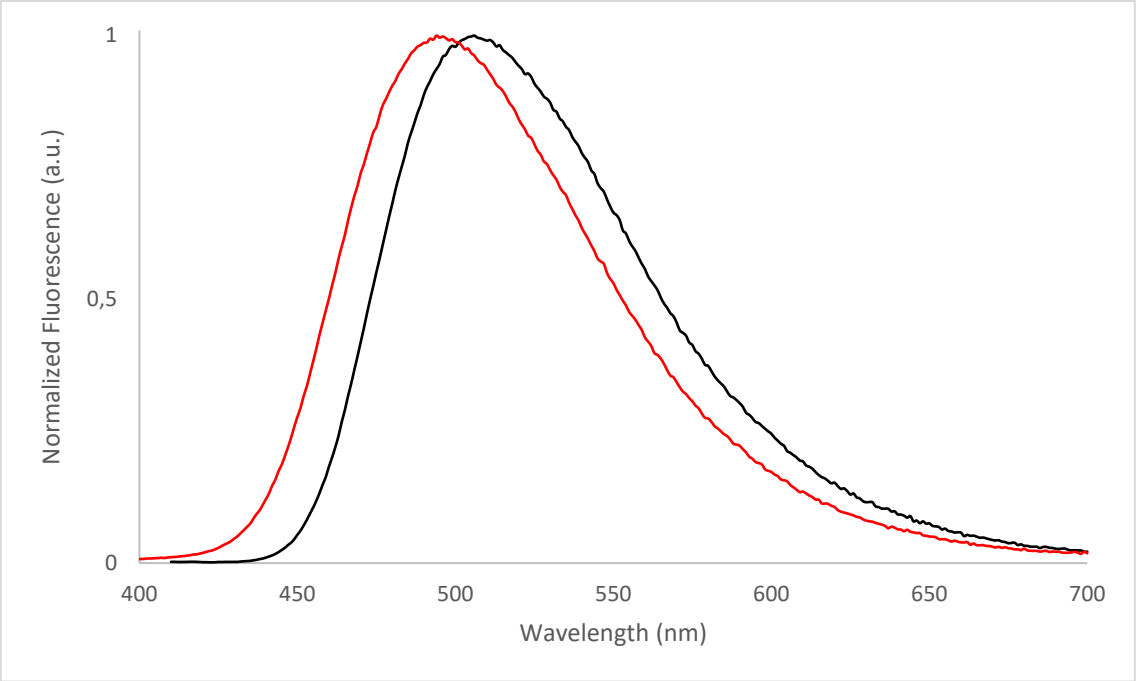

Figure S15: Normalized emission spectra of **C2** in toluene solution excited at 400 nm (black) and in PMMA film excited at 370 nm (red) at 298 K.

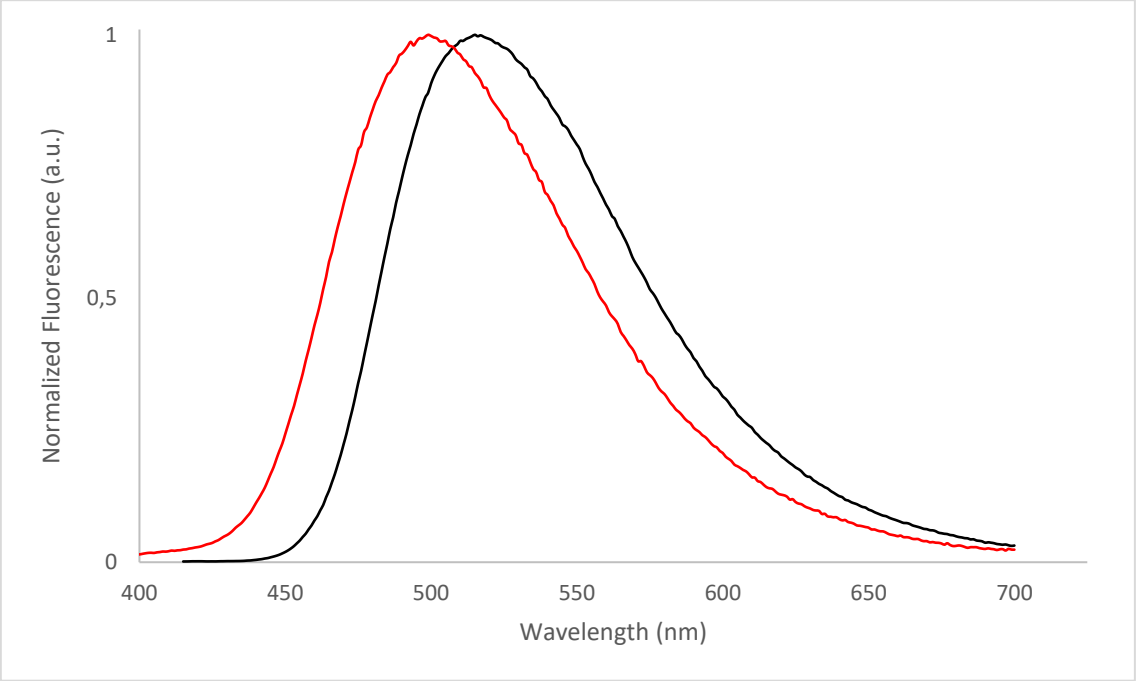

Figure S16: Normalized emission spectra of **C3** in toluene solution excited at 405 nm (black) and in PMMA film excited at 370 nm (red) at 298 K.

Luminescence at 77K

Every following spectra were measured in 2-methyltetrahydrofuran at 77K

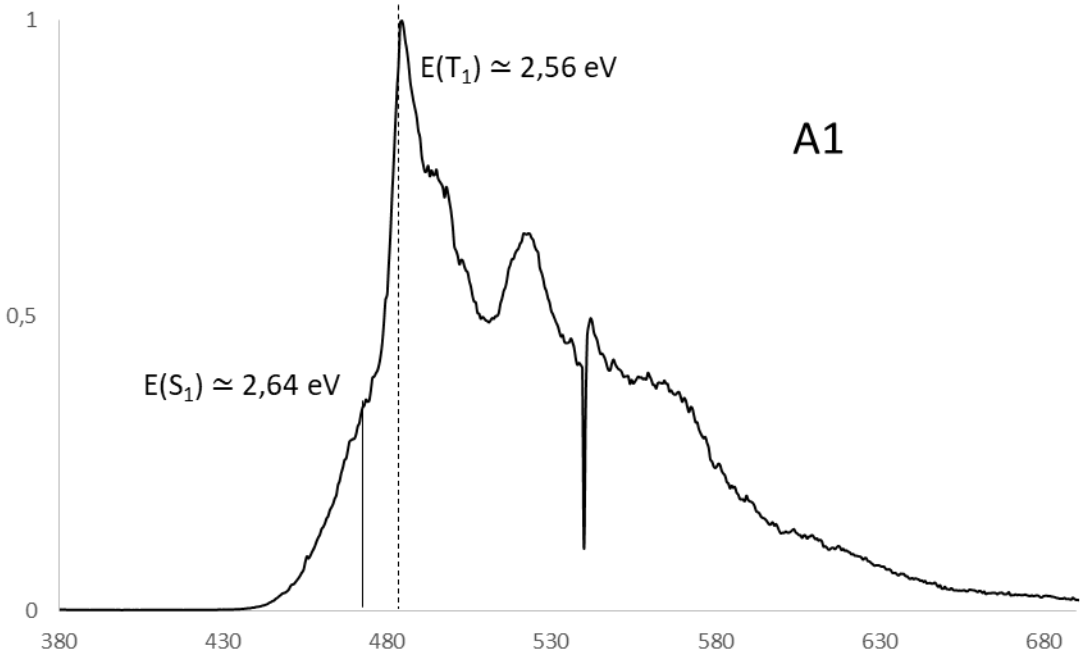

Figure S17: Normalized luminescence spectrum of **A1** in 2-methyltetrahydrofuran at 77 K excited at 370 nm. Black solid and dashed lines represent supporting lines to estimate S_1 and T_1 energy ($E(S_1)$=2.64 eV; $E(T_1)$=2.56 eV).

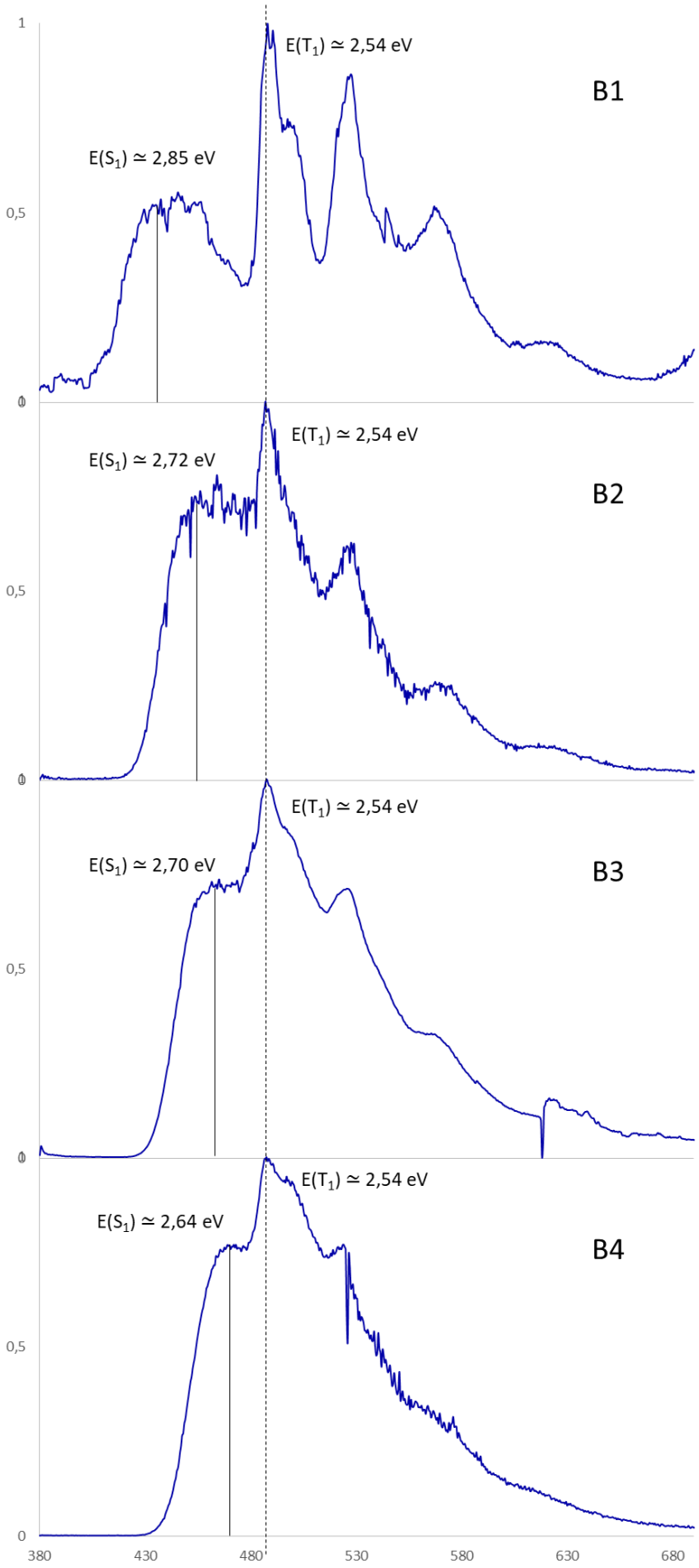

Figure S18: Normalized luminescence spectrum of B serie in 2-methyltetrahydrofuran at 77 K excited at 370 nm. Black solid dashed lines represent supporting lines to estimate S_1 and T_1 energy.

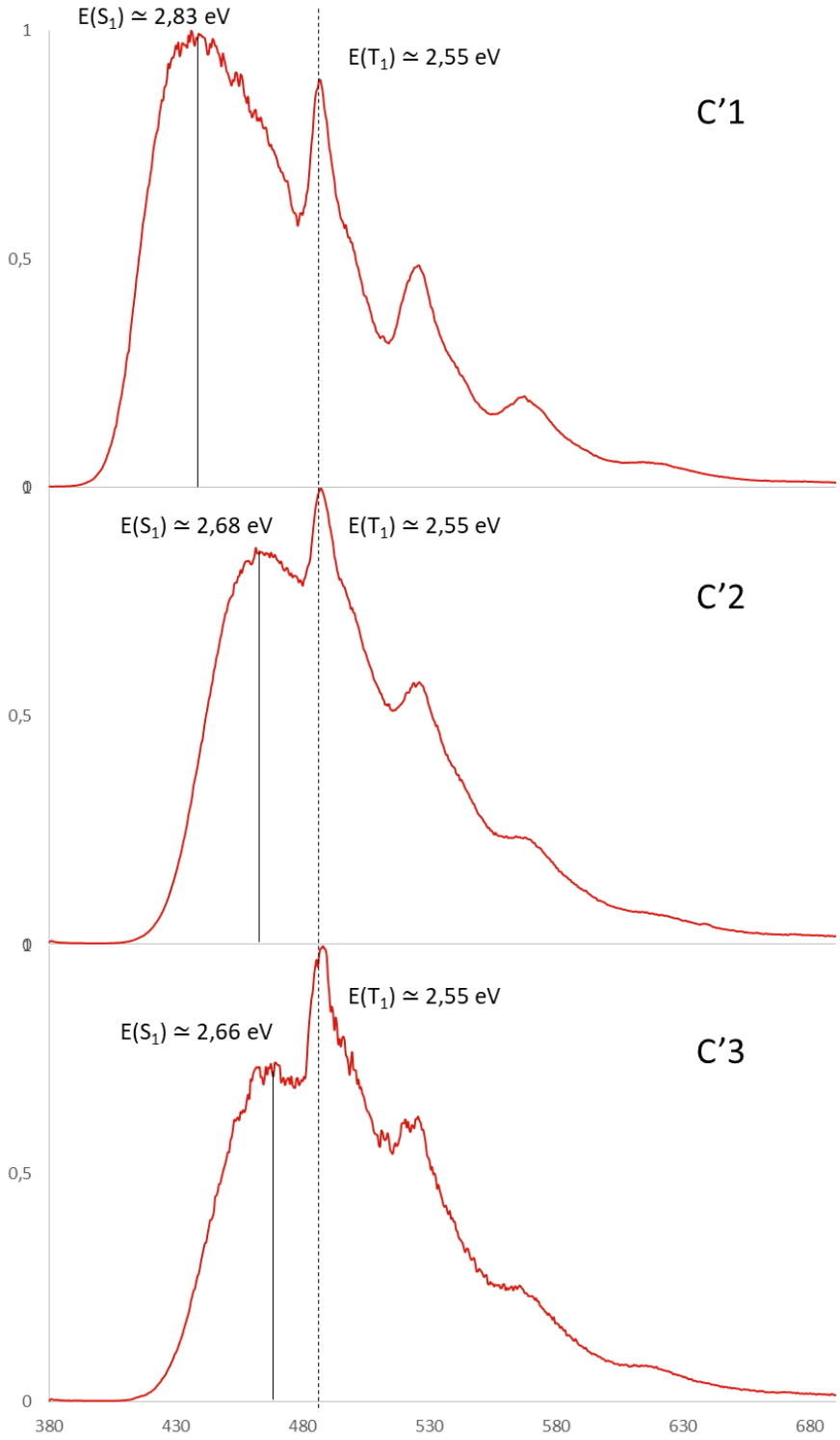

Figure S19: Normalized luminescence spectrum of C' serie in 2-methyltetrahydrofuran at 77 K excited at 370 nm. Black solid and dashed lines represent supporting lines to estimate S_1 and T_1 energy.

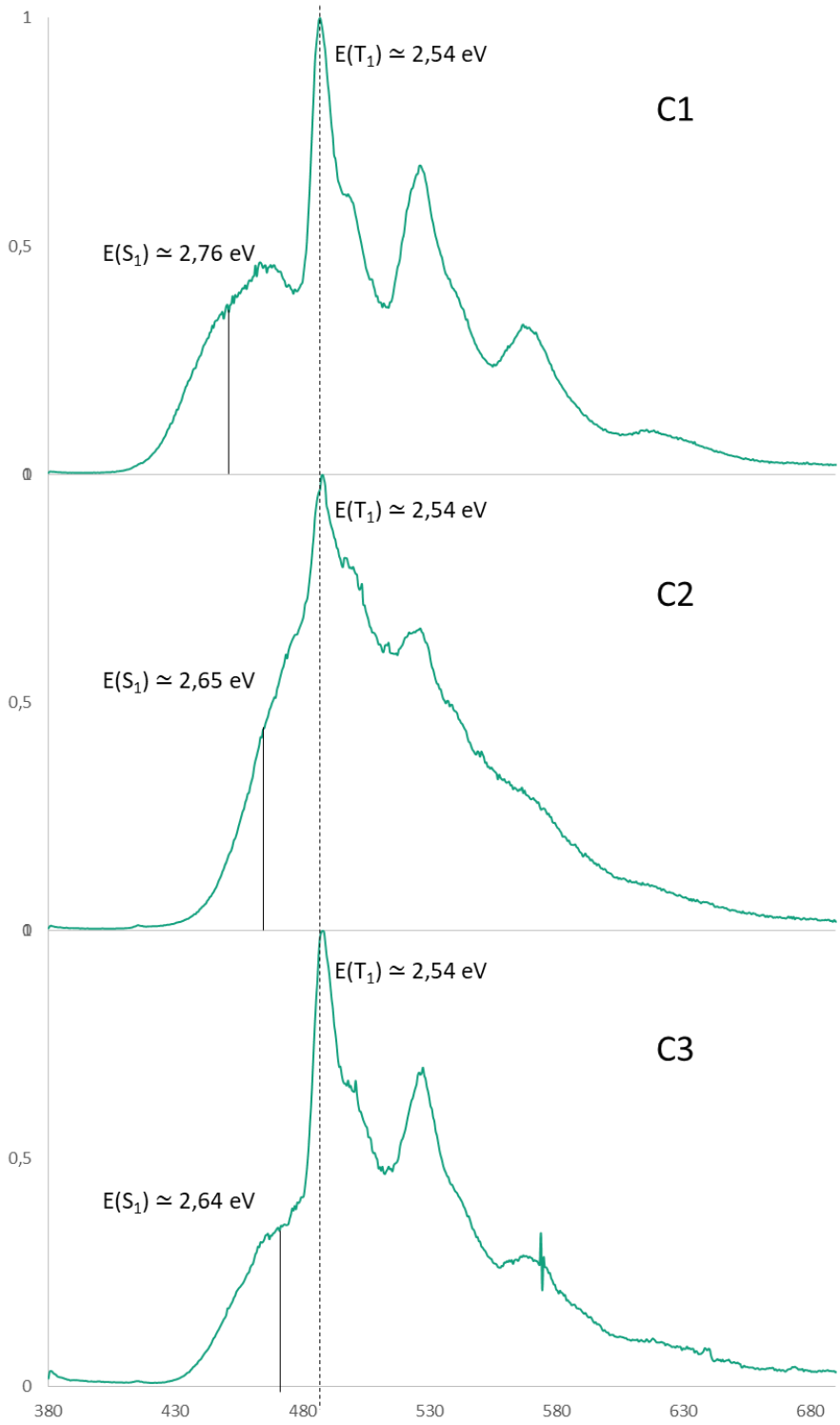

Figure S20: Normalized luminescence spectrum of C serie in 2-methyltetrahydrofuran at 77 K excited at 370 nm. Black solid and dashed lines represent supporting lines to estimate S_1 and T_1 energy.

Summary table :

Compound	$E(S_1)$ (eV)	$E(T_1)$ (eV)	ΔE_{ST} (eV)
B1	2,85	2,54	0,31
B2	2,72	2,54	0,18
B3	2,70	2,54	0,16
B4	2,64	2,54	0,10
C'1	2,83	2,55	0,28
C'2	2,68	2,55	0,13
C'3	2,66	2,55	0,11
C1	2,76	2,54	0,22
C2	2,65	2,54	0,11
C3	2,64	2,54	0,1
A1	2,64	2,56	0,08

Table S2: Experimental evaluation of $E(S_1)$, $E(T_1)$ and ΔE_{ST} for every compounds

CD and g_{abs}:

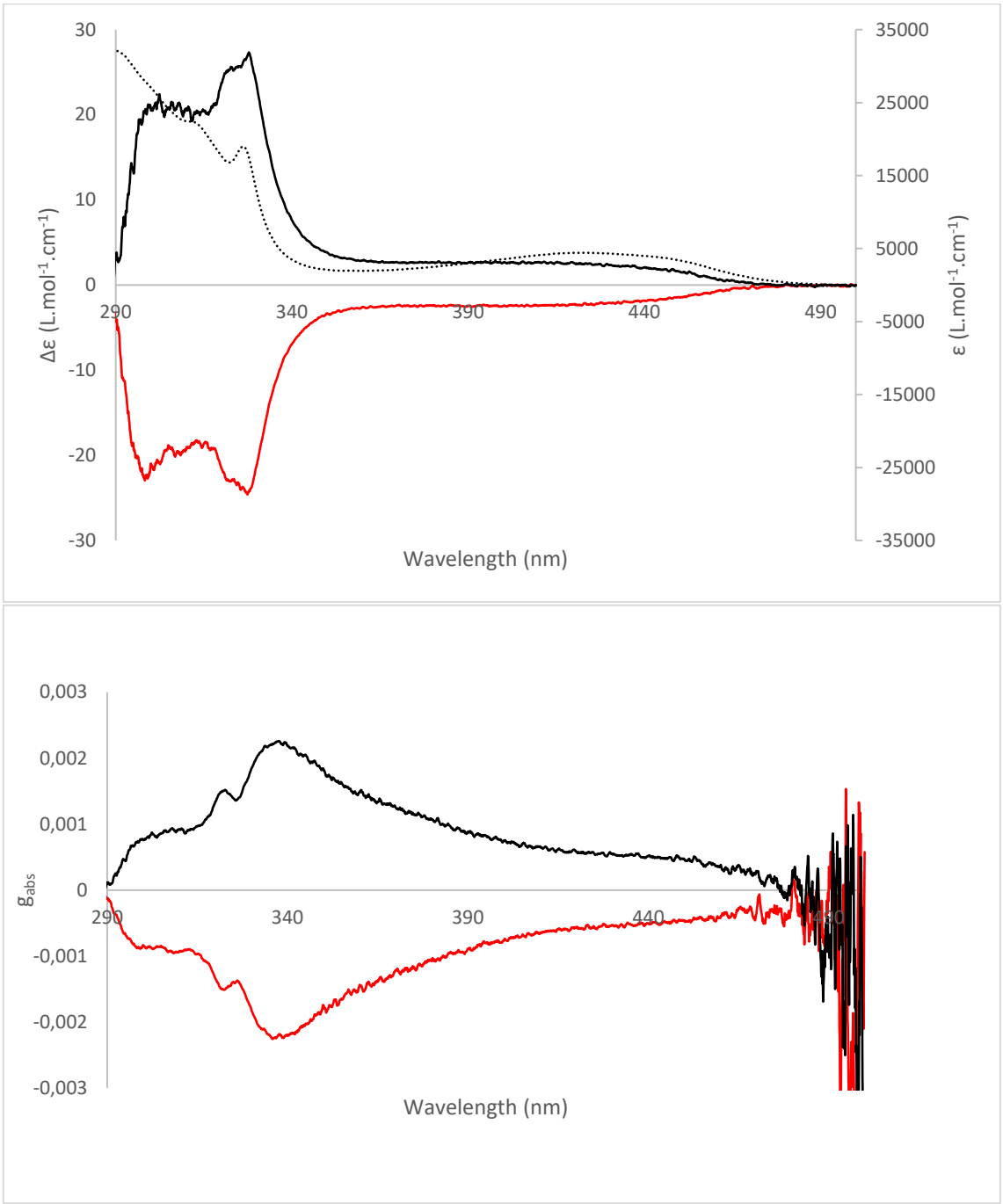

Figure S21: Top: ECD spectra of **A1** (*S* enantiomer in red, *R* enantiomer in black) and UV-vis spectrum of **A1** (dashed lines) at 298 K in toluene solution. Bottom: absorption dissymetry factor g_{abs} spectra of **A1** (*S* enantiomer in red, *R* enantiomer in black) at 298 K in toluene solution.

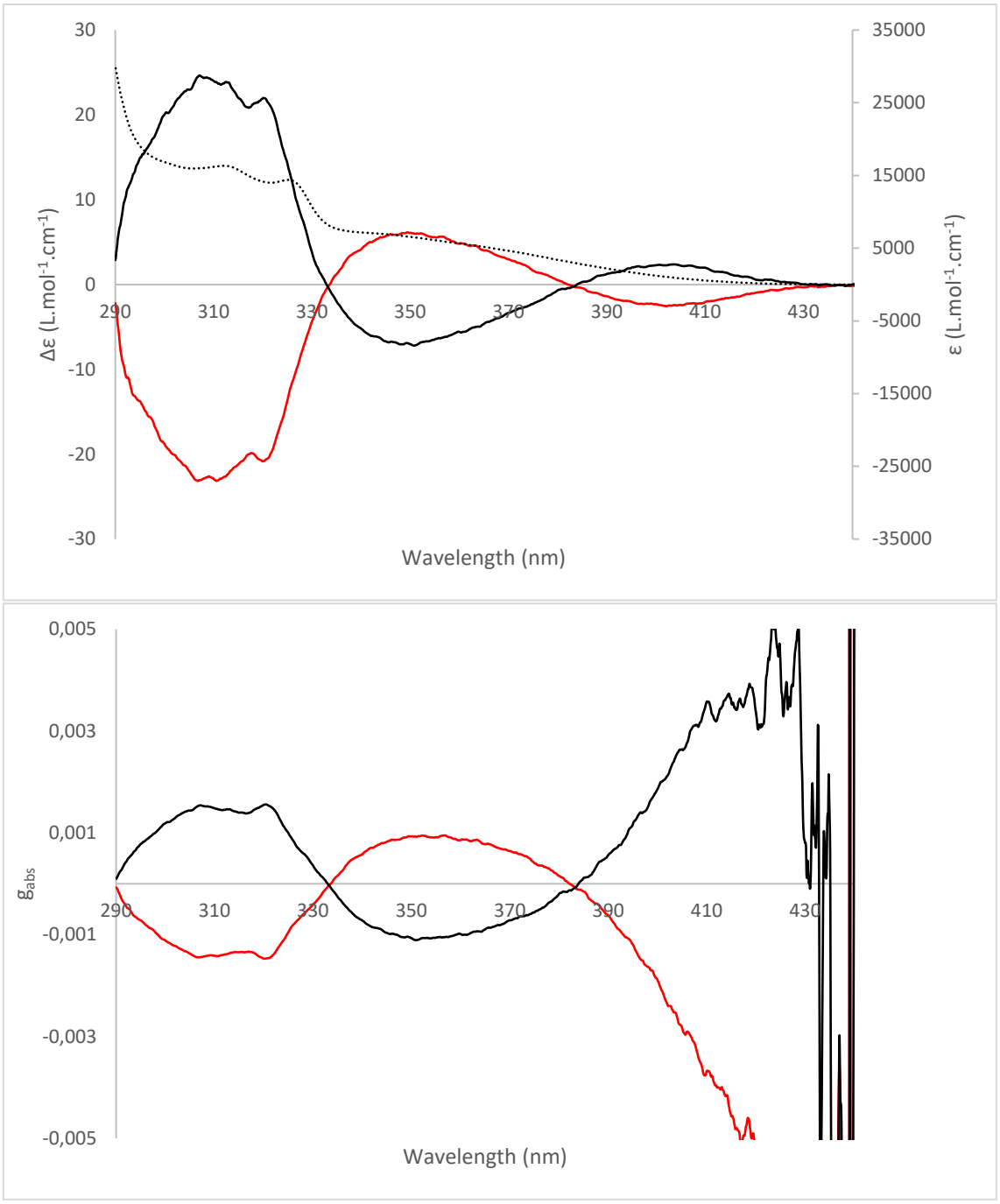

Figure S22: Top: ECD spectra of **B1** (*S* enantiomer in red, *R* enantiomer in black) and UV-vis spectrum of **B1** (dashed lines) at 298 K in toluene solution. Bottom: absorption dissymetry factor g_{abs} spectra of **B1** (*S* enantiomer in red, *R* enantiomer in black) at 298 K in toluene solution.

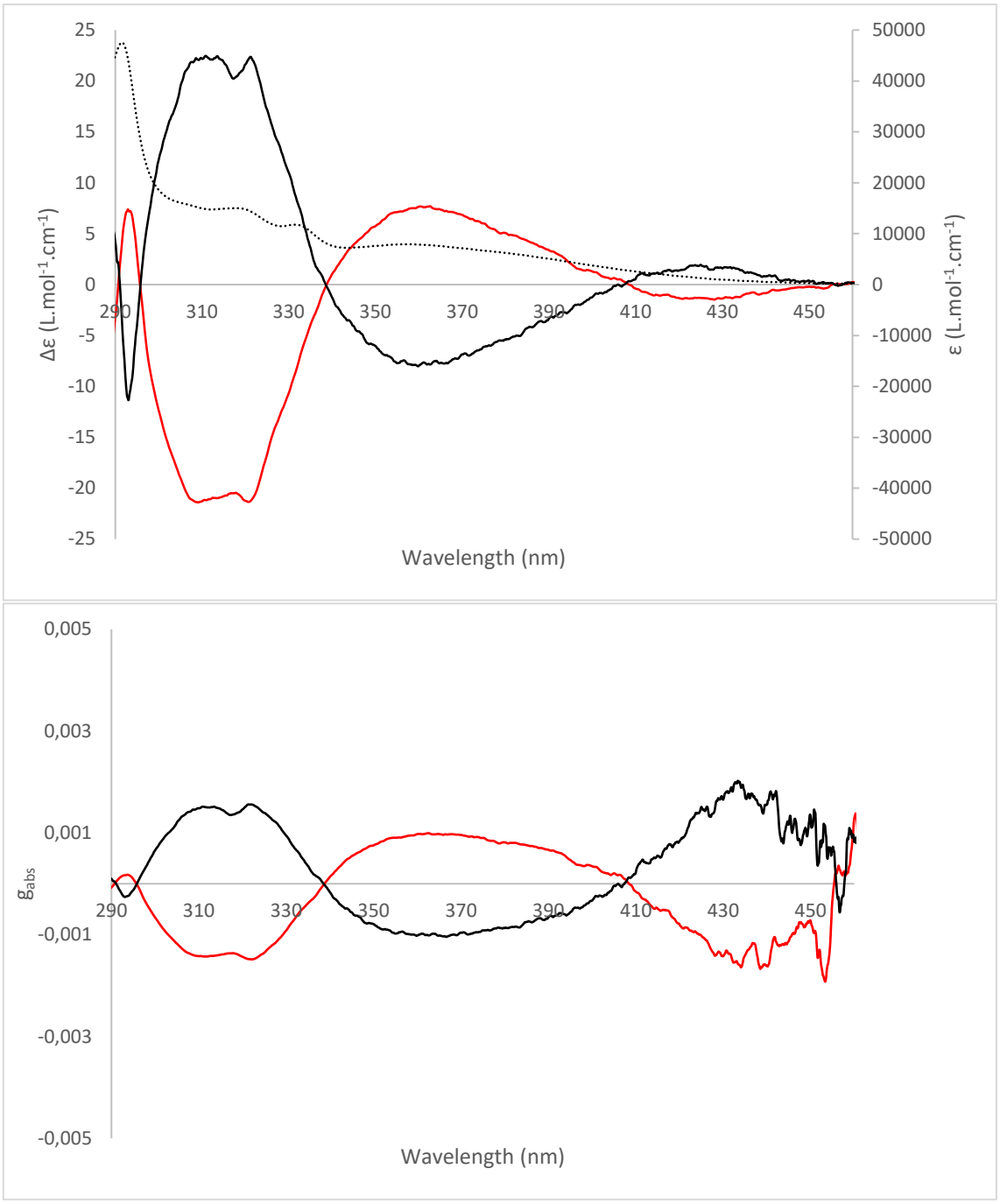

Figure S23: Top: ECD spectra of **B2** (*S* enantiomer in red, *R* enantiomer in black) and UV-vis spectrum of **B2** (dashed lines) at 298 K in toluene solution. Bottom: absorption dissymetry factor g_{abs} spectra of **B2** (*S* enantiomer in red, *R* enantiomer in black) at 298 K in toluene solution.

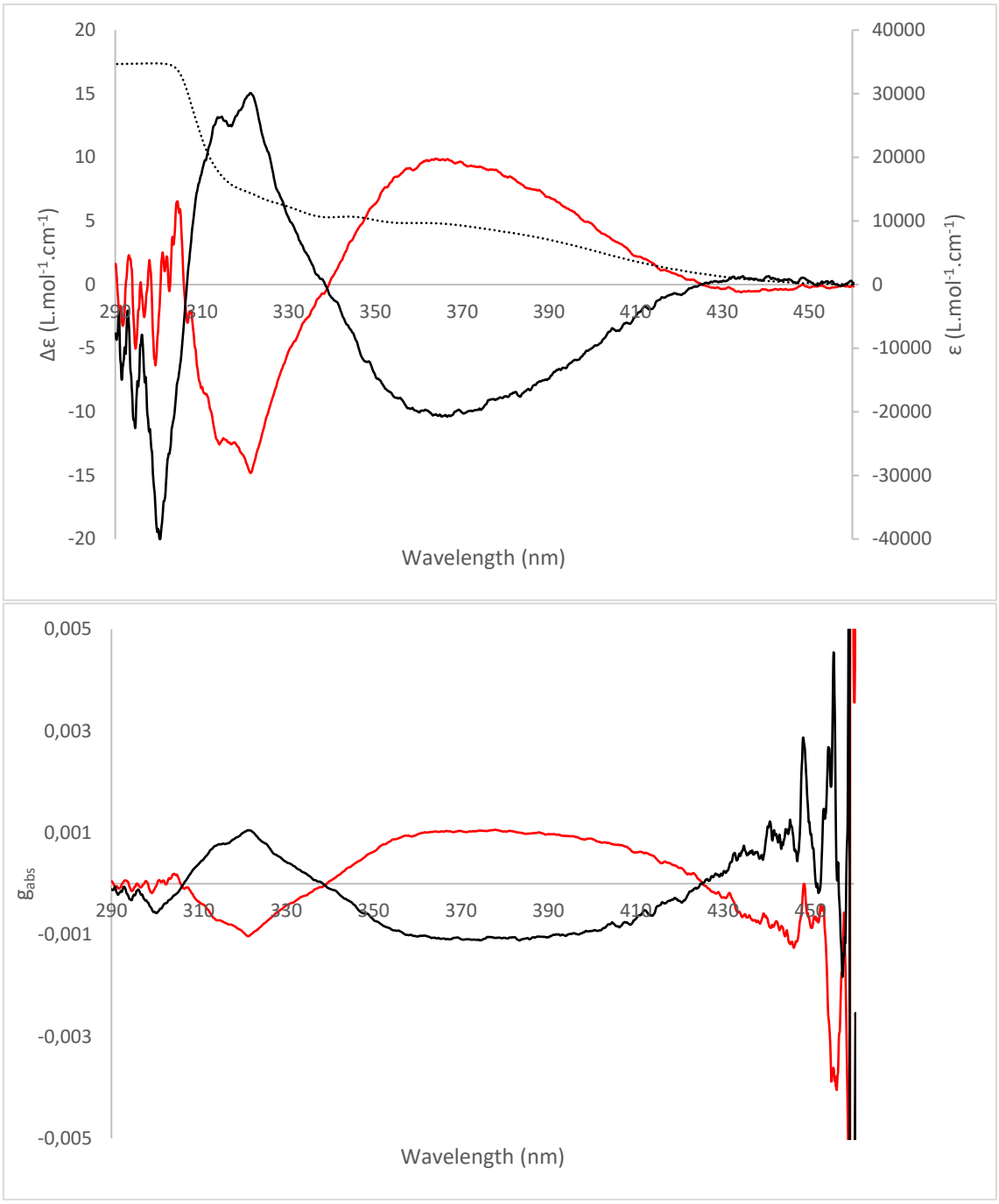

Figure S24: Top: ECD spectra of **B3** (*S* enantiomer in red, *R* enantiomer in black) and UV-vis spectrum of **B3** (dashed lines) at 298 K in toluene solution. Bottom: absorption dissymetry factor g_{abs} spectra of **B3** (*S* enantiomer in red, *R* enantiomer in black) at 298 K in toluene solution.

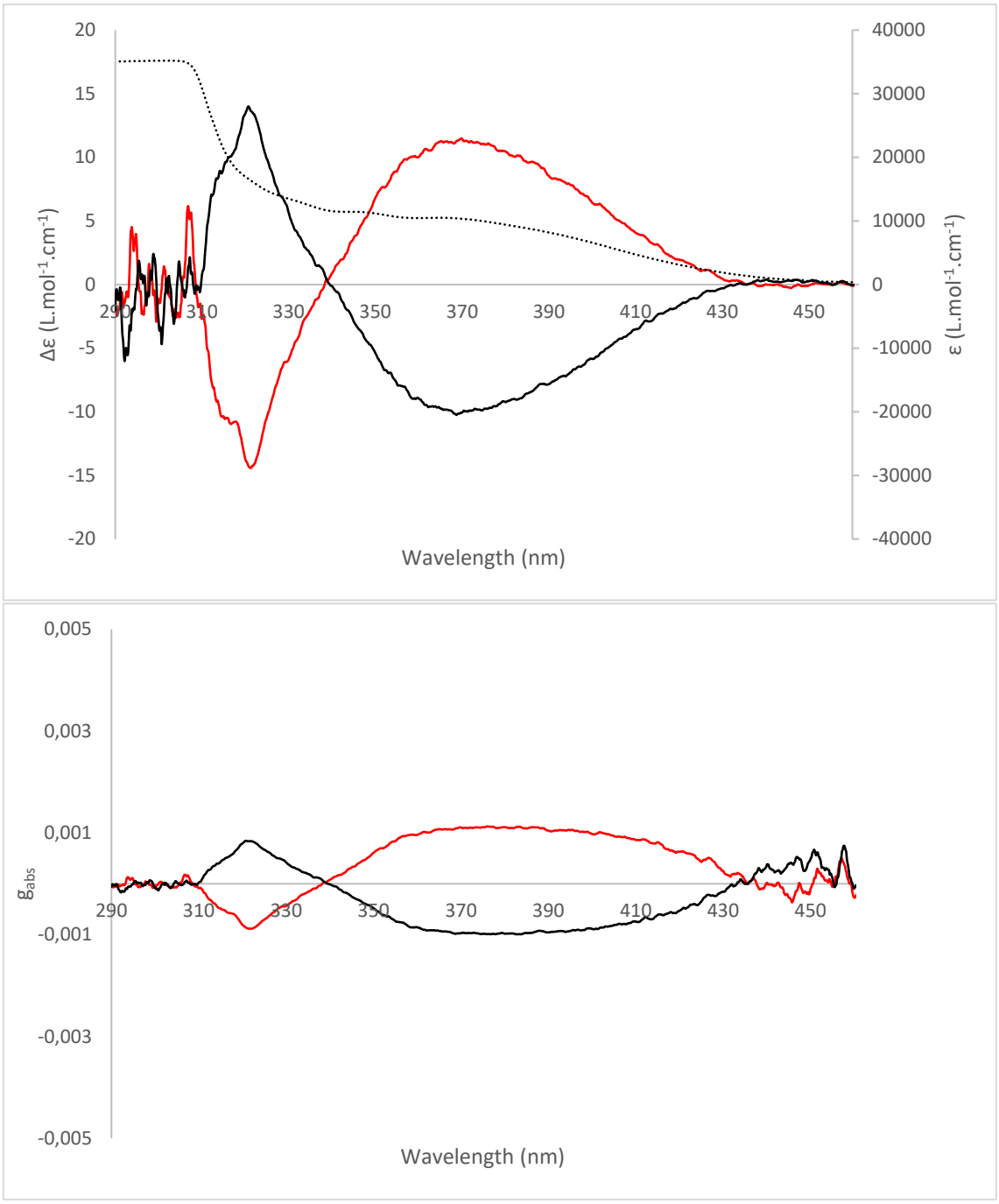

Figure S25: Top: ECD spectra of **B4** (*S* enantiomer in red, *R* enantiomer in black) and UV-vis spectrum of **B4** (dashed lines) at 298 K in toluene solution. Bottom: absorption dissymetry factor g_{abs} spectra of **B4** (*S* enantiomer in red, *R* enantiomer in black) at 298 K in toluene solution.

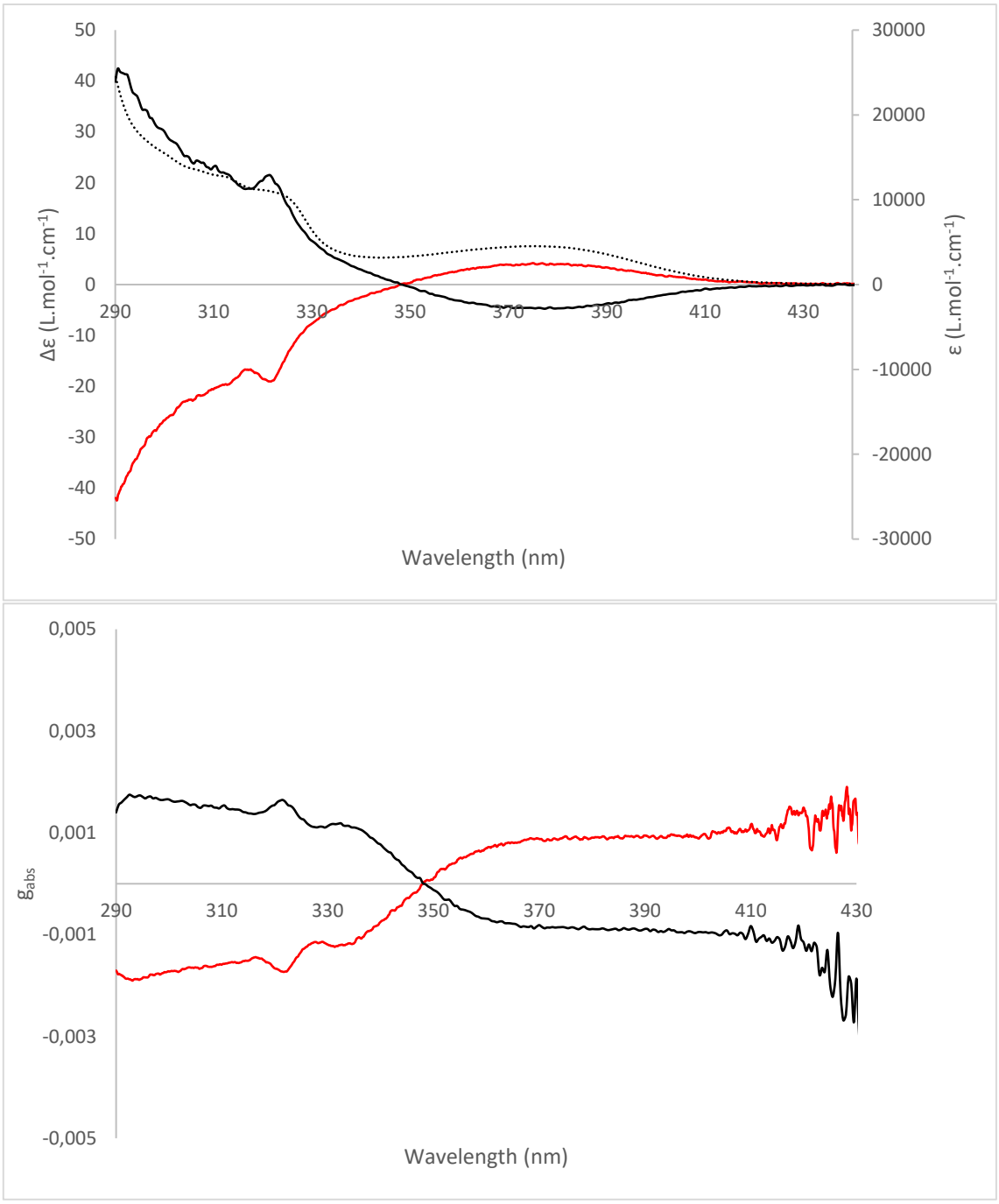

Figure S26: Top: ECD spectra of **C'1** (*S* enantiomer in red, *R* enantiomer in black) and UV-vis spectrum of **C'1** (dashed lines) at 298 K in toluene solution. Bottom: absorption dissymetry factor g_{abs} spectra of **C'1** (*S* enantiomer in red, *R* enantiomer in black) at 298 K in toluene solution.

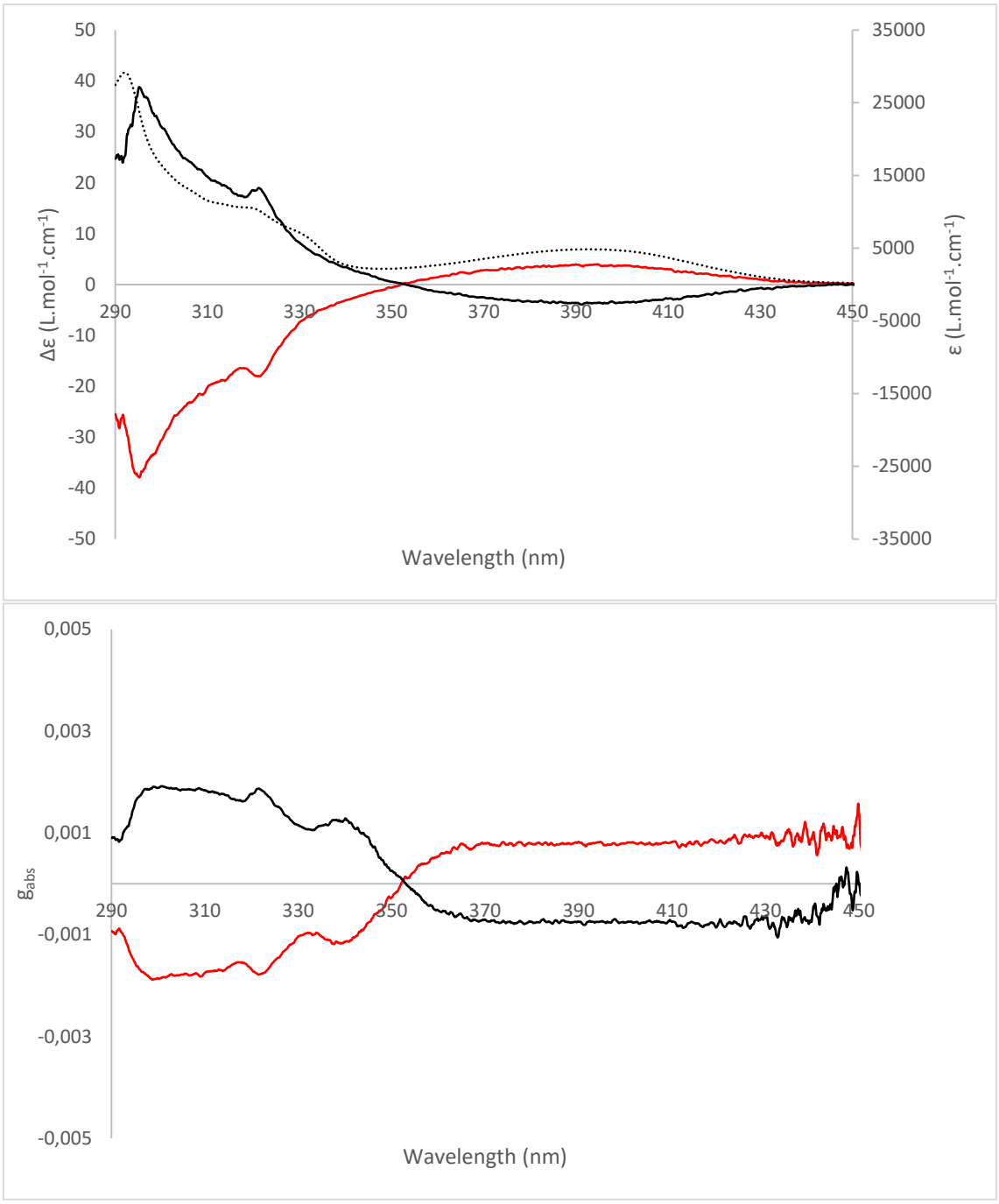

Figure S27: Top: ECD spectra of **C'2** (*S* enantiomer in red, *R* enantiomer in black) and UV-vis spectrum of **C'2** (dashed lines) at 298 K in toluene solution. Bottom: absorption dissymetry factor g_{abs} spectra of **C'2** (*S* enantiomer in red, *R* enantiomer in black) at 298 K in toluene solution.

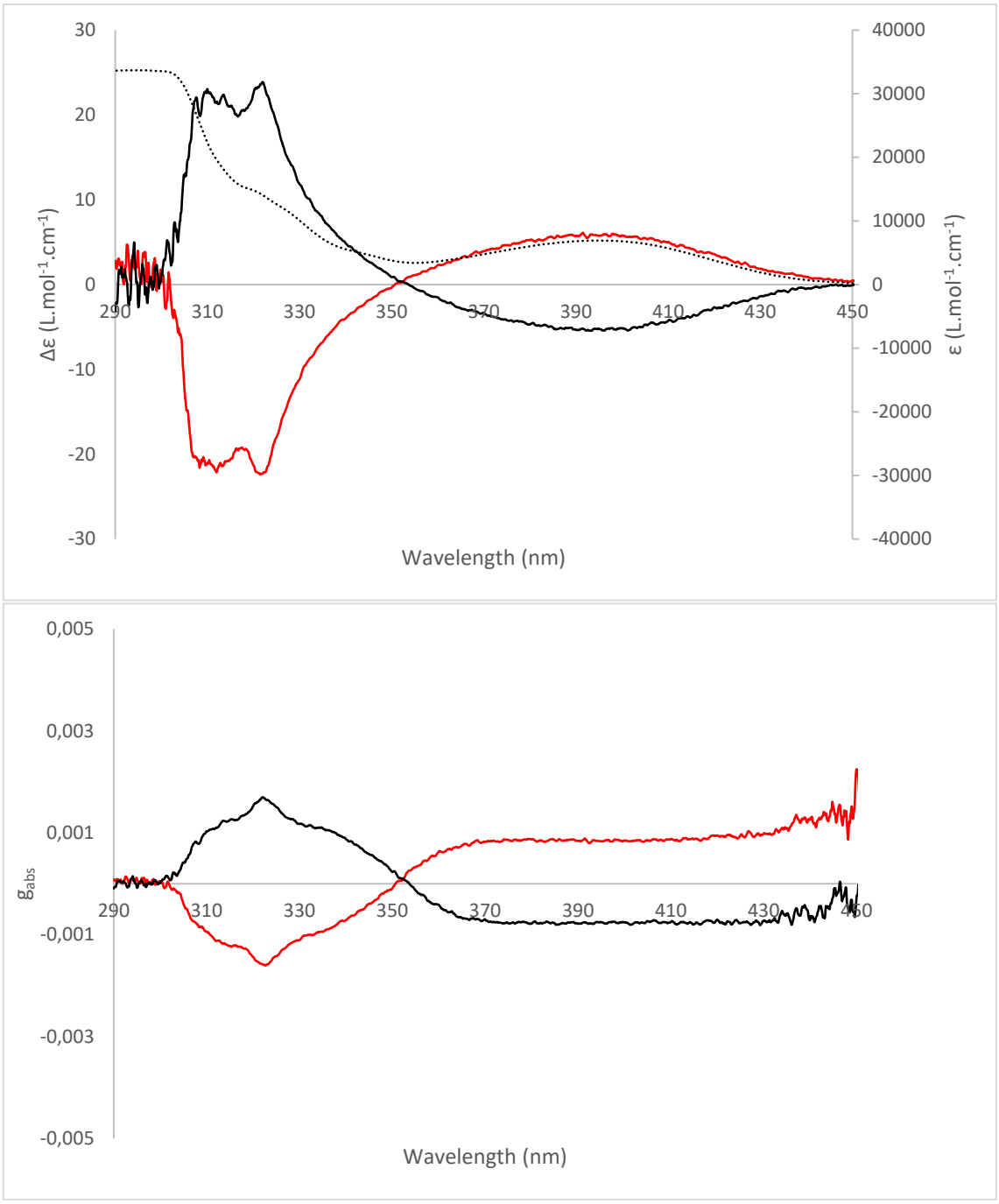

Figure S28: Top: ECD spectra of **C'3** (*S* enantiomer in red, *R* enantiomer in black) and UV-vis spectrum of **C'3** (dashed lines) at 298 K in toluene solution. Bottom: absorption dissymetry factor g_{abs} spectra of **C'3** (*S* enantiomer in red, *R* enantiomer in black) at 298 K in toluene solution.

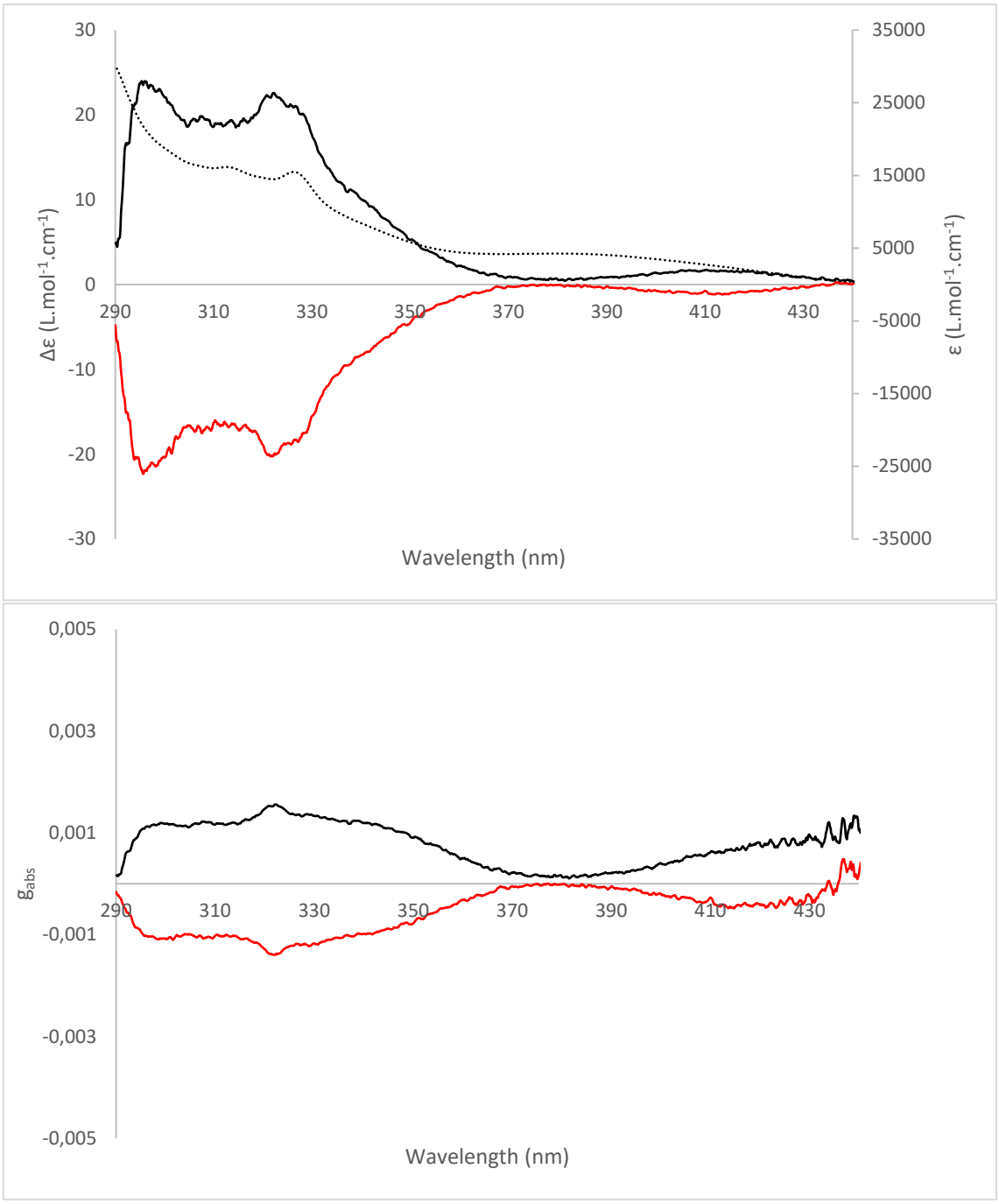

Figure S29: Top: ECD spectra of **C1** (*S* enantiomer in red, *R* enantiomer in black) and UV-vis spectrum of **C1** (dashed lines) at 298 K in toluene solution. Bottom: absorption dissymetry factor g_{abs} spectra of **C1** (*S* enantiomer in red, *R* enantiomer in black) at 298 K in toluene solution.

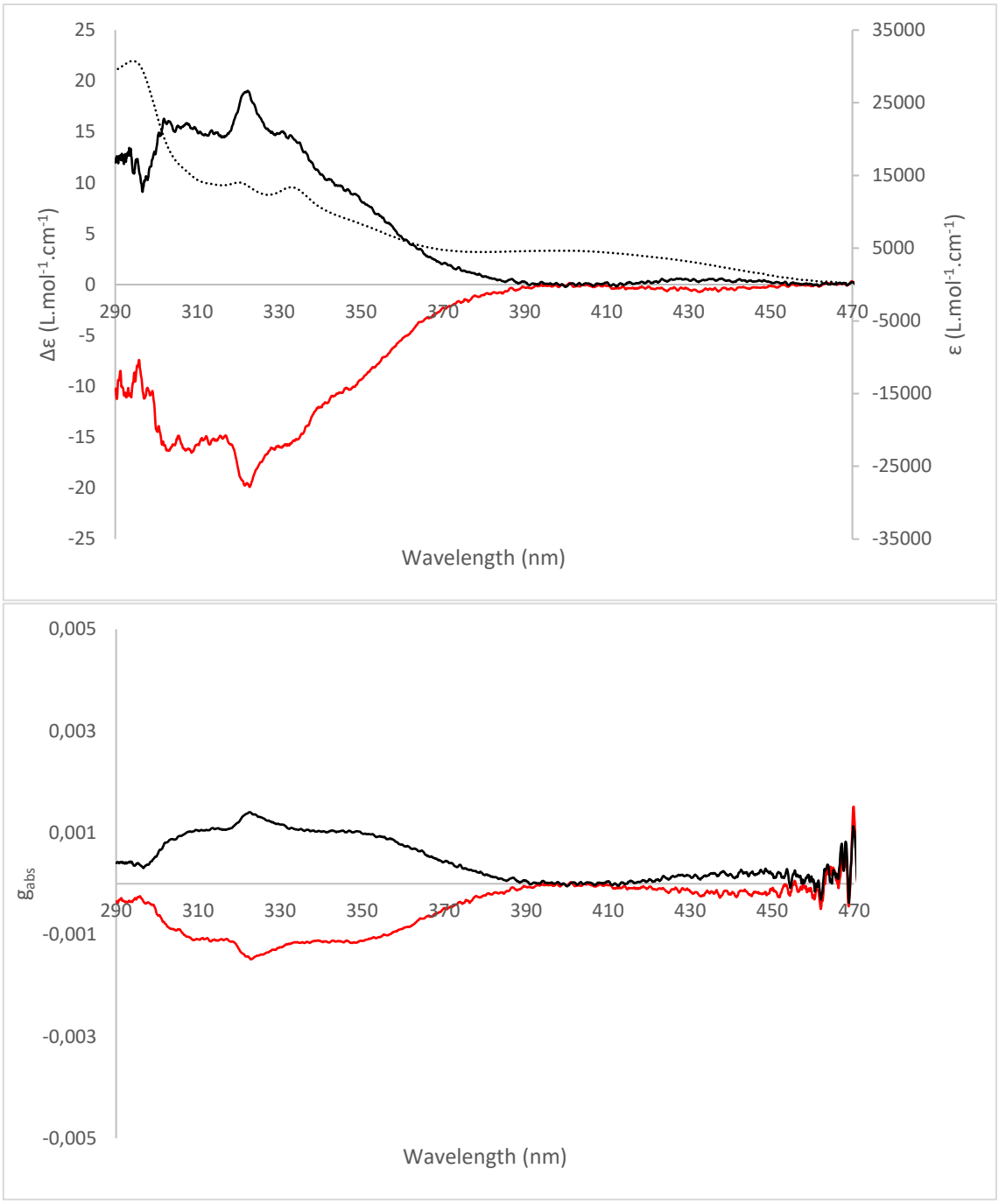

Figure S30: Top: ECD spectra of **C2** (*S* enantiomer in red, *R* enantiomer in black) and UV-vis spectrum of **C2** (dashed lines) at 298 K in toluene solution. Bottom: absorption dissymetry factor g_{abs} spectra of **C2** (*S* enantiomer in red, *R* enantiomer in black) at 298 K in toluene solution.

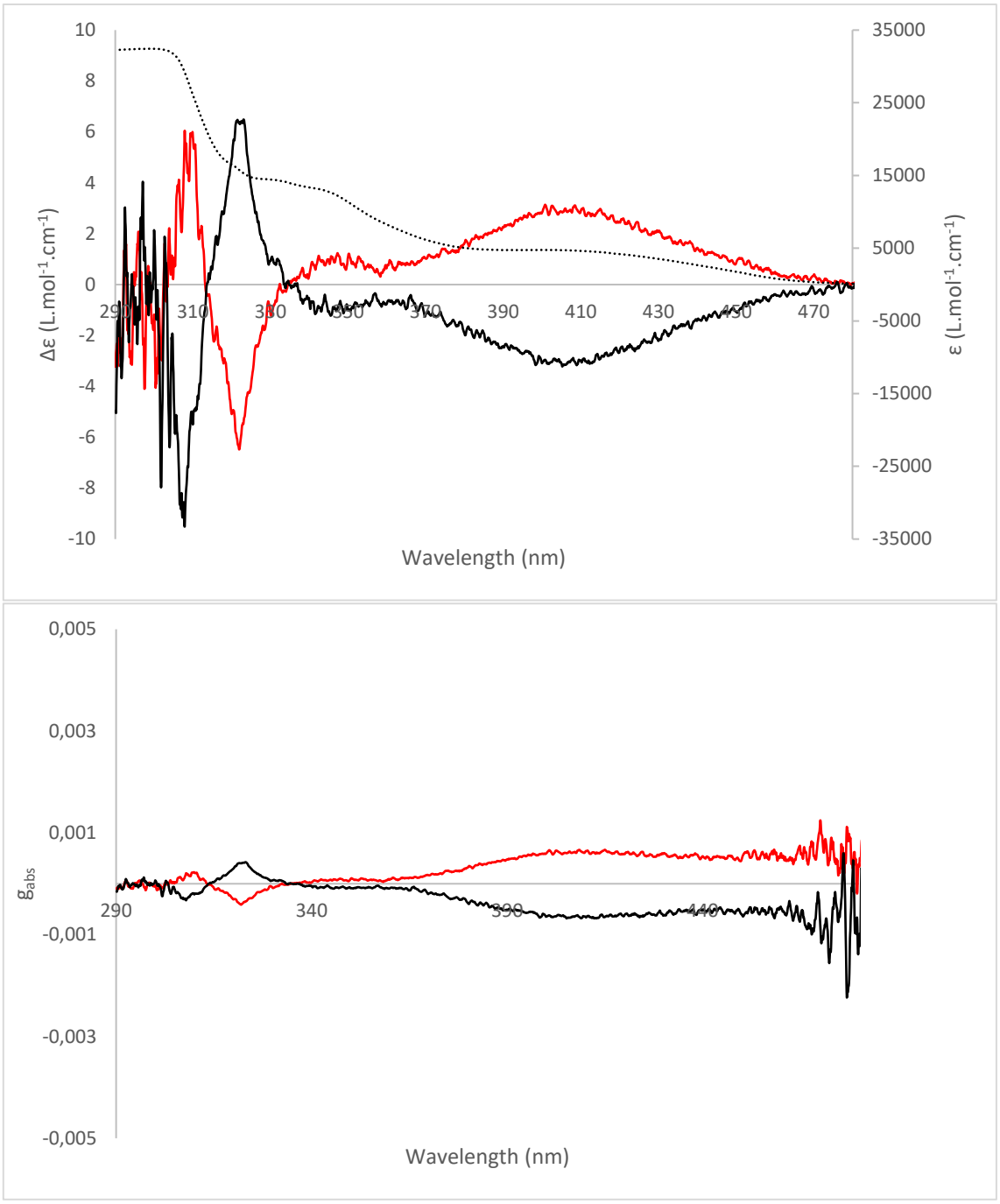

Figure S31: Top: ECD spectra of **C3** (*S* enantiomer in red, *R* enantiomer in black) and UV-vis spectrum of **C3** (dashed lines) at 298 K in toluene solution. Bottom: absorption dissymetry factor g_{abs} spectra of **C3** (*S* enantiomer in red, *R* enantiomer in black) at 298 K in toluene solution.

CPL and g_{lum} :

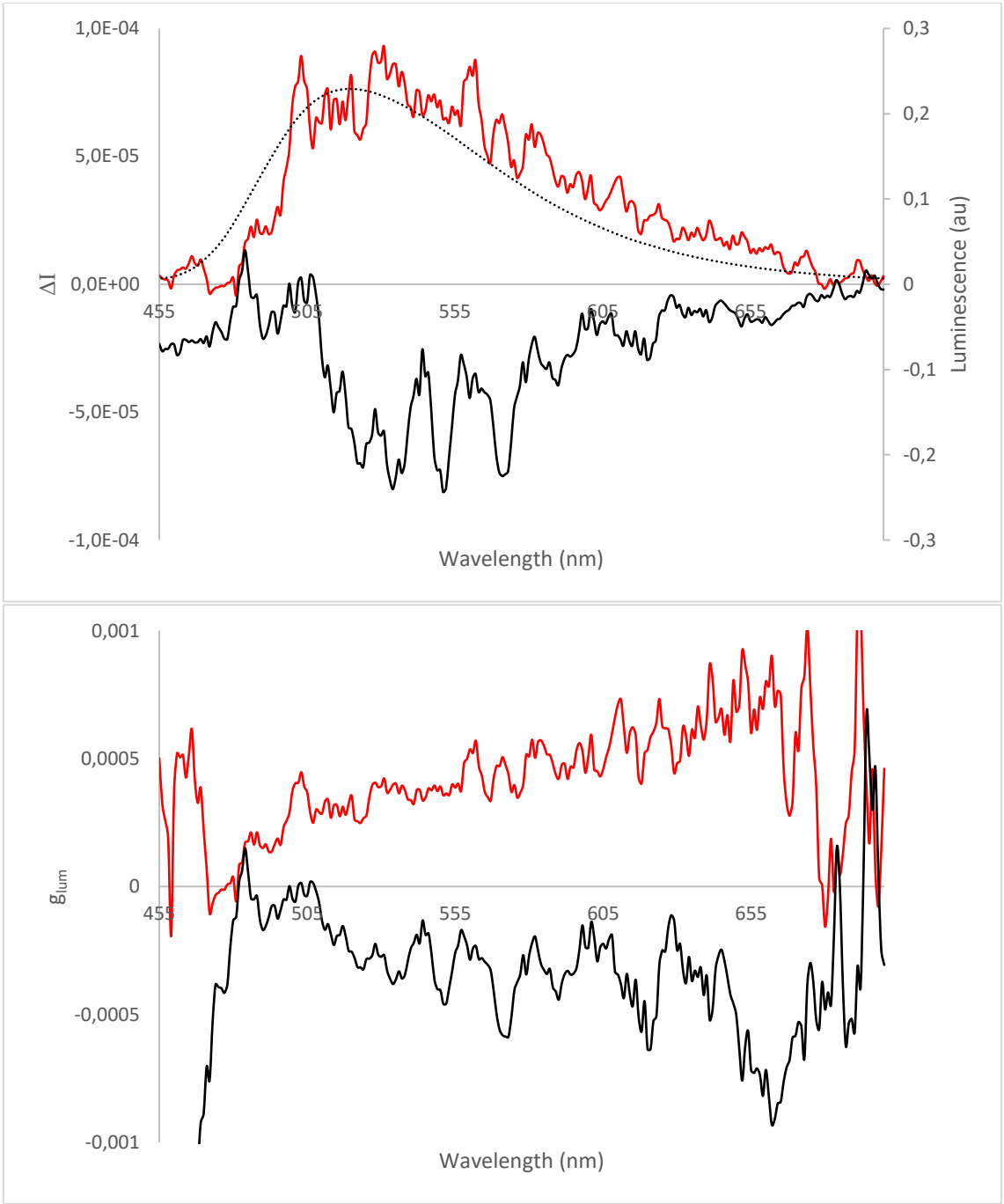

Figure S32: Top: CPL spectra of **A1** (*S* enantiomer in red, *R* enantiomer in black) and emission spectrum of **A1** (dashed lines) at 298 K in toluene solution excited at 420 nm. Bottom: emission dissymetry factor g_{lum} spectra of **A1** (*S* enantiomer in red, *R* enantiomer in black) at 298 K in toluene solution excited at 420 nm.

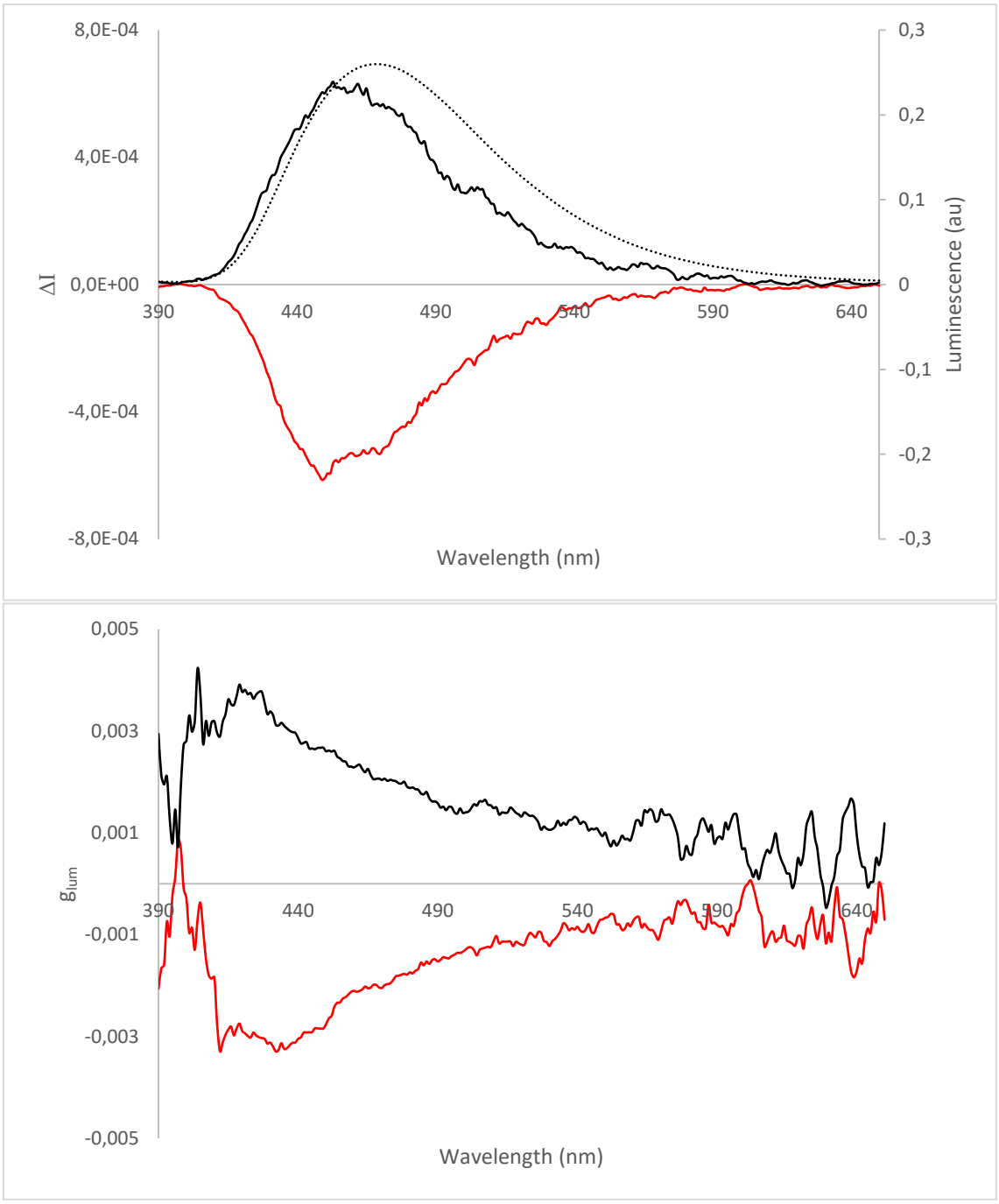

Figure S33: Top: CPL spectra of **B1** (*S* enantiomer in red, *R* enantiomer in black) and emission spectrum of **B1** (dashed lines) at 298 K in toluene solution excited at 350 nm. Bottom: emission dissymetry factor g_{lum} spectra of **B1** (*S* enantiomer in red, *R* enantiomer in black) at 298 K in toluene solution excited at 350 nm.

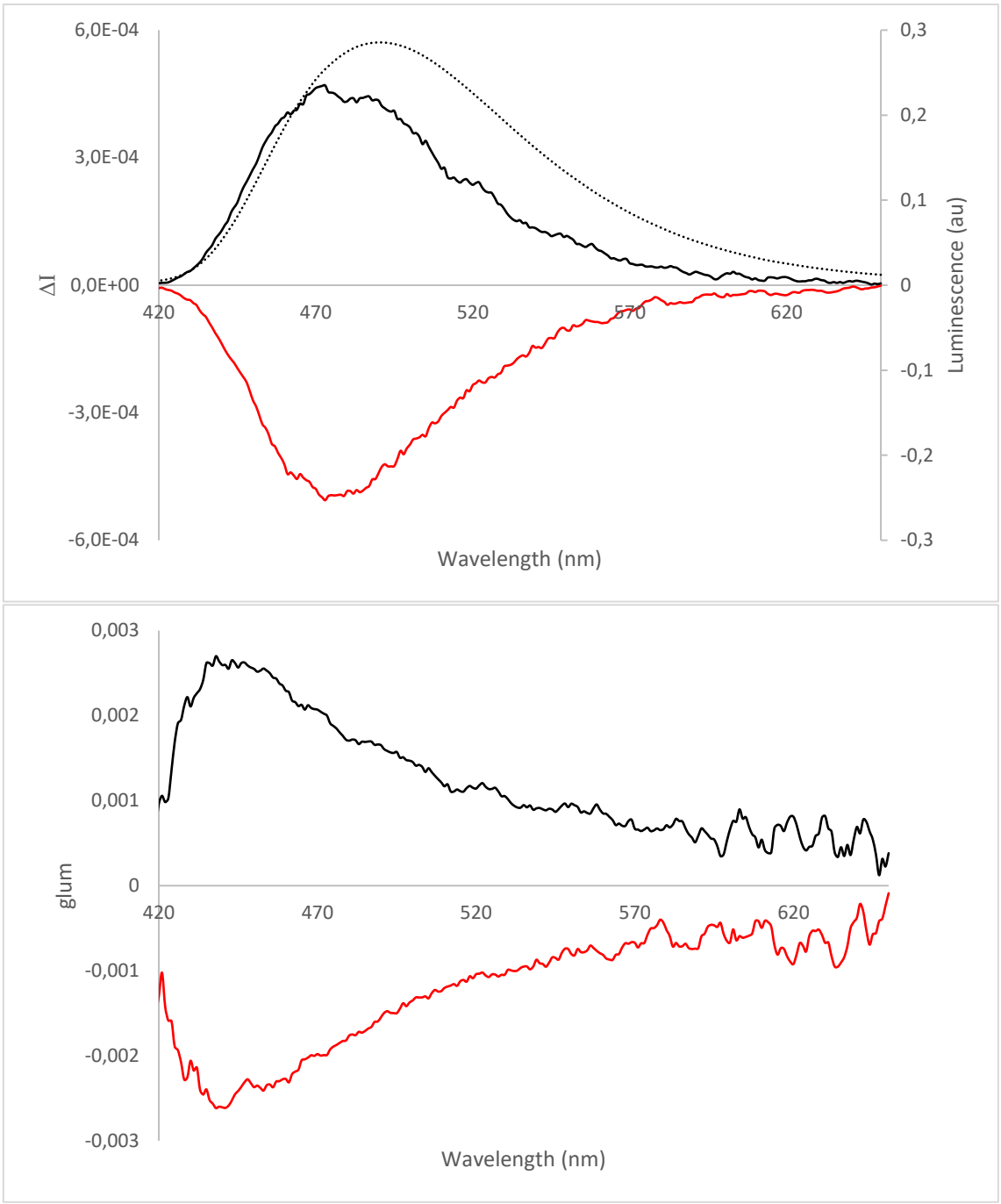

Figure S34: Top: CPL spectra of **B2** (*S* enantiomer in red, *R* enantiomer in black) and emission spectrum of **B2** (dashed lines) at 298 K in toluene solution excited at 360 nm. Bottom: emission dissymetry factor g_{lum} spectra of **B2** (*S* enantiomer in red, *R* enantiomer in black) at 298 K in toluene solution excited at 360 nm.

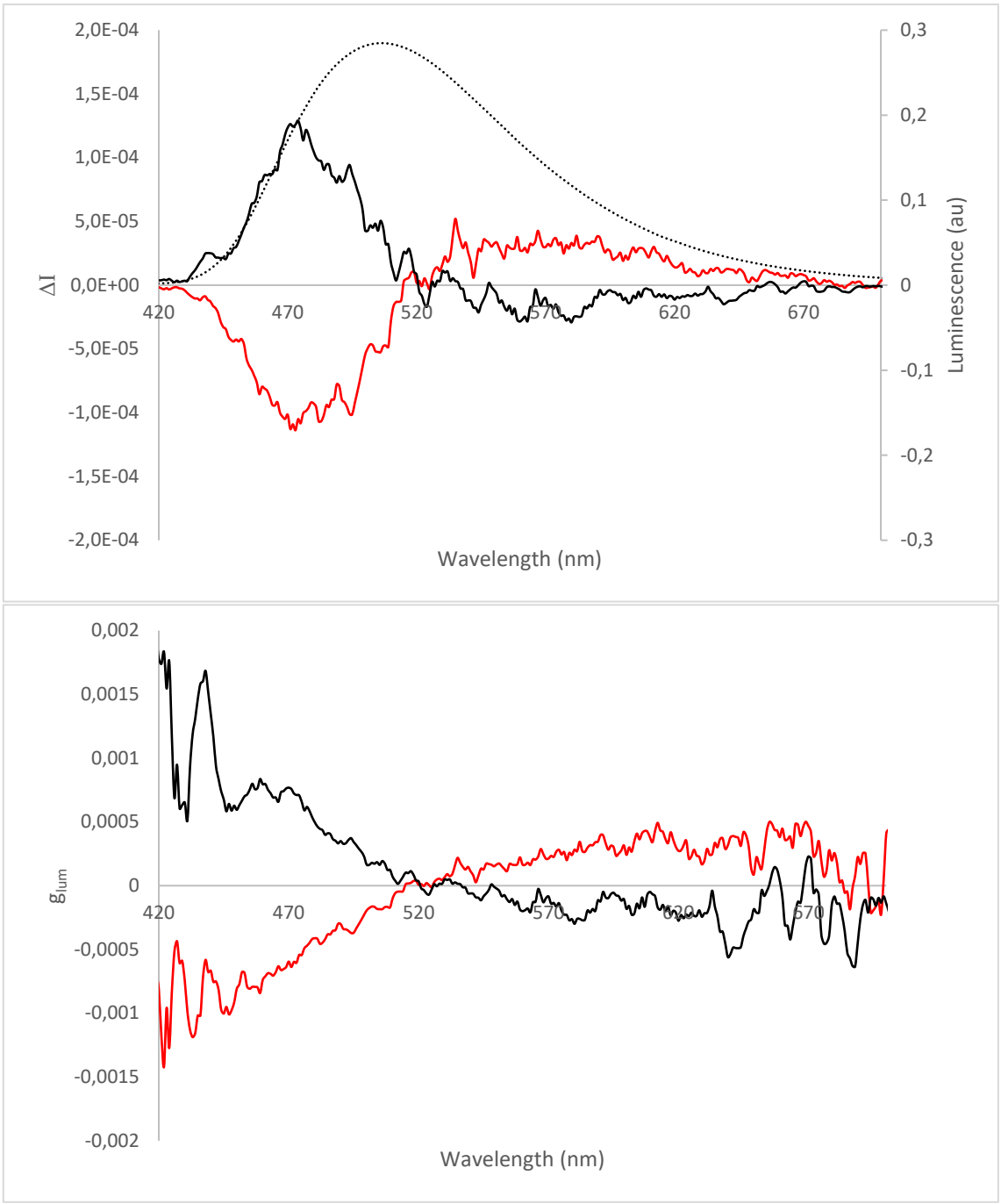

Figure S35: Top: CPL spectra of **B3** (*S* enantiomer in red, *R* enantiomer in black) and emission spectrum of **B3** (dashed lines) at 298 K in toluene solution excited at 360 nm. Bottom: emission dissymetry factor g_{lum} spectra of **B3** (*S* enantiomer in red, *R* enantiomer in black) at 298 K in toluene solution excited at 360 nm.

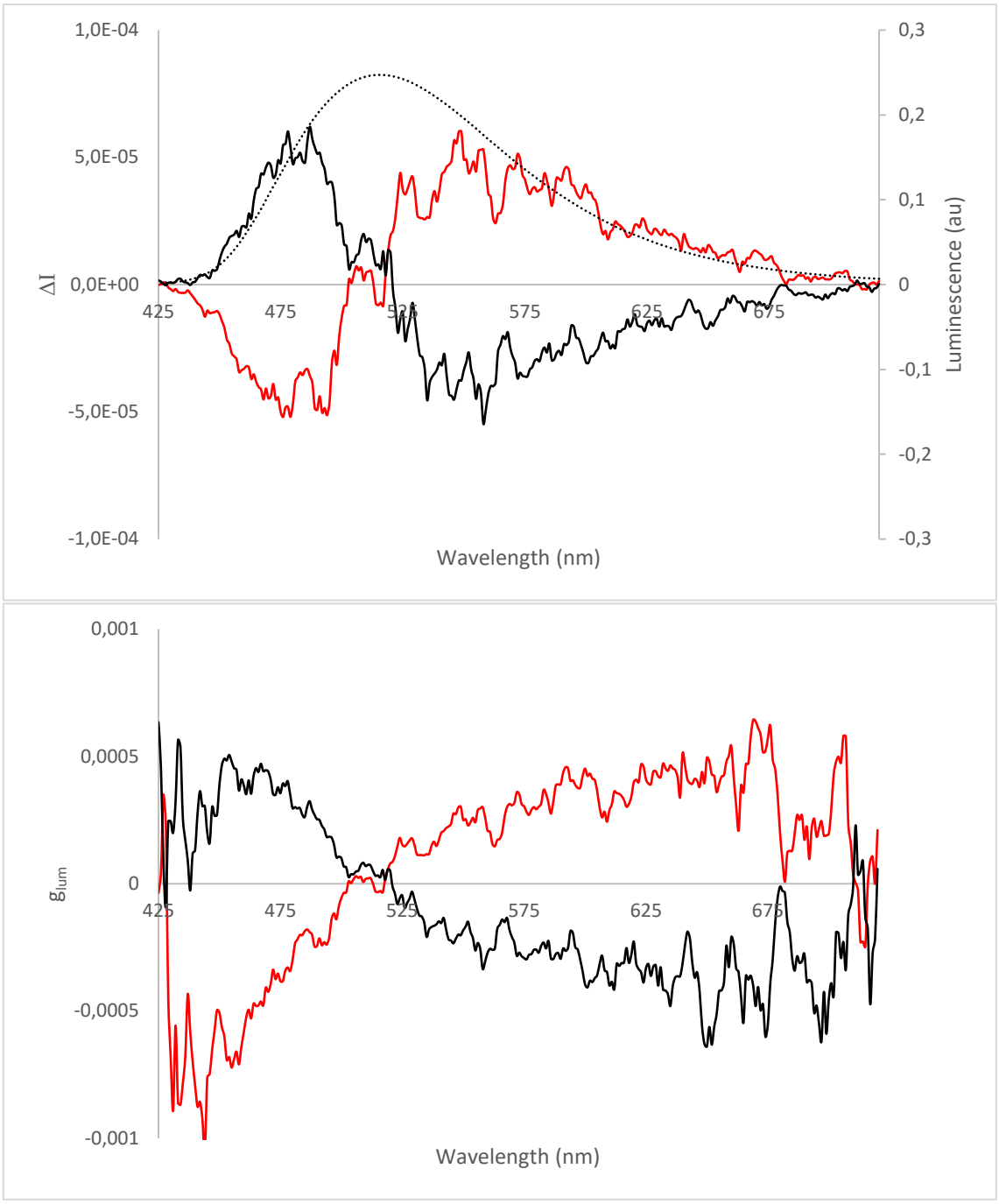

Figure S36: Top: CPL spectra of **B4** (*S* enantiomer in red, *R* enantiomer in black) and emission spectrum of **B4** (dashed lines) at 298 K in toluene solution excited at 370 nm. Bottom: emission dissymetry factor g_{lum} spectra of **B4** (*S* enantiomer in red, *R* enantiomer in black) at 298 K in toluene solution excited at 370 nm.

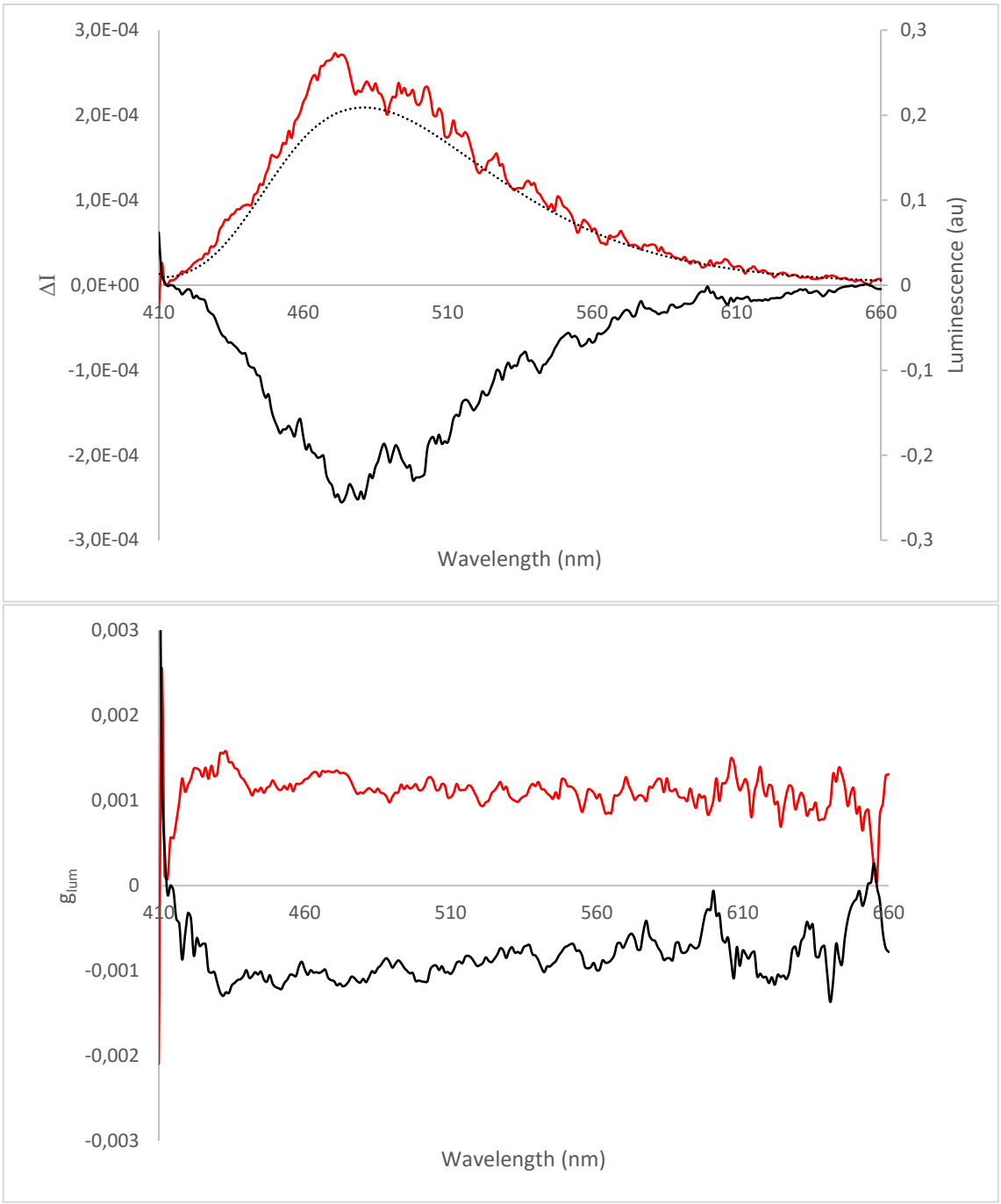

Figure S37: Top: CPL spectra of **C'1** (*S* enantiomer in red, *R* enantiomer in black) and emission spectrum of **C'1** (dashed lines) at 298 K in toluene solution excited at 378 nm. Bottom: emission dissymetry factor g_{lum} spectra of **C'1** (*S* enantiomer in red, *R* enantiomer in black) at 298 K in toluene solution excited at 378 nm.

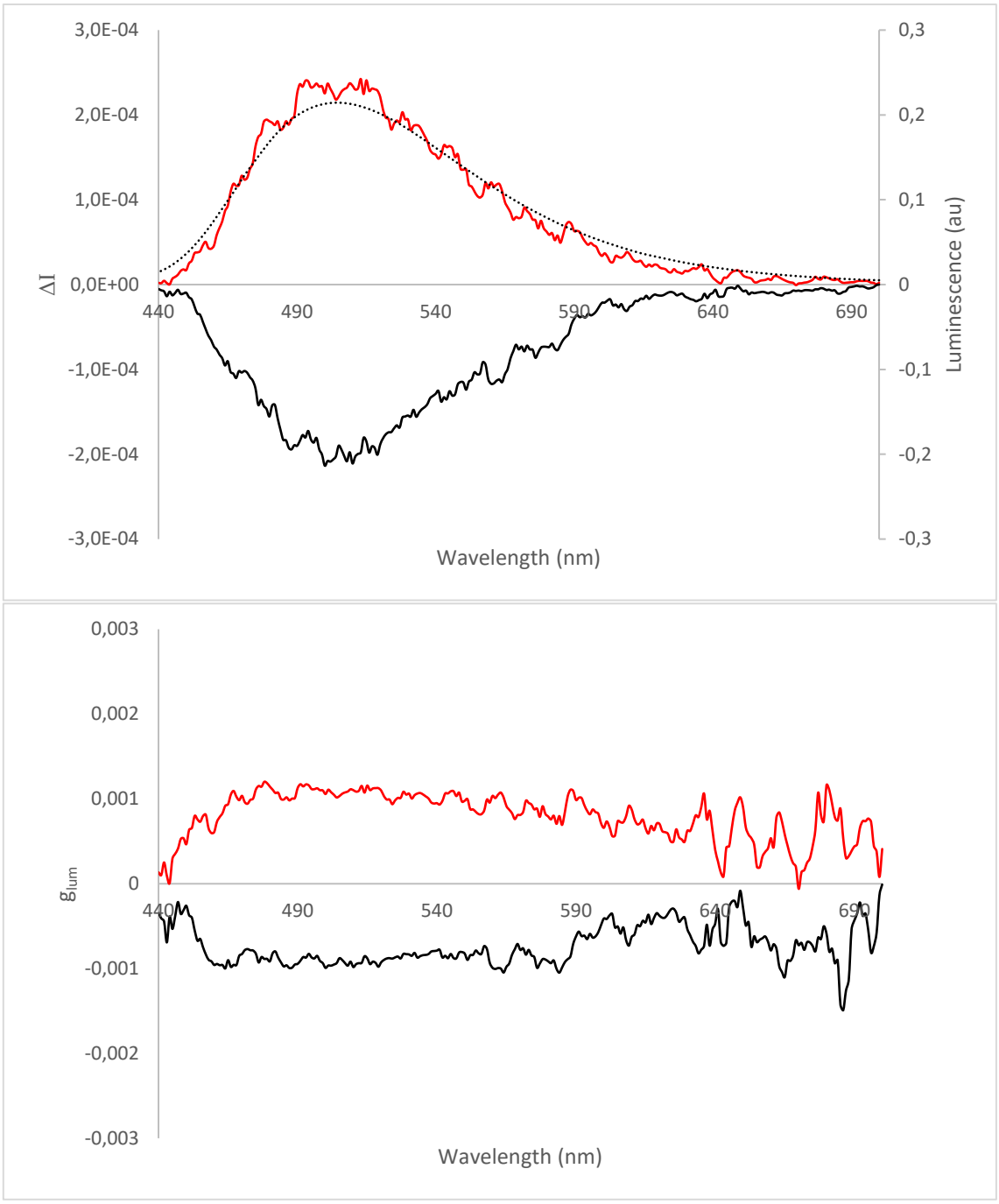

Figure S38: Top: CPL spectra of **C'2** (*S* enantiomer in red, *R* enantiomer in black) and emission spectrum of **C'2** (dashed lines) at 298 K in toluene solution excited at 395 nm. Bottom: emission dissymetry factor g_{lum} spectra of **C'2** (*S* enantiomer in red, *R* enantiomer in black) at 298 K in toluene solution excited at 395 nm.

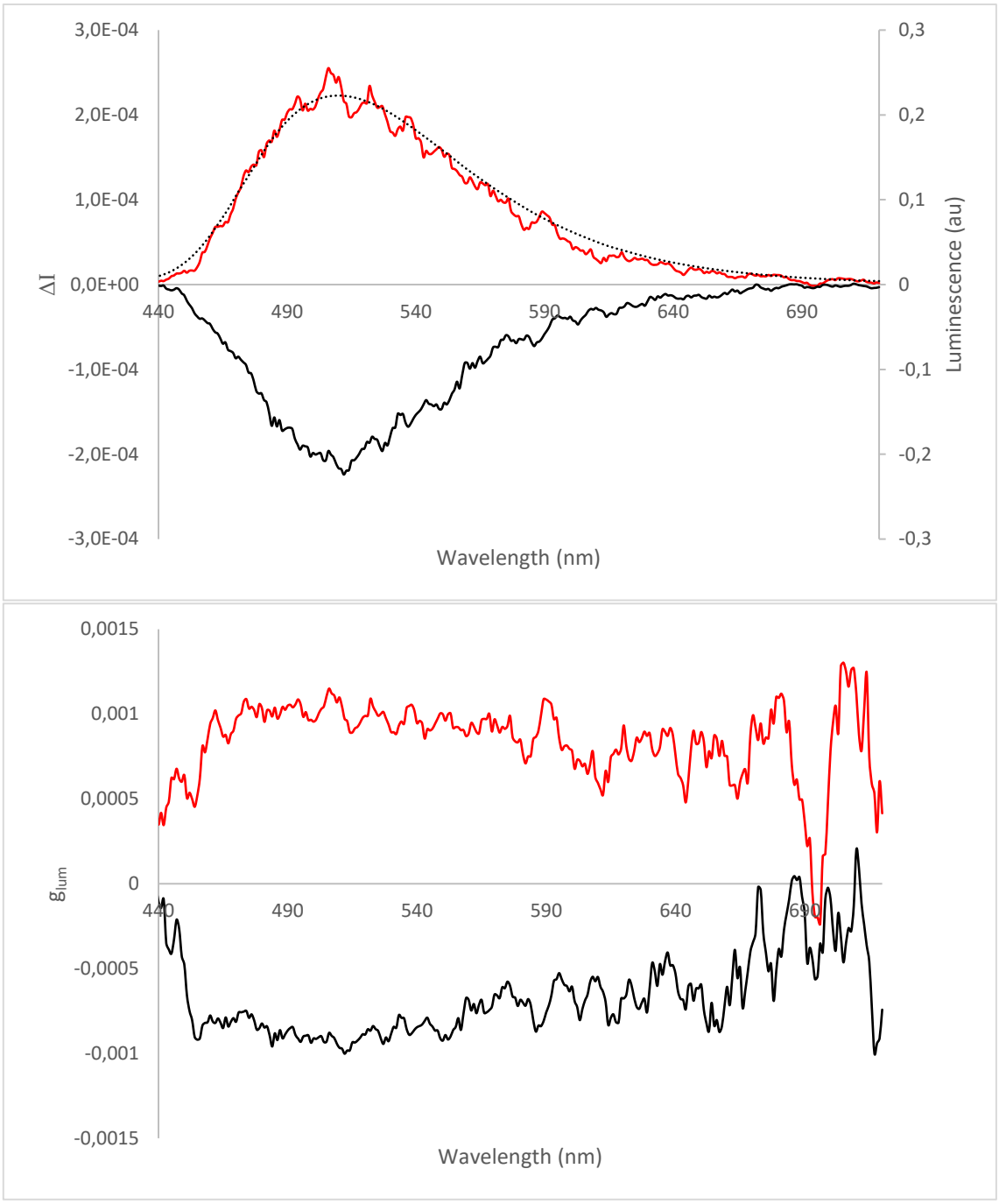

Figure S39: Top: CPL spectra of **C'3** (*S* enantiomer in red, *R* enantiomer in black) and emission spectrum of **C'3** (dashed lines) at 298 K in toluene solution excited at 395 nm. Bottom: emission dissymetry factor g_{lum} spectra of **C'3** (*S* enantiomer in red, *R* enantiomer in black) at 298 K in toluene solution excited at 395 nm.

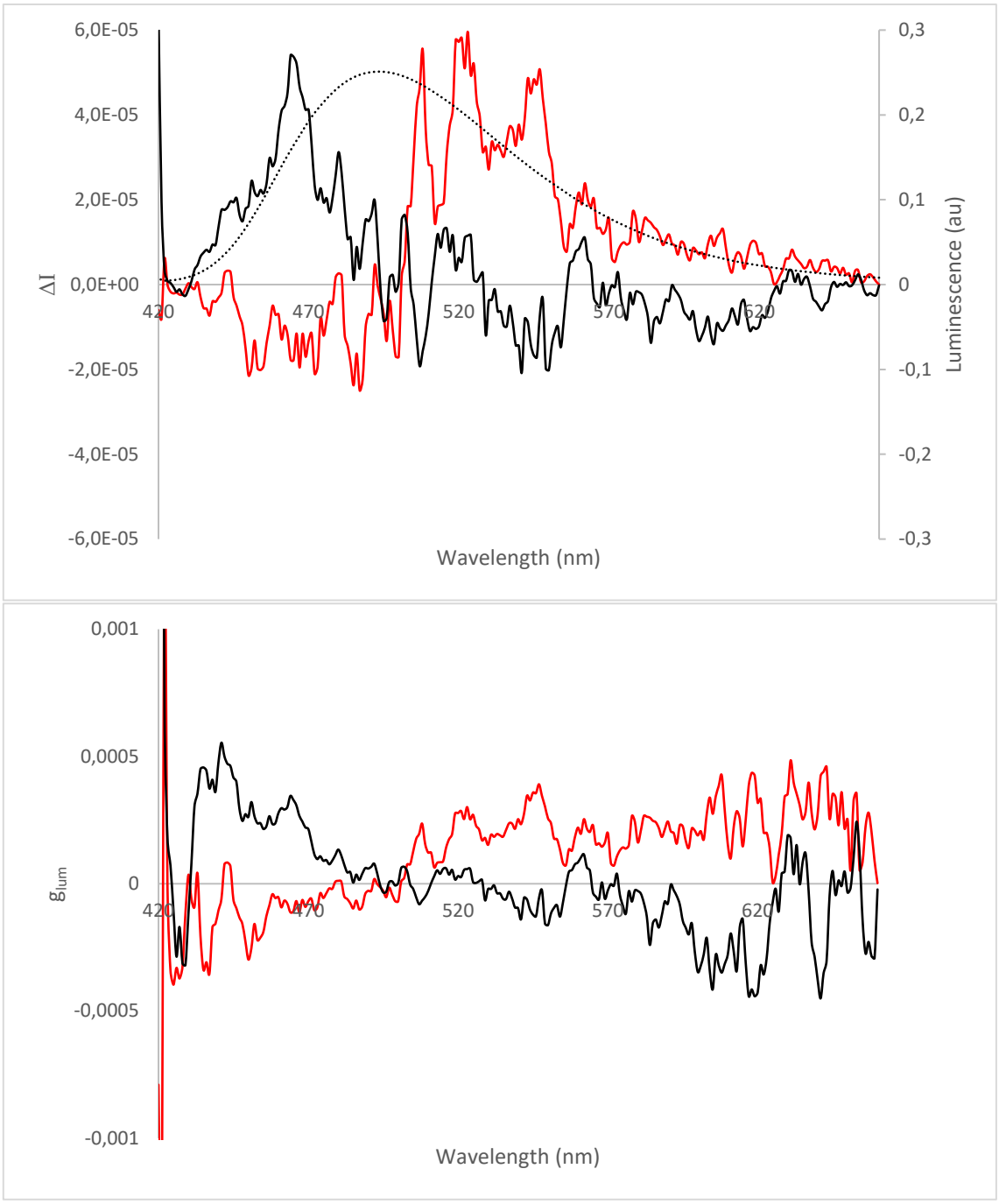

Figure S40: Top: CPL spectra of **C1** (*S* enantiomer in red, *R* enantiomer in black) and emission spectrum of **C1** (dashed lines) at 298 K in toluene solution excited at 380 nm. Bottom: emission dissymetry factor g_{lum} spectra of **C1** (*S* enantiomer in red, *R* enantiomer in black) at 298 K in toluene solution excited at 380 nm.

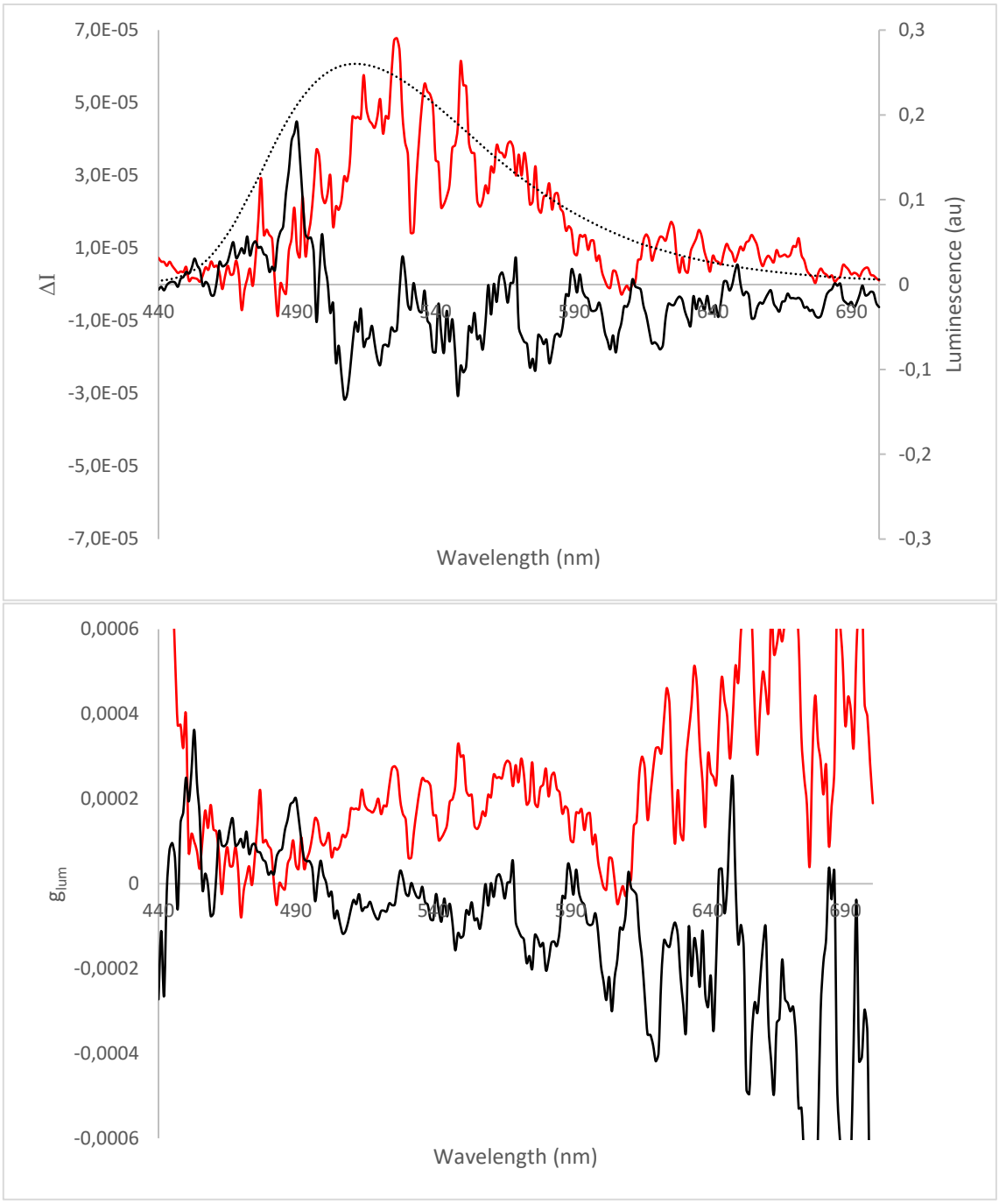

Figure S41: Top: CPL spectra of **C2** (*S* enantiomer in red, *R* enantiomer in black) and emission spectrum of **C2** (dashed lines) at 298 K in toluene solution excited at 395 nm. Bottom: emission dissymetry factor g_{lum} spectra of **C2** (*S* enantiomer in red, *R* enantiomer in black) at 298 K in toluene solution excited at 395 nm.

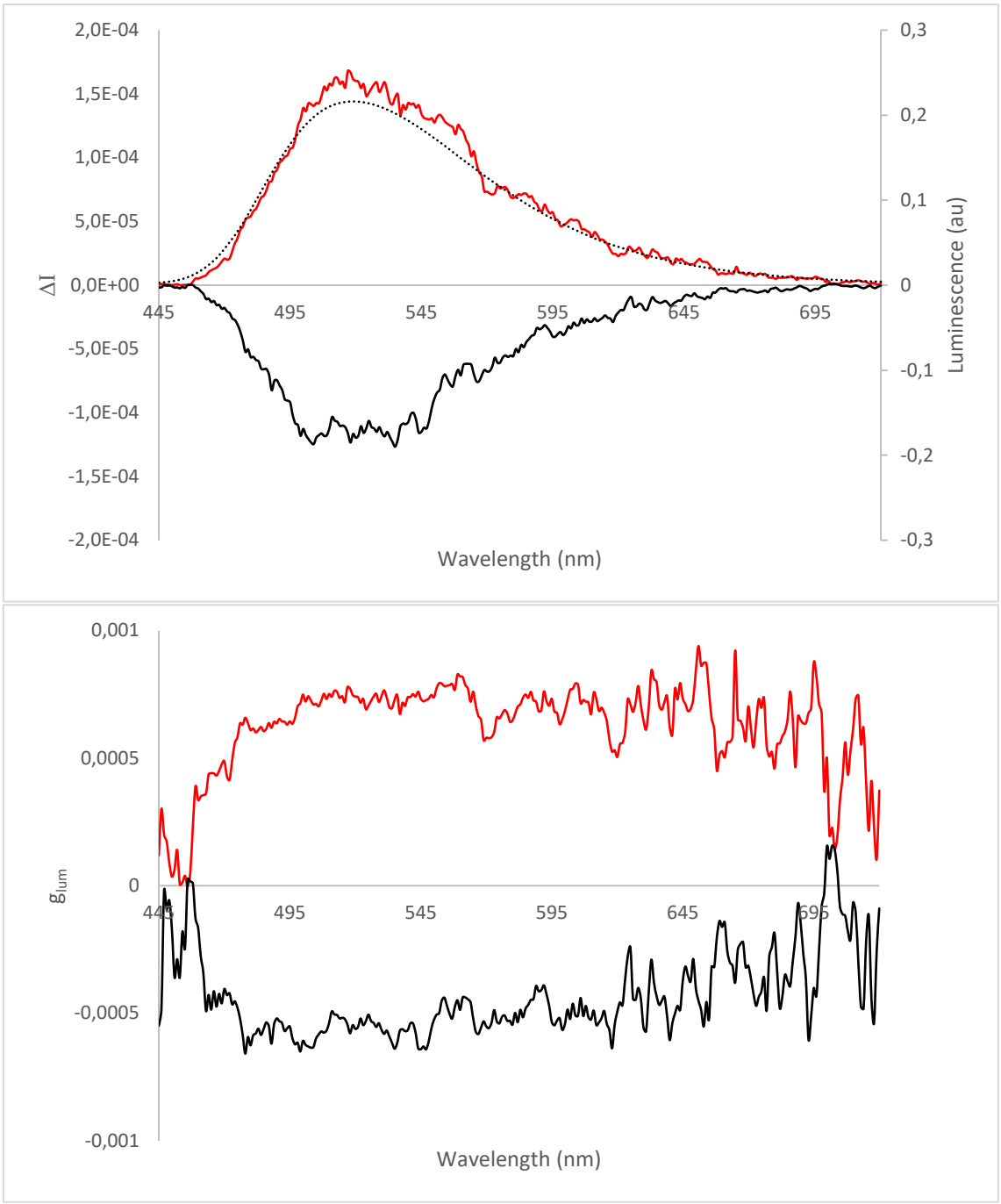

Figure S42: Top: CPL spectra of **C3** (*S* enantiomer in red, *R* enantiomer in black) and emission spectrum of **C3** (dashed lines) at 298 K in toluene solution excited at 400 nm. Bottom: emission dissymetry factor g_{lum} spectra of **C3** (*S* enantiomer in red, *R* enantiomer in black) at 298 K in toluene solution excited at 400 nm.

AIE properties :

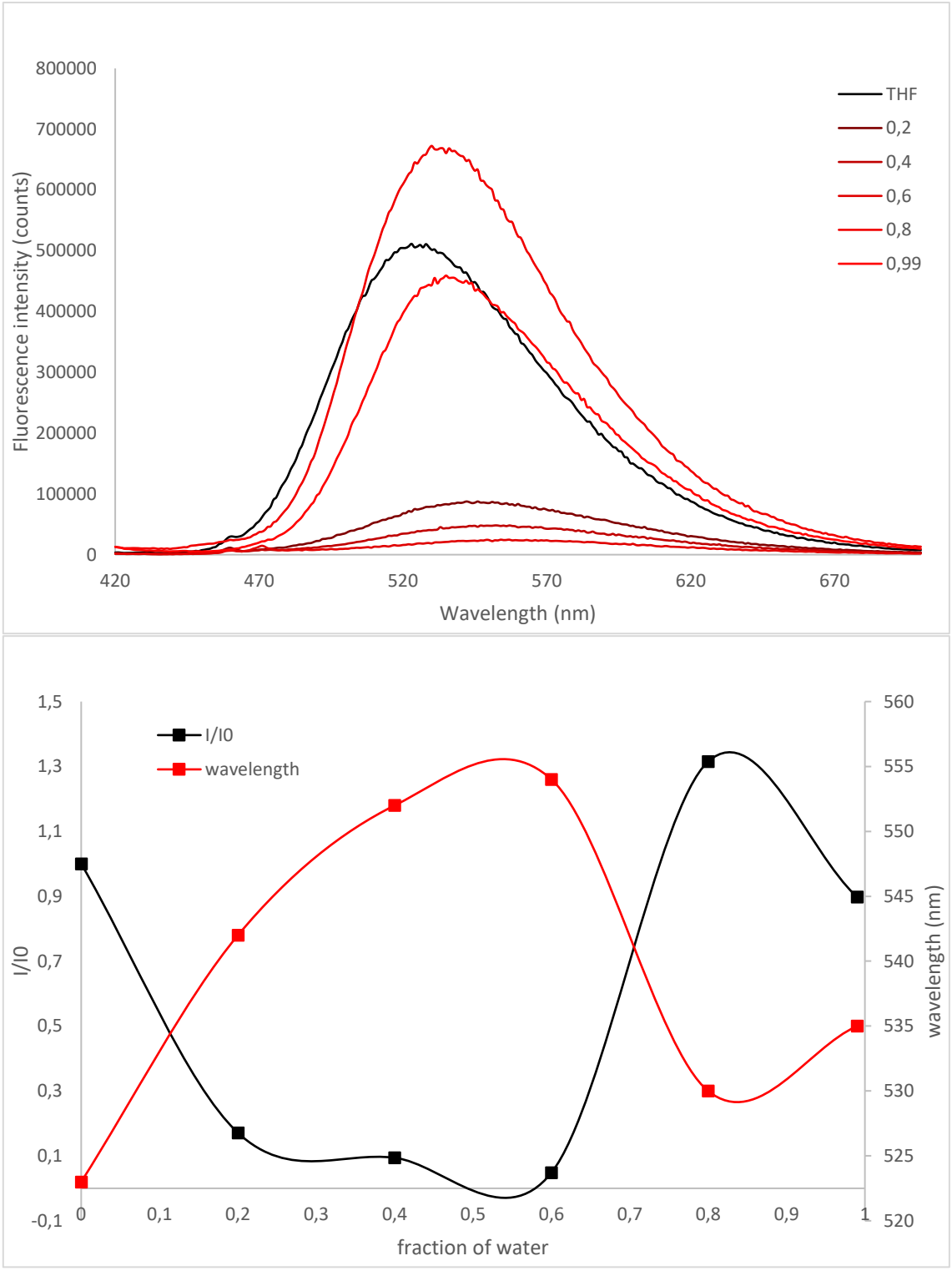

Figure S43: Top: Fluorescence intensity against wavelength depending on fraction of water (f_w) of **A1** at 298 K excited at 410 nm. Bottom: relative photoluminescence intensity (in black) and emission maximum wavelength against fraction of water (f_w) of **A1** at 298 K in toluene solution excited at 410 nm.

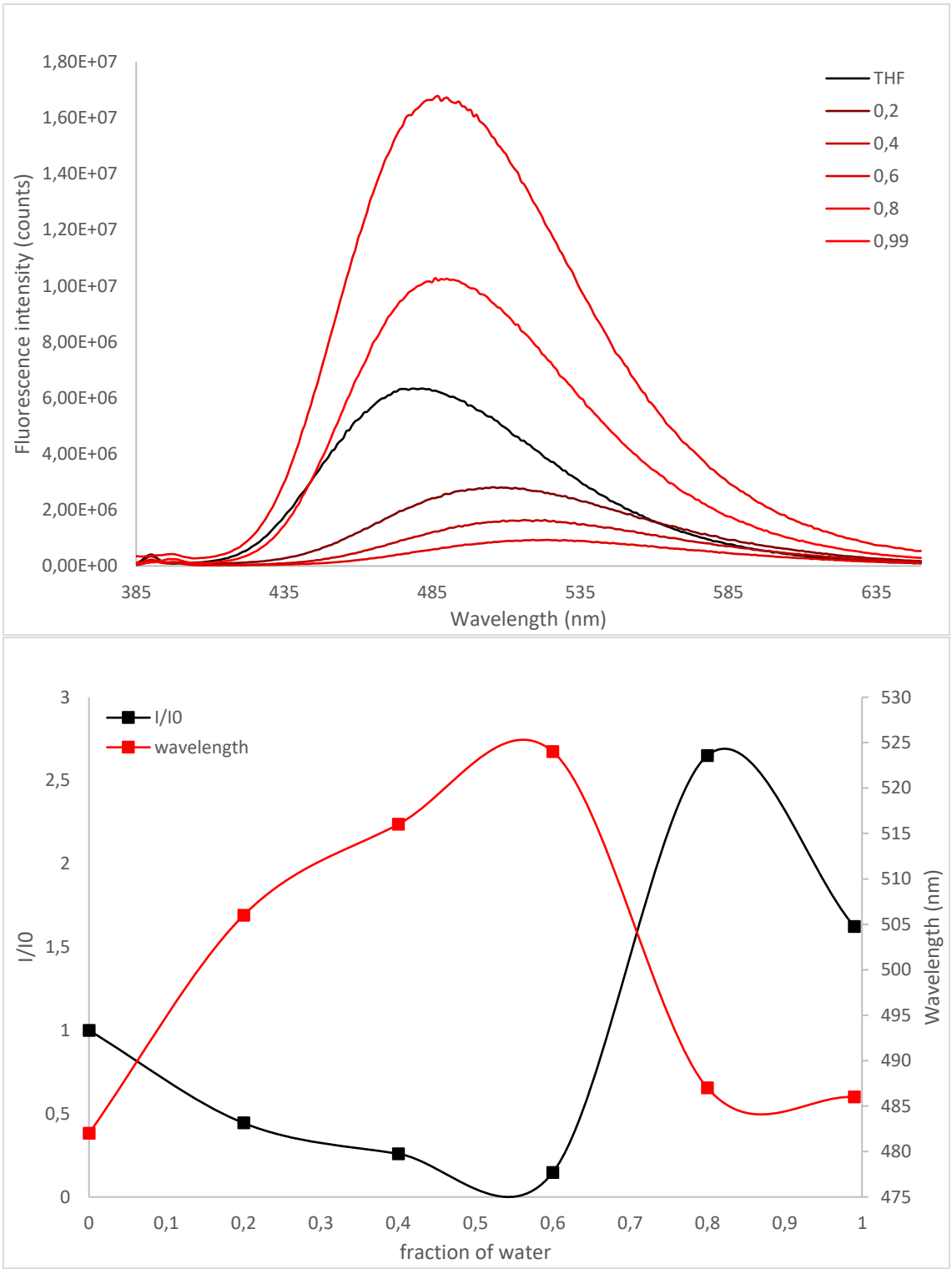

Figure S44: Top: Fluorescence intensity against wavelength depending on fraction of water (f_w) of **B1** at 298 K excited at 375 nm. Bottom: relative photoluminescence intensity (in black) and emission maximum wavelength against fraction of water (f_w) of **B1** at 298 K in toluene solution excited at 375 nm.

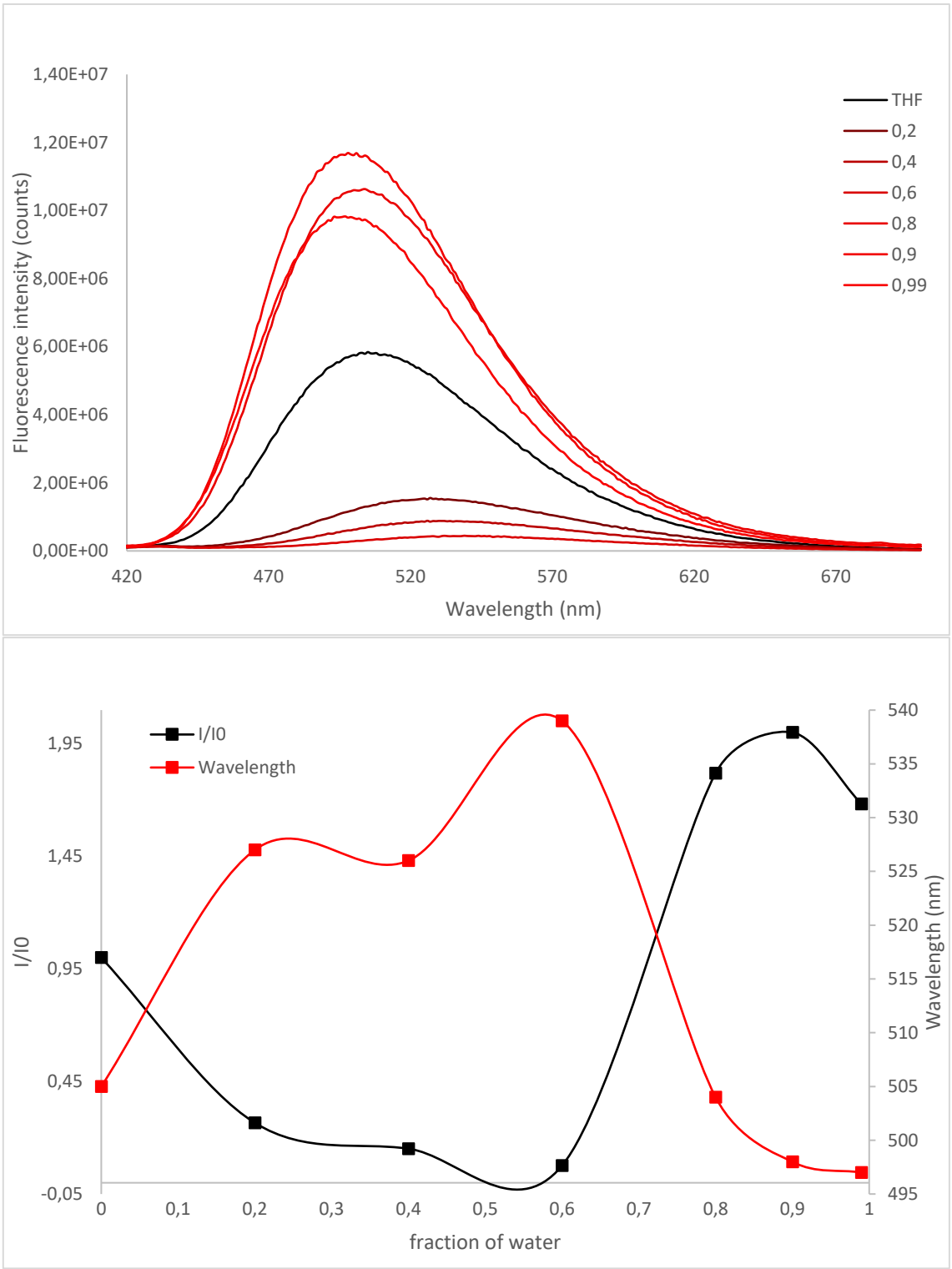

Figure S45: Top: Fluorescence intensity against wavelength depending on fraction of water (f_w) of **B2** at 298 K excited at 410 nm. Bottom relative photoluminescence intensity (in black) and emission maximum wavelength against fraction of water (f_w) of **B2** at 298 K in toluene solution excited at 410 nm.

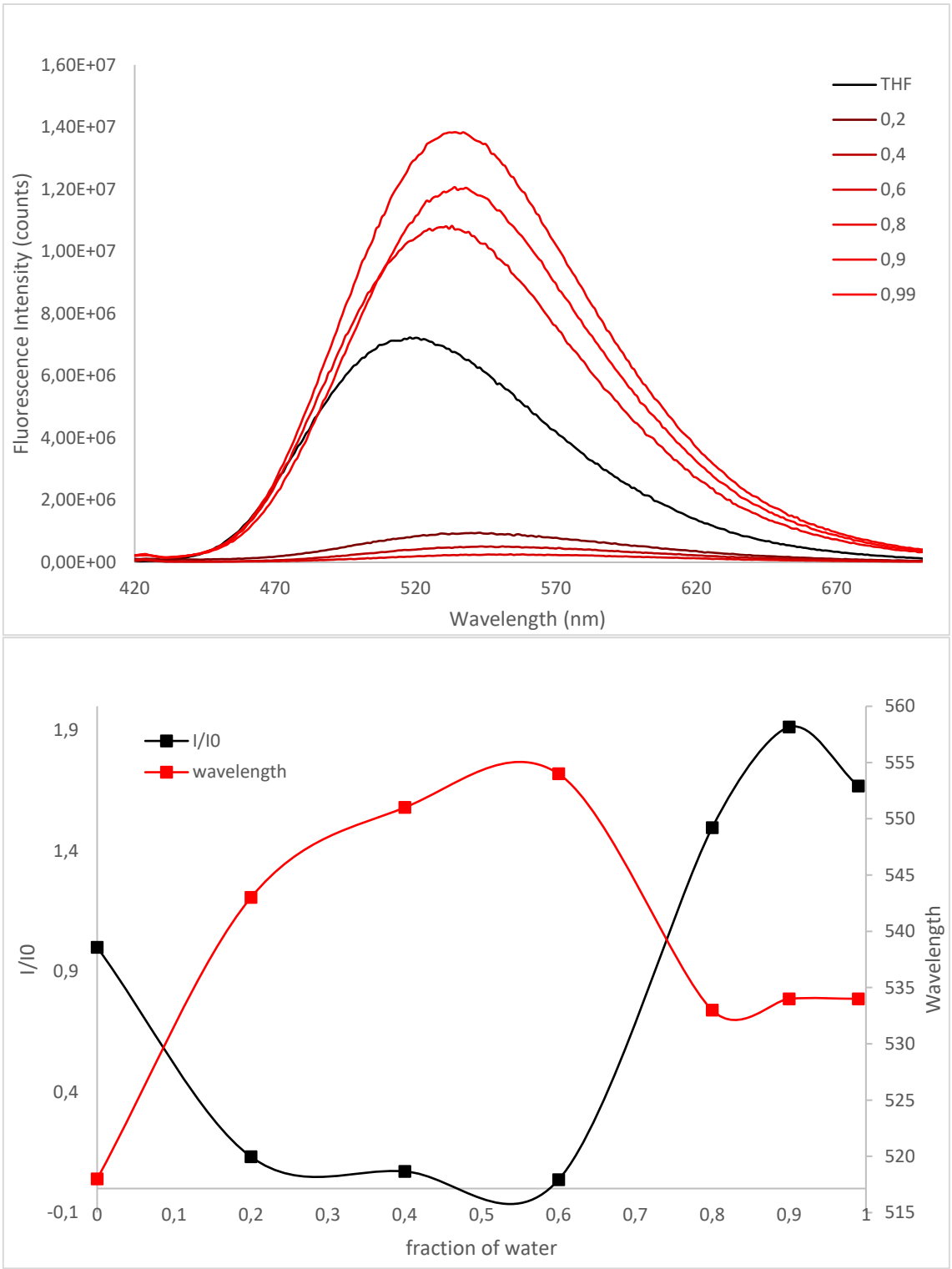

Figure S46: Top: Fluorescence intensity against wavelength depending on fraction of water (f_w) of **B3** at 298 K excited at 410 nm. Bottom: relative photoluminescence intensity (in black) and emission maximum wavelength against fraction of water (f_w) of **B3** at 298 K in toluene solution excited at 410 nm.

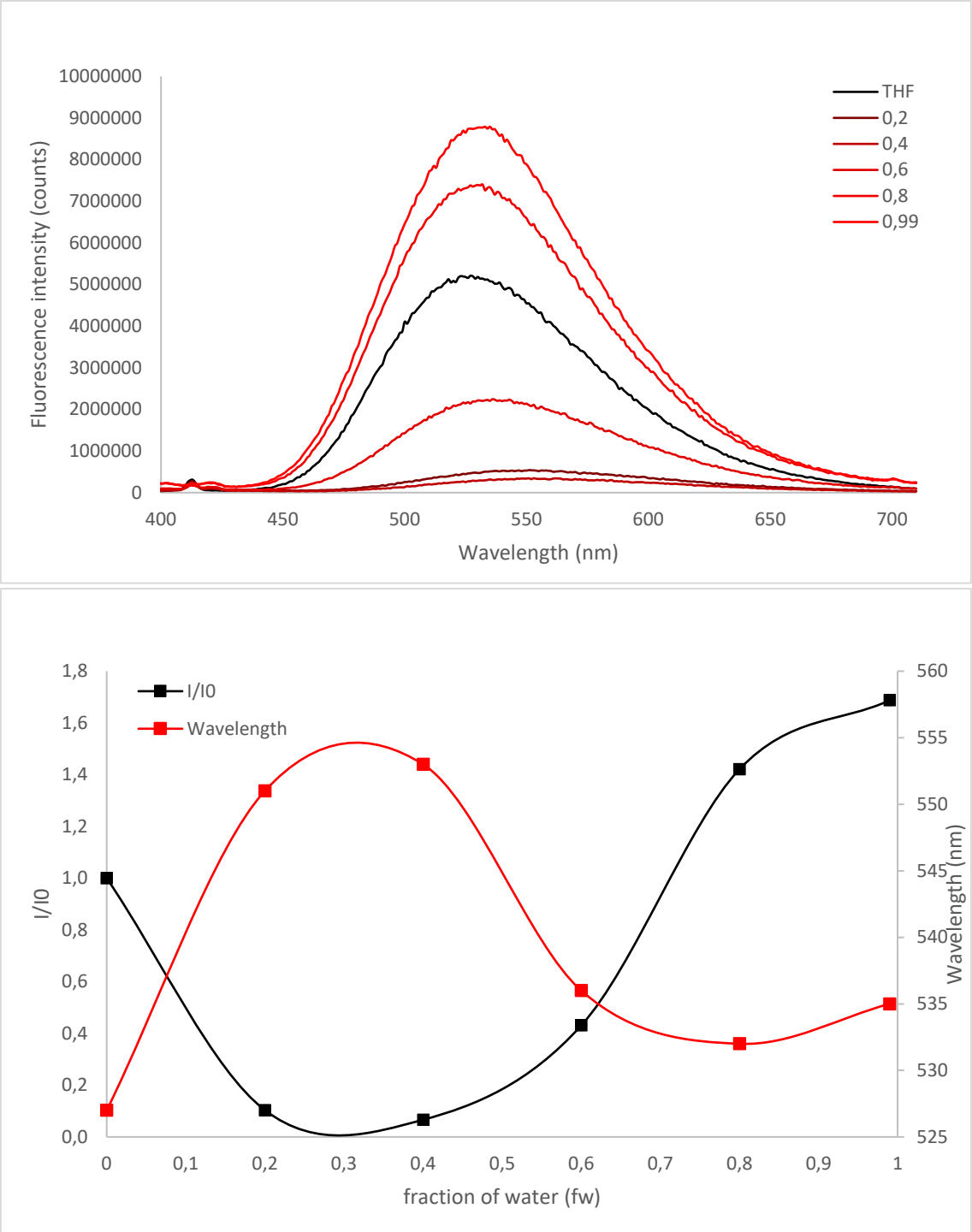

Figure S47: Top: Fluorescence intensity against wavelength depending on fraction of water (f_w) of **B4** at 298 K excited at 363 nm. Bottom: relative photoluminescence intensity (in black) and emission maximum wavelength against fraction of water (f_w) of **B4** at 298 K in toluene solution excited at 363 nm.

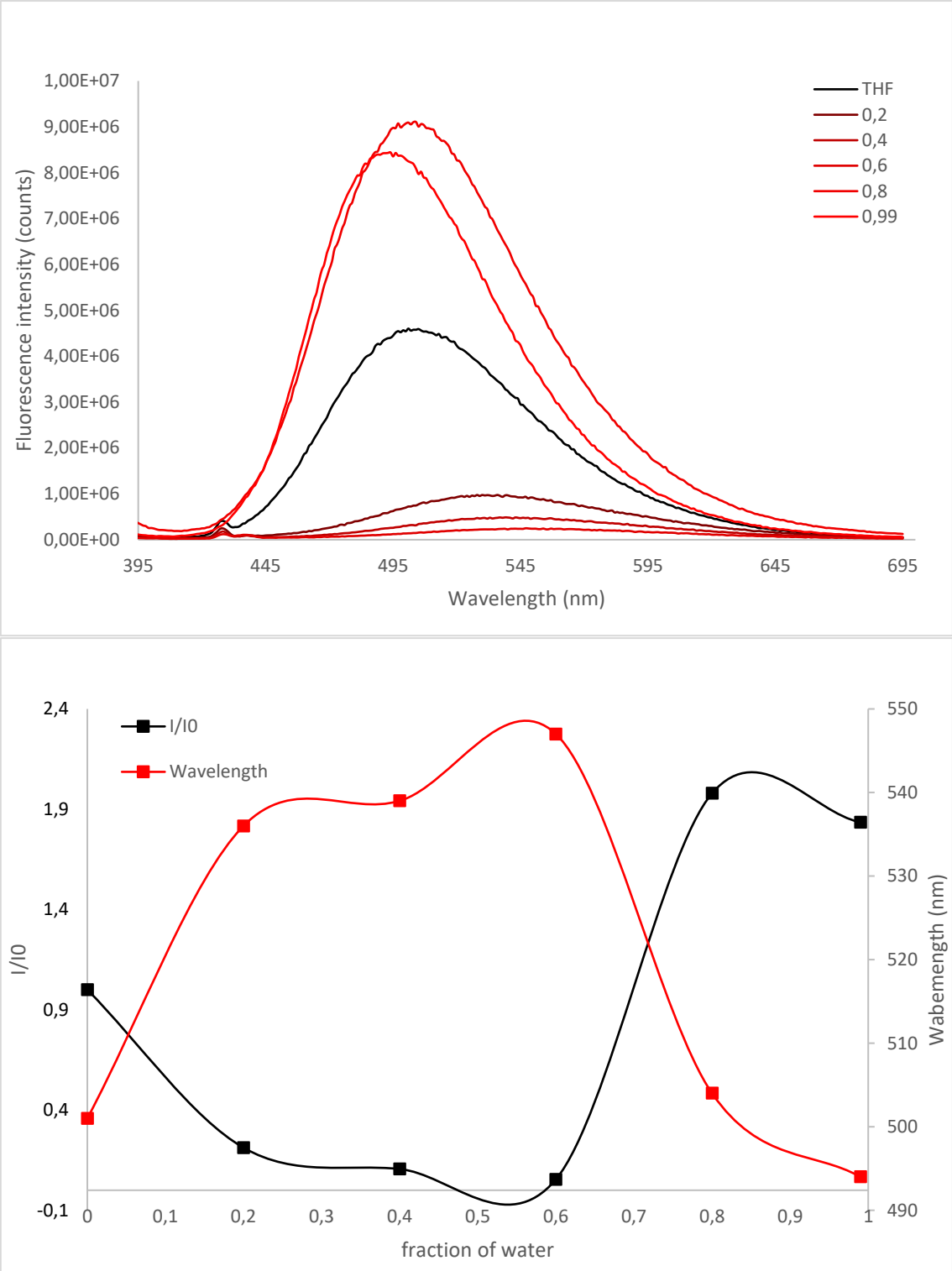

Figure S48: Top: Fluorescence intensity against wavelength depending on fraction of water (f_w) of **C'1** at 298 K excited at 380 nm. Bottom: relative photoluminescence intensity (in black) and emission maximum wavelength against fraction of water (f_w) of **C'1** at 298 K in toluene solution excited at 380 nm.

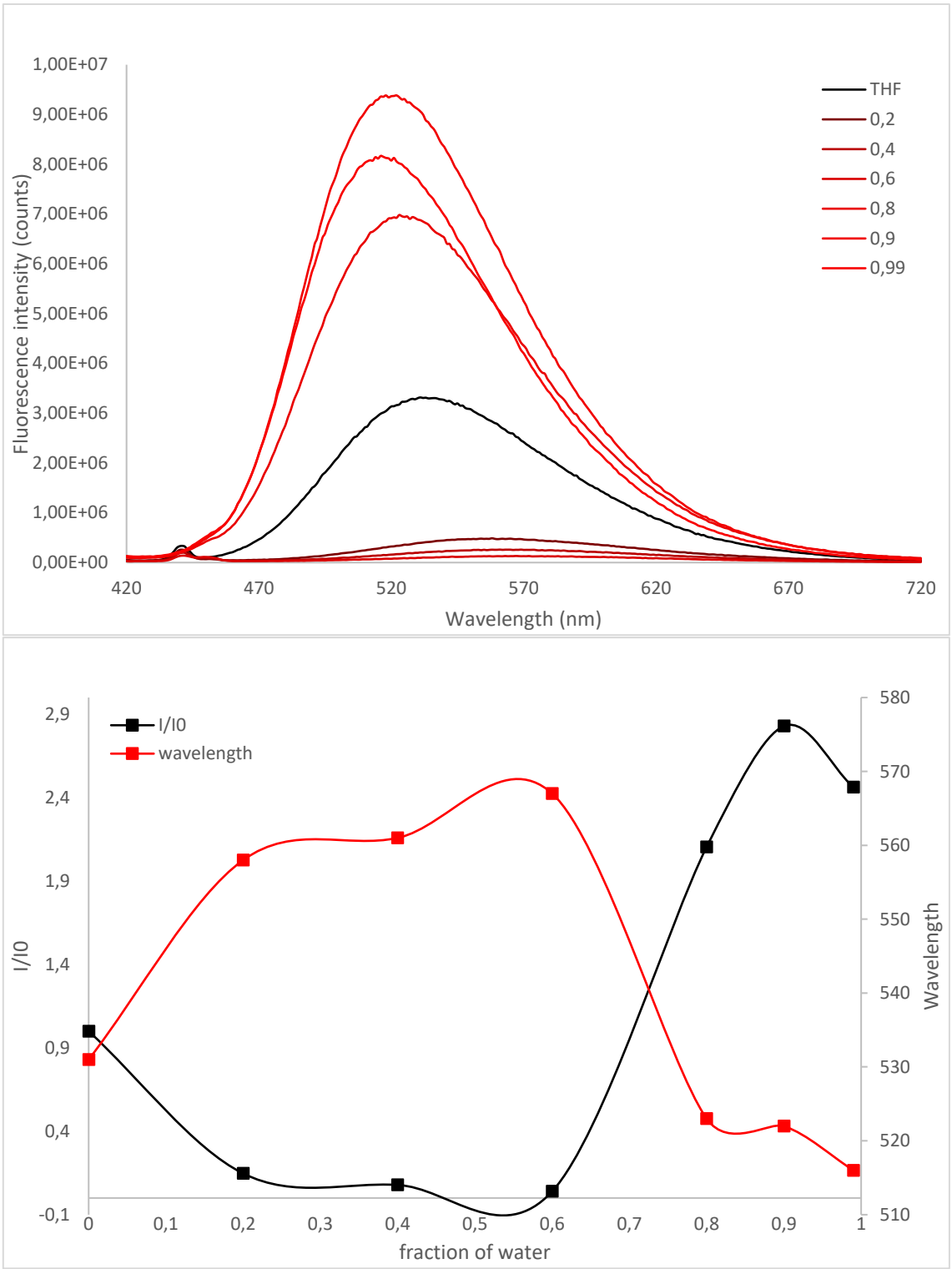

Figure S49: Top: Fluorescence intensity against wavelength depending on fraction of water (f_w) of **C'2** at 298 K excited at 410 nm. Bottom: relative photoluminescence intensity (in black) and emission maximum wavelength against fraction of water (f_w) of **C'2** at 298 K in toluene solution excited at 410 nm.

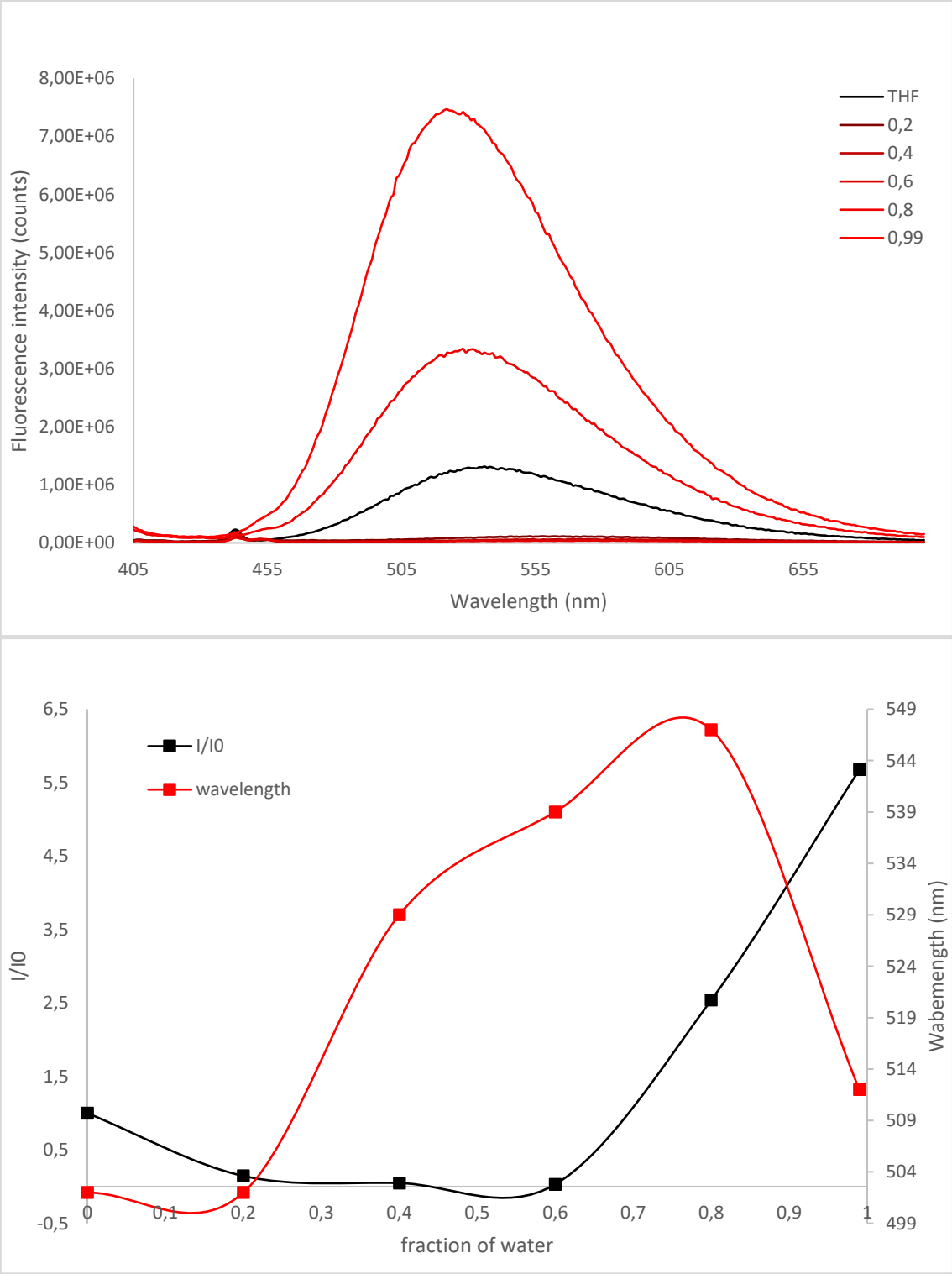

Figure S50: Top: Fluorescence intensity against wavelength depending on fraction of water (f_w) of **C'3** at 298 K excited at 390 nm. Bottom: relative photoluminescence intensity (in black) and emission maximum wavelength against fraction of water (f_w) of **C'3** at 298 K in toluene solution excited at 390 nm.

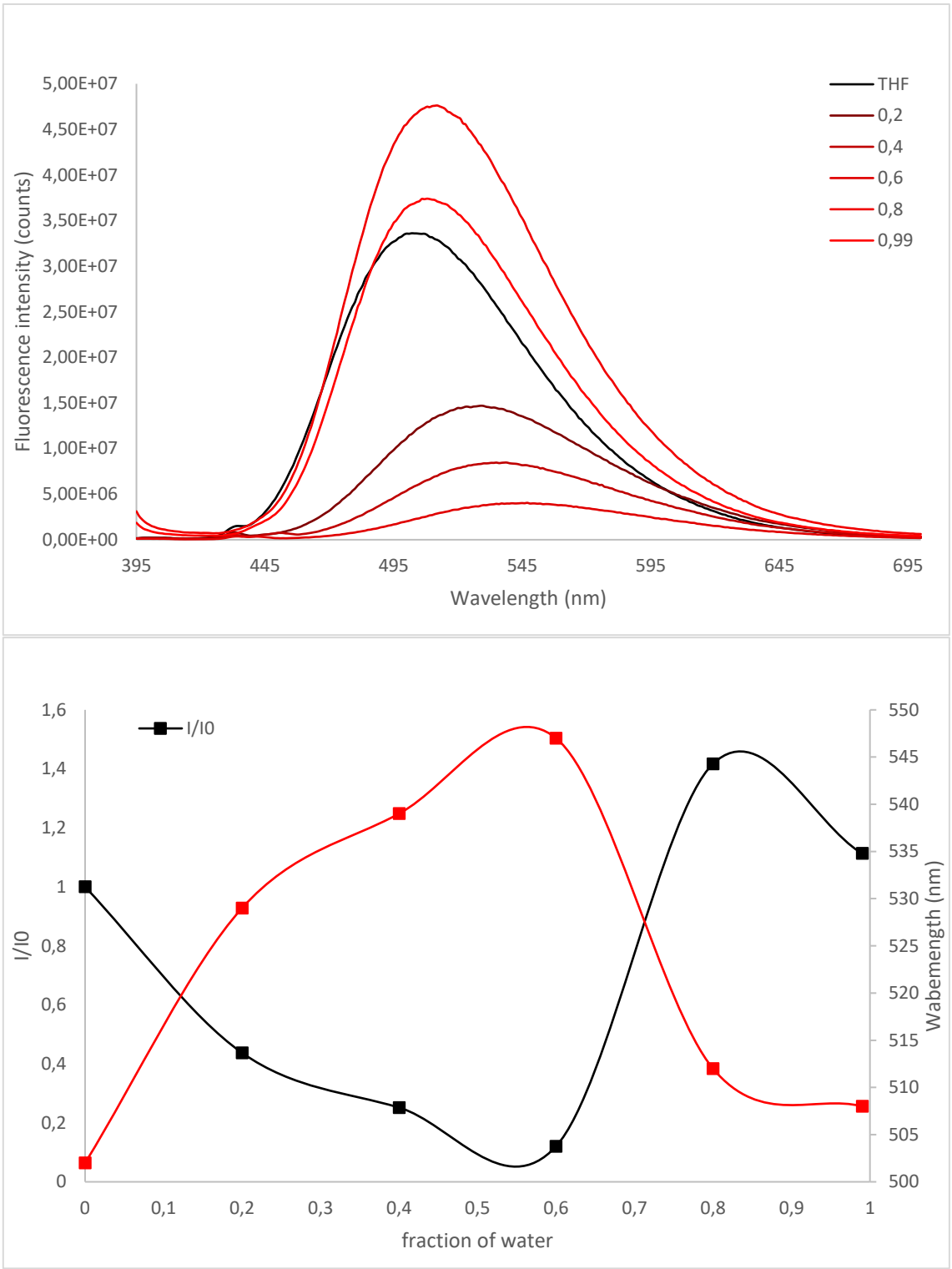

Figure S51: Top: Fluorescence intensity against wavelength depending on fraction of water (f_w) of **C1** at 298 K excited at 385 nm. Bottom: relative photoluminescence intensity (in black) and emission maximum wavelength against fraction of water (f_w) of **C1** at 298 K in toluene solution excited at 385 nm.

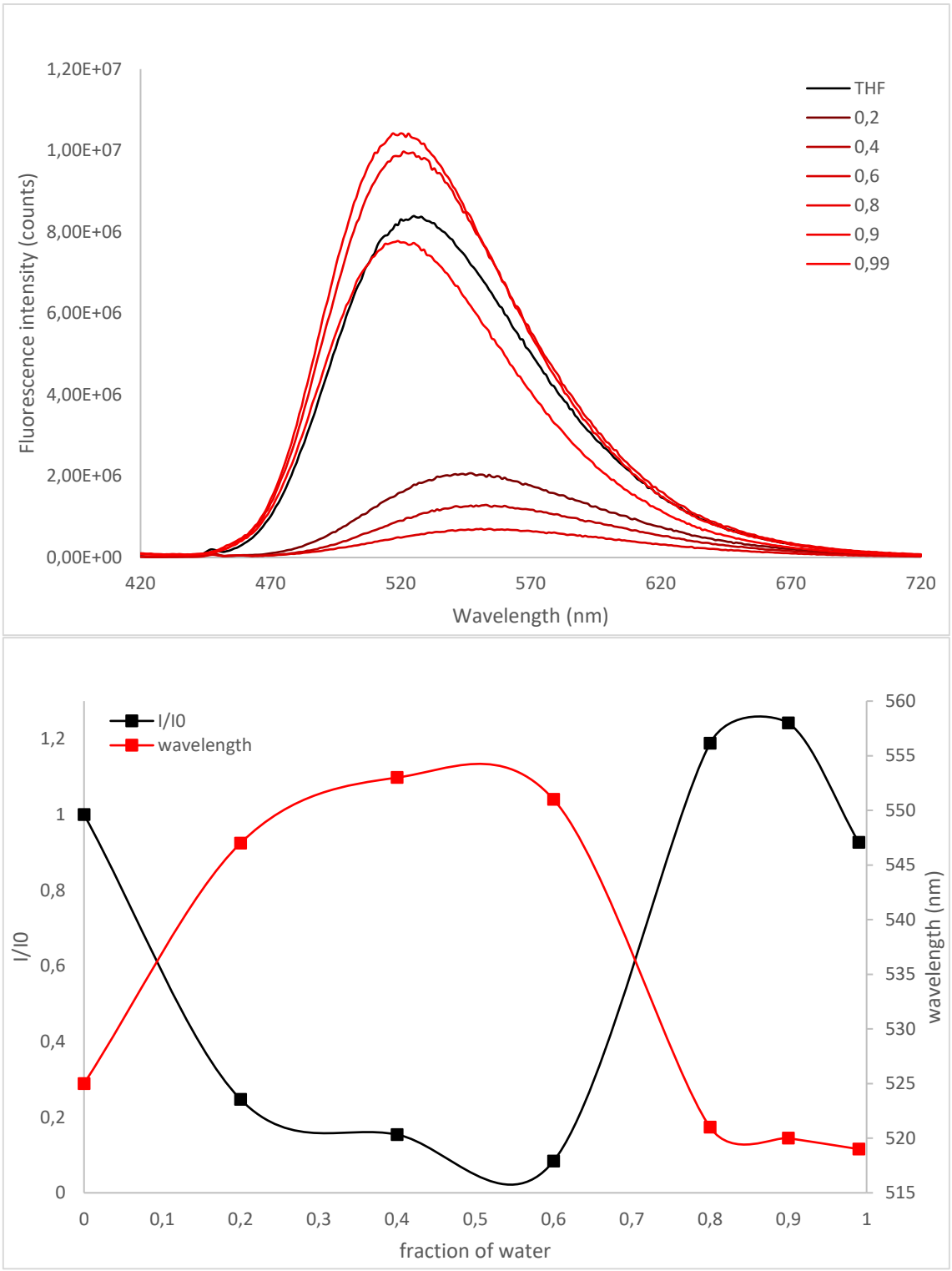

Figure S52: Top: Fluorescence intensity against wavelength depending on fraction of water (f_w) of **C2** at 298 K excited at 410 nm. Bottom: relative photoluminescence intensity (in black) and emission maximum wavelength against fraction of water (f_w) of **C2** at 298 K in toluene solution excited at 410 nm.

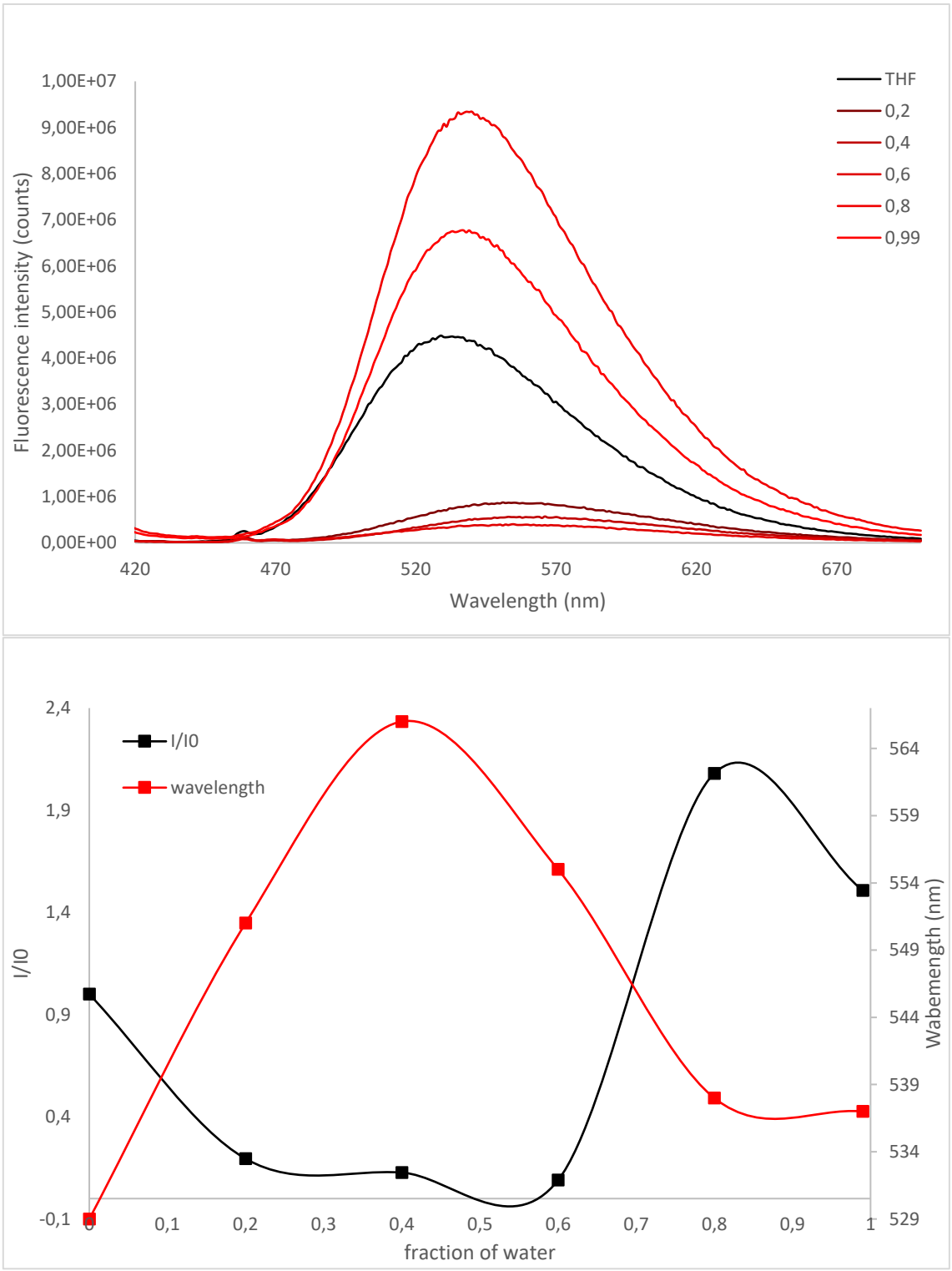

Figure S53: Top: Fluorescence intensity against wavelength depending on fraction of water (f_w) of **C3** at 298 K excited at 415 nm. Bottom: relative photoluminescence intensity (in black) and emission maximum wavelength against fraction of water (f_w) of **C3** at 298 K in toluene solution excited at 415 nm.

Photoluminescence lifetime

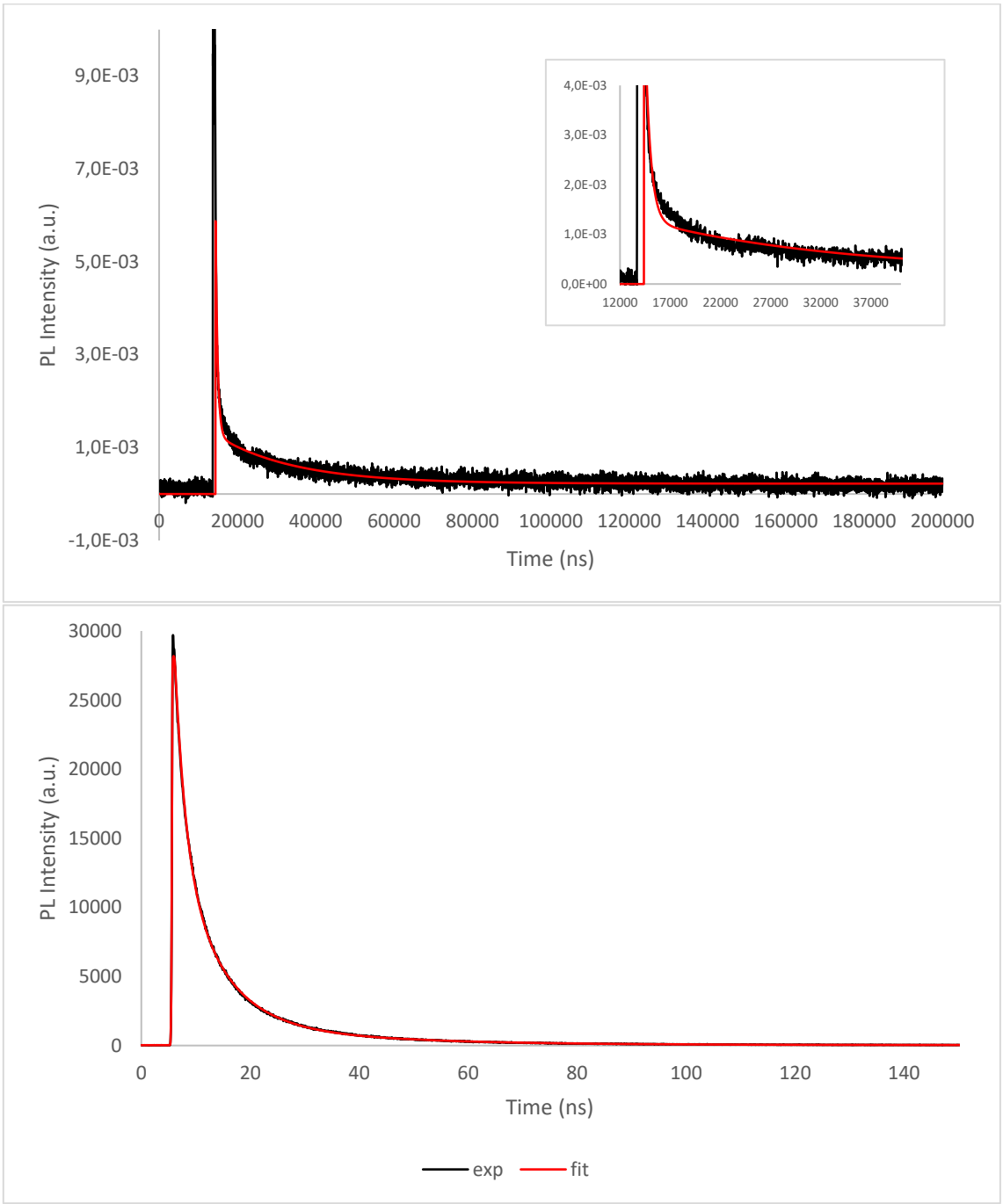

Figure S54: Top: Photoluminescence decay (µs regime) of **B1** in PMMA film at 298 K. Bottom: Photoluminescence decay (ns regime) of **B1** in PMMa film at 298 K. Instrumental response in black and exponential fit in red.

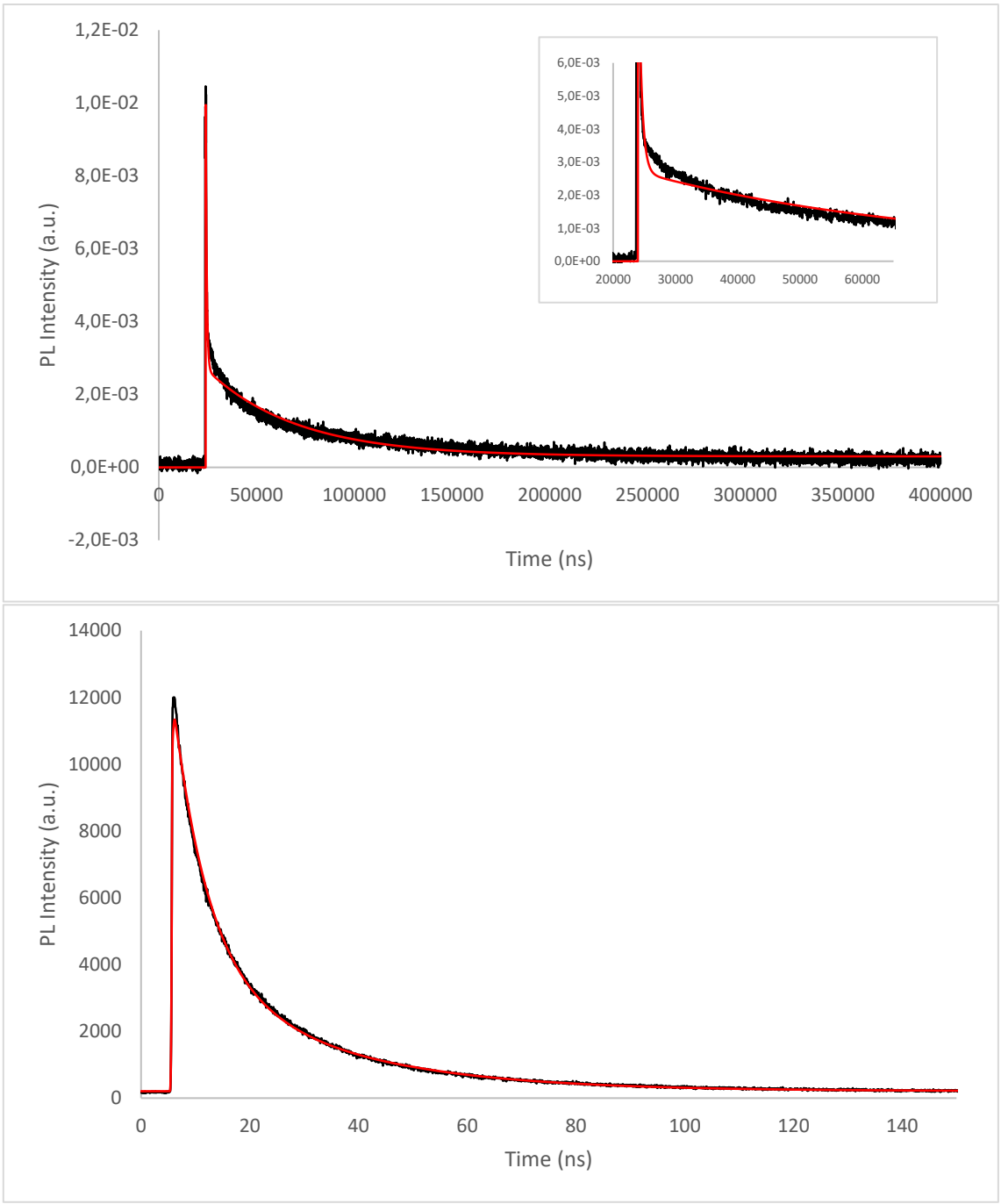

Figure S55: Top: Photoluminescence decay (µs regime) of **B2** in PMMA film at 298 K. Bottom: Photoluminescence decay (ns regime) of **B2** in PMMa film at 298 K. Instrumental response in black and exponential fit in red.

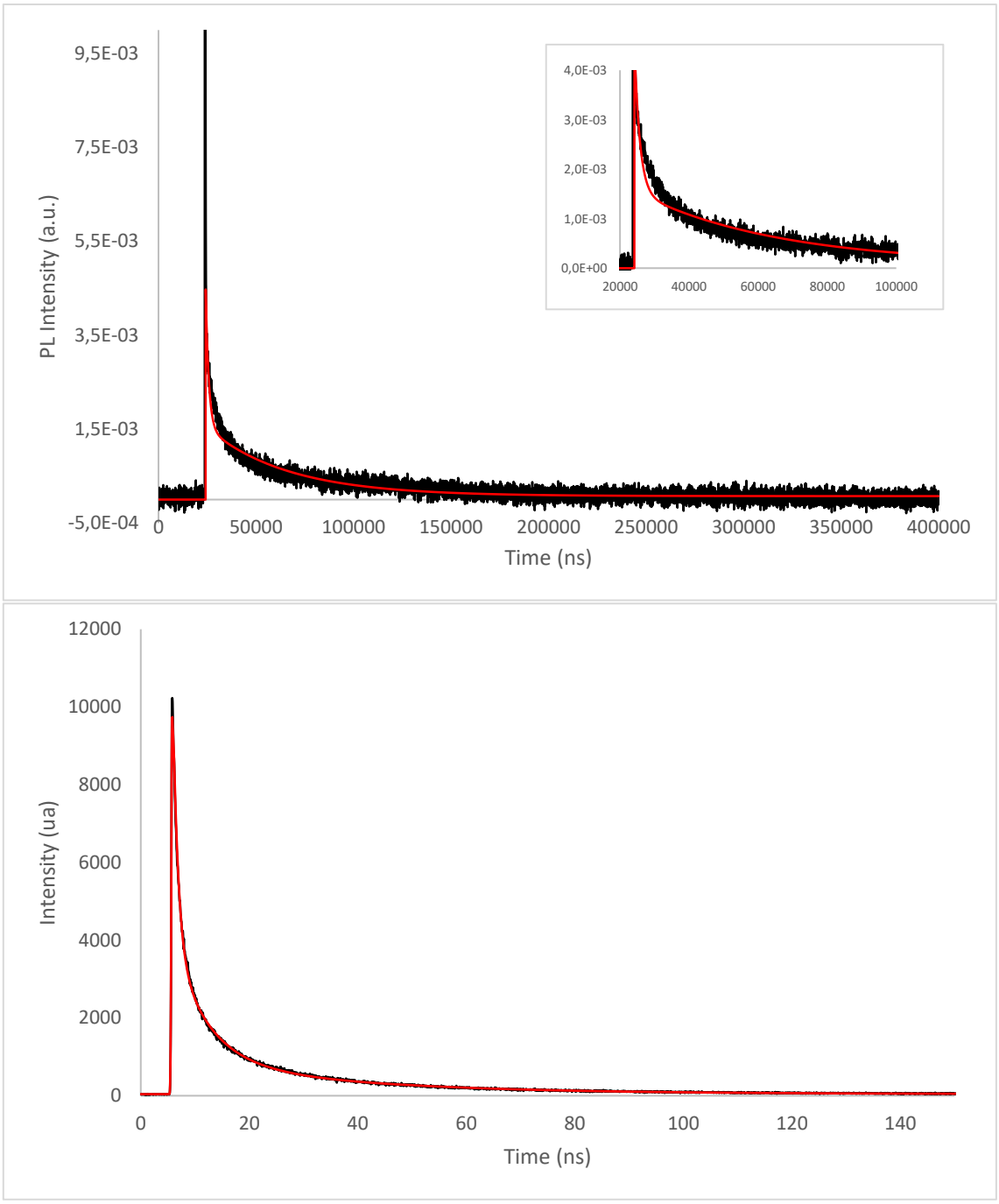

Figure S56: Top: Photoluminescence decay (µs regime) of **B3** in PMMA film at 298 K. Bottom: Photoluminescence decay (ns regime) of **B3** in PMMa film at 298 K. Instrumental response in black and exponential fit in red.

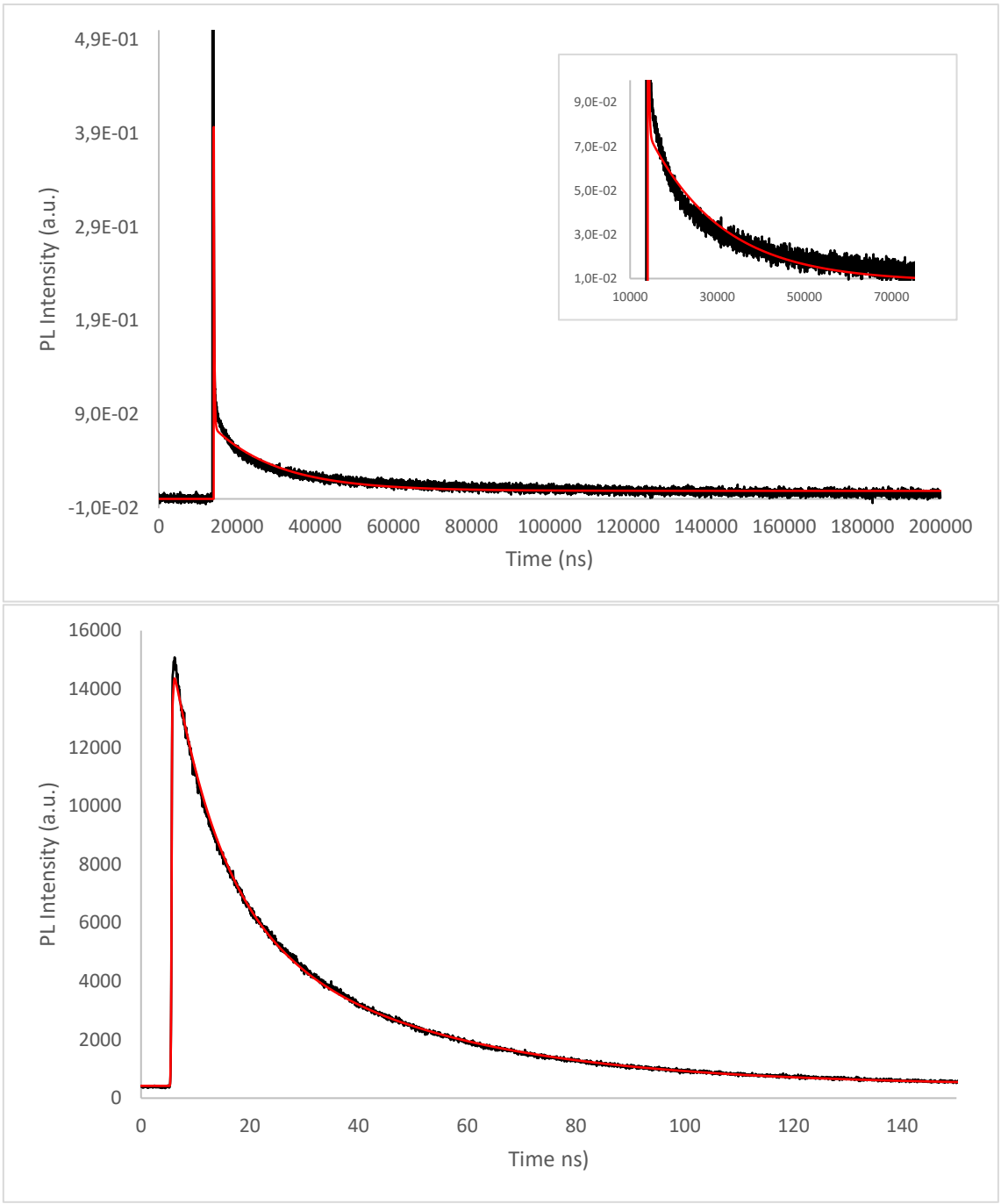

Figure S57: Top: Photoluminescence decay (µs regime) of **B4** in PMMA film at 298 K. Bottom: Photoluminescence decay (ns regime) of **B4** in PMMa film at 298 K. Instrumental response in black and exponential fit in red.

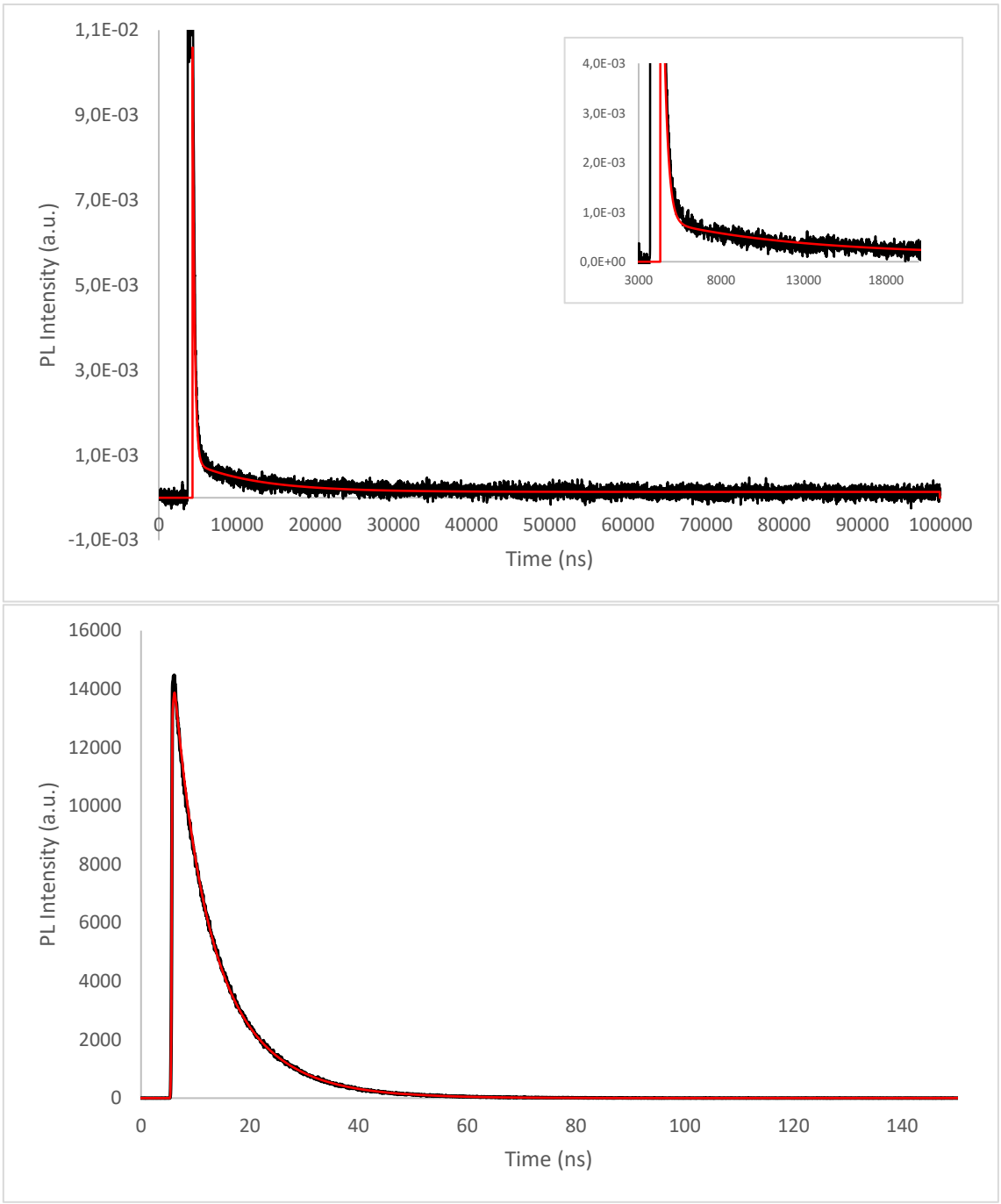

Figure S58: Top: Photoluminescence decay (µs regime) of **C'1** in PMMA film at 298 K. Bottom: Photoluminescence decay (ns regime) of **C'1** in PMMa film at 298 K. Instrumental response in black and exponential fit in red.

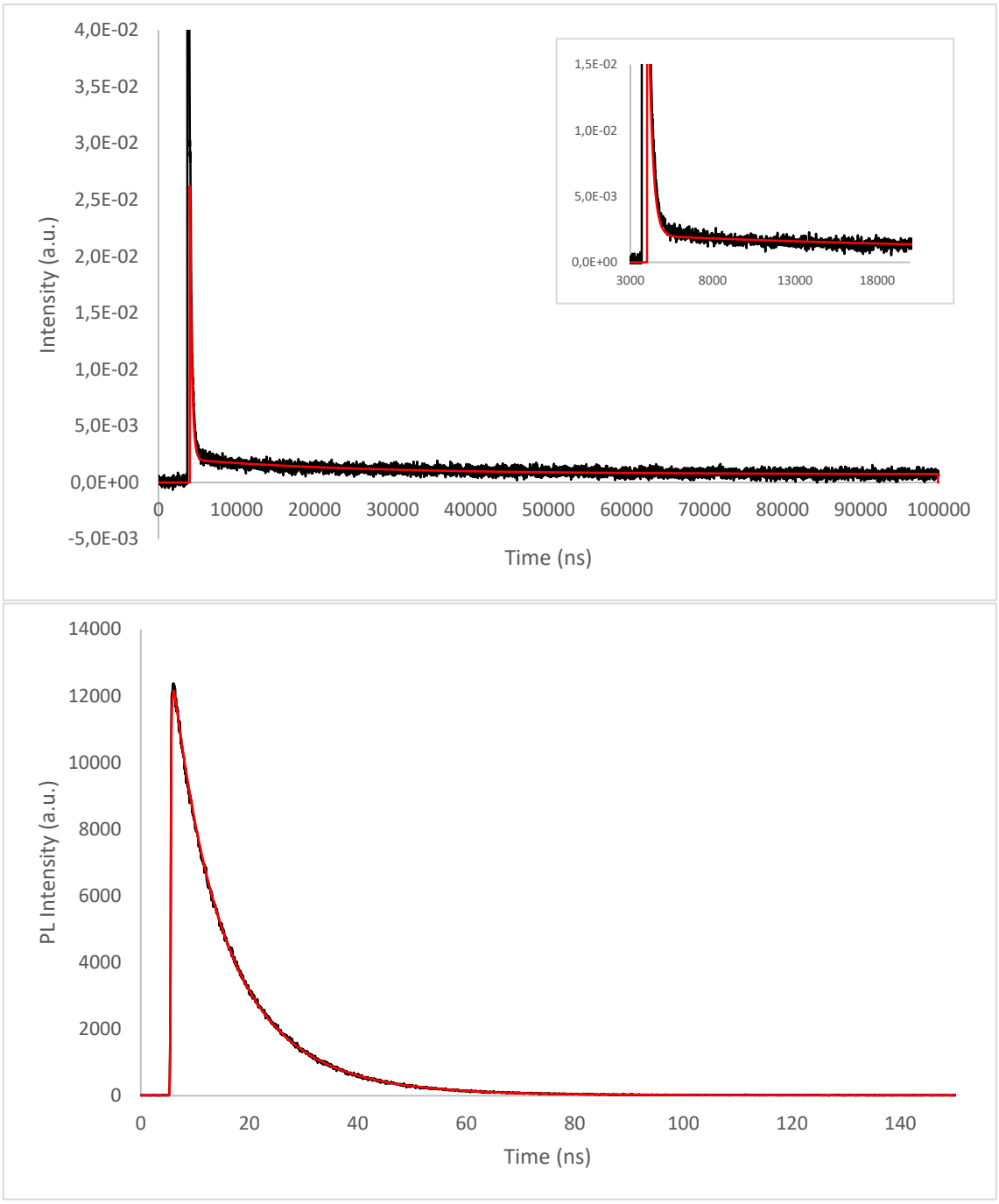

Figure 59: Top: Photoluminescence decay (µs regime) of **C'2** in PMMA film at 298 K. Bottom: Photoluminescence decay (ns regime) of **C'2** in PMMa film at 298 K. Instrumental response in black and exponential fit in red.

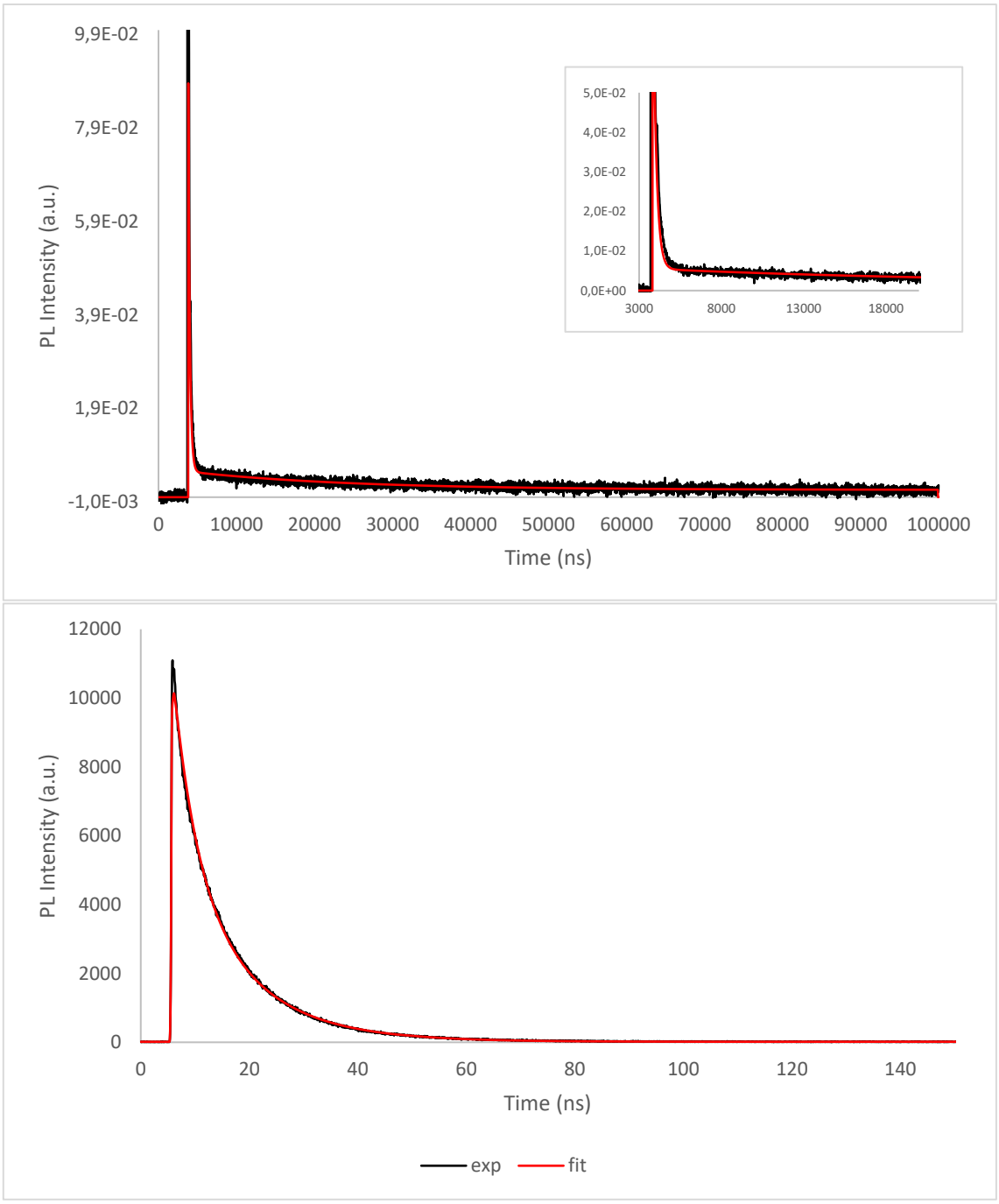

Figure S60: Top: Photoluminescence decay (µs regime) of **C'3** in PMMA film at 298 K. Bottom: Photoluminescence decay (ns regime) of **C'3** in PMMa film at 298 K. Instrumental response in black and exponential fit in red.

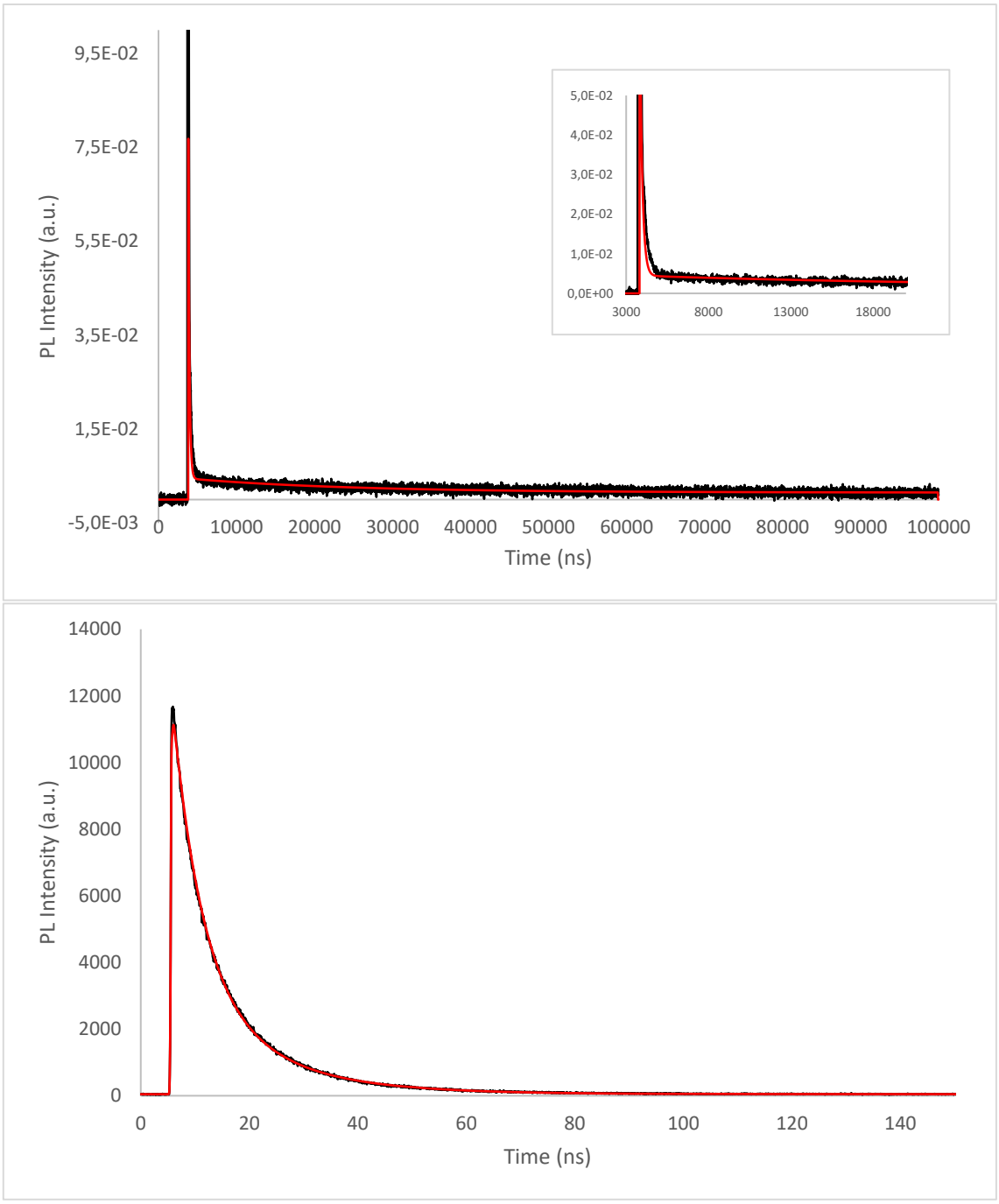

Figure S61: Top: Photoluminescence decay (µs regime) of **C1** in PMMA film at 298 K. Bottom: Photoluminescence decay (ns regime) of **C1** in PMMa film at 298 K. Instrumental response in black and exponential fit in red.

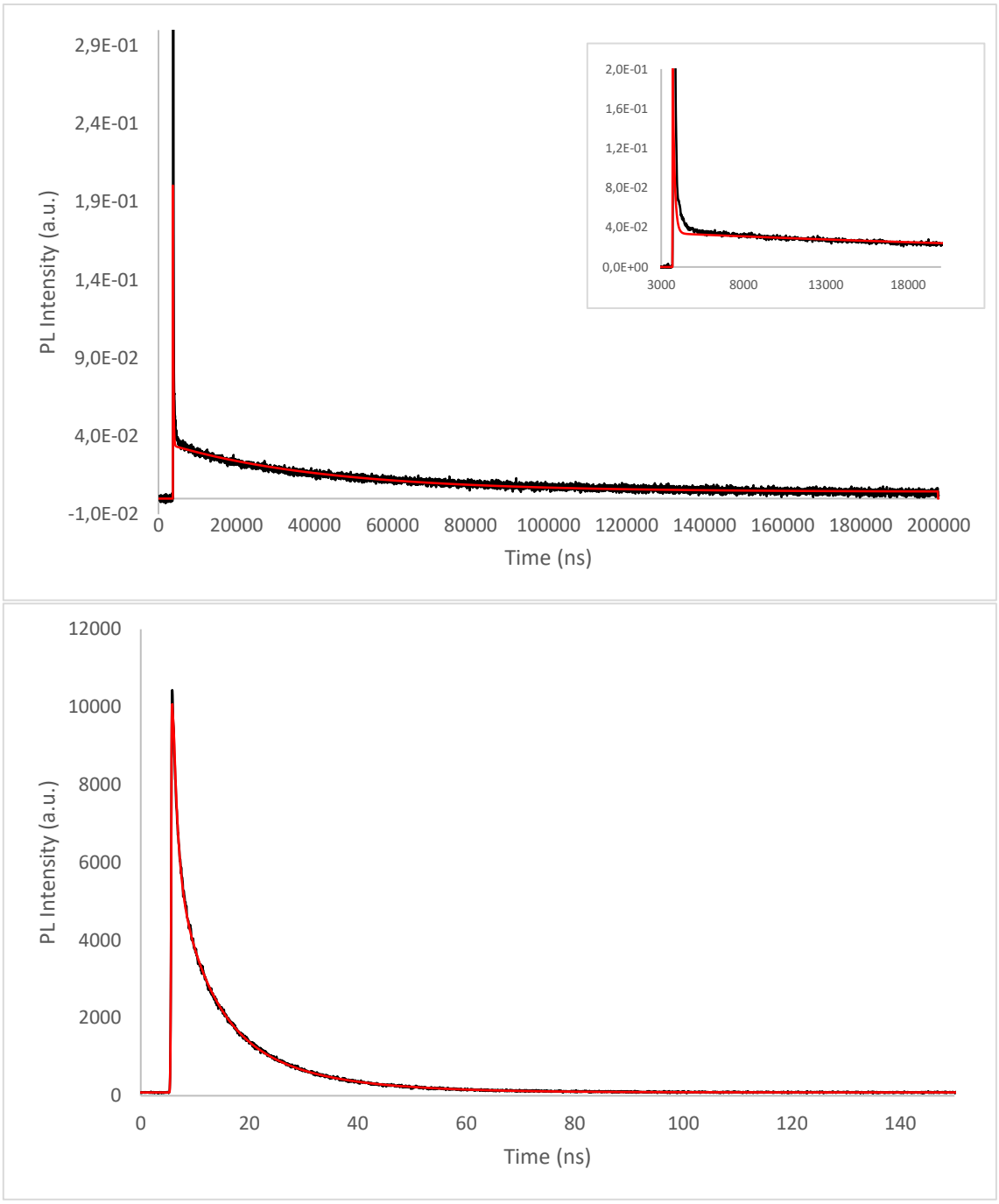

Figure S62: Top: Photoluminescence decay (μs regime) of **C2** in PMMA film at 298 K. Bottom: Photoluminescence decay (ns regime) of **C2** in PMMa film at 298 K. Instrumental response in black and exponential fit in red.

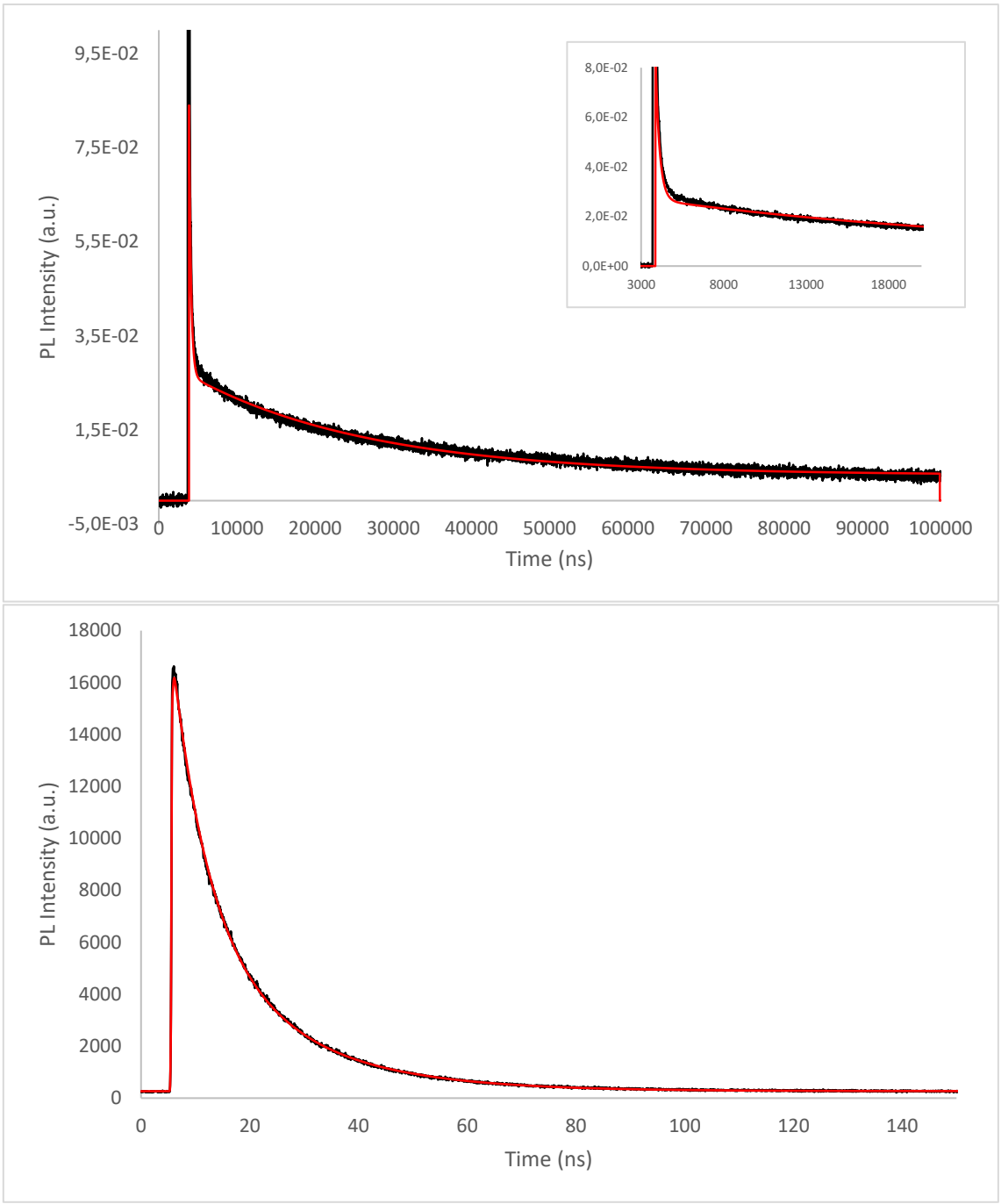

Figure S63: Top: Photoluminescence decay (µs regime) of **C3** in PMMA film at 298 K. Bottom: Photoluminescence decay (ns regime) of **C3** in PMMa film at 298 K. Instrumental response in black and exponential fit in red.

Compound	Φ_F (PMMA film)	R_{prompt}	$R_{delayed}$	Φ_{PF}	Φ_{PF}	k_{PF} (×10^6 s^{-1})	k_{DF} (×10^3 s^{-1})	k_{ISC} (×10^6 s^{-1})	k_{RISC} (×10^3 s^{-1})	Φ_{ISC}	Φ_{RISC}
B1	0,07	0,27	0,73	0,02	0,05	3,02	3,18	1,93	0,16	0,64	0,05
B2	0,16	0,04	0,96	0,01	0,15	0,46	3,32	0,44	0,51	0,96	0,13
B3	0,18	0,07	0,93	0,01	0,17	2,30	3,94	2,12	0,65	0,92	0,14
B4	0,22	0,05	0,95	0,01	0,21	0,47	12,6	0,45	2,67	0,95	0,18
C'1	0,29	0,31	0,69	0,09	0,20	9,39	19,1	5,16	3,84	0,55	0,18
C'2	0,46	0,18	0,82	0,08	0,38	7,99	16,1	6,24	6,11	0,78	0,29
C'3	0,42	0,18	0,82	0,07	0,34	8,70	15,6	6,81	5,33	0,78	0,27
C1	0,20	0,15	0,85	0,03	0,17	3,68	7,73	3,01	1,31	0,82	0,15
C2	0,41	0,02	0,98	0,01	0,40	1,47	9,96	1,44	4,00	0,98	0,29
C3	0,47	0,03	0,97	0,01	0,46	1,20	19,9	1,17	9,14	0,97	0,32

Table S3: Photophysical constants of PMMA films of every compounds

Abbreviations: Φ_F, absolute photoluminescence quantum yield; R_{prompt} and $R_{delayed}$, individual component ratio for respectively prompt and delayed fluorescence ($R_{prompt} = \frac{\tau_{PF} \times A_{PF}}{\sum \tau_i \times A_i}$ and $R_{delayed} = 1 - R_{prompt}$, where A_i is preexponential term for lifetime τ_i); Φ_{PF} and Φ_{PF} , fluorescent and delayed components, respectively, determined from the total Φ_F and the proportion of the integrated area of each of the components in the transient spectra to the total integrated area; k_{PF} and k_{DF}, respectively, prompt and delayed fluorescence decay rate; k_{ISC}, internal conversion decay rate from S_1 to T_1; k_{RISC} intersystem crossing decay rate from S_1 to T_1; Φ_{ISC} and Φ_{RISC}, respectively, intersystem crossing and reverse intersystem crossing quantum yield.

The quantum efficiency and rates constants were determined using the following equations according to Huang's method[S13]

$$\Phi_{PF} = \Phi_F \times R_{prompt}$$

$$\Phi_{DF} = \Phi_F \times R_{delayed}$$

$$k_{PF} = \frac{\Phi_{PF}}{\tau_{PF}}$$

$$k_{DF} = \frac{\Phi_{DF}}{\tau_{DF}}$$

$$k_{ISC} = \frac{\Phi_{DF}}{\Phi_{DF} + \Phi_{PF}} k_{PF}$$

$$k_{RISC} = \frac{k_{DF} \times k_{PF}}{k_{ISC}} \times \frac{\Phi_{DF}}{\Phi_{PF}}$$

$$\Phi_{ISC} = \frac{k_{ISC}}{k_{PF}}$$

$$\Phi_{RISC} = \frac{k_{RISC}}{k_{DF} + k_{RISC} \times \Phi_{ISC}}$$

Cyclic Voltammetry

Summary table :

	E_{ox} (V)	E_{red} (V)
compound **B1**	1,55	-1,40
compound **B2**	1,44	-1,37
compound **B3**	1,44	-1,37
compound **B4**	1,36	-1,37
compound **C'1**	1,54	-1,30
compound **C'2**	1,47	-1,34
compound **C'3**	1,44	-1,30
compound **C1**	1,43	-1,34
compound **C2**	1,33	-1,40
compound **C3**	1,38 (1,54)[a]	-1,34

[a]Compound **C3** displays two oxidative potentials

Table S4: Oxidative and reductive potentials for every product

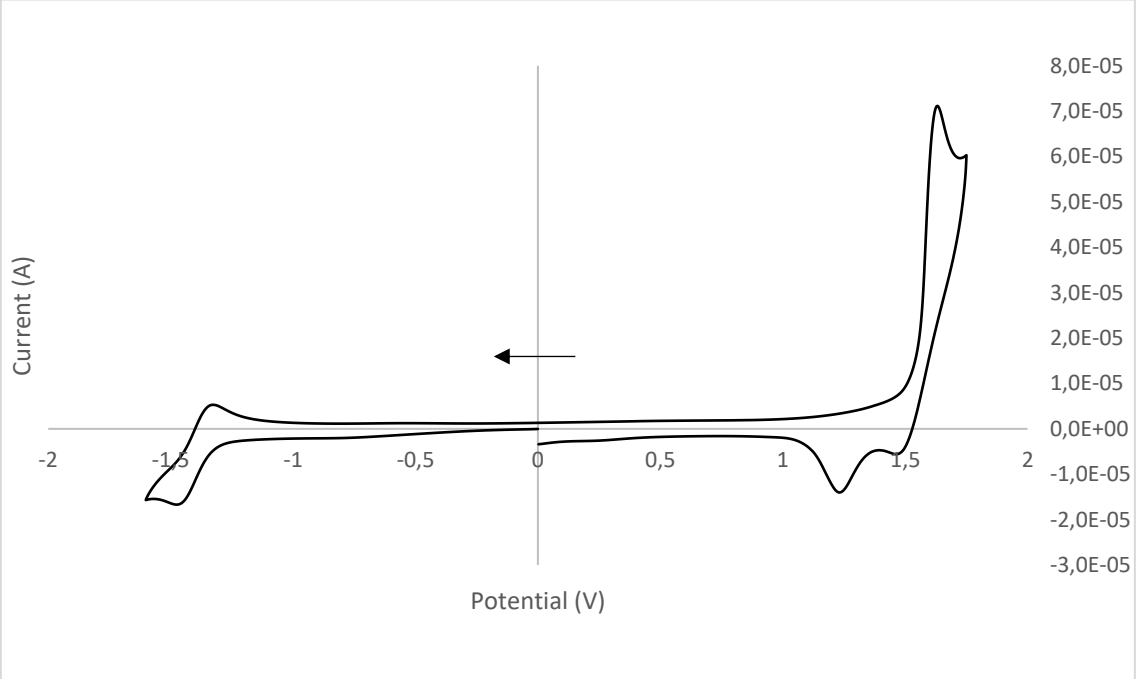

Figure S64: Cyclic voltametry graph for compound **B1.**

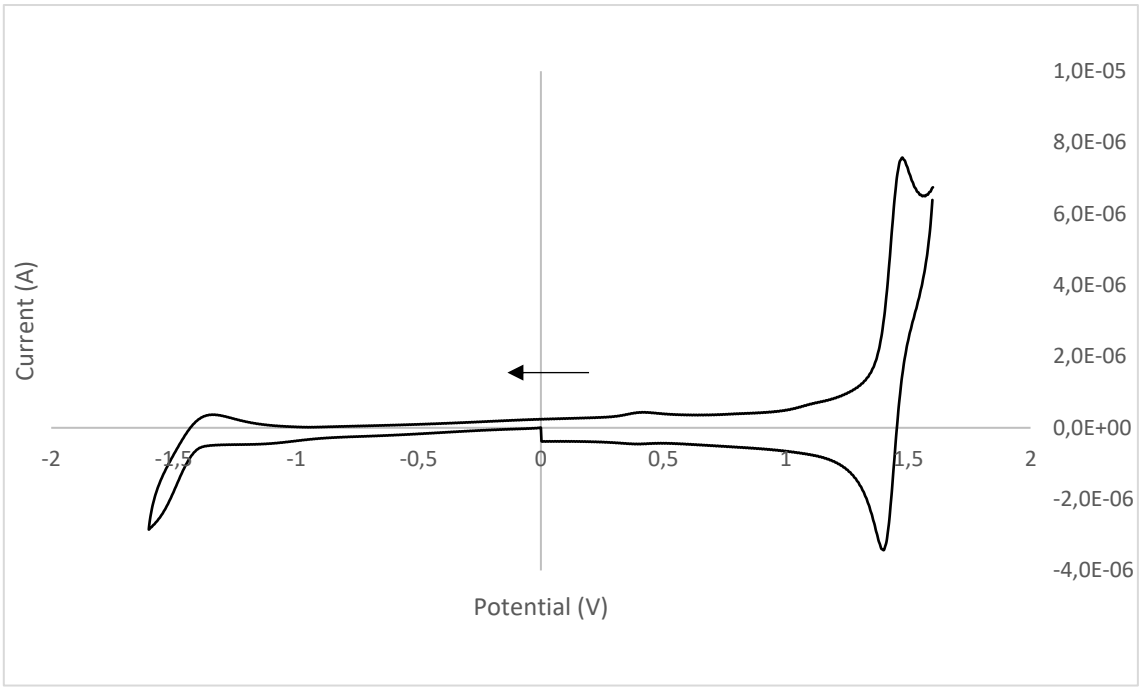

Figure S65: Cyclic voltametry graph for compound **B2.**

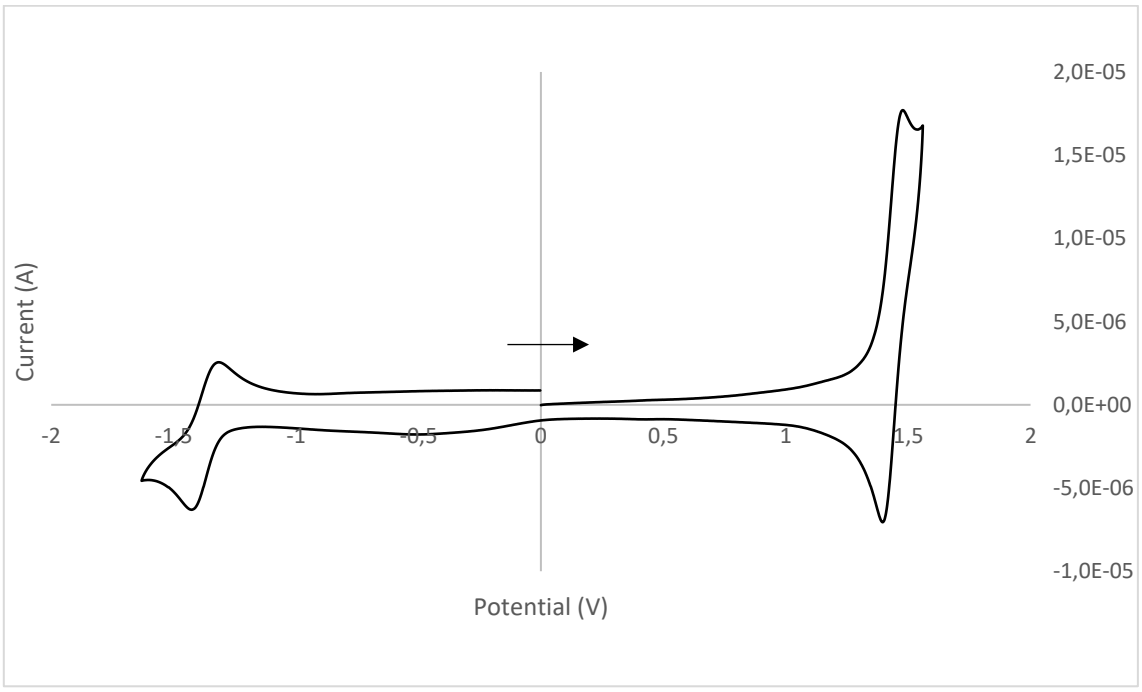

Figure S66: Cyclic voltametry graph for compound **B3.**

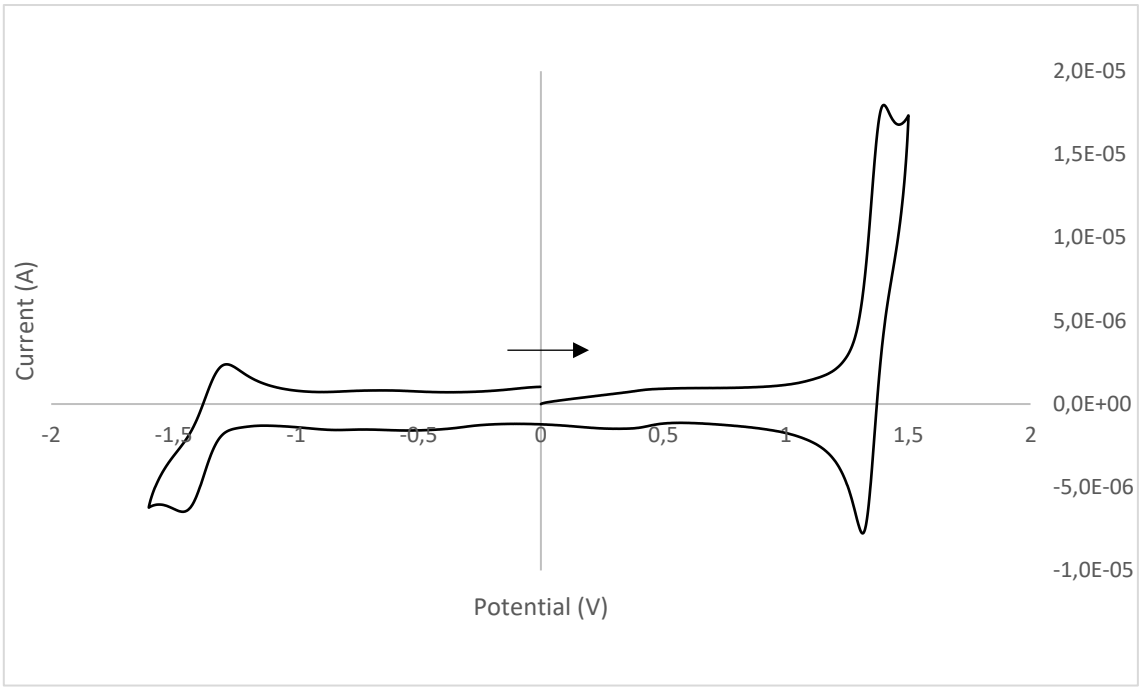

Figure S67: Cyclic voltametry graph for compound **B4.**

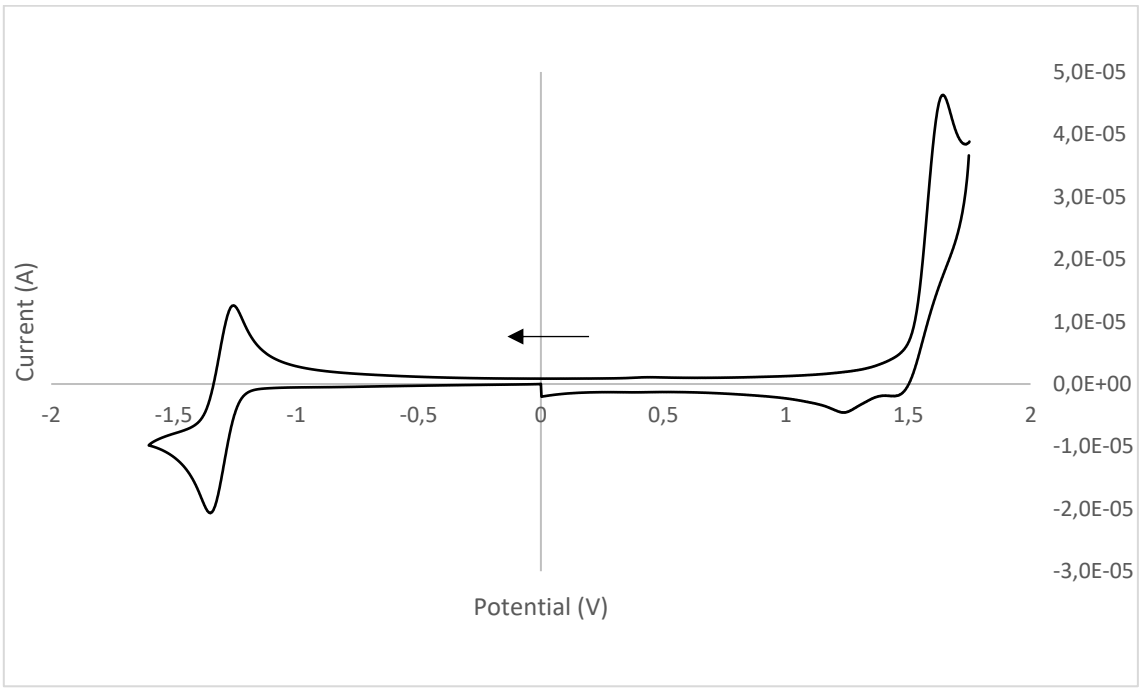

Figure S68: Cyclic voltametry graph for compound **C'1.**

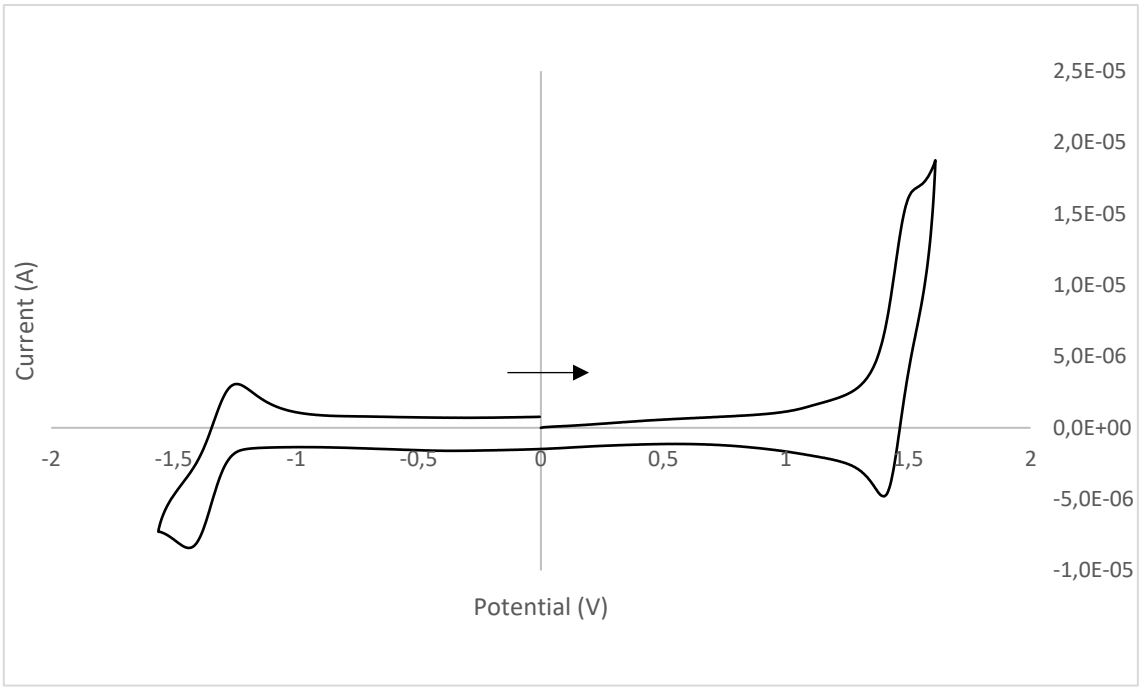

Figure S69: Cyclic voltametry graph for compound **C'2.**

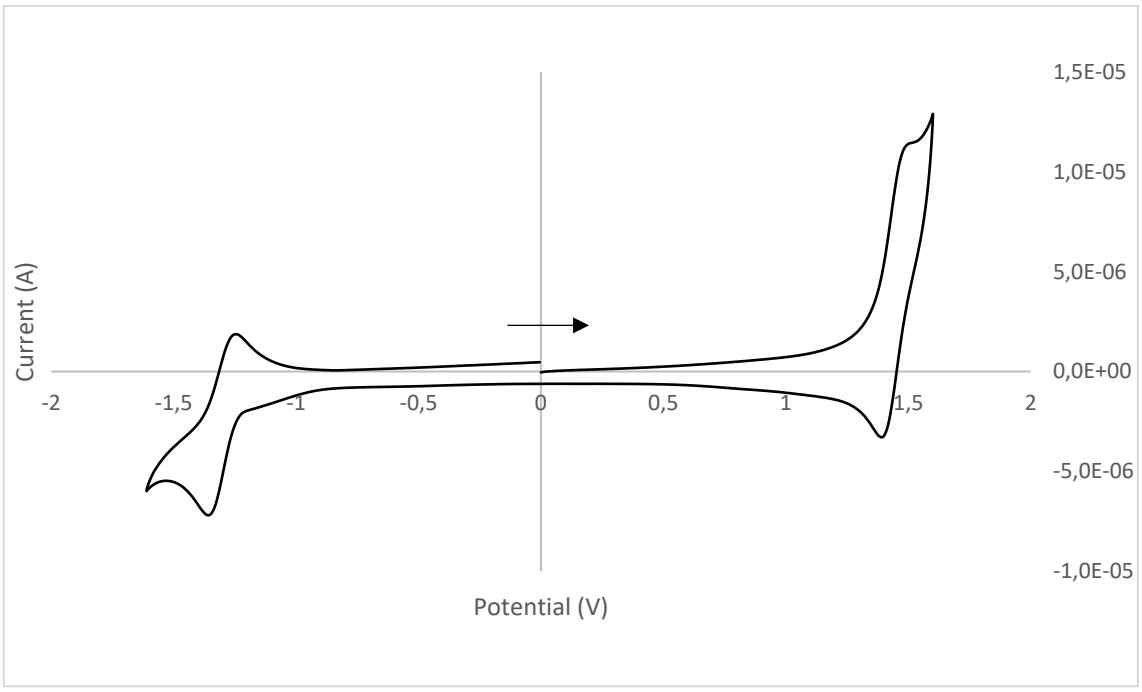

Figure S70: Cyclic voltametry graph for compound **C'3.**

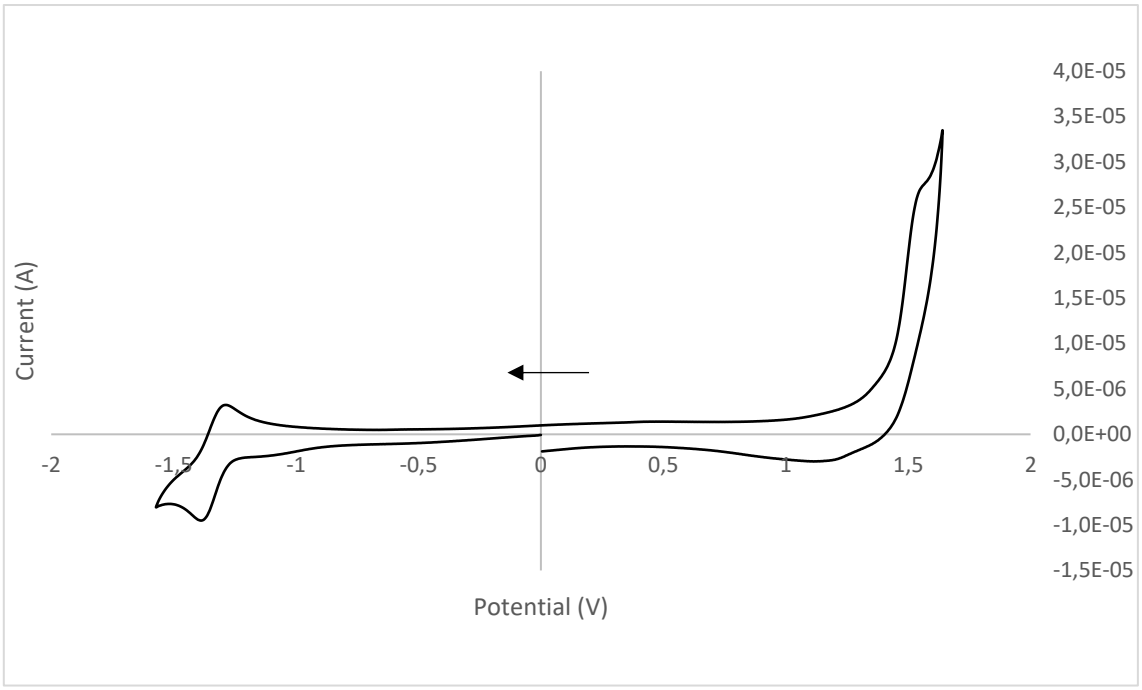

Figure S71: Cyclic voltametry graph for compound **C1.**

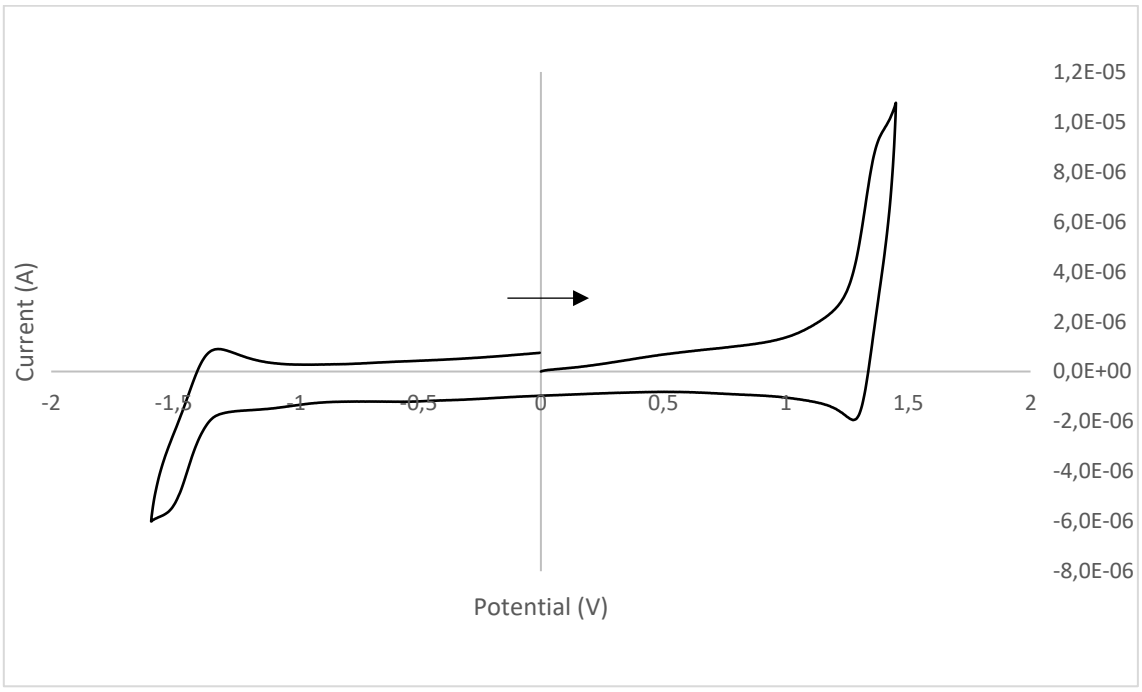

Figure S72: Cyclic voltametry graph for compound **C2.**

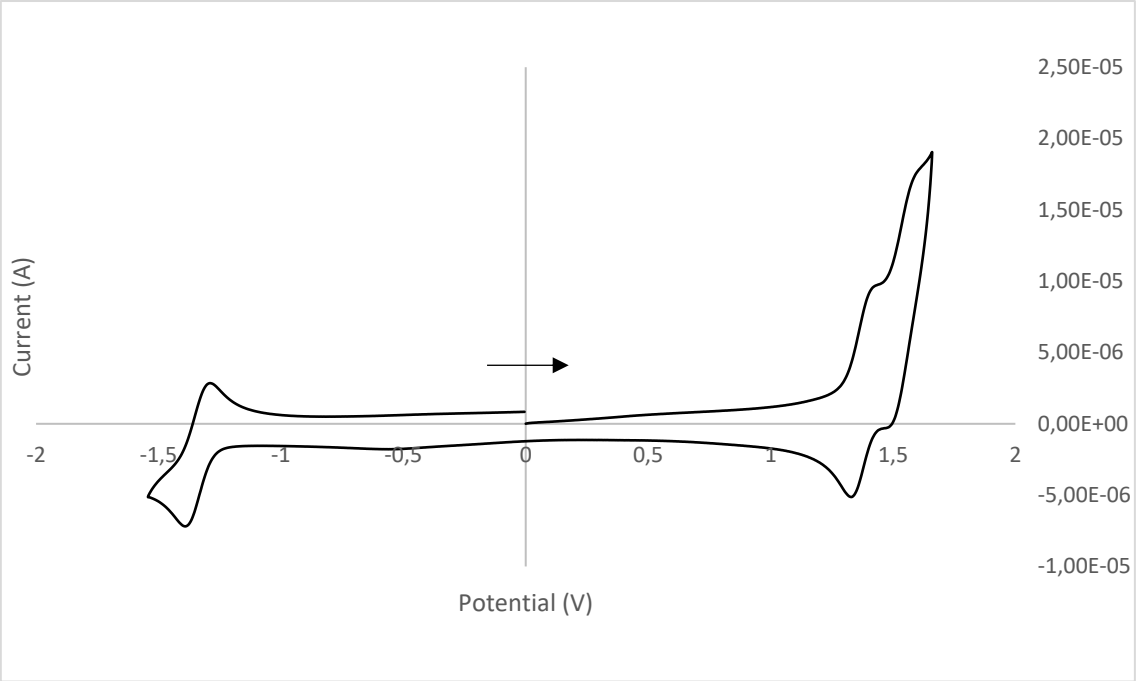

Figure S73: Cyclic voltametry graph for compound **C3.**

Computational results

Simulated UV-vis spectra

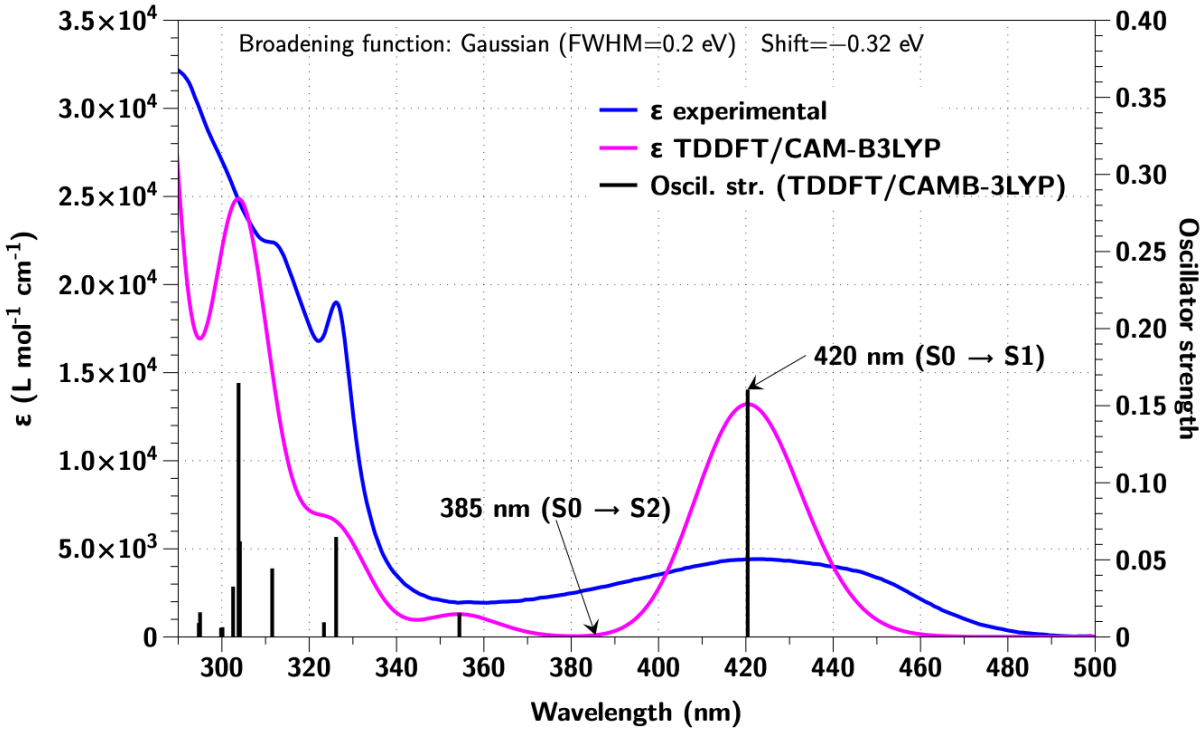

Figure S74: Comparison of the simulated UV-vis spectrum of **A1**. A spectral shift has been applied (-0.32 eV). Calculated excitation energy and oscillator strength indicated as 'stick' spectra (black), experimental and simulated spectra indicated as blue and pink curve respectively.

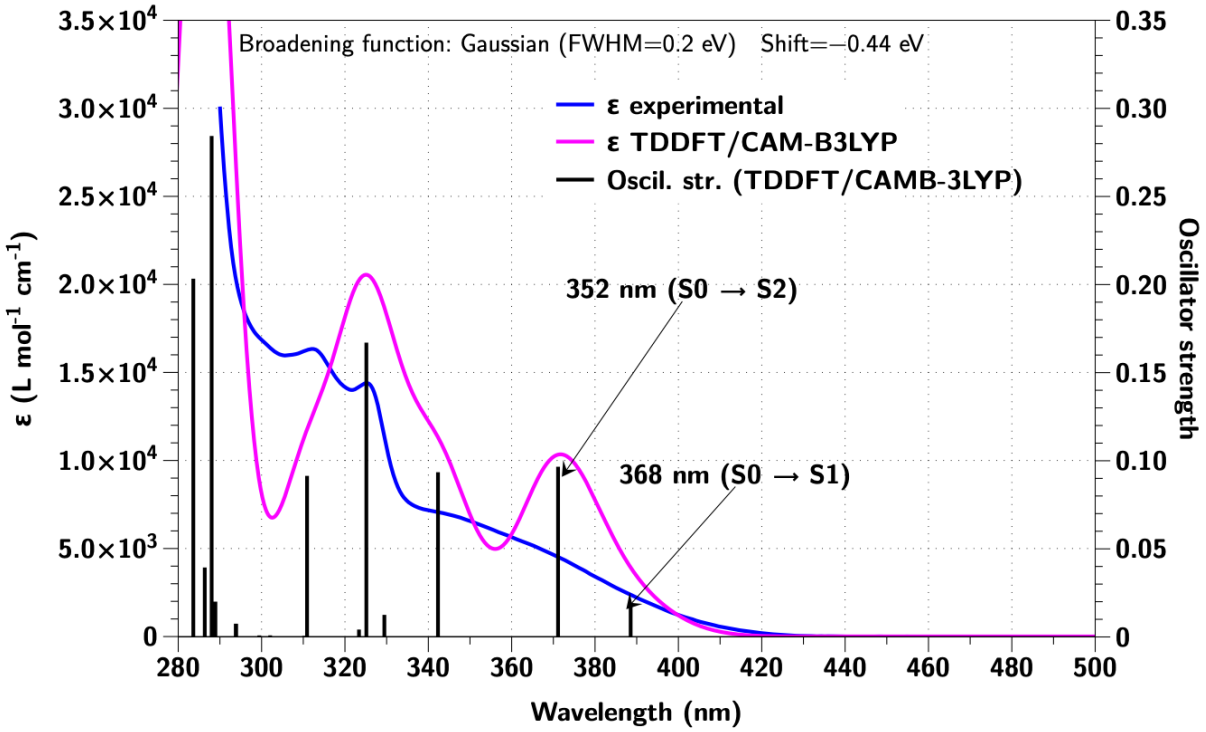

Figure S75: Comparison of the simulated UV-vis spectrum of **B1**. A spectral shift has been applied (-0.44 eV). Calculated excitation energiy and oscillator strength indicated as 'stick' spectra (black), experimental and simulated spectra indicated as blue and pink curve respectively.

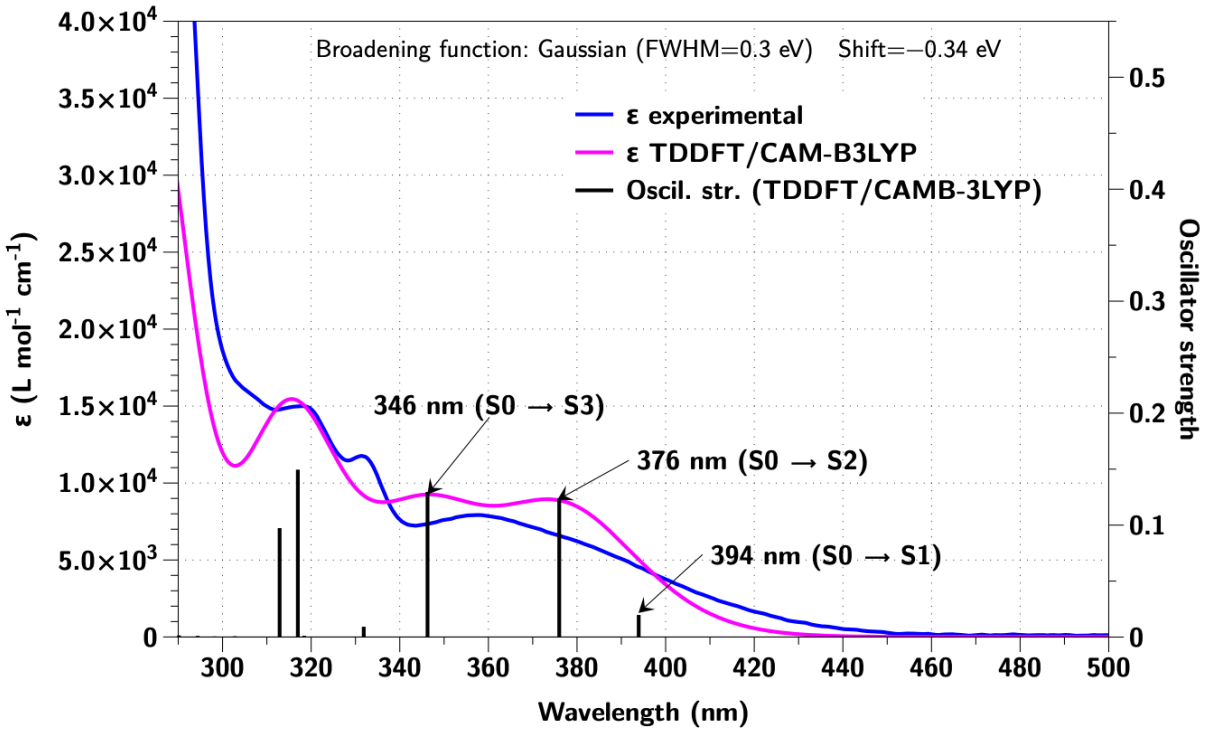

Figure S76: Comparison of the simulated UV-vis spectrum of **B2**. A spectral shift has been applied (-0.34 eV). Calculated excitation energy and oscillator strength indicated as 'stick' spectra (black), experimental and simulated spectra indicated as blue and pink curve respectively.

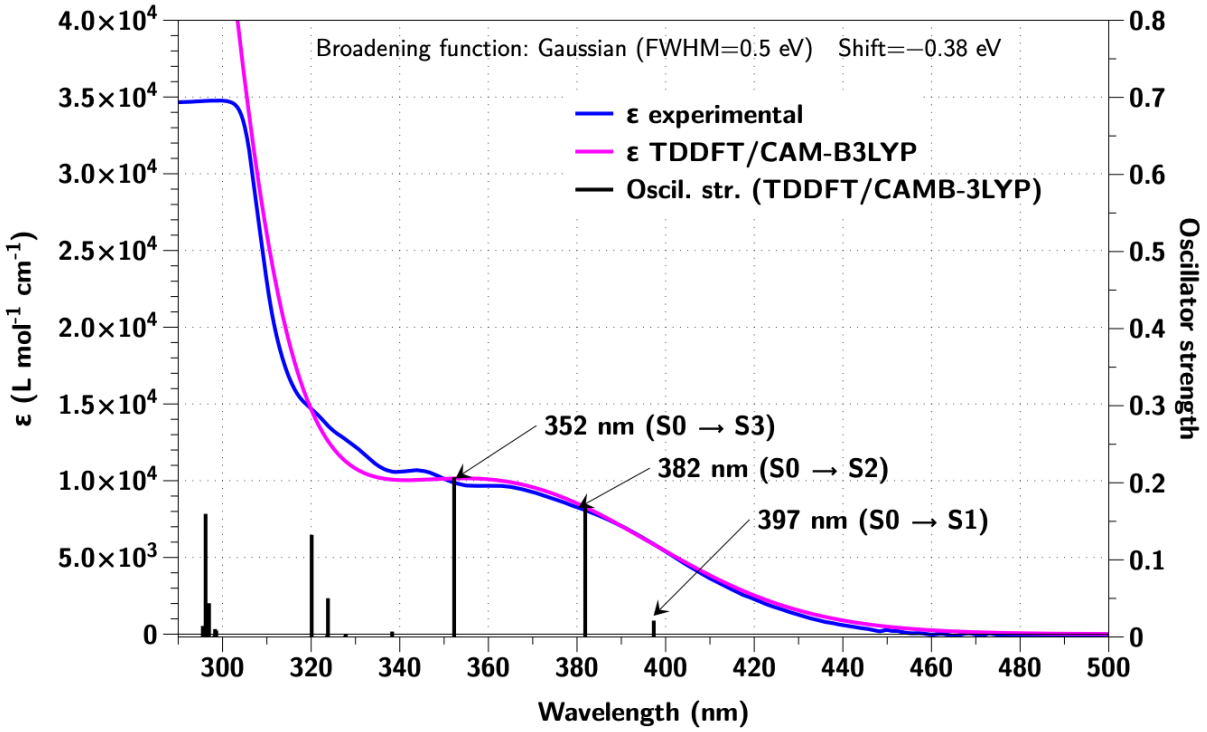

Figure S77: Comparison of the simulated UV-vis spectrum of **B3**. A spectral shift has been applied (-0.38 eV). Calculated excitation energy and oscillator strength indicated as 'stick' spectra (black), experimental and simulated spectra indicated as blue and pink curve respectively.

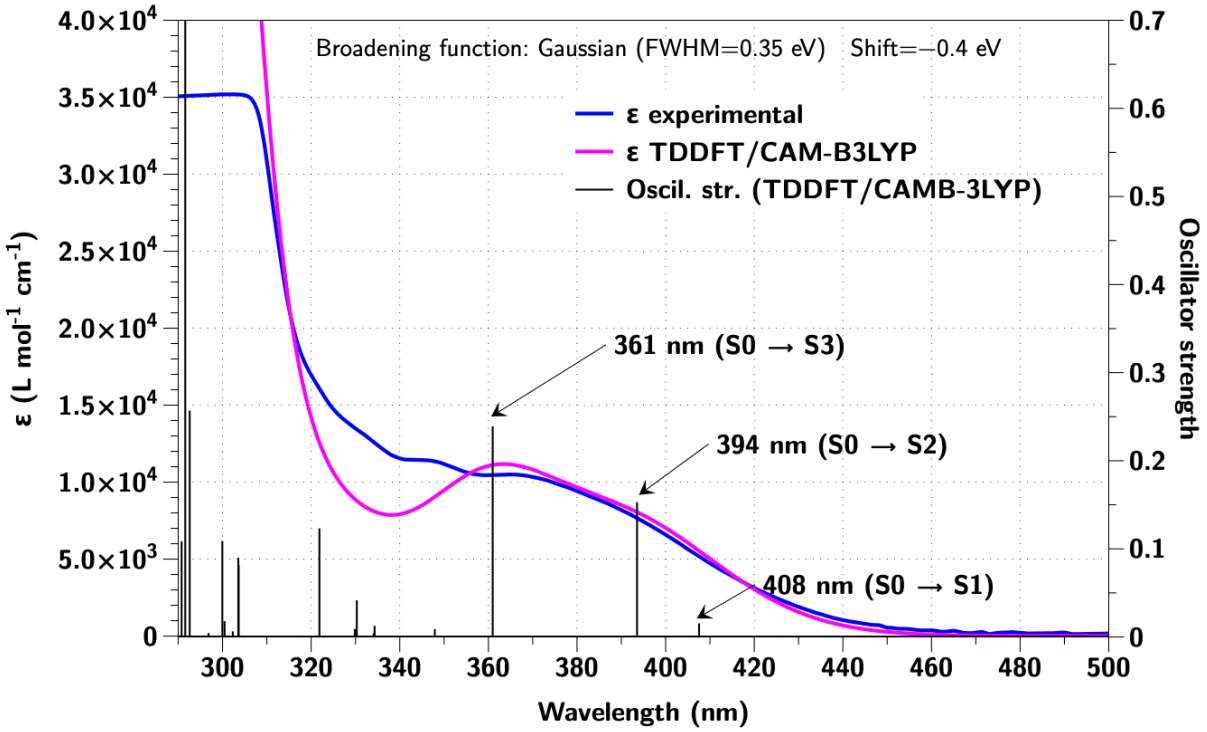

Figure S78: Comparison of the simulated UV-vis spectrum of **B4**. A spectral shift has been applied (-0.4 eV). Calculated excitation energy and oscillator strength indicated as 'stick' spectra (black), experimental and simulated spectra indicated as blue and pink curve respectively.

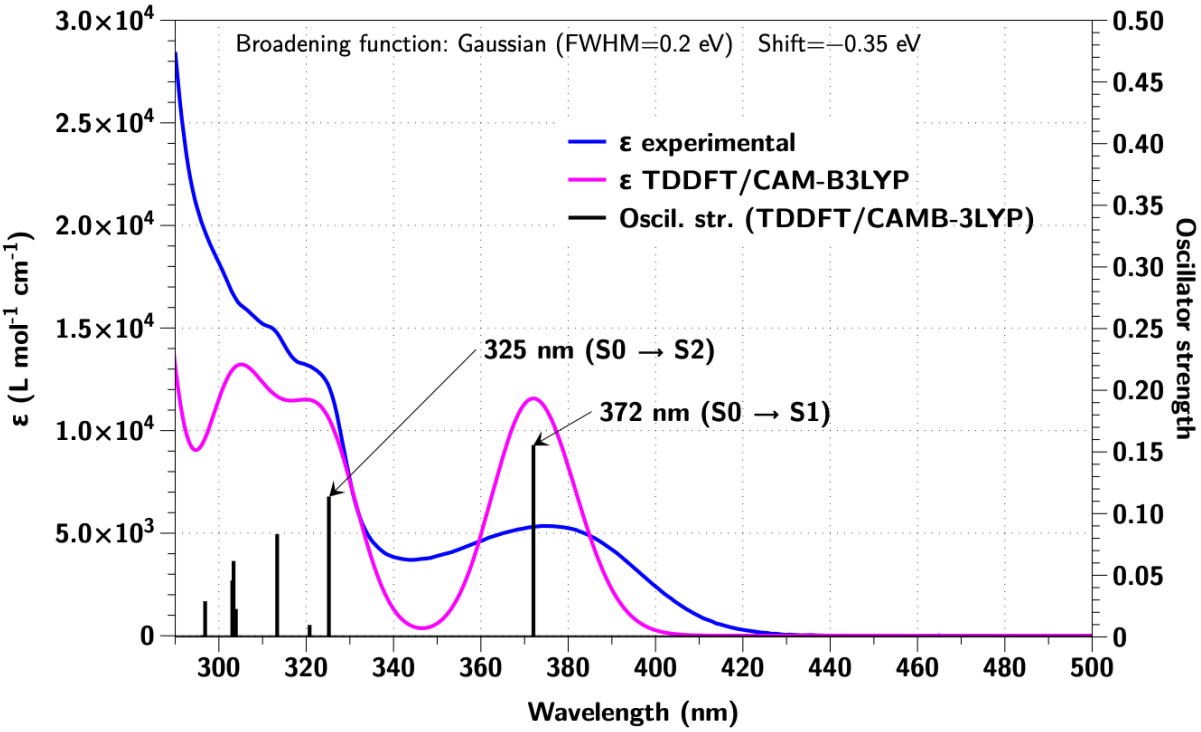

Figure S79: Comparison of the simulated UV-vis spectrum of **C'1**. A spectral shift has been applied (-0.35 eV). Calculated excitation energy and oscillator strength indicated as 'stick' spectra (black), experimental and simulated spectra indicated as blue and pink curve respectively.

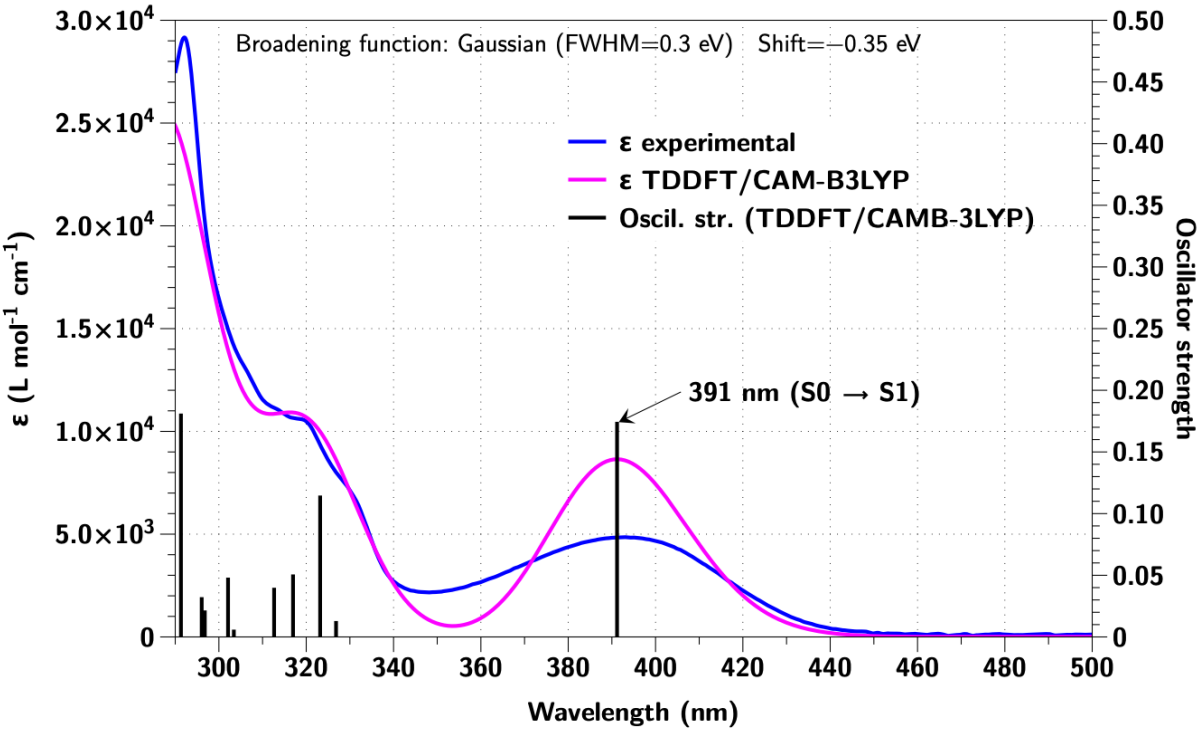

Figure S80: Comparison of the simulated UV-vis spectrum of **C'2**. A spectral shift has been

applied (-0.35 eV). Calculated excitation energy and oscillator strength indicated as 'stick' spectra (black), experimental and simulated spectra indicated as blue and pink curve respectively.

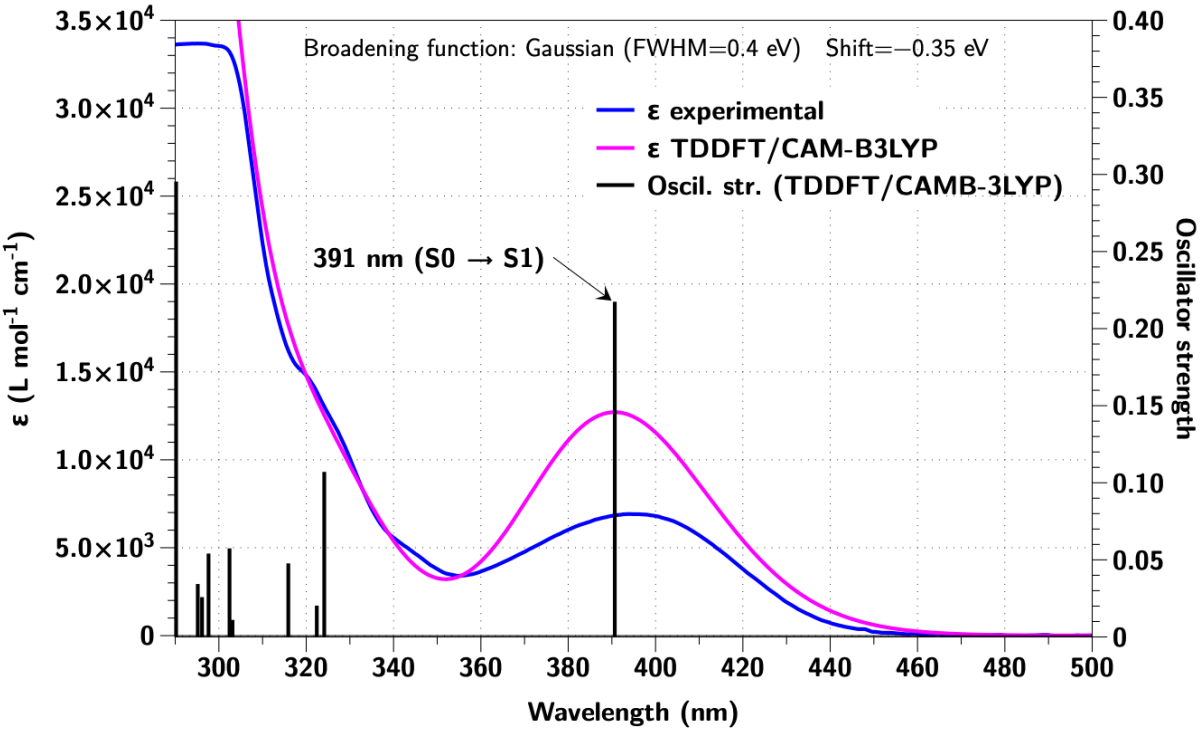

Figure S81: Comparison of the simulated UV-vis spectrum of **C'3**. A spectral shift has been applied (-0.35 eV). Calculated excitation energy and oscillator strength indicated as 'stick' spectra (black), experimental and simulated spectra indicated as blue and pink curve respectively.

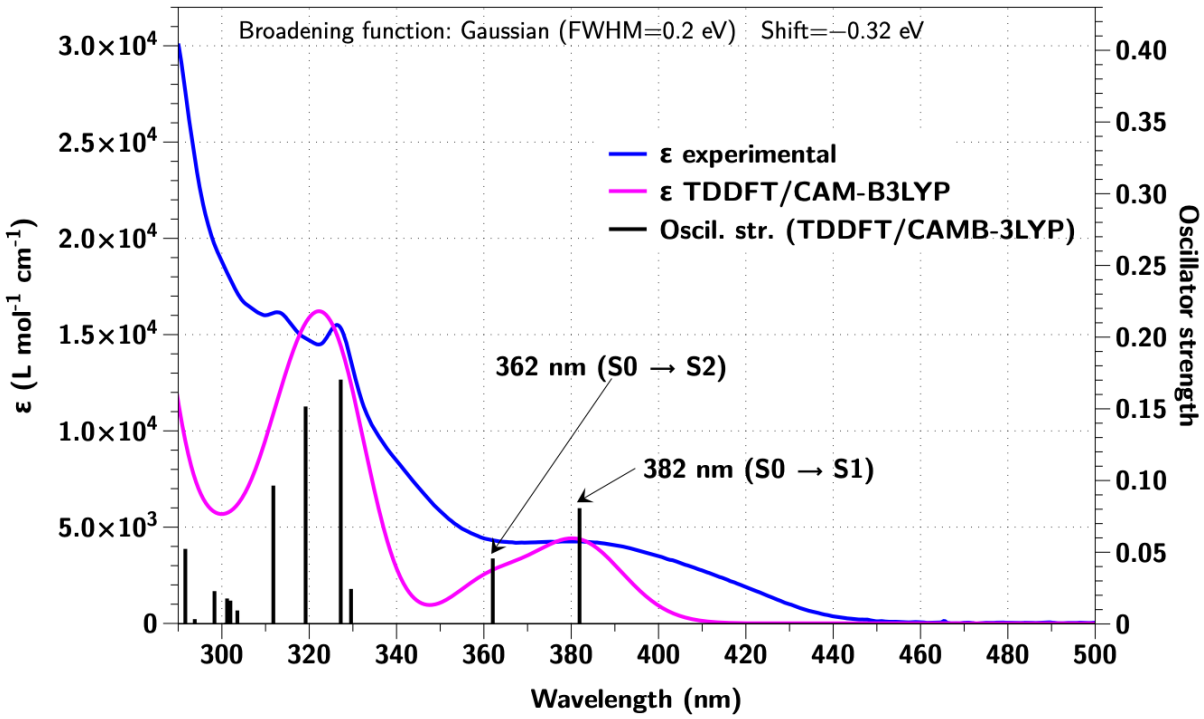

Figure S82: Comparison of the simulated UV-vis spectrum of **C1**. A spectral shift has been applied (-0.32 eV). Calculated excitation energy and oscillator strength indicated as 'stick' spectra (black), experimental and simulated spectra indicated as blue and pink curve respectively.

Simulated ECD spectra

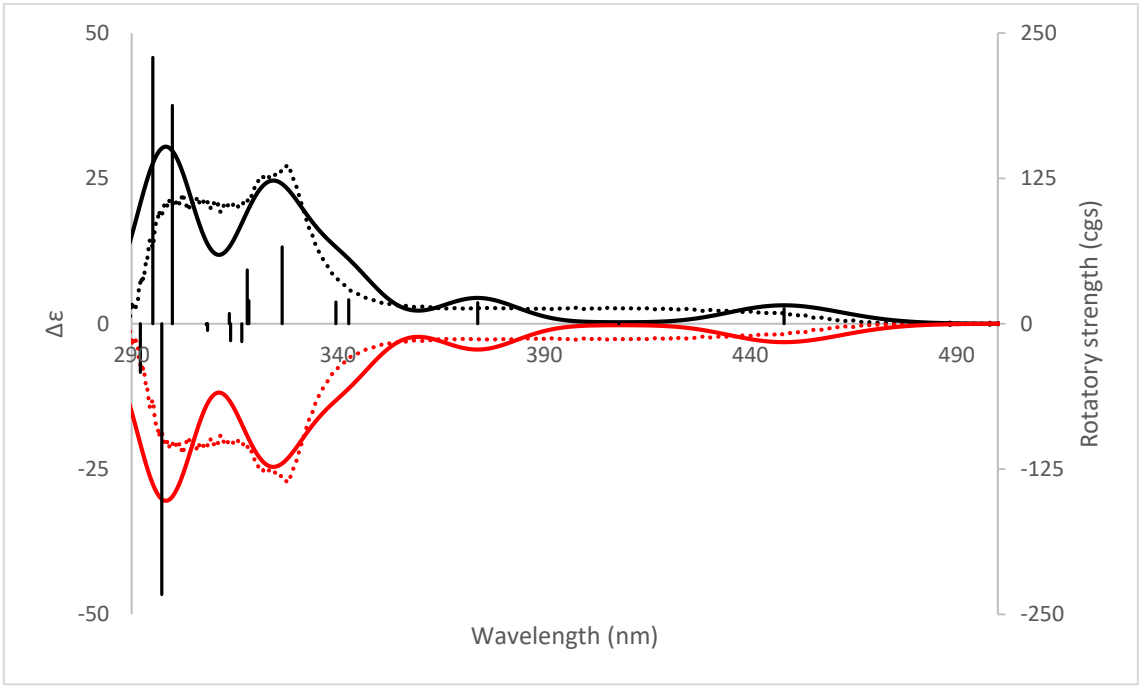

Figure S83: Comparison of the simulated ECD spectra of **A1**. A spectral shift has been applied (-0.51 eV). Calculated excitation energy and oscillator strength indicated as 'stick' spectra (black),

experimental spectra are indicated as dashed lines, simulated spectra are indicated as solid lines (*S* enantiomer in red, *R* enantiomer in black).

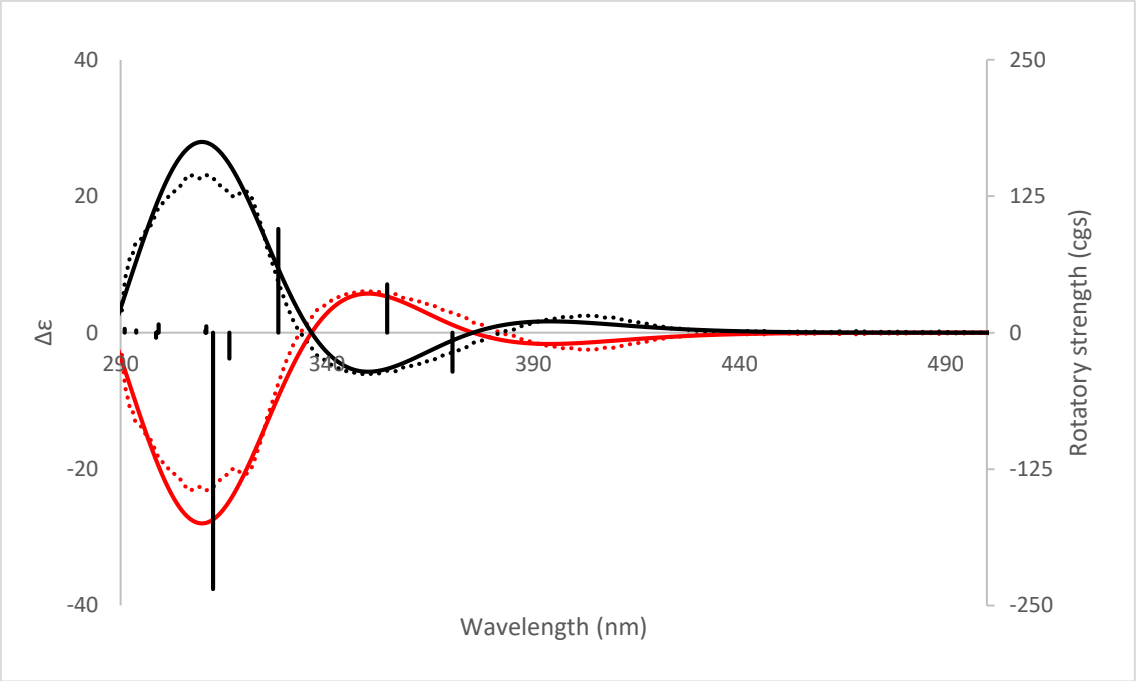

Figure S84: Comparison of the simulated ECD spectra of **B1**. A spectral shift has been applied (-0.28 eV). Calculated excitation energy and oscillator strength indicated as 'stick' spectra (black), experimental spectra are indicated as dashed lines, simulated spectra are indicated as solid lines (*S* enantiomer in red, *R* enantiomer in black).

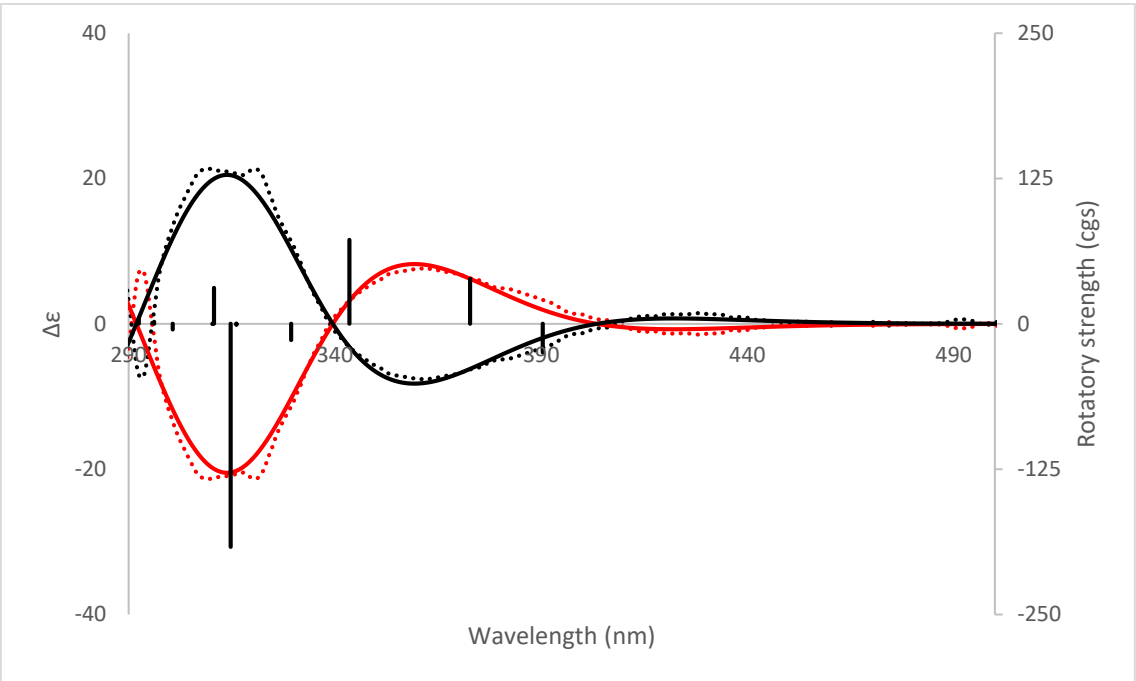

Figure S85: Comparison of the simulated ECD spectra of **B2**. A spectral shift has been applied (-0.32 eV). Calculated excitation energy and oscillator strength indicated as 'stick' spectra (black), experimental spectra are indicated as dashed lines, simulated spectra are indicated as solid lines (*S* enantiomer in red, *R* enantiomer in black).

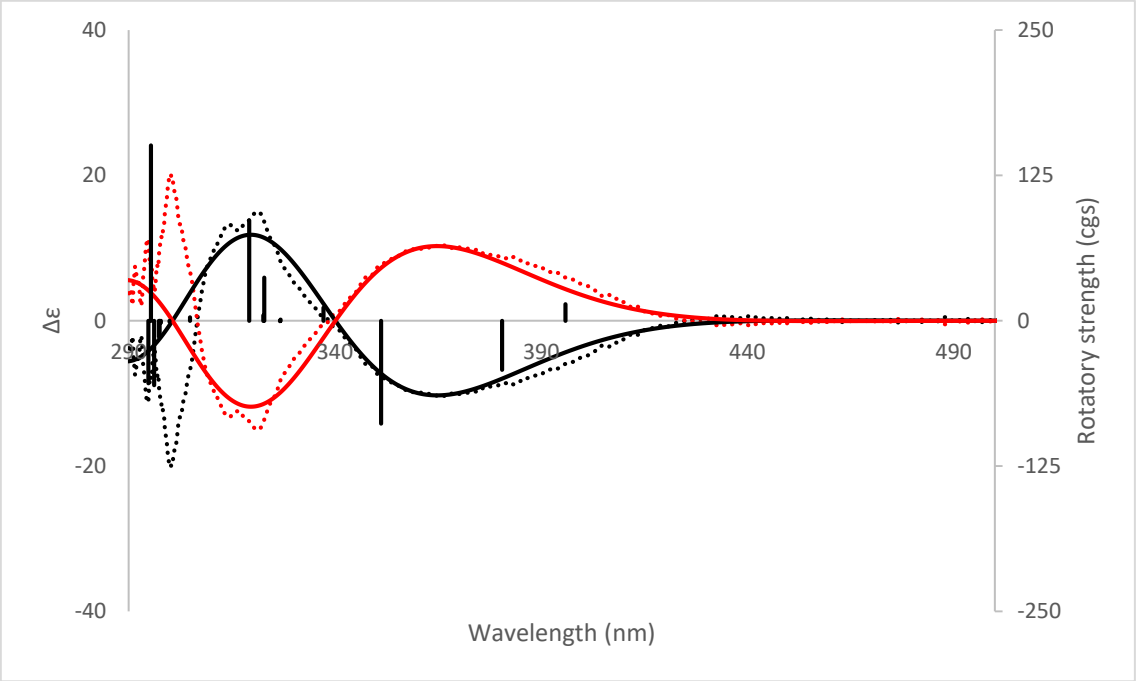

Figure S86: Comparison of the simulated ECD spectra of **B3**. A spectral shift has been applied (-0.37 eV). Calculated excitation energy and oscillator strength indicated as 'stick' spectra (black), experimental spectra are indicated as dashed lines, simulated spectra are indicated as solid lines (*S* enantiomer in red, *R* enantiomer in black).

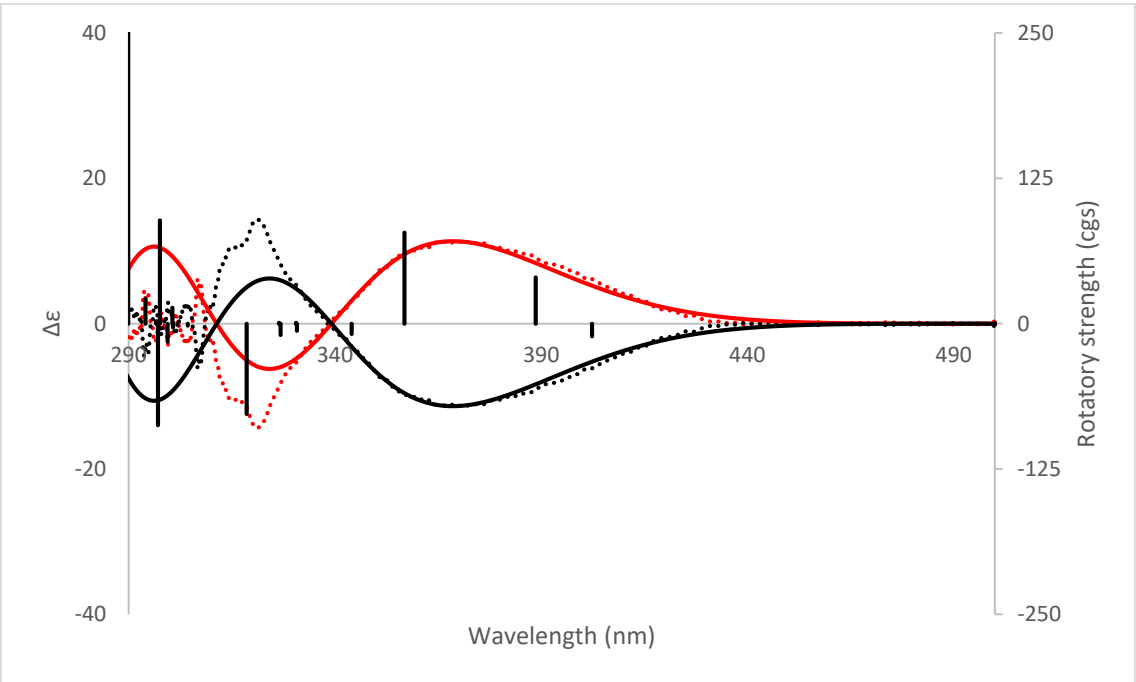

Figure S87: Comparison of the simulated ECD spectra of **B4**. A spectral shift has been applied (-0.36 eV). Calculated excitation energy and oscillator strength indicated as 'stick' spectra (black), experimental spectra are indicated as dashed lines, simulated spectra are indicated as solid lines (*S* enantiomer in red, *R* enantiomer in black).

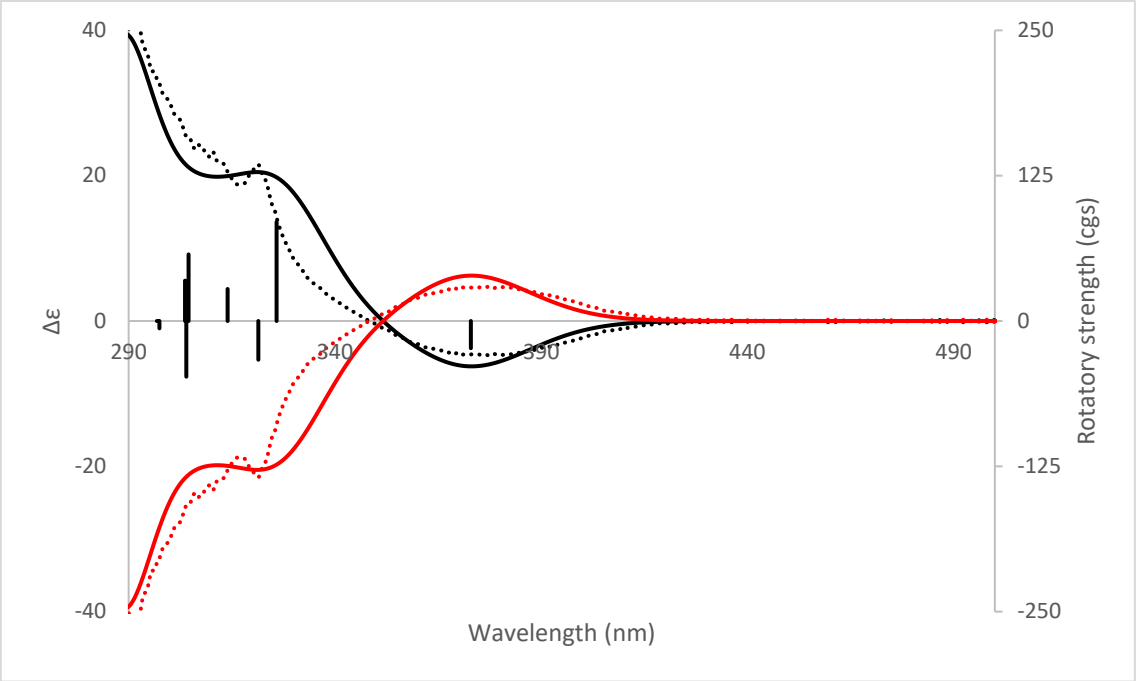

Figure S88: Comparison of the simulated ECD spectra of **C'1**. A spectral shift has been applied (-0.36 eV). Calculated excitation energy and oscillator strength indicated as 'stick' spectra (black), experimental spectra are indicated as dashed lines, simulated spectra are indicated as solid lines (*S* enantiomer in red, *R* enantiomer in black).

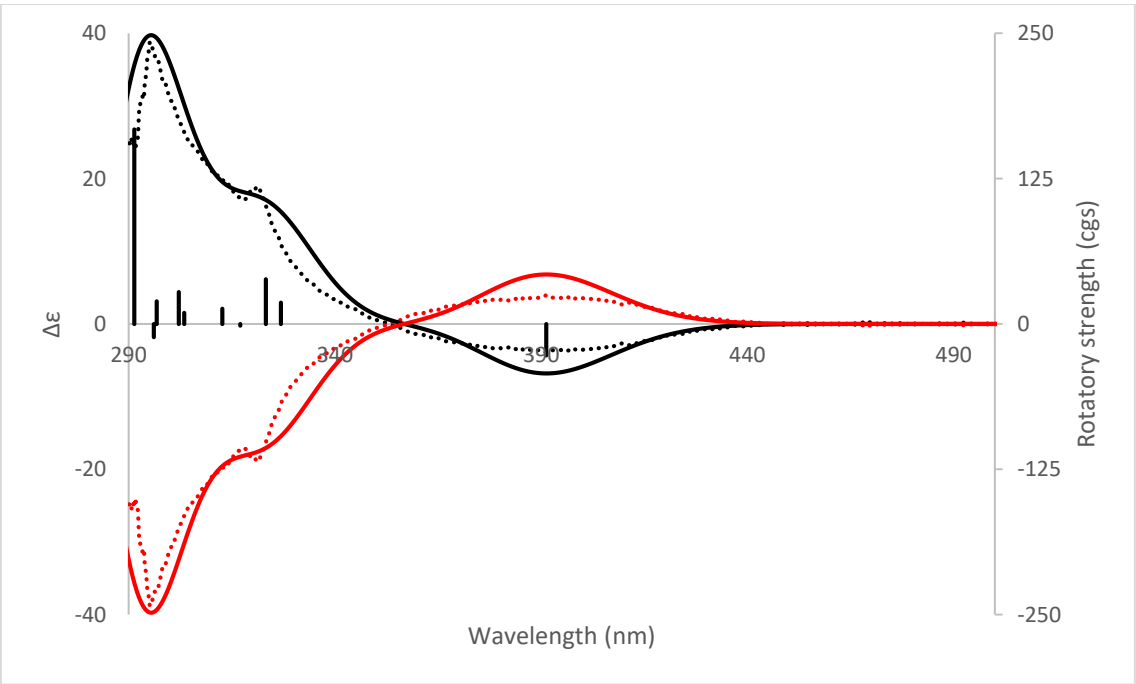

Figure S89: Comparison of the simulated ECD spectra of **C'2**. A spectral shift has been applied (-0.36 eV). Calculated excitation energy and oscillator strength indicated as 'stick' spectra (black), experimental spectra are indicated as dashed lines, simulated spectra are indicated as solid lines (*S* enantiomer in red, *R* enantiomer in black).

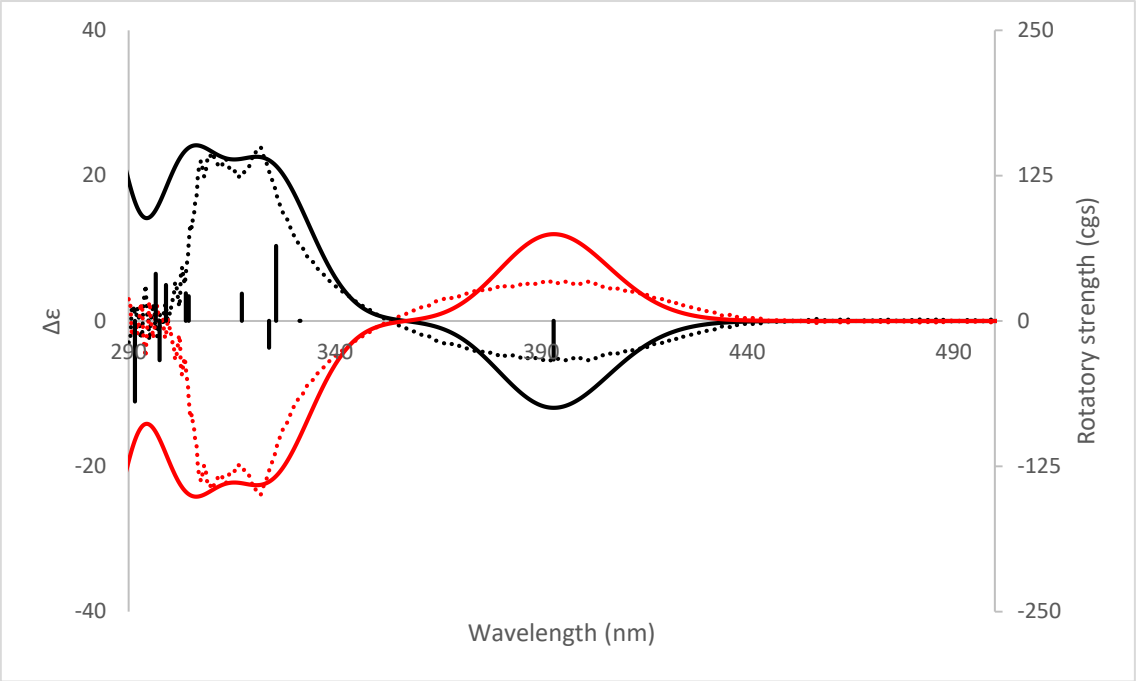

Figure S90: Comparison of the simulated ECD spectra of **C'3**. A spectral shift has been applied (-0.37 eV). Calculated excitation energy and oscillator strength indicated as 'stick' spectra (black), experimental spectra are indicated as dashed lines, simulated spectra are indicated as solid lines (*S* enantiomer in red, *R* enantiomer in black).

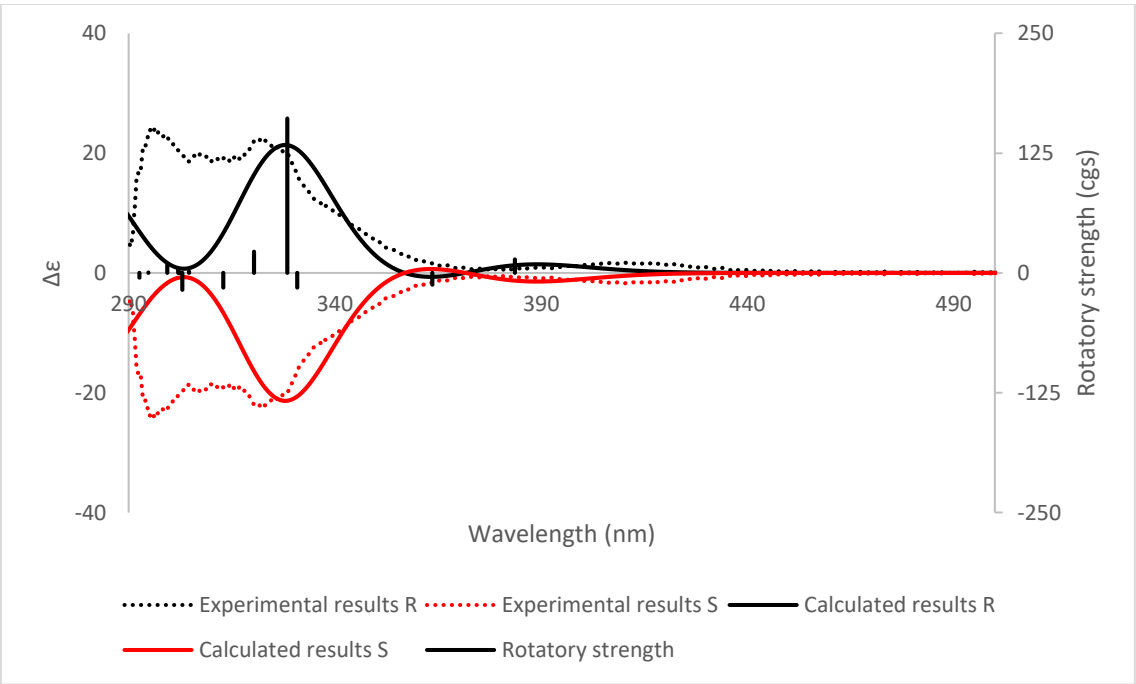

Figure S91: Comparison of the simulated ECD spectra of **C1**. A spectral shift has been applied (-0.33 eV). Calculated excitation energy and oscillator strength indicated as 'stick' spectra (black), experimental spectra are indicated as dashed lines, simulated spectra are indicated as solid lines (*S* enantiomer in red, *R* enantiomer in black).

Transition dipole moments values

For $S_0 \rightarrow S_1$ transition:

	A1	B1	B4	C1	C'1	C2	C'2	C3	C'3
μ_e	1,4148	0,4478	0,4271	0,9611	1,3123	1,0787	1,4213	1,1768	1,5874
μ_m	0,0194	0,1325	0,0533	0,0870	0,5014	0,0797	0,5203	0,1102	0,5573
θ	0,0000	179,9900	176,1880	69,0718	94,3188	48,7757	94,4379	103,3014	94,5732
g	0,0550	-1,1839	-0,4981	0,1294	-0,1151	0,1948	-0,1133	-0,0862	-0,1120

Table S5: Transition dipole moment values for $S_0 \rightarrow S_1$ transition

For $S_0 \rightarrow S_2$ transition:

	A1	B1	B4	C1	C'1	C2	C'2	C3	C'3
μ_e	0,0125	1,0213	1,3255	0,7054	1,0559	0,8065	0,3491	0,3302	0,0439
μ_m	0,1606	0,2750	0,2451	0,1147	0,5118	0,0853	0,2274	0,7879	0,2084
θ	18,6199	74,7882	74,9068	108,8830	70,4844	109,5550	32,4722	13,1682	86,5396
g	48,5742	0,2826	0,1926	-0,2106	0,6476	-0,1415	2,1978	9,2931	1,1457

Table S6: Transition dipole moment values for $S_0 \rightarrow S_2$ transition

Optimized geometries at different states

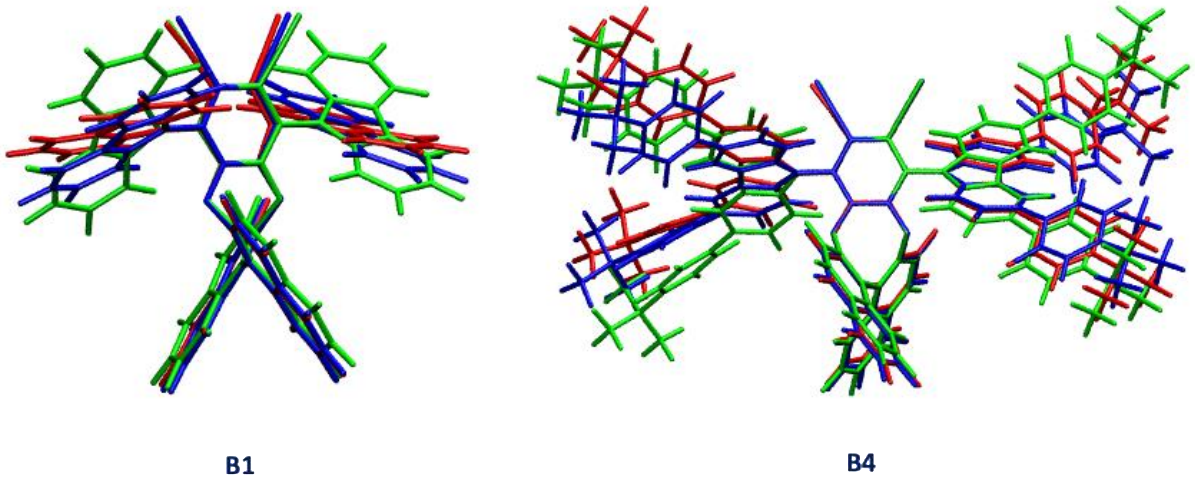

Figure S92: DFT/PBE0 S0, S1 and T1 state optimized geometries. S0 in blue, S1 in red and T1 in green color.

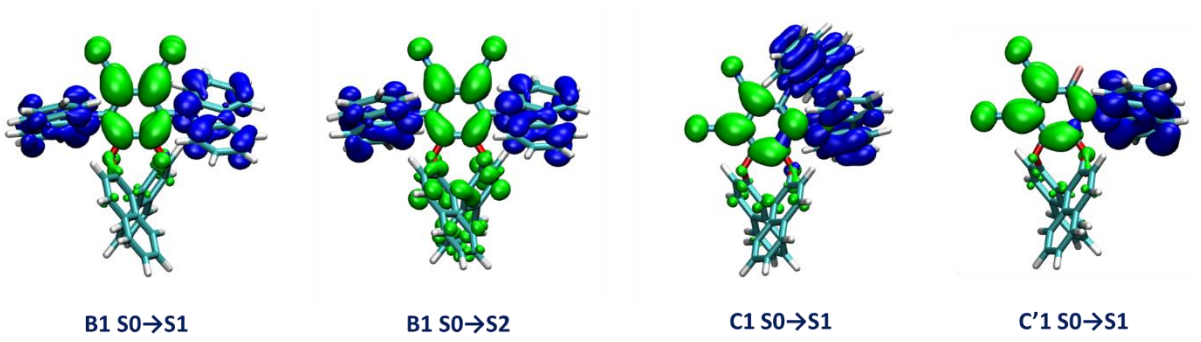

Figure S93: Holes and electrons distributions for selected transitions. Blue and green isosurfaces (0.001) represent hole and electrons respectively.

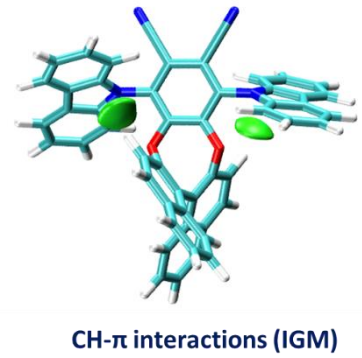

Figure S94: CH-π interactions for compound **B1**represented as green ellipsoids using IGM (Independent Gradient Model)

B1r optical and chiroptical data

Relative quantum yield in aerated toluene solution for B1r: 0.056

Relative quantum yield in degazed toluene solution for B1r: 0.062

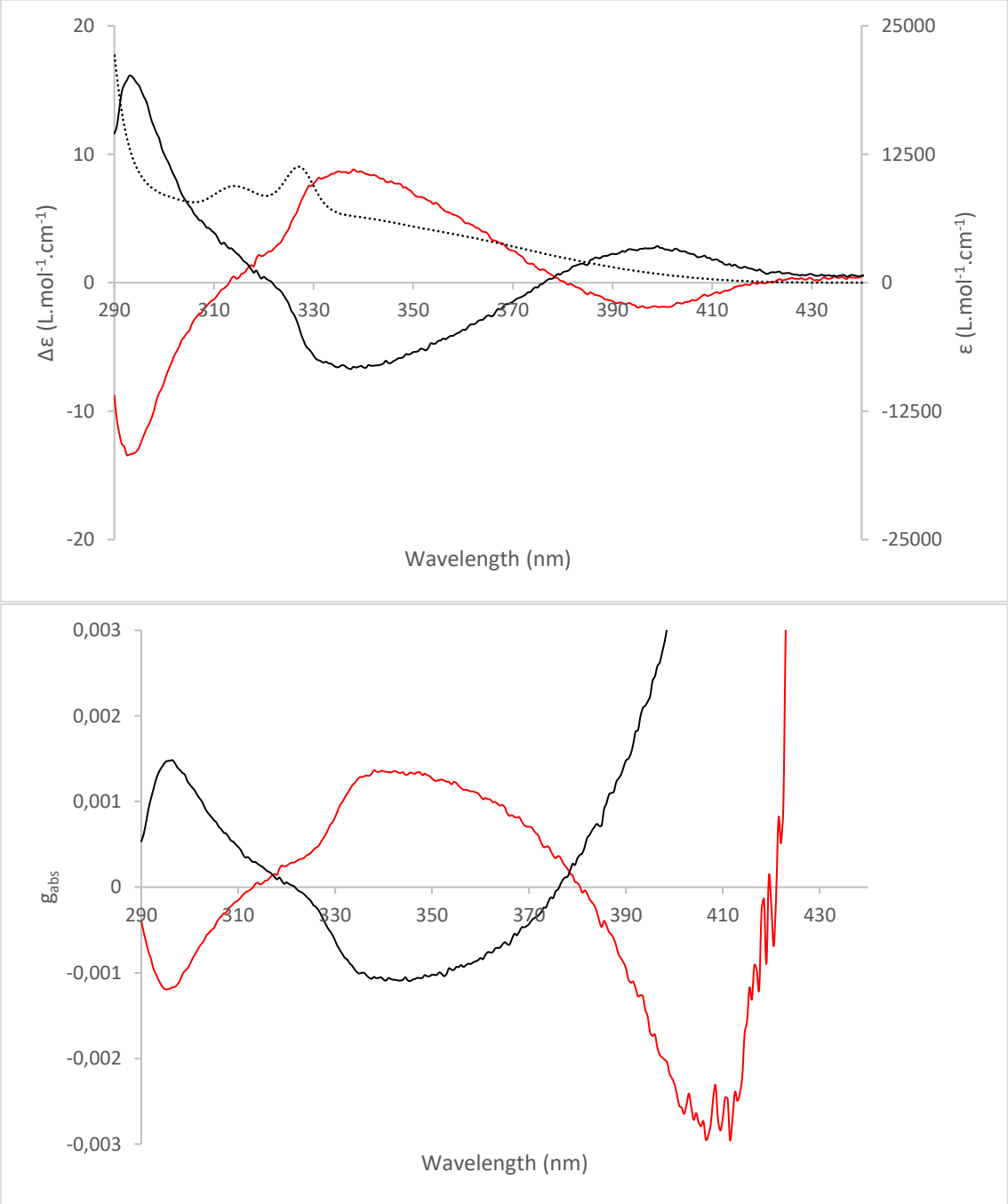

Figure S95: Top: ECD spectra of **B1r** (*S* enantiomer in red, *R* enantiomer in black) and UV-vis spectrum of **B1r** (dashed lines) at 298 K in toluene solution. Bottom: absorption dissymetry factor g_{abs} spectra of **B1r** (*S* enantiomer in red, *R* enantiomer in black) at 298 K in toluene solution.

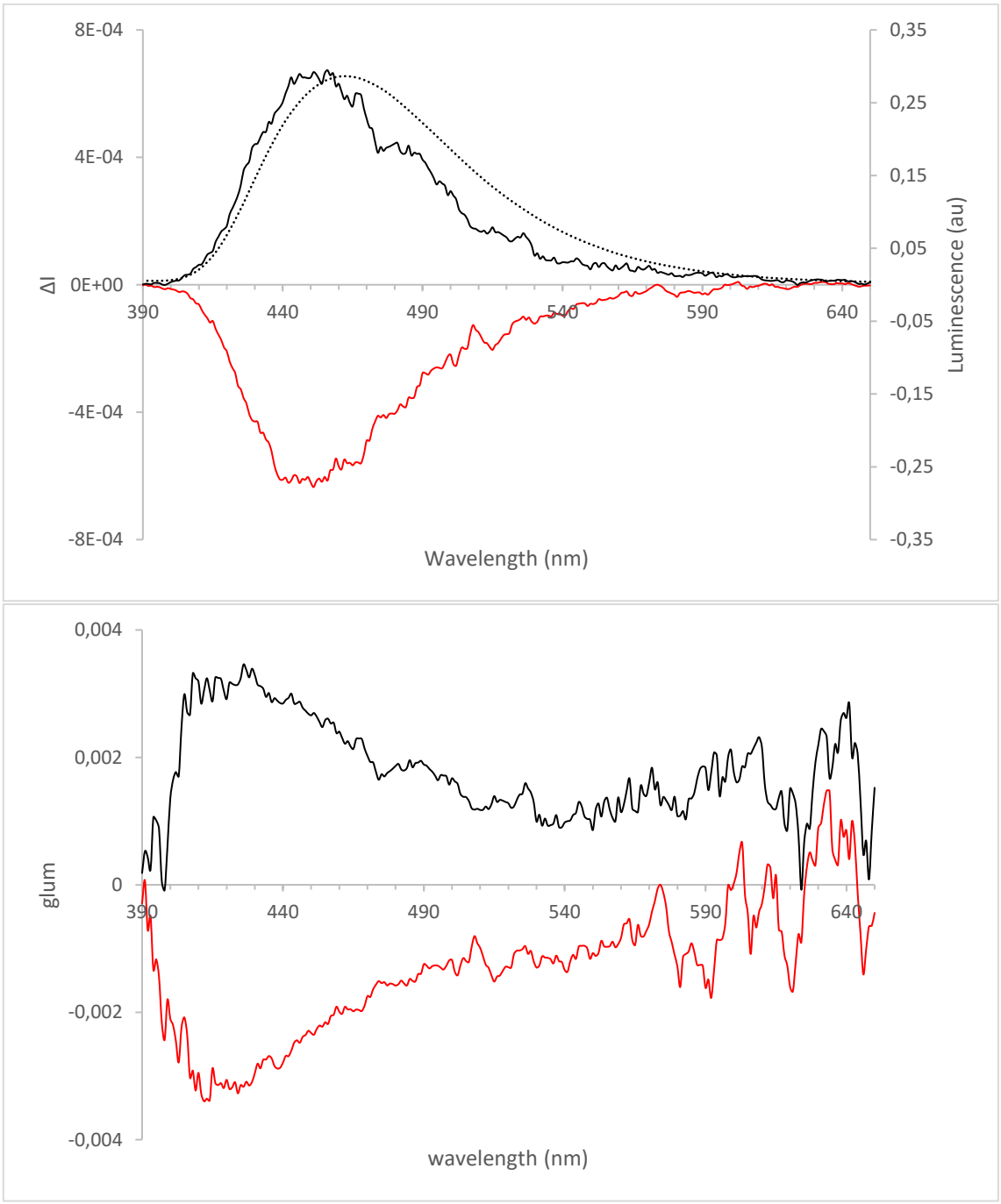

Figure S96: Top: CPL spectra of **B1r** (*S* enantiomer in red, *R* enantiomer in black) and emission spectrum of **B1r** (dashed lines) at 298 K in toluene solution excited at 350 nm. Bottom: emission dissymetry factor g_{lum} spectra of **B1r** (*S* enantiomer in red, *R* enantiomer in black) at 298 K in toluene solution excited at 350 nm.

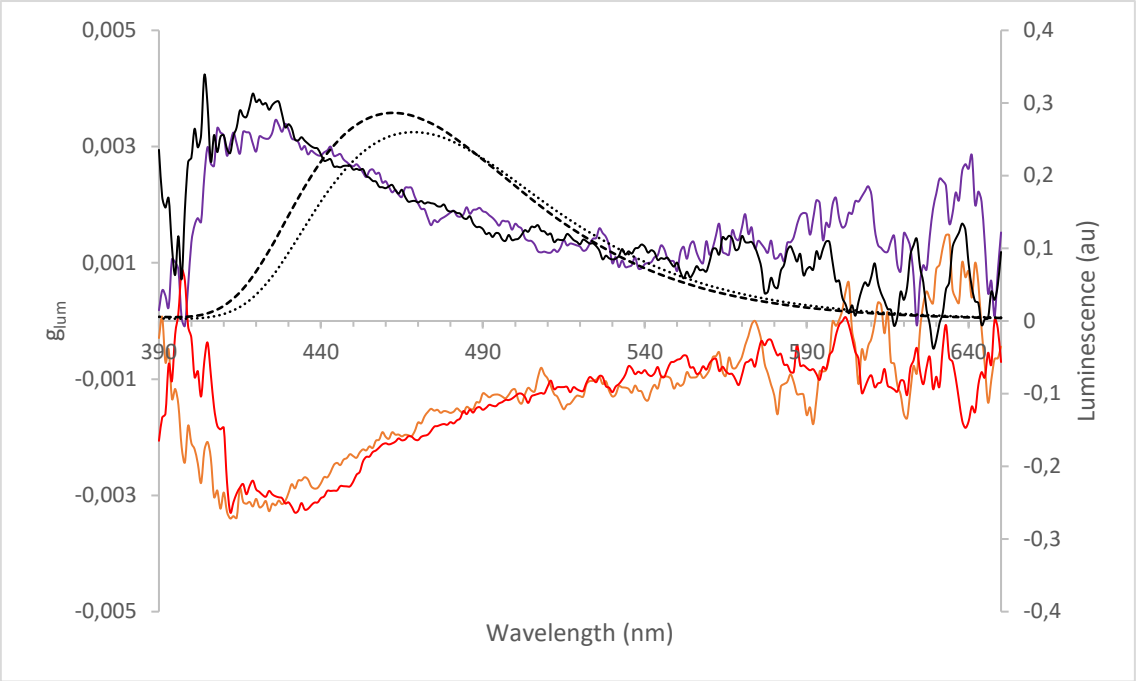

Figure S97: Comparison of emission dissymetry factor g_{lum} spectra of **B1** and **B1r** (*S* enantiomer in red and orange, *R* enantiomer in black and purple respectively) and emission spectra of **B1** and **B1r** (dotted line and dashed line respectively) at 298 K in toluene solution excited at 350 nm.

OLED manufacturing

The manufacturing of OLED stacks includes metal, organic, and dielectric thin film deposition. It is performed by vacuum evaporation in a dedicated thin film deposition tool (Super Spectros 200 from Kurt J. Lesker company) routinely used for OLED manufacturing. This tool is connected to a glove box equipped with an Atomic Layer Deposition (ALD) reactor where OLEDs are encapsulated by an alumina thin film[S14] prior to exposure to air and optoelectronic characterization. The OLEDs are processed on an 8 inch-silicon wafer with more than 50 individual OLEDs per wafer, each having an active area of 0.26 cm^2. The full stack comprises an Al-Cu bottom cathode covered with a thin passivation layer (TiN) on which the OLED stack is deposited before encapsulation. The organic OLED stack (see Figure 15 a) comprises successive layers including electron injection and transport layers (EIL/ETL), a hole blocking layer (HBL), an emissive layer (EML), and hole transport and injection layers (HTL/HIL). On top of this, an ultra-thin silver (Ag) layer is deposited as anode. Finally, a SiO/Al_2O_3 bilayer is used as a thin film encapsulation against moisture and oxygen to ensure long term OLED functionality. The EML layer is a mCP matrix doped with 15 to 20% by volume of C'3 chiral dopant (*S* or *R* enantiomer). This doping is controlled in-situ by using QCM monitoring (quartz crystal microbalance) of the deposition rates of both elements.

Top-emission OLED technology: Optical cavity effect

The top-emission OLED design of Figure 15 a) involves building an organic stack sandwiched between two metallic electrodes. As a result, this architecture induces an optical cavity effect that mitigates and filters part of the electroluminescent light generated by the mCP and the chiral dopant emitting layer.

This effect is highlighted in Figure S98 where a bottom-emission OLED is compared to a top-emission one. In a bottom-emission OLED the light exit electrode is fully transparent (glass covered with Indium Tin Oxide –ITO). In a top-emission OLED, the extracted light exits through a very thin semi-transparent metallic electrode.[S14] As a result, while in a bottom-emission device most of the electroluminescent light is directly extracted though the bottom ITO/glass substrate, in a top-emission device the electroluminescent light is submitted to various multi-reflections that induce optical interference effect and at the end wavelength selectivity in the spectrum of extracted light (filtering). In addition, since the top-electrode is partly absorbing, the intensity of extracted light is noticeably attenuated which is not the case in a bottom-emission OLED.

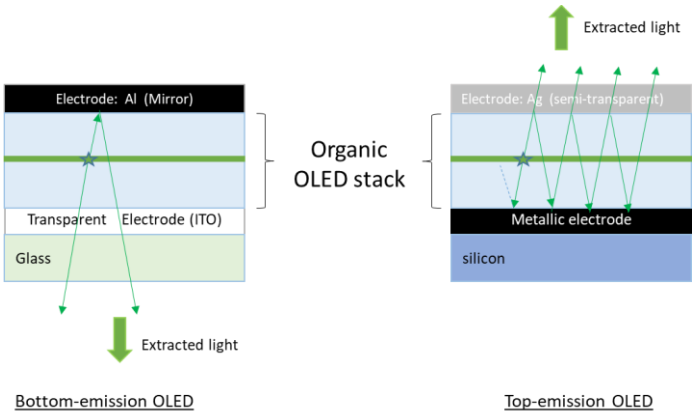

Figure S98: sketch of typical bottom- and top- emission OLED architectures

We can estimate the effect of the optical cavity on the resulting OLED emission intensity in a top-emission OLED. Figure S99 below presents the Photoluminescence (PL) spectrum measured at normal incidence on a pure **C'3** (*S* enantiomer) layer (green area).

We define T(λ) as measured spectral transmittance of C'3 (*S* enantiomer) OLED cavity. Actually, we measured the surface reflectance R(λ) at normal incidence on the semi-transparent anode side (Figure 15). We then assume T=1-R since the R value takes into account most of the cavity absorption. If we convolve both curves, we obtain the solid black line OLED spectrum. Assuming a better cavity alignment with **C'3** (*S* enantiomer) emission spectrum (dashed pink cavity transmittance), convolving with the green spectrum gives the solid pink OLED spectrum.

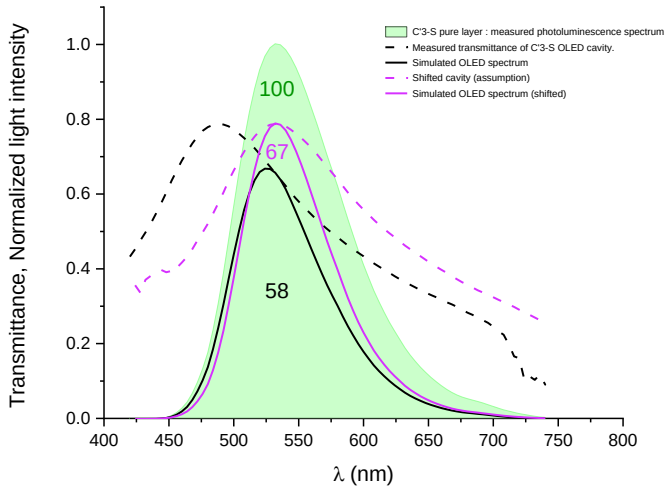

Figure S99: Comparison between the PL spectrum measured at normal incidence on a pure C'3 (*S* enantiomer) layer and the calculated OLED emission spectra with the experimental OLED cavity (solid black line) and with a better aligned OLED cavity (solid pink line). The figures on the graph correspond to the normalized integrated area of each corresponding curve. Dashed curved are the transmittance of experimental and corrected OLED cavities.

In our **C'3** (*S* enantiomer) OLED the measured cavity was found to have it's maximum transmission at 490 nm while the photoluminescence (PL) peak of **C'3** (*S* enantiomer) is higher (532 nm). As a result, the top-emission OLED is slightly blue-shifted and extracts only 58% of total available light. A perfect cavity alignment with PL maximum gives at the best +15% extracted light (58=>67). Moreover, compared to a bottom emission OLED where most (~100%) of the light emitted by the EML layer is extracted, in a top-emission OLED we can only expect extracting 2/3 of available light maximum with an optical cavity perfectly matching the light spectrum emission peak.

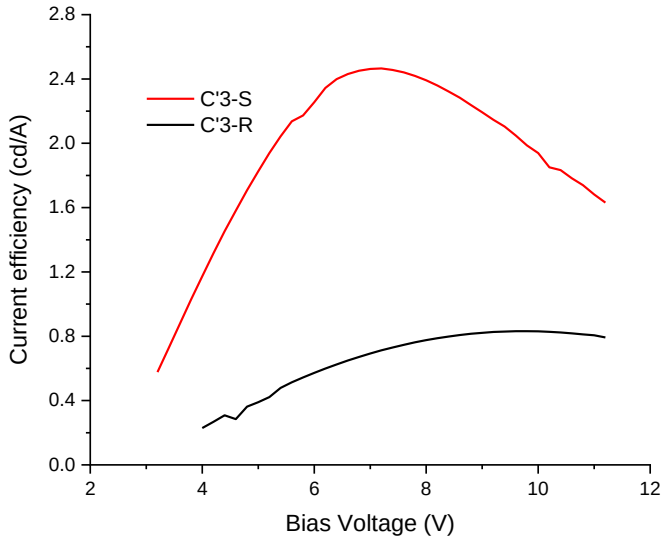

Figure S100: Current effiency-bias voltage characteristics of OLEDs made with C'3-*(S)* (red) and C'3-(R) (black).

Current density and luminance versus voltage characteristics have been simultaneously recorded with a PR - 655 spectrascan spectrophotometer attached to a programmable Keithley 2400 voltage‑current source. All measurements have been carried out at room temperature under ambient atmosphere.

Crystallography

The data for compounds **A1**·CH_2Cl_2 and **B1**·$2C_5H_5N$ were collected at 100(2) K on a Nonius Kappa-CCD area detector diffractometer[S15] using graphite-monochromated Mo Kα radiation (λ = 0.71073 Å). The crystals were introduced into glass capillaries with a protective coating of Paratone-N oil (Hampton Research). The unit cell parameters were determined from ten frames, then refined on all data. The data (combinations of φ- and ω-scans with a minimum redundancy of at least 4 for 90% of the reflections) were processed with HKL2000.[S16] Absorption effects were corrected empirically with the program SCALEPACK[S16] for compound **A1**·CH_2Cl_2, and no correction was performed for compound **B1**·$2C_5H_5N$. The structures were solved by intrinsic phasing with SHELXTS[S17] and refined by full-matrix least-squares on F^2 with SHELXL-2014.[S18] All non-hydrogen atoms were refined with anisotropic displacement parameters. The hydrogen atoms were introduced at calculated positions and they were treated as riding atoms with an isotropic displacement parameter equal to 1.2 times that of the parent atom. Voids in the structures of those compounds indicate the presence of other, unresolved solvent molecules, whose contribution to the structure factors was taken into account with PLATON/SQUEEZE.[S19]

Crystal data for A1·CH_2Cl_2. $C_{53}H_{30}Cl_2N_4O_2$, M = 825.71, monoclinic, space group $P2_1$, a = 16.0812(7), b = 8.7358(4), c = 17.1922(7) Å, β = 116.567(2)°, V = 2160.18(17) Å^3, Z = 2, μ = 0.197 mm^{-1}, F(000) = 852. . Refinement of 551 parameters on 8151 independent reflections out of 102119 measured reflections led to R_1 = 0.044 , wR_2 = 0.120, S = 1.124, Flack parameter = -0.03(8).

Crystal data for B1·$2C_5H_5N$. $C_{62}H_{38}N_6O_2$, M = 898.98, monoclinic, space group $P2_1$, a = 13.1668(3), b = 14.5178(4), c = 14.6278(5) Å, β = 112.899(2)°, V = 2575.79(13) Å^3, Z = 2, μ = 0.071 mm^{-1}, F(000) = 936. Refinement of 631 parameters on 5081 independent reflections out of 84843 measured reflections led to R_1 = 0.062 , wR_2 = 0.188, S = 1.037. In the absence of a suitable anomalous scatterer, the refined Flack parameter was inconclusive, so that the Friedel pairs have been merged.

CCDC-1995065 (**A1**·CH_2Cl_2) and CCDC-1995066 (**B1**·$2C_5H_5N$) contain the supplementary crystallographic data. These data can be obtained free of charge from The Cambridge Crystallographic Data Centre via www.ccdc.cam.ac.uk/data_request/cif.

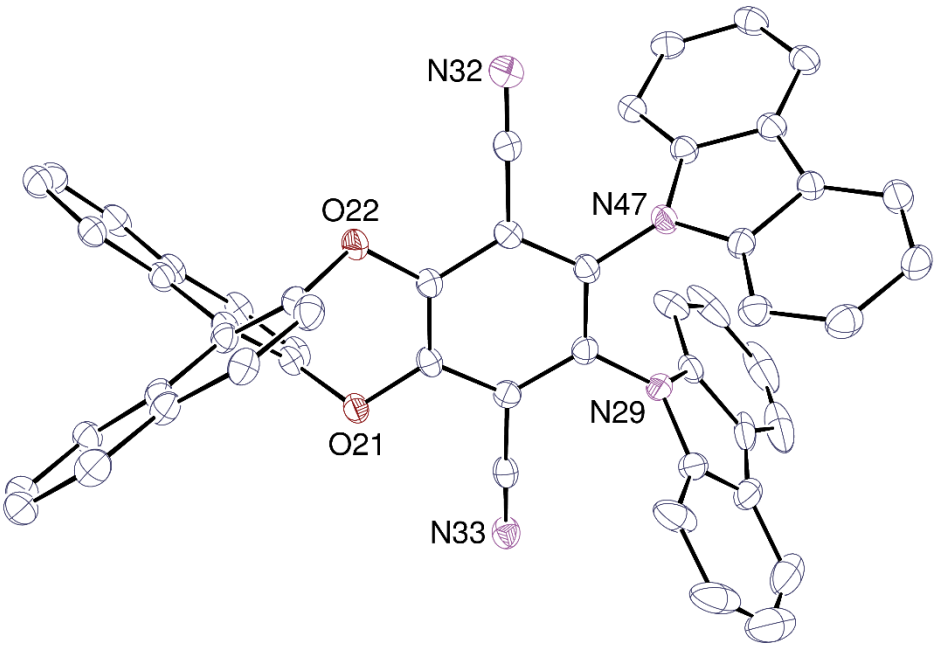

Figure S101: View of compound A1 in the crystal structure of **A1**·CH_2Cl_2. Displacement ellipsoids are shown at the 30 % probability level. Hydrogen atoms are omitted.

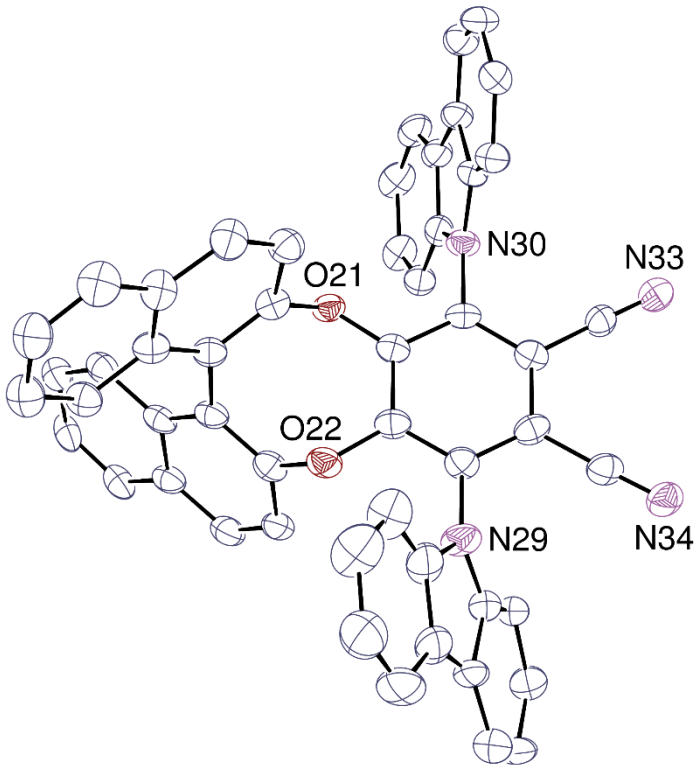

Figure S102: View of compound B1 in the crystal structure of **B1·2C_5H_5N**. Displacement ellipsoids are shown at the 30 % probability level. Hydrogen atoms are omitted.

NMR data

19F NMR spectra from mixture **3** and **4**:

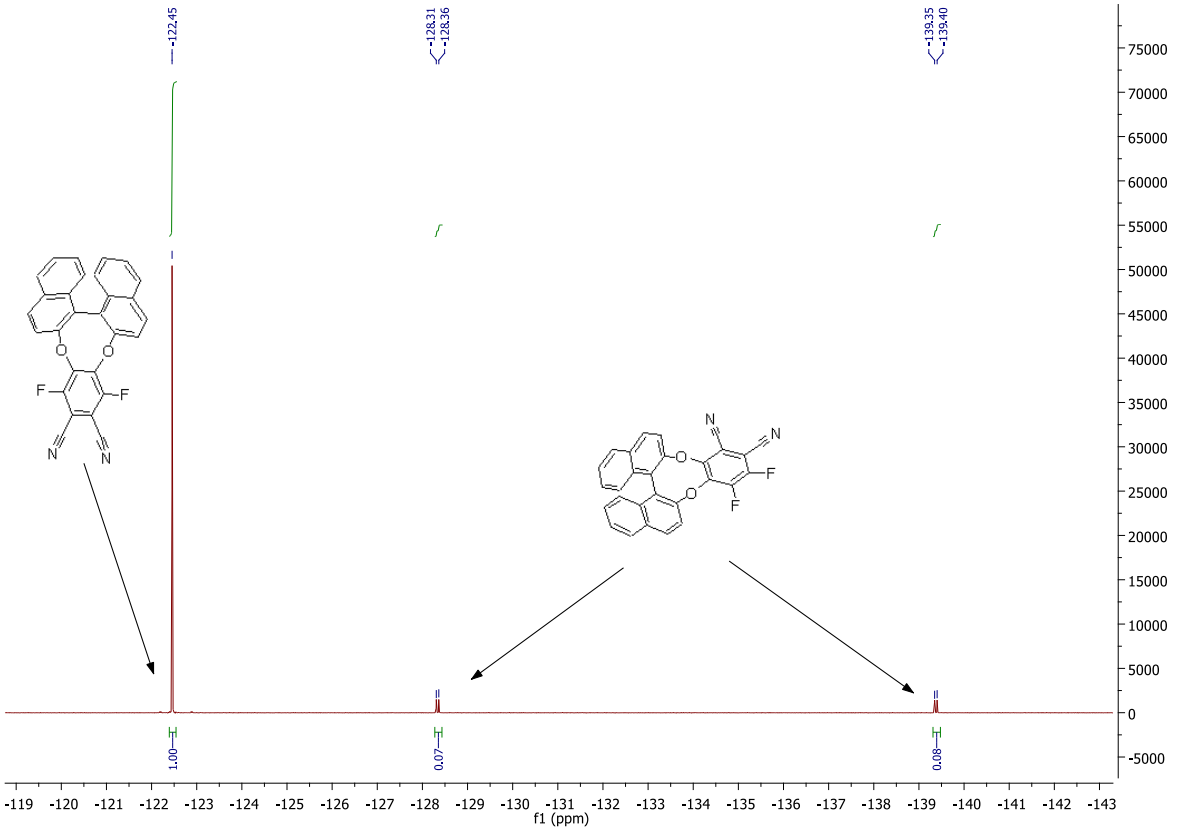

Figure S103: ^{19}F NMR spectrum of the reaction mixture involving 1 and *(S)/(R)*-(-)-1,1'-bi(2-naphthol) at room temperature (298 K) .

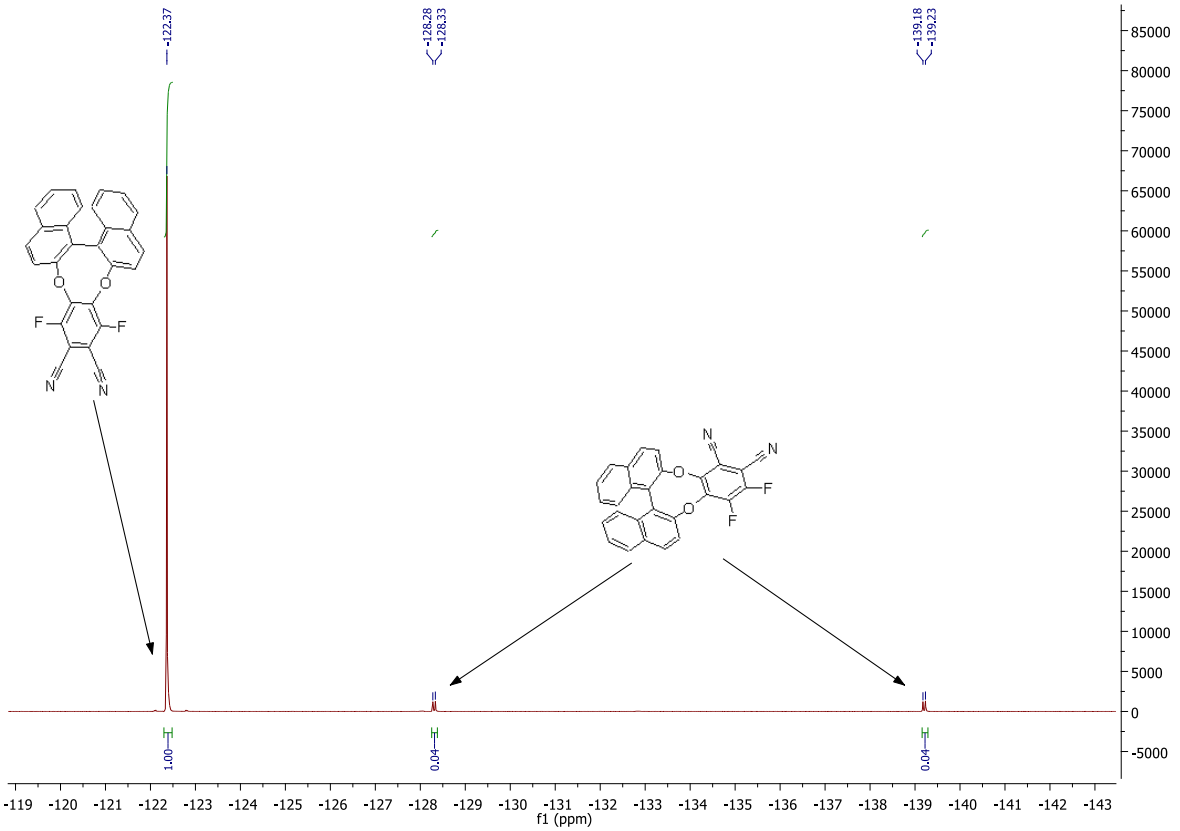

Figure S104: ^{19}F NMR spectrum of the reaction mixture involving 1 and *(S)/(R)*-(-)-1,1'-bi(2-naphthol) at 0°C temperature.

Compound **B1:**

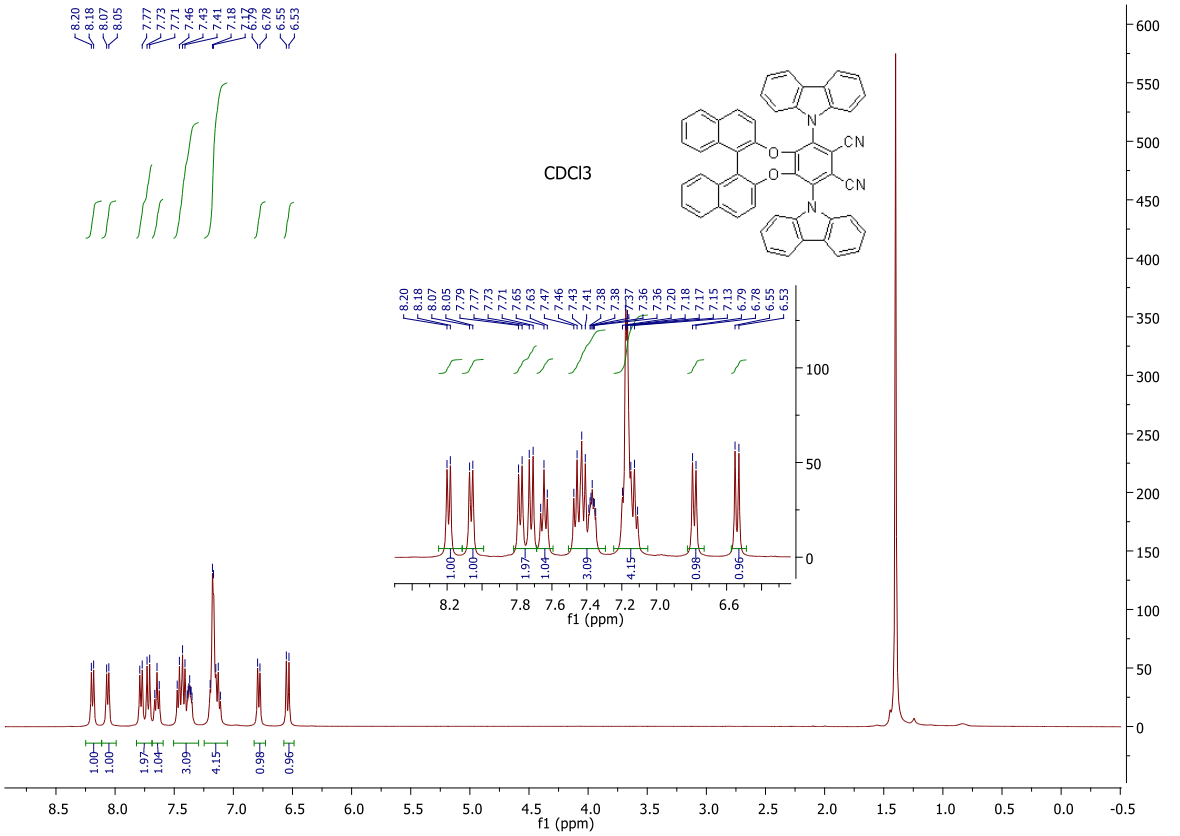

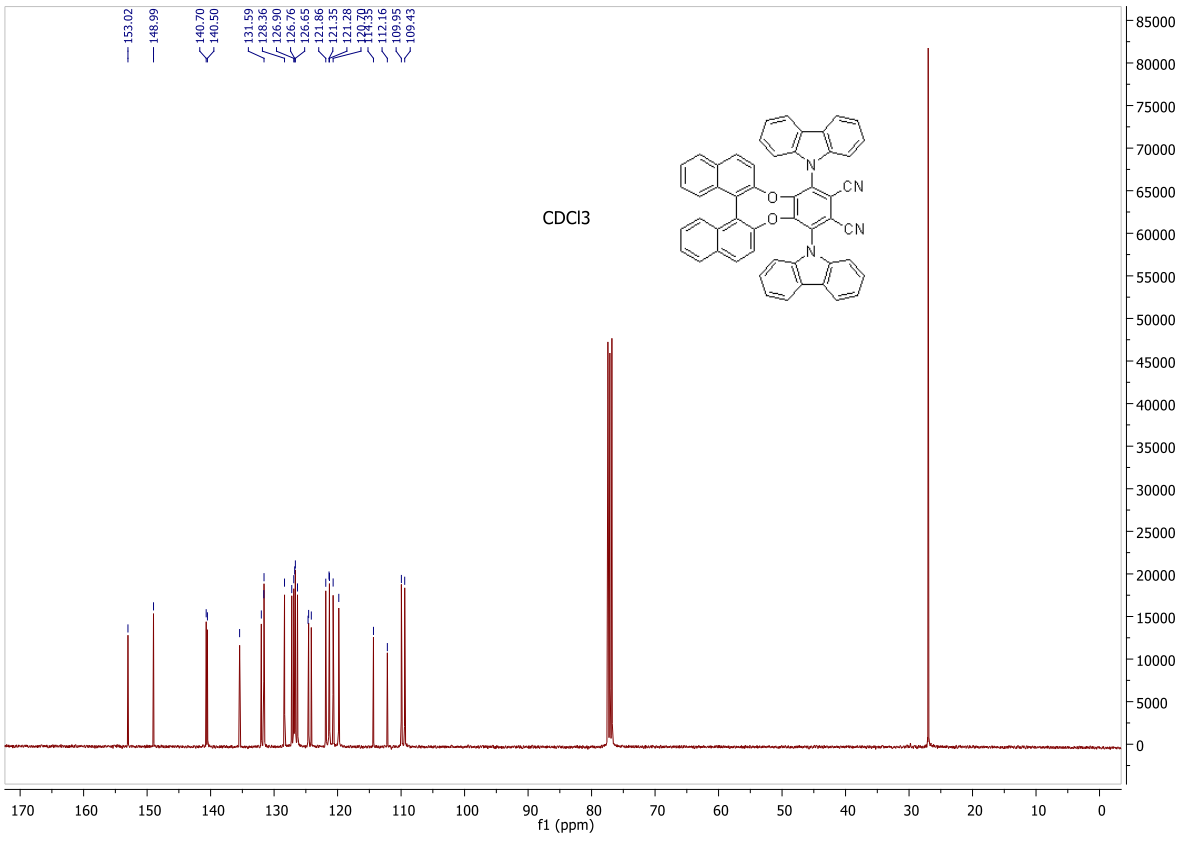

Compound **B1r** :

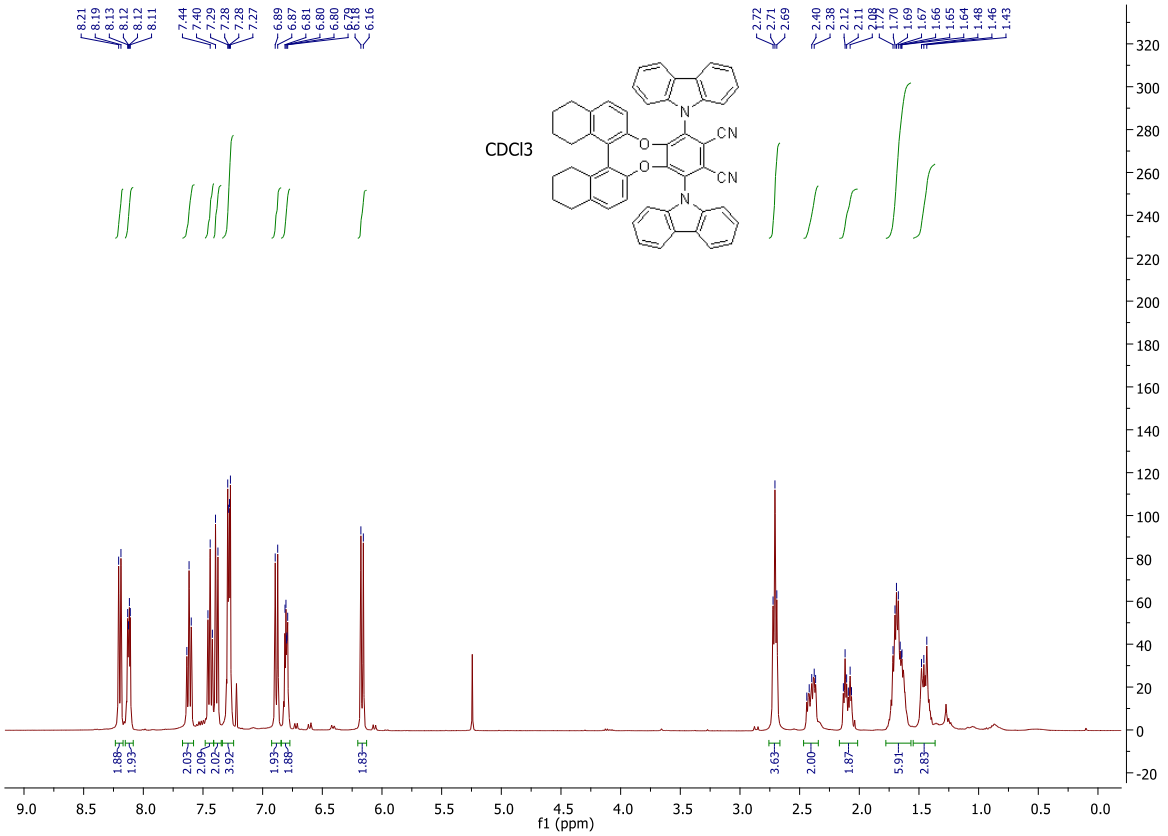

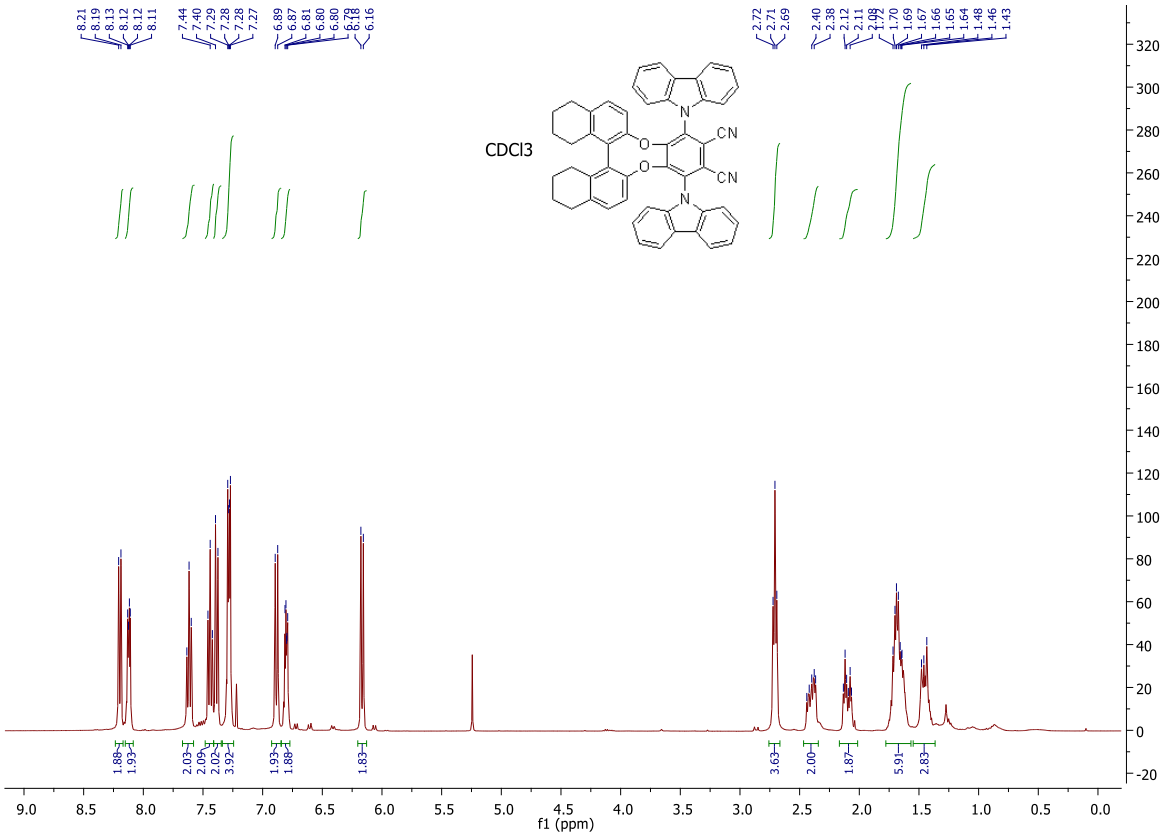

Compound **B2**:

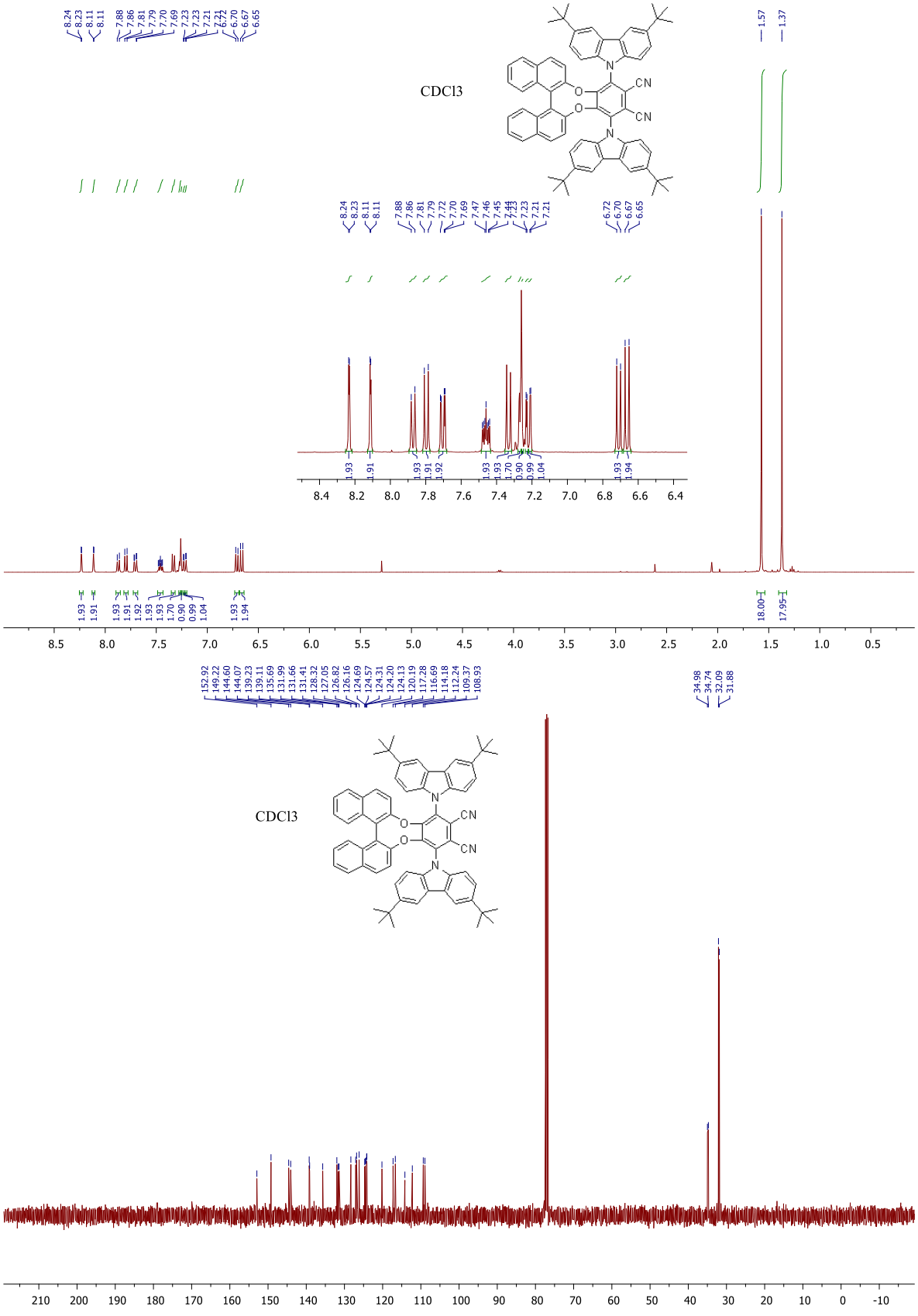
CDCl3
CN
CN
N
O
O
8.24
8.23
8.11
8.11
7.88
7.86
7.81
7.79
7.72
7.70
7.69
7.47
7.46
7.45
7.23
7.21
7.21
6.72
6.70
6.67
6.65
1.57
1.37
1.93
1.91
1.93
1.91
1.92
1.93
1.93
1.70
0.90
0.99
1.04
1.93
1.94
18.00
17.95
8.5
8.0
7.5
7.0
6.5
6.0
5.5
5.0
4.5
4.0
3.5
3.0
2.5
2.0
1.5
1.0
0.5
152.92
149.22
144.60
144.07
139.23
139.11
135.69
131.99
131.66
131.41
128.32
127.05
126.82
126.16
124.69
124.57
124.31
124.20
124.13
120.19
117.28
116.69
114.18
112.24
109.37
108.93
34.98
34.74
32.09
31.88
CDCl3
CN
CN
N
O
O
210
200
190
180
170
160
150
140
130
120
110
100
90
80
70
60
50
40
30
20
10
0
-10

Compound **B3**:

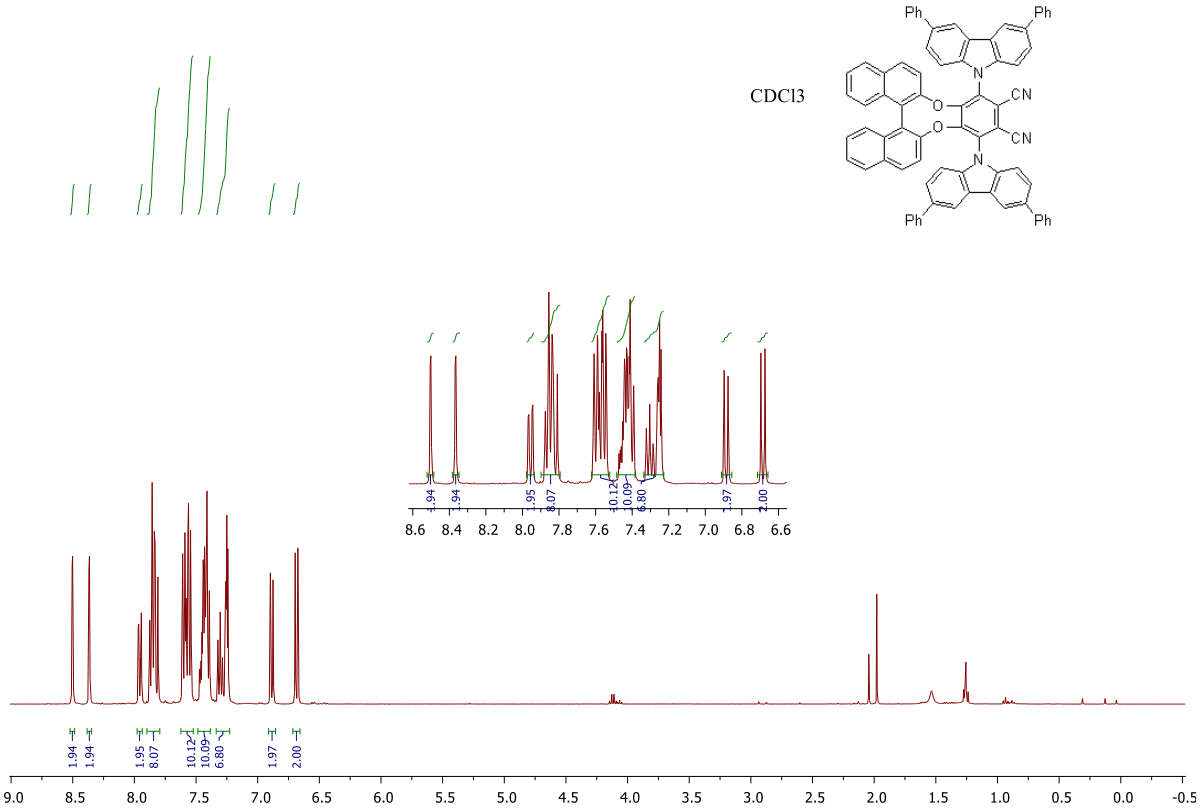
CDCl3
Ph
Ph
N
O
O
CN
CN
N
Ph
Ph
1.94
1.94
1.95
8.07
10.12
10.09
6.80
1.97
2.00
9.0
8.5
8.0
7.5
7.0
6.5
6.0
5.5
5.0
4.5
4.0
3.5
3.0
2.5
2.0
1.5
1.0
0.5
0.0
-0.5

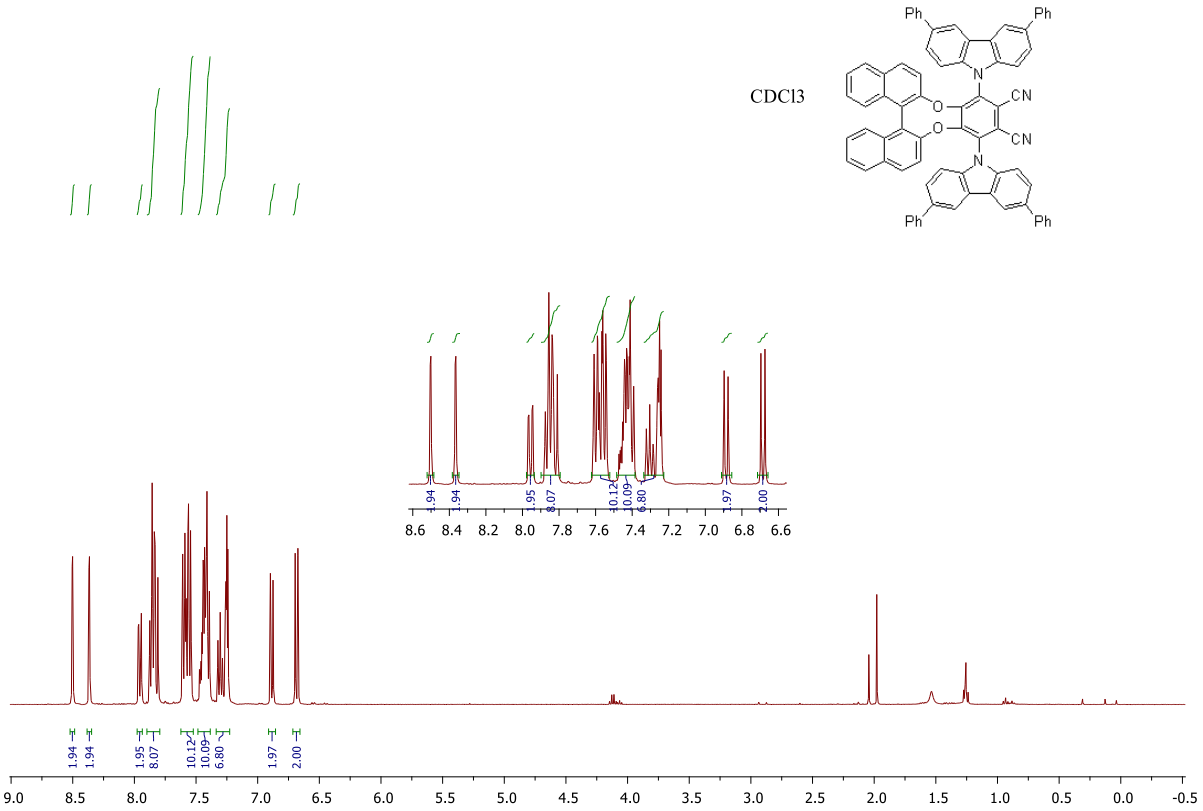
CDCl3
Ph
Ph
N
O
O
CN
CN
N
Ph
Ph
1.94
1.94
1.95
8.07
10.12
10.09
6.80
1.97
2.00
9.0
8.5
8.0
7.5
7.0
6.5
6.0
5.5
5.0
4.5
4.0
3.5
3.0
2.5
2.0
1.5
1.0
0.5
0.0
-0.5

Compound **B4** :

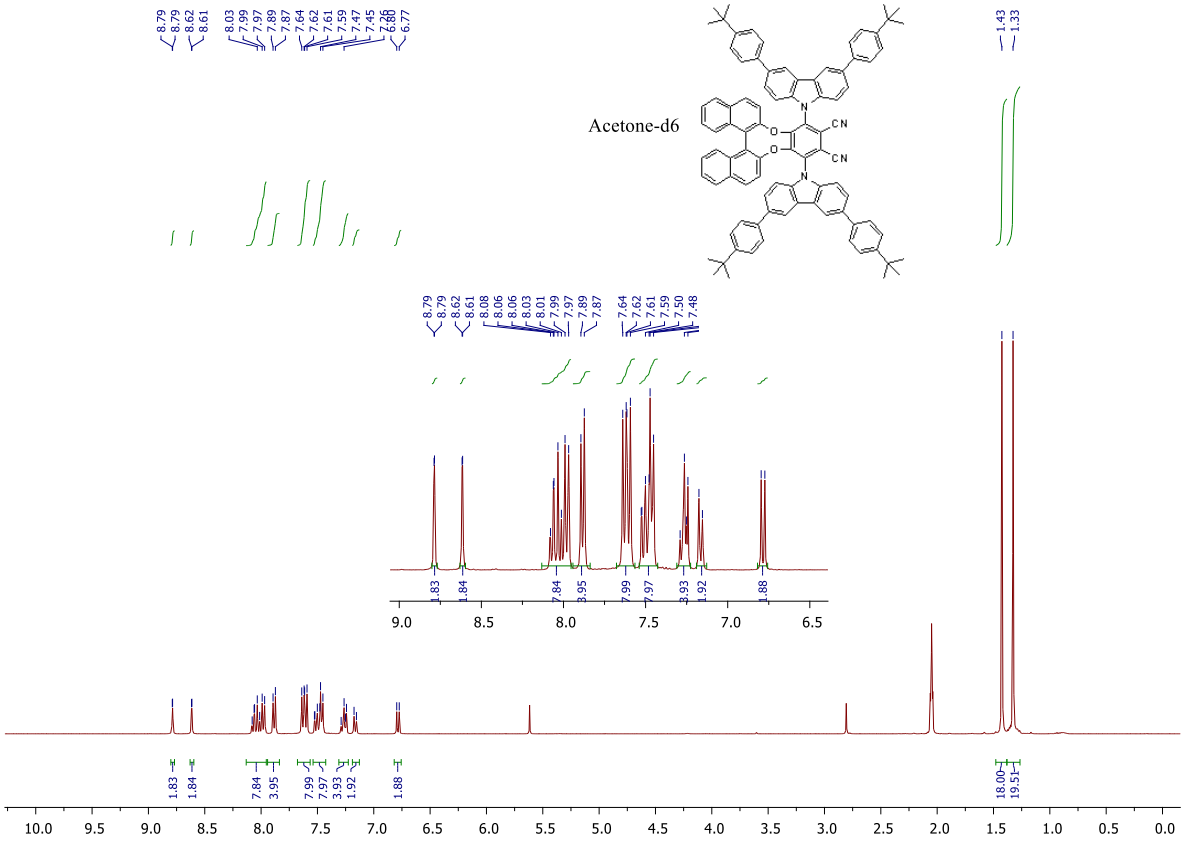

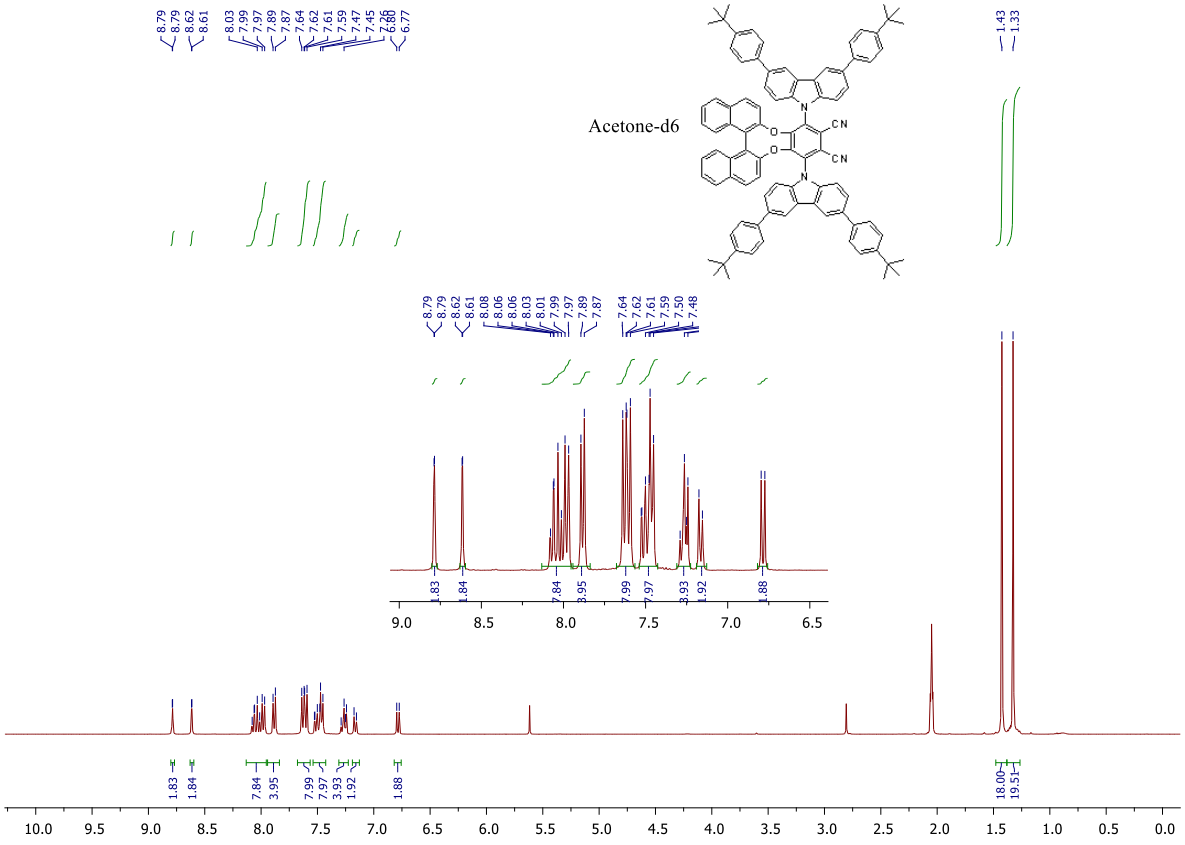

Compound **C'1** :

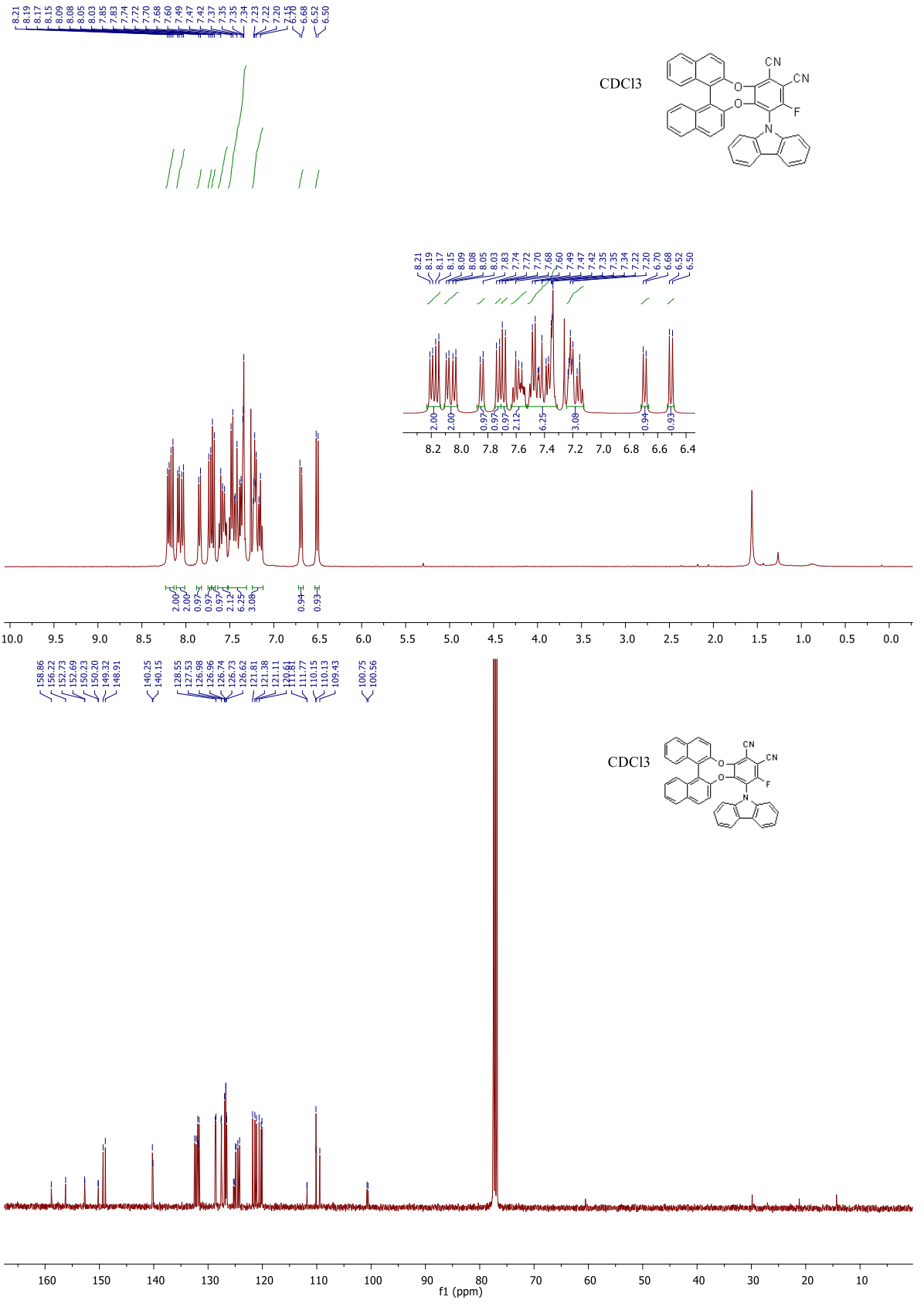

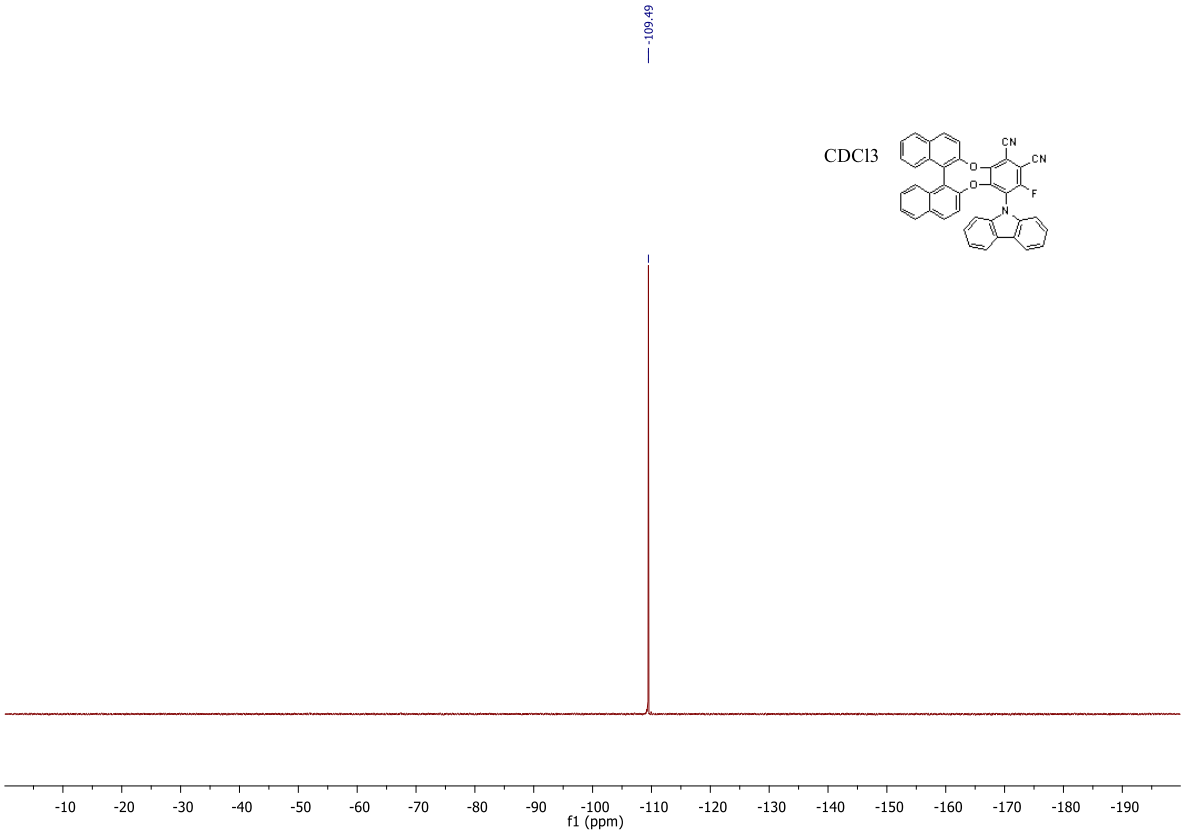
-109.49
CDCl3
CN
CN
F
O
O
N
-10 -20 -30 -40 -50 -60 -70 -80 -90 -100 -110 -120 -130 -140 -150 -160 -170 -180 -190
f1 (ppm)

Compound **C'2** :

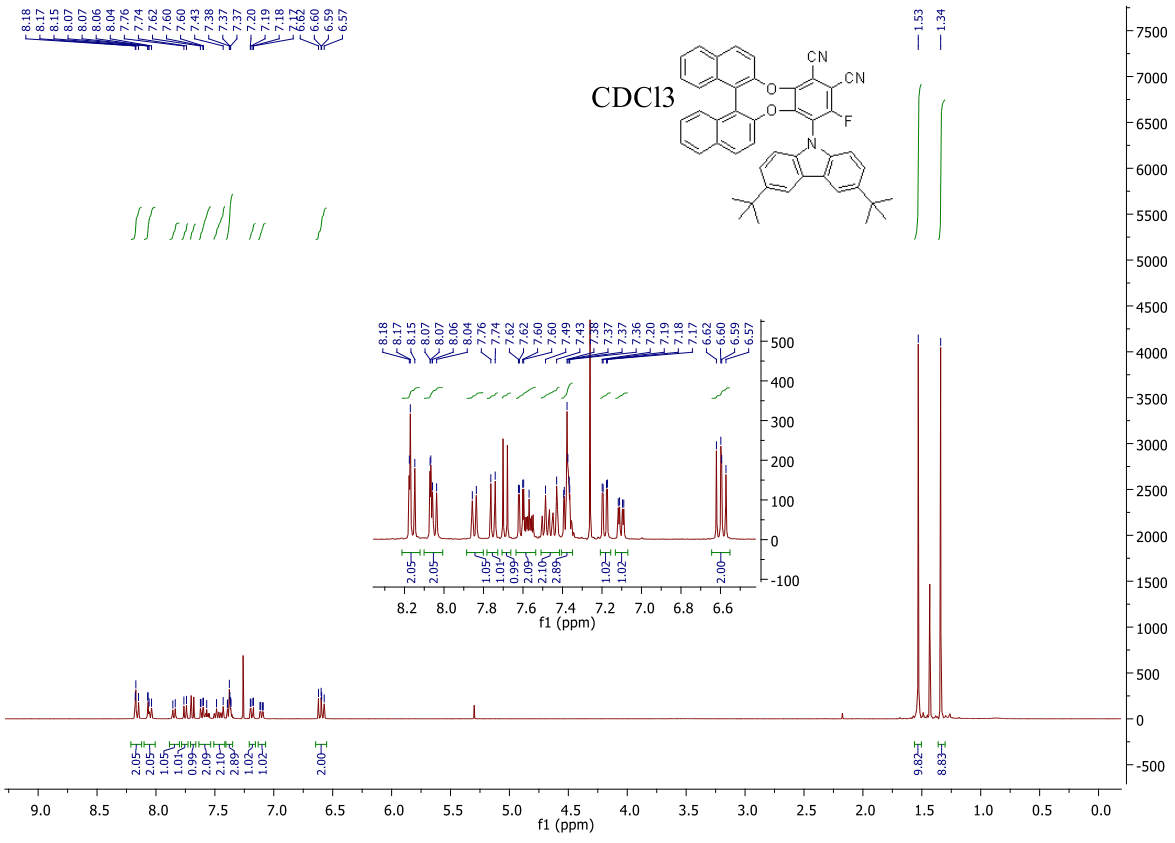
8.18 8.17 8.15 8.07 8.07 8.06 8.04 7.76 7.74 7.62 7.60 7.60 7.43 7.38 7.37 7.37 7.20 7.19 7.18 7.17 6.62 6.60 6.59 6.57
1.53
1.34
CDCl3
CN
CN
F
O
O
N
2.05 2.05 1.05 1.01 0.99 2.09 2.10 2.89 1.02 1.02 2.00
9.82 8.83
9.0 8.5 8.0 7.5 7.0 6.5 6.0 5.5 5.0 4.5 4.0 3.5 3.0 2.5 2.0 1.5 1.0 0.5 0.0
f1 (ppm)

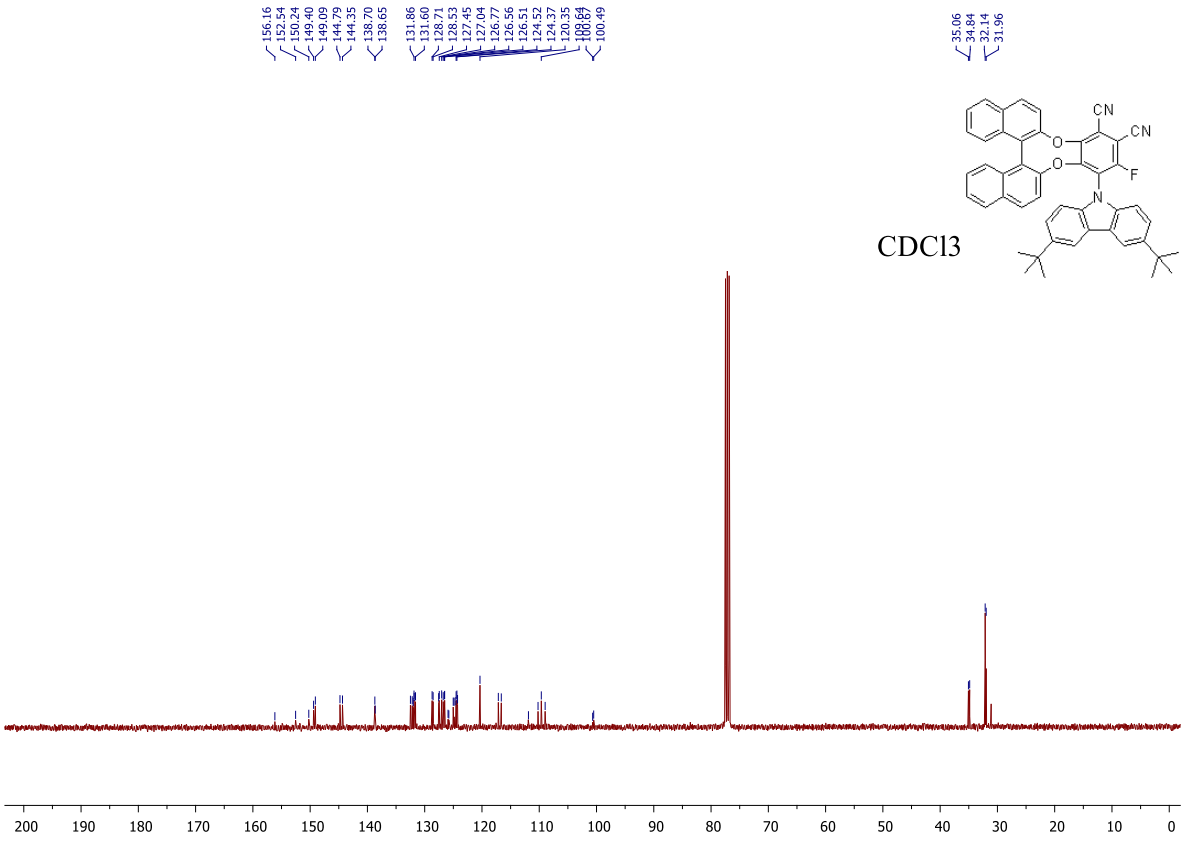

^{19}F NMR (376 MHz, CDCl$_3$) δ -109.00.

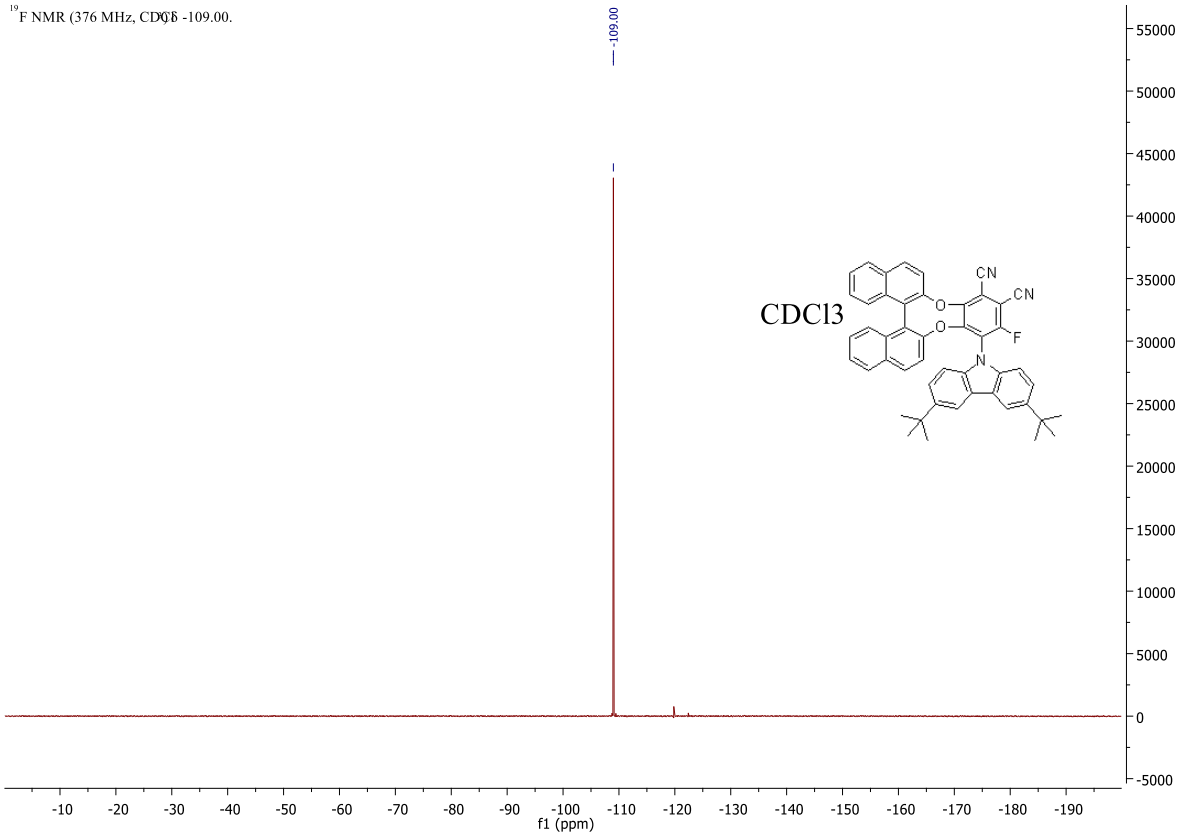

Compound **C'3** :

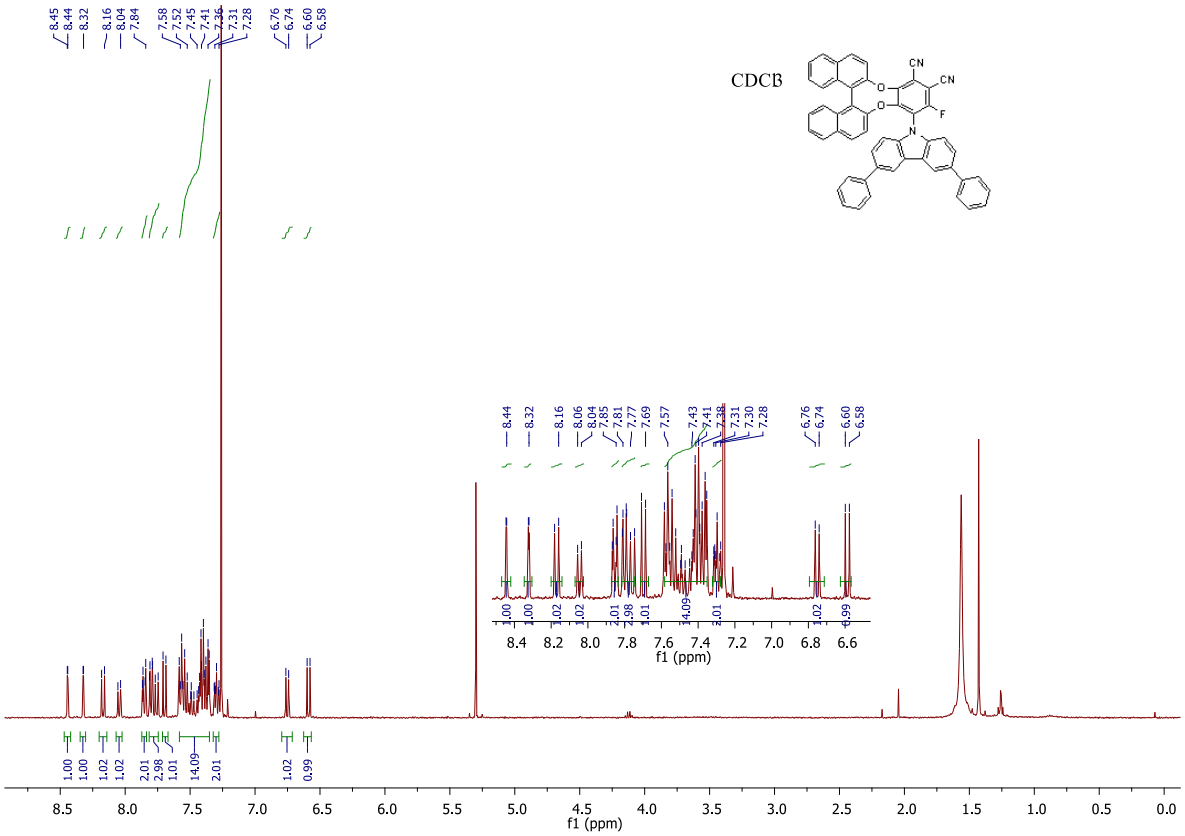

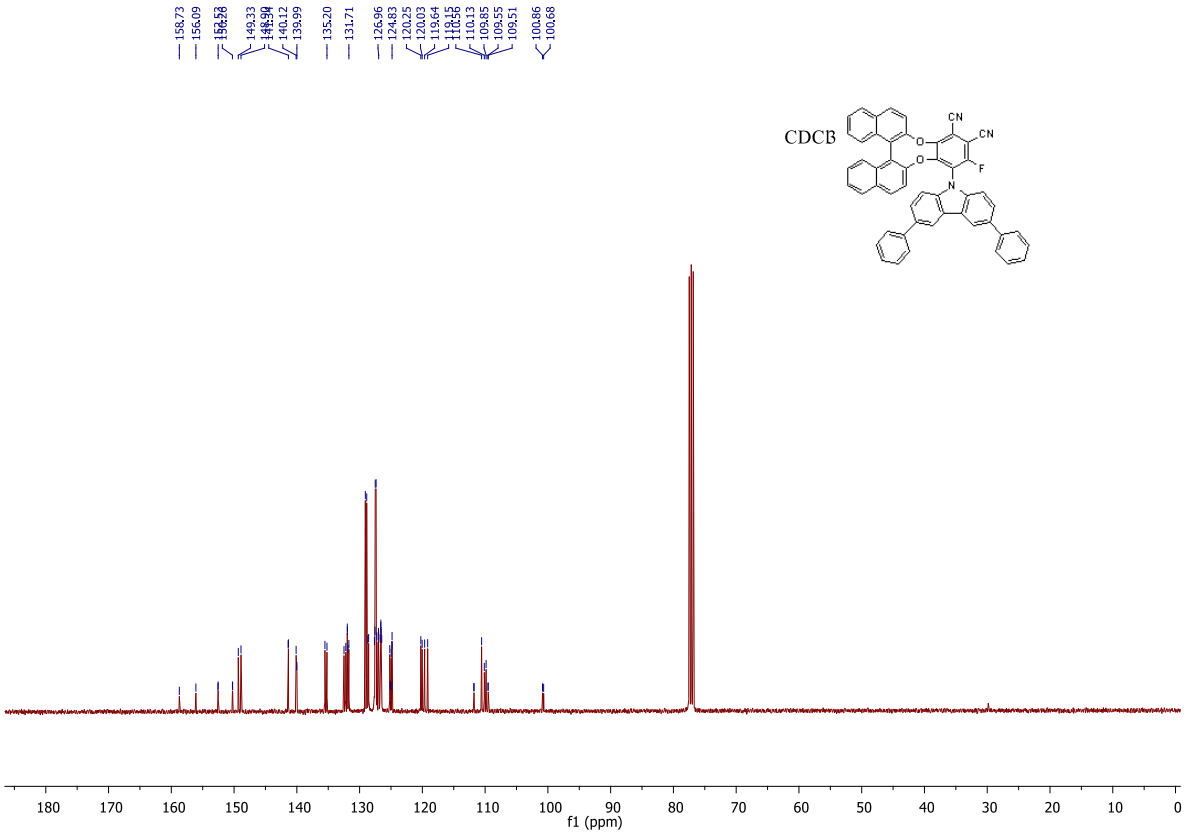

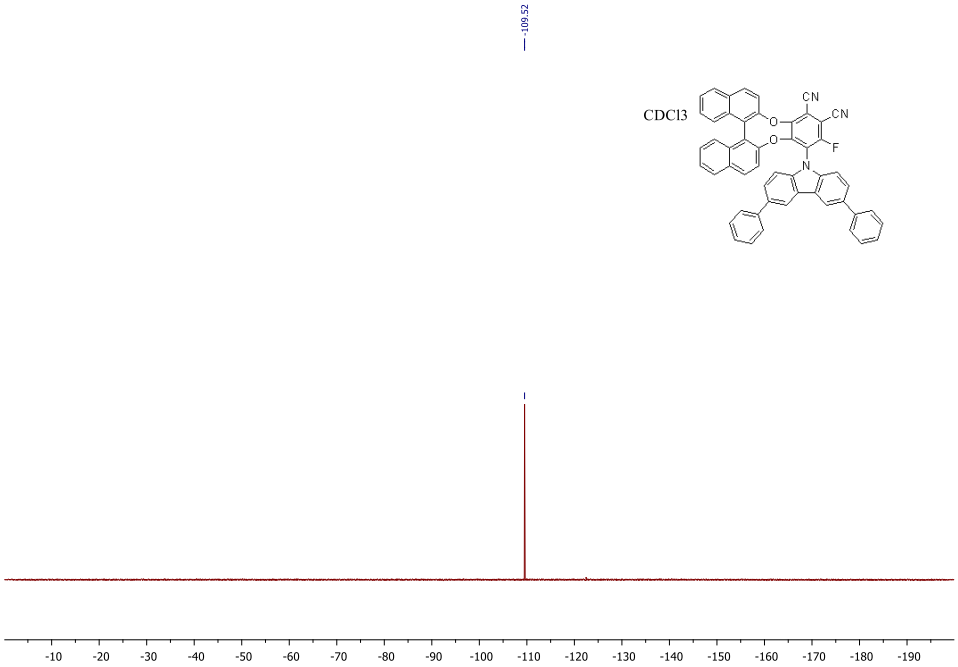
-109.52
CDCl3
CN
CN
F
O
O
N
-10 -20 -30 -40 -50 -60 -70 -80 -90 -100 -110 -120 -130 -140 -150 -160 -170 -180 -190

Compound **C1** :

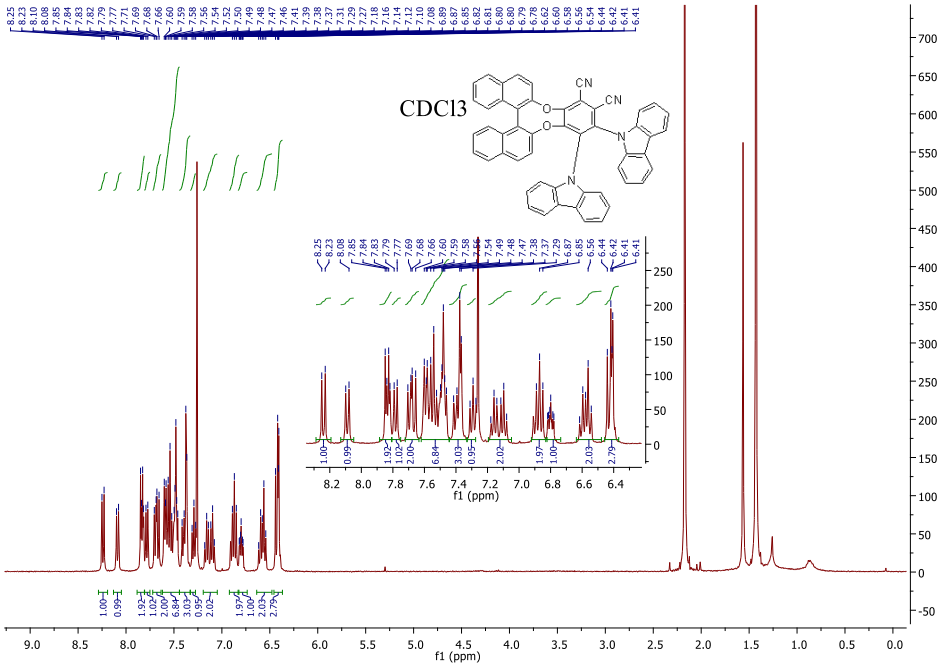
CDCl3
CN
CN
O
O
N
f1 (ppm)
9.0 8.5 8.0 7.5 7.0 6.5 6.0 5.5 5.0 4.5 4.0 3.5 3.0 2.5 2.0 1.5 1.0 0.5 0.0

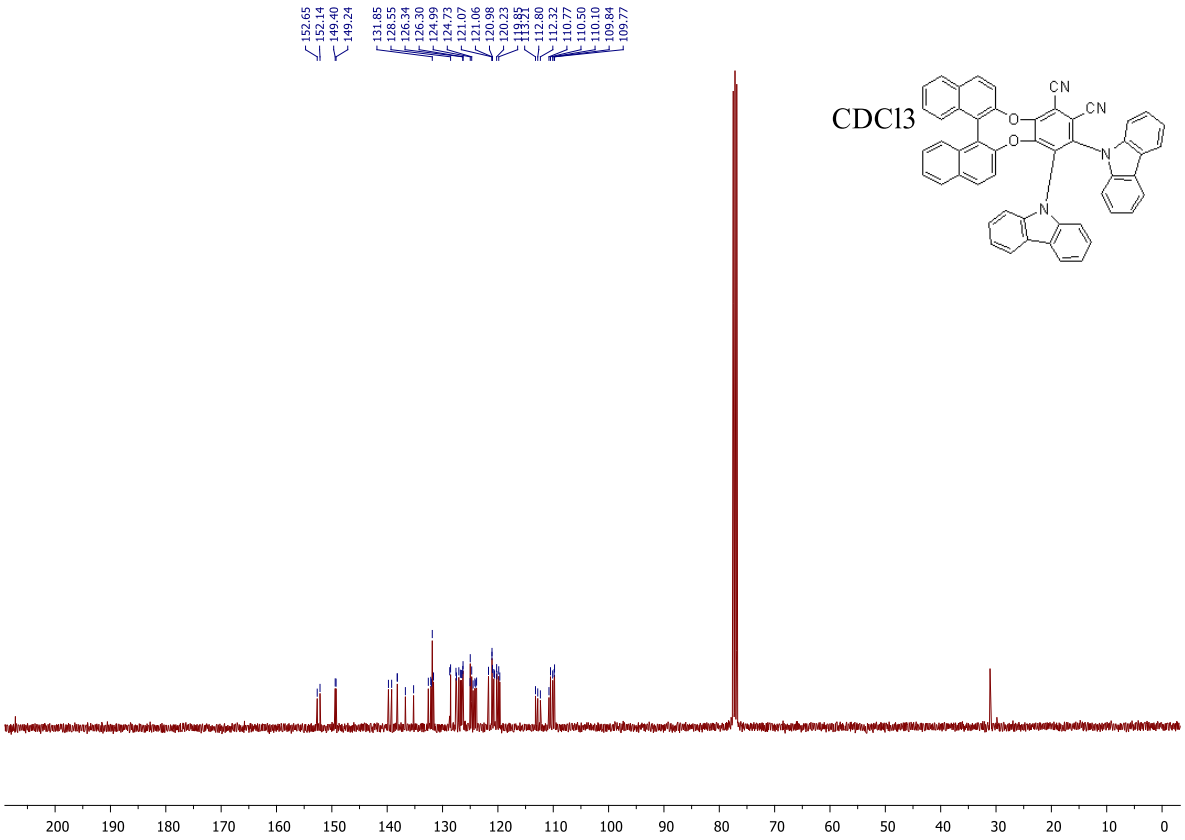

Compound **C2**:

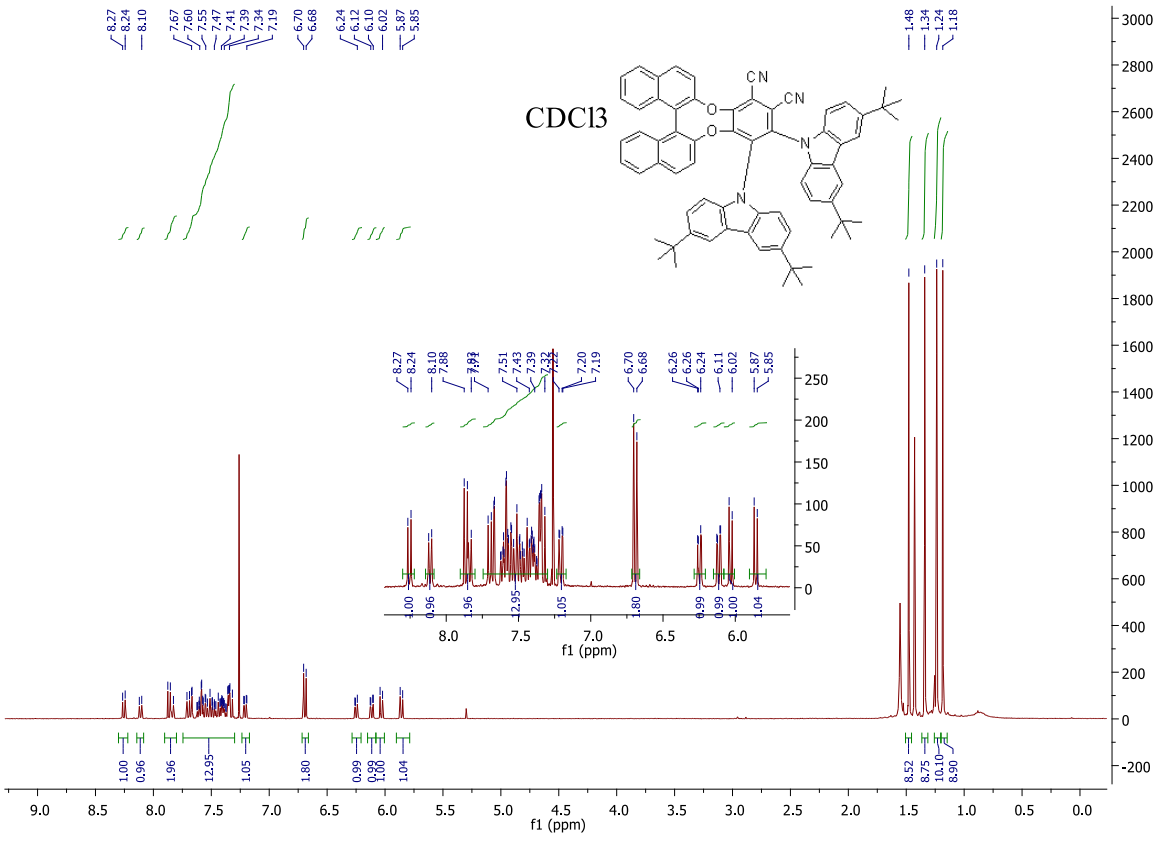

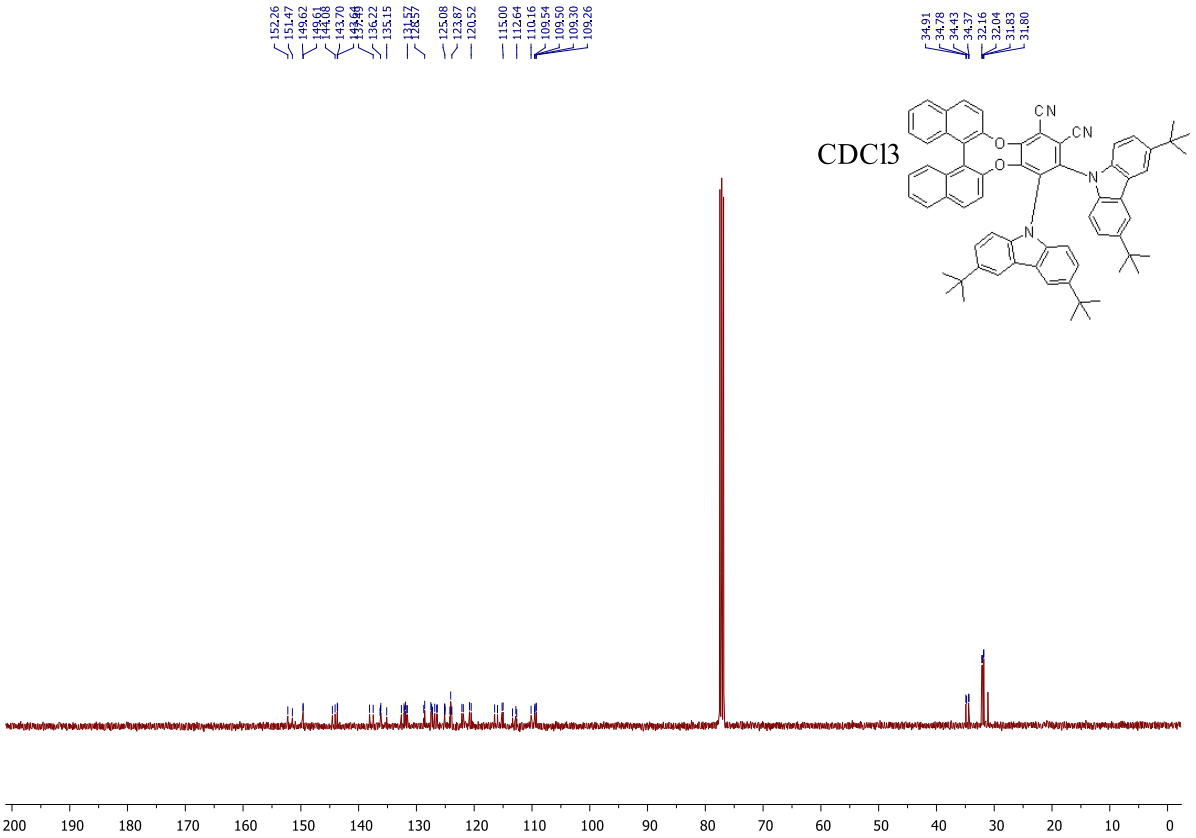

Compound **C3** :

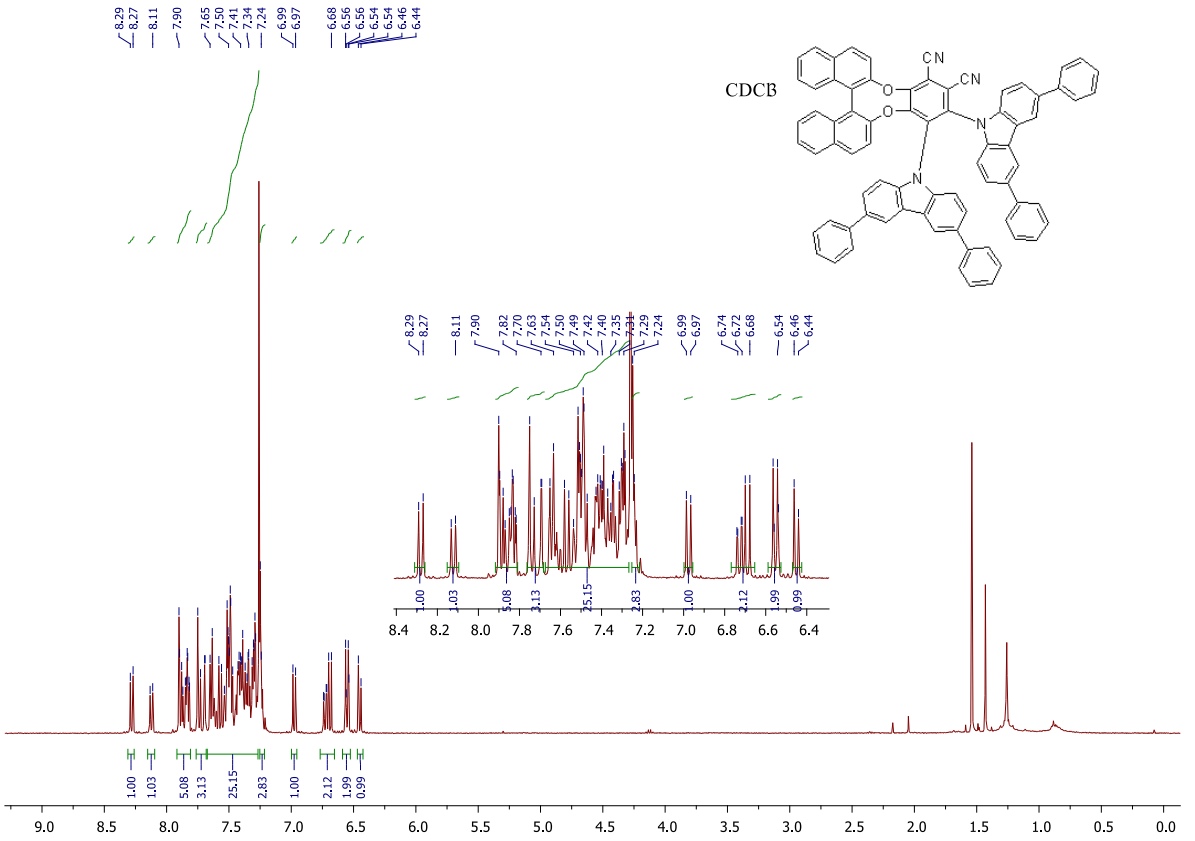

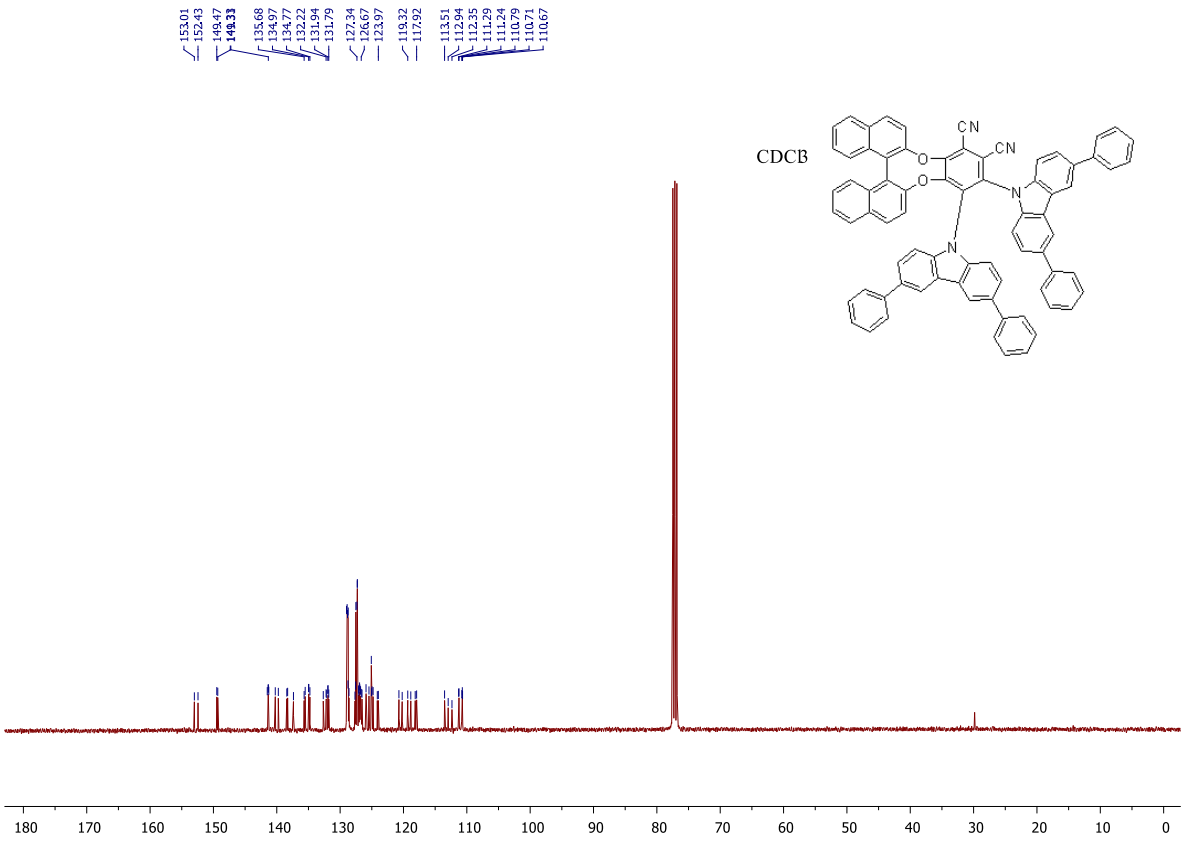

3,6-dibromocarbazole :

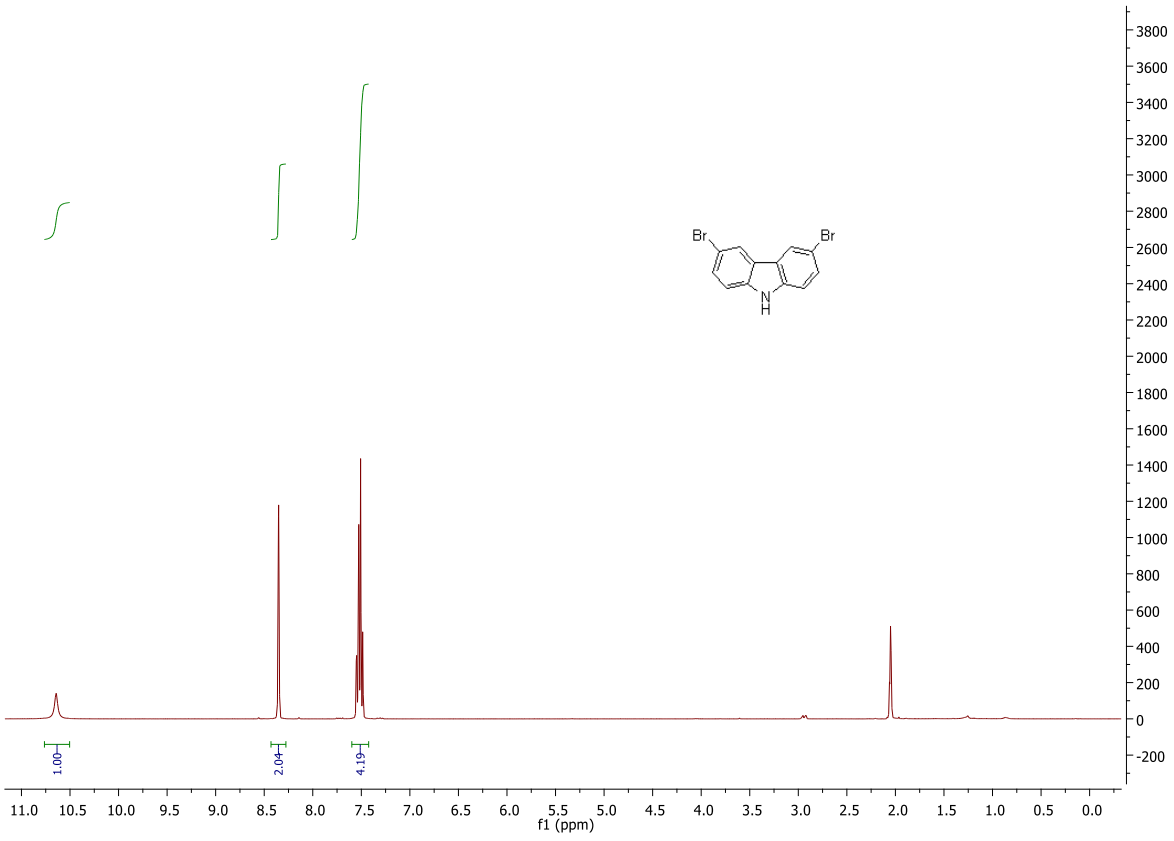

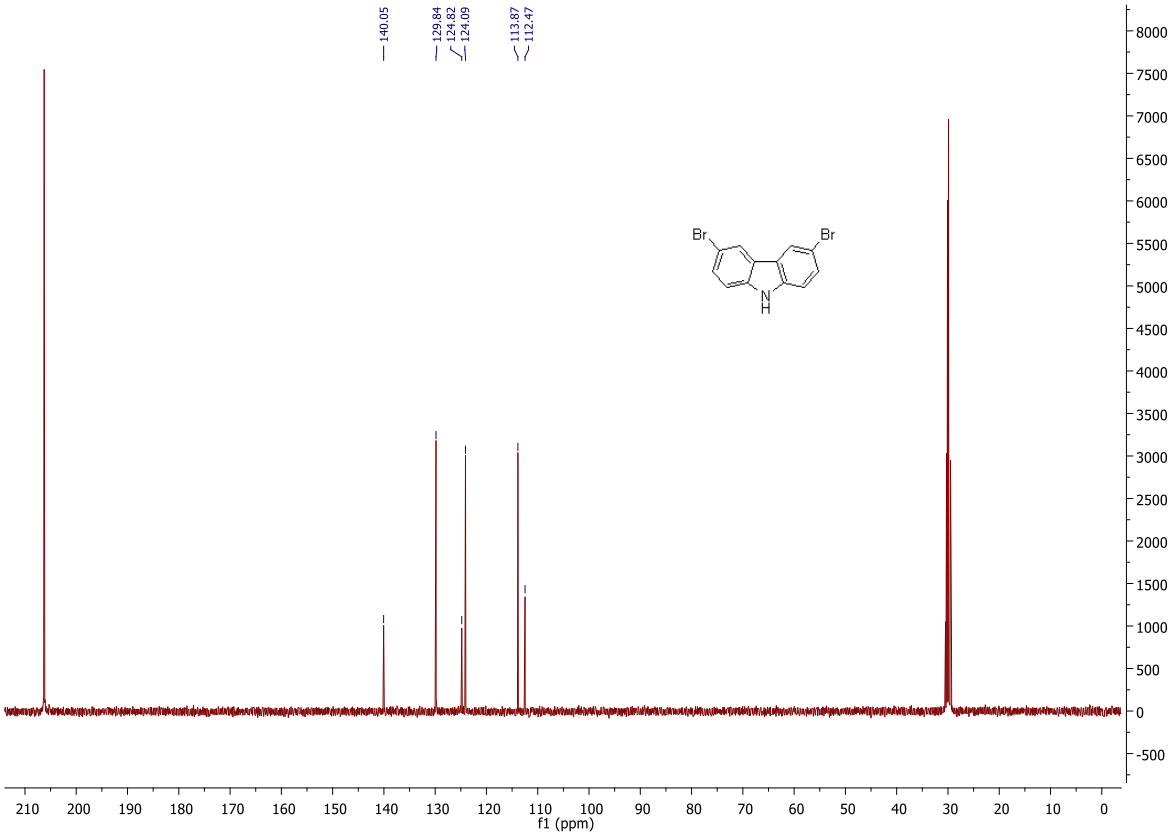
140.05
129.84
124.82
124.09
113.87
112.47
Br
Br
N
H
f1 (ppm)

Compound **5d** :

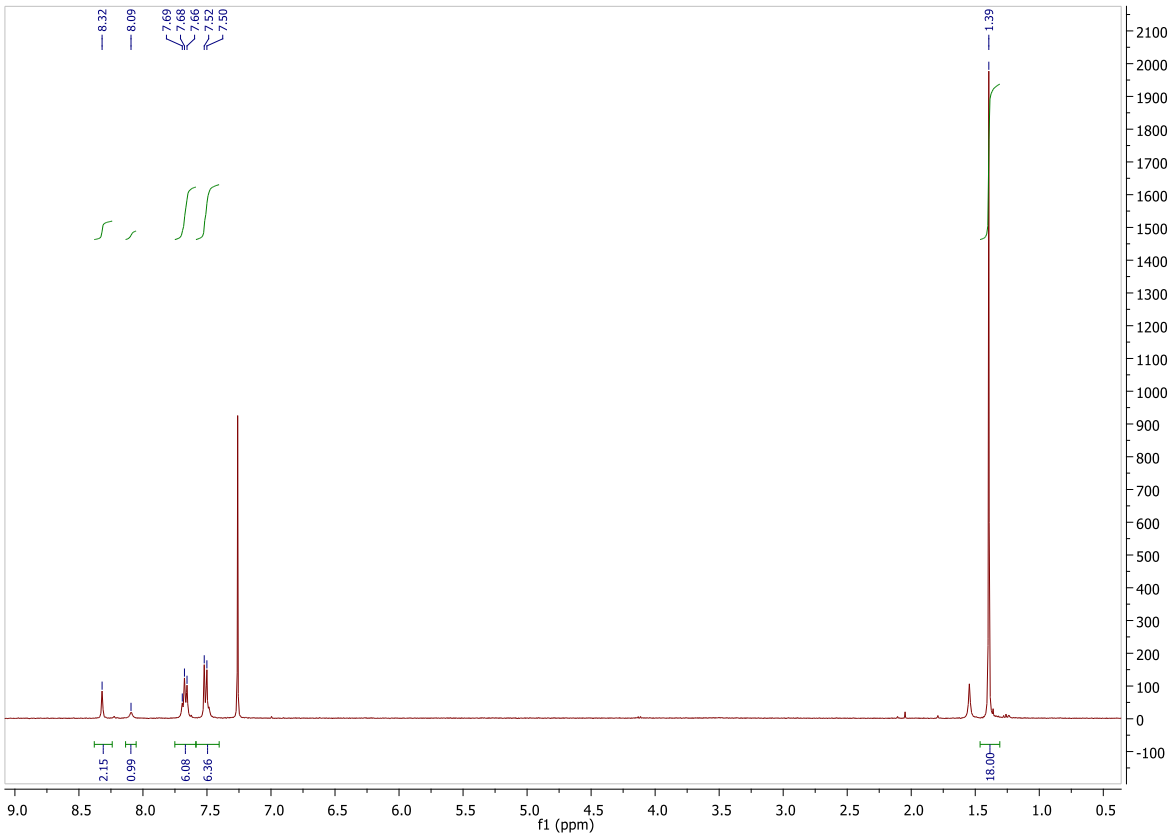
8.32
8.09
7.69
7.68
7.66
7.52
7.50
1.39
2.15
0.99
6.08
6.36
18.00
f1 (ppm)

References:

S1: Brunet, E.; Jiménez, L.; de Victoria-Rodriguez, M.; Luu, V. ; Muller, G.; Juanes, O.;Rodríguez-Ubis, J. C. *Microporous Mesoporous Mater.* **2013**, 169, 222, and references therein.

S2: Dekkers, H. P. J. M.; Moraal, P. F.; Timper, J. M.; Riehl, J. P. *Appl. Spectrosc.* **1985**, 39, 818.

S3: T. Yanai, D. P. Tew, N. C. Handy, *Chem. Phys. Lett.*, **2004**, 393, 51.

S4: F. Neese, *WIREs Comput. Mol. Sci.*, **2018**, 8, e1327.

S5: O. Vahtras, J. Almlöf, M. W. Feyereisen, *Chem. Phys. Lett.*, **1993**, 213, 514.

S6: S. Grimme, J. Antony, S. Ehrlich, H. Krieg, *J. Chem. Phys.*, **2010**, 132, 154104.

S7: S. Grimme , S. Ehrlich , L. Goerigk, *J. Comput. Chem.*, **2011**, 32, 1456.

S8: F. Weigend, R. Ahlrichs, *Phys. Chem. Chem. Phys.*, **2005**, 7, 3297.

S9: T. Lu, F. Chen, *J. Comput. Chem.*, **2012**, 33, 580.

S10: W. Humphrey, A. Dalke, K. Schulten, *J. Molec. Graphics*, **1996**, 14, 33.

S11: C. Lefebvre, G. Rubez, H. Khartabil, J.-C. Boisson, J. Contreras-García, E. Hénon, *Phys. Chem. Chem. Phys.*, **2017**,19, 17928.

S12: H. Tanaka, Y. Inoue and T. Mori , *ChemPhotoChem*, **2018**, 2 , 386

S13: Tao, Y.; Yuan, K.; Chen, T.; Xu, P.; Li, H.; Chen, R.; Zheng, C.; Zhang, L.; Huang, W. *Adv. Mater.* **2014**, *26*, 7931-7958.

S14: S. Taverne, B. Caron, S. Gétin, O. Lartigue, C. Lopez, S. Meunier-Della-Gatta, V. Gorge, M. Reymermier, B. Racine, T. Maindron, E. Quesnel, *J. Appl. Phys.*, **2018**, 123, 023108

S15: R. W. W. Hooft, COLLECT, Nonius BV, Delft, The Netherlands, 1998.

S16: Z. Otwinowski and W. Minor, Methods Enzymol., 1997, 276, 307.

S17: G. M. Sheldrick, Acta Crystallogr., Sect. A, 2015, 71, 3.

S18: G. M. Sheldrick, Acta Crystallogr., Sect. C, 2015, 71, 3.

S19: Spek, A. L. PLATON SQUEEZE: a Tool for the Calculation of the Disordered Solvent Contribution to the Calculated Structure Factors. Acta Crystallogr., Sect. C: Struct. Chem. 2015, 71, 9−18.